Double Parton Distributions

Perturbative splitting, sum rules, and models

Dissertation zur Erlangung
des Doktorgrades der Naturwissenschaften (Dr. rer. nat.)
der Fakultät für Physik der Universität Regensburg

vorgelegt von

Peter Plößl

aus

Nabburg

im Jahr 2019

Acknowledgements

As this thesis would not have been possible in its present form without the support from a number of people, I want to express my gratitude for this. First of all I would like to thank my supervisor, Professor Andreas Schäfer, who sparked my interest in high energy physics with an extensive lecture on theoretical and experimental particle physics. As a result of this I joined his group for my Bachelor's thesis and stayed throughout my Master's degree and finally for my PhD.

For my Master's thesis I started working on multiple partonic interactions (MPIs) in collaboration with Markus Diehl and Jonathan Gaunt who have been collaborators from this day on. For this I would like to thank them, as they took their time to explain many of the subtleties encountered in perturbative QCD in general and MPIs in particular. Markus Diehl was basically my second supervisor during my PhD and always had extremely valuable input whenever I was stuck with a problem. Collaborating with Jonathan Gaunt for the final project of my PhD greatly improved my understanding of perturbative QCD calculations, for which I am very grateful. I would also like to thank Daniel Lang who worked with me on the sum rule improved DPD models and helped quite a lot with the numerical implementation.

For the great times during numerous lunch and coffee breaks I would like to thank my fellow graduate students, many of whom became close friends over the course of the years. In particular I am thankful to Jakob Simeth and Max Emmerich with whom I shared an office. At this point it should not go unmentioned that also many of my close friends supported me in one way or another, for which I am very grateful.

And finally, last but not least, I would like to thank my family – my parents, my sister, and my grandma – for being supportive of me in every way possible for so many years. Without them and their continued support I probably would have given up somewhere along the way.

Abstract

The overarching topic of this thesis is double parton scattering (DPS), which describes the situation when two individual hard scattering reactions occur in a single hadron-hadron collision. In some regions of phase space DPS may give sizeable contributions to the production of multi-particle final states and thus be an important background to single parton scattering (SPS). Not only this, but DPS is also an interesting phenomena in its own right, as it gives insight into the correlations of partons inside of hadrons. Therefore a theoretical description of such processes from first principles is required. Such a prescription is obtained in the form of a factorisation theorem akin to the one known from SPS, with a central building block being the double parton distributions (DPDs). However, these DPDs are presently basically unknown as experimental data is still lacking.

One of the few general theoretical constraints for DPDs are the number and momentum sum rules proposed by Gaunt and Stirling. In chapter 3 of this thesis a proof is presented that the DPD sum rules are valid at all orders in the strong coupling for renormalised distributions. As by-products of this proof the all order form of the inhomogeneous evolution equation for momentum space DPDs can be derived and it can be shown how the inhomogeneous term in this equation is related to the contribution of a short distance $1 \rightarrow 2$ splitting to the DPDs. It can furthermore be shown that the $1 \rightarrow 2$ evolution kernels in the inhomogeneous term fulfil number and momentum sum rules closely resembling the ones for DPDs.

In chapter 4 the sum rules considered in chapter 3 are used to construct improved position space DPD models. To this end it is first shown how position space DPDs can be matched onto the momentum space DPDs for which the sum rules have been shown to be valid. Following this an initial DPD model consisting of an intrinsic part and a contribution from the perturbative $1 \rightarrow 2$ splitting is iteratively refined in order to obtain the best possible agreement with the DPD sum rules. In particular, this highlighted that a good agreement with the momentum and equal flavour number sum rules is not possible without taking into account the $1 \rightarrow 2$ splitting contribution. Finally the dependence of the agreement with the sum rules on the renormalisation scale and the cut-off scale introduced by the matching onto momentum space DPDs is investigated.

As the $1 \rightarrow 2$ splitting contribution has been shown to be quite important for DPS it is extensively studied in chapter 5. In particular, the next-to-leading order (NLO) expression for this splitting is the only missing quantity required for NLO DPS calculations.

Therefore this splitting is calculated at NLO in perturbation theory for unpolarised colour singlet DPDs in all partonic channels using state of the art techniques. From this momentum and position space $1 \to 2$ splitting kernels as well as the $1 \to 2$ evolution kernels needed in the inhomogeneous evolution equation of momentum space DPDs are extracted at NLO. As a cross-check for the correctness of the results the agreement of the $1 \to 2$ evolution kernels with the sum rules derived in chapter 3 is explicitly verified. Finally various kinematic limits of the momentum space splitting kernels and the evolution kernels are discussed.

Contents

Contents

List of Figures

1. Introduction

One of the great successes of physics in the 20th century was the establishment of the Standard Model of particle physics (SM) as the theory of the known microscopic interactions in a combined effort of theoretical and experimental particle physicists. Within the framework now known as the SM the interactions of elementary particles via the fundamental forces are on one hand described by the electroweak theory which is a unification of the theories describing the electromagnetic interaction – Quantum ElectroDynamics (QED) – and the weak interaction – Quantum FlavourDynamics (QFD) – responsible for radioactive decays, and on the other hand by the theory of strong interactions – Quantum ChromoDynamics (QCD) – governing how quarks interact to form hadrons, while gravitation is completely neglected in the SM. Incorporating a quantum theory of gravitation that is compatible with general relativity into the SM is one of the most important steps towards a unified description of the fundamental interactions. Nevertheless, even without this[1] the SM has proven remarkably successful in predicting experimental results, with its latest and probably best known (at least to the general public) success being the discovery of the Higgs boson at the Large Hadron Collider (LHC). The existence of this elusive particle had been predicted already in the 1960's as a fundamental building block of the SM and its experimental observation was celebrated as the completion of the SM. However, the failure to account for the effects of gravitation is not the only weakness of the SM as it also fails to explain the observed matter-antimatter asymmetry as well as the existence of dark matter and dark energy. Phenomena associated with these – and other – things not explained by the SM are referred to as beyond Standard Model (BSM) physics and are a very active field of research within the particle physics community with great experimental efforts invested in the observation of such phenomena. Despite this so far no direct evidence of BSM physics has been detected, suggesting that deviations from the SM predictions are – at currently accessible energies – very small. This implies that not only increased experimental accuracy and higher collision energies are required in order to discover BSM effects, but also the precision of theoretical predictions has to be pushed further.

Currently the largest uncertainties are associated with predictions regarding the strong interaction, on one hand due to the fact that the coupling constant of the strong interaction is comparably large, and on the other hand because calculations within QCD tend to be quite a bit more involved than for example in QED such that calculations of higher order terms in the perturbative expansion tend to become cumbersome. Besides

---

[1]The reason for this is that at the energies – and thus also distances – probed at present day colliders gravitation can be neglected compared to the other fundamental forces.

this, most QCD calculations and event generators only take leading power contributions into account while the full plethora of possible (power suppressed) QCD effects is not taken into account in a systematic manner. One example are so called multiple partonic interactions (MPIs) which can contribute to the production of multiple hard final states. Consider to this end the simplest MPI reaction, namely double parton scattering (DPS), which is also the largest of the MPI contributions. The typical assumption in hadron-hadron collisions is that the final state with an associated hard scale Q is produced in a single parton scattering (SPS) event where one parton from one of the colliding hadrons scatters of a single parton in the second colliding hadron, while the remaining partons do not partake in any hard scatterings and fly off as beam remnants. In the case that the final state can be divided into two subsets A and B with associated hard scales Q_A and Q_B the final states can furthermore be produced by so called double parton scattering (DPS) events where two partons from each colliding hadron enter distinct hard scatterings. Experimental evidence of DPS has already been found in the 1980's and 1990's as can be seen in references [1–5] and also more recently at the LHC as evidenced by the results in references [6–18]. In particular it is expected that especially after the rather recent energy upgrade at the LHC and even more so at possible future higher energy hadron colliders the rate of MPI events will further increase as will be discussed in a bit. A generalisation of the situation with two distinct subsets in the final state to the case of multiple distinct subsets in the final state which can be produced by MPIs arises naturally following the rationale for DPS above. However, when integrated cross sections are considered already DPS is is power suppressed compared to SPS by Λ^2/Q^2 where Λ is a generic hadronic scale while Q is the smaller of the two hard scales Q_A and Q_B. Despite of this suppression DPS can nevertheless compete with SPS in some cases where the production of the final states via SPS involves small coupling constants or higher orders in the coupling constant, with the most well known of these probably being the production of a same sign WW pair as described in references [19–24]. When cross sections differential in the transverse momenta of the final states are considered it has been shown in references [25–28] that for small transverse momenta of the final states DPS contributes at leading power, comparable to the SPS contributions. In references [29–31] is has furthermore been pointed out that DPS gives sizeable contributions to the overall cross sections in the case of a large rapidity separation between the two subsets A and B in the final state. As mentioned above, the relative importance of DPS compared to SPS is expected increase with increasing collision energy. This can be understood if one considers that on one hand with increasing collision energy smaller and smaller momentum fractions of the constituent partons are probed while on the other hand the DPS cross section is expected to scale like the fourth power of a parton distribution whereas SPS scales like the second power of a parton distribution. Since parton distributions exhibit a strong growth for small momentum fractions this leads to an enhancement of DPS relative to SPS. While the inclusion of MPIs and in particular DPS in perturbative cross section calculations is required in order to improve theoretical precision, MPIs are interesting to study in their own right, as they give access to a detail picture of hadron structure

that is not accessible in SPS reactions. In particular the study of MPI processes makes it possible to obtain information about correlations between the partons making up hadrons as well as their distribution in transverse momentum space.

A systematic description of MPIs from first principles requires the extension of the well-known SPS factorisation theorems to the case of multiple hard interactions, giving rise to multi parton distributions in close analogy to the regular single parton distributions (PDFs). First steps in this direction were already taken in the 1980's when physicists first gained interest in MPIs as evidenced by references [32, 33] and a more stringent theoretical treatment was developed more recently with a particular focus on DPS as this is naturally the leading of the MPI contributions. In recent years quite some progress has been made towards a complete proof of factorisation for DPS in close analogy to the proofs of SPS factorisation theorems, especially in references [26, 34–36]. Furthermore a framework has been developed in reference [35] that allows for a clean separation of SPS and DPS contributions in regions of phase space where they overlap. At this point the theoretical framework for DPS calculations – even at higher orders – has reached a level of sophistication comparable to the SPS factorisation theorems. Nevertheless it is still not quite possible to perform DPS cross section calculations from first principles as a crucial ingredient in the DPS factorisation formula is still missing – the double parton distributions (DPDs) which contain the non-perturbative part of the full DPS cross section. As these DPDs are genuine nonperturbative quantities they cannot be calculated in perturbation theory and either have to be obtained from experimental data or using nonperturbative methods like lattice computations. Since DPS signals are generally small compared to the SPS case and an experimental determination of DPDs requires huge amounts of data the former is not possible at present and even though quite a lot of progress has been made regarding the extraction of parton distributions from lattice data the situation for DPDs is not as favourable there either. In order to still be able to compute DPS cross sections many physicists resort to what is known as the DPS pocket formula in which the DPS cross section is factorised into a product of SPS cross sections divided by a so called effective cross section. Such a factorised form of the DPS cross section arises when DPDs are approximated by simple products of PDFs multiplied by a spatial profile function, neglecting even the most basic correlations of the partons inside a hadron. A possible way to do better than this approach is to construct more sophisticated DPD models incorporating at least the most basic correlations. To this end any type of constraint placed upon the DPD models is valuable input and one possible constraint is the behaviour of the DPDs at small transverse separation between the two partons. In this regime the DPDs are dominated by what is referred to as the $1 \rightarrow 2$ splitting contribution in which the two partons arise from a short-distance splitting of a single parton. In this limit the DPDs can be expressed in terms of a convolution of perturbative $1 \rightarrow 2$ splitting kernels and regular PDFs. This $1 \rightarrow 2$ splitting contribution and its effect an DPDs and the DPS cross section has already been studied extensively in references [25, 26, 28, 35, 37–44]. A second kind of constraint was proposed by Gaunt and Stirling in reference [45] in the form of sum rules corresponding to the conservation of quark flavour and momentum

which momentum space DPDs have to fulfil, reaffirming the interpretation of DPDs as probability densities.

The main aim of this thesis is to gain a better understanding how to model DPDs in a way that most closely resembles the physical reality. To this end first a brief review of the underlying theory of QCD is presented in section 2.1 followed by an overview over the more specific DPS theory in section 2.2 where first the derivation of factorisation theorems for DPS is discussed in section 2.2.1 before definitions and properties of DPDs are addressed in section 2.2.2. In their original work on the DPD sum rules Gaunt and Stirling noted that the sum rules remain valid under LO renormalisation group evolution, given that they are fulfilled at the initial renormalisation scale. As the DPD sum rules provide one of the only constraints placed on DPDs it is of utmost importance to make sure that they are indeed valid in QCD at any scale. A first proof of this using light-cone wave functions was given in appendix C of reference [46]. However, while the framework of light-cone wave functions allows to keep track of kinematic and combinatorial factors, basically recovering the probabilistic parton model interpretation, the subtleties of renormalisation have not been fully taken into account in the proof presented in reference [46]. In chapter 3 this will be rectified by a detailed analysis of the UV singularities in DPDs and the effect of renormalisation on the validity of the sum rules. In particular it will be shown that the sum rules are indeed valid for renormalised DPDs to all orders in perturbation theory. Following this analysis the sum rules – together with the LO expression for the perturbative $1 \rightarrow 2$ splitting contribution to DPDs – will be used in chapter 4 to construct a sum rule improved position space DPD model. To this end the model suggested in reference [35] is used as a starting point for iterative refinement of this model with help of the sum rules. Following this a calculation of the $1 \rightarrow 2$ splitting contribution at NLO will be presented in chapter 5. The results obtained there are the last missing step towards NLO DPD models and subsequently also NLO DPS cross section calculations within the framework introduced in reference [35]. Finally a brief summary of the results obtained in chapters 3 to 5 will be presented in chapter 6 along with a discussion of work in progress and future directions.

2. Theory

2.1. Quantum ChromoDynamics

Before moving on to the actual research work of this dissertation, a short introduction to the underlying theory – Quantum ChromoDynamics (QCD) – is presented in this section. QCD is the microscopic theory of the so called strong interaction describing the interactions of quarks and gluons which are bound by this interaction to form hadrons, for example protons and neutrons which make up everyday matter, but also more elusive particles like π mesons. Together with the electroweak interaction and the Higgs mechanism QCD forms the standard model of particle physics (SM) which to this day is in astonishing agreement with experimental data, despite enormous efforts to find deviations which are known to exist because of some theoretical flaws within the standard model. Of the theories making up the standard model QCD is the most non-trivial one, but as a result of this also the one with the most interesting features. This is largely due to the fact that the strong coupling constant is comparatively large and that QCD is a non-abelian gauge theory, leading to self interactions of the force carrying gluons. In what follows, a short history of the development of QCD – following loosely the presentation in Collins book on perturbative QCD [47] – will be given, as this nicely illustrates the remarkable features of the strong interaction.

2.1.1. A brief history of QCD

The first discoveries leading to the development of the theory now known as QCD date back to the 1950's when experimental particle physics discovered more and more new particles in accelerator experiments. In the years following these discoveries theoreticians suggested different ways to explain the observed spectrum of particles, classifying them according to their measured properties like charge and spin. One of the most successful of these was Gell-Mann's eightfold-way introduced in reference [48] which organized the discovered particles according to their spin and charge quantum numbers in representations of the $SU(3)$ group and even allowed to predict the existence of the Ω^- baryon which at this time had not been discovered yet. Building on this Gell-Mann and, independently, Zweig formulated the quark model in references [49–51] which assumed that the observed particles were not elemental, but rather made up from fermionic spin $\frac{1}{2}$ particles of (approximately) the same mass called quarks, of which three different flavours – up (u), down (d), and strange (s) – exist, resulting in the

observed (approximate) $SU(3)$ symmetry. The particle spectrum can further be divided into mesons, constituted of two quarks, and baryons, made up from three quarks. As both mesons and baryons have integer charge it is natural that the quarks should have fractional charges, namely $+\frac{2}{3}$ for the up and $-\frac{1}{3}$ for the down and strange quarks. Explaining the observed particle spectrum, in particular the spin $\frac{3}{2}$ Δ^{++} baryon, consisting of three up quarks, required the introduction of an additional quantum number called colour, taking on three different values, as otherwise the spin-statistics theorem would forbid the existence of the Δ^{++}. One major drawback of the quark model was the fact that, while it was capable of explaining experimental data, the postulated constituents of the discovered particles could not be observed in experiments which lead to some scepticism.

A different, less experimentally driven, approach to describe the strong interaction was that of Yang and Mills who in reference [52] introduced the novel concept of non-abelian gauge theories, in contrast to the gauge theories existing at that time, in particular Quantum Electro Dynamics (QED), which were based on abelian gauge groups. However, a direct application of these non-abelian gauge theories seemed infeasible at this time – before the advent of the quark model – as it was assumed that the fields in the Lagrangian of such a theory should correspond directly to the observed particles which had to be massless in order to maintain gauge invariance, in contradiction with the observed massive particles. Nevertheless further progress in this direction was made by Faddeev and Popov who showed how non-abelian gauge theories can be quantized using generating functionals [53], and finally 't Hooft and Veltman proved that these theories are renormalisable [54]. Together with the discovery that masses could be generated by spontaneous symmetry breaking [55, 56] and the insight from the quark model this made Yang-Mills theories viable candidates for a quantum field theory of the strong interaction.

Results of the deep inelastic scattering (DIS) experiments at SLAC where electrons were accelerated to high energies and fired at protons and neutrons in atomic nuclei making up a fixed target led to the development of the so called parton model by Feynman [57]. The cross section of such a scattering event can be factorised into a leptonic tensor $L_{\mu\nu}$ and a hadronic tensor $W^{\mu\nu}$ which can be further decomposed into so called structure functions. Feynman suggested that hadrons are made up of so called partons which in DIS can be considered to be free massless particles. The reason for this assumption is rather intuitive as in the centre-of-mass frame of the collision the hadrons get Lorentz contracted along the collision axis. On the timescale of the scattering the individual partons can then indeed be thought of as non-interacting which makes it possible to neglect the strong interactions and only consider the electromagnetic interactions described by QED. The cross section can then be described as a product of a partonic cross section and what is referred to as a parton distribution function (PDF) which is basically the probability to find a given parton with a given longitudinal momentum

fraction inside a hadron. One remarkable prediction of the parton model is Bjorken scaling, implying that the structure functions measured in the DIS experiments should be independent of the momentum transfer Q between the electron and the hadron which was indeed in pretty good agreement with experimental data. If this Bjorken scaling were exact it would require the coupling of the strong interaction to tend to zero in the ultra-violet (UV), and even for the observed approximate Bjorken scaling the strong interaction should become very weak at high energies, or correspondingly at small distances.

In 1973 Gross, Wilczek and Politzer showed that for not too many matter fields non-abelian gauge theories exhibit exactly this behaviour, namely asymptotic freedom [58–60]. This was the final missing piece for the non-abelian gauge theory suggested by Fritzsch, Gell-Mann, and Leutwyler as a description of the strong interaction [61, 62] to be consistent with all the known requirements it should fulfil. Not only did the work by Gross, Wilczek and Politzer imply that the coupling of the strong interaction decreases with increasing energies, but also the opposite behaviour for low energies, which could explain why it seemed to be impossible to detect free quarks. The basic part of the Lagrangian of the theory now known as QCD has the following form

$$\mathcal{L}_{\text{QCD}} = \sum_{j=1}^{n_f} \overline{\psi}_{0,j} \left(i\slashed{D} - m_0 \right) \psi_{0,j} - \frac{1}{4} \left(F_{0,\mu\nu}^a \right)^2 , \tag{2.1}$$

where the sum over flavours indices includes the three quarks of the quark model – up, down, and strange – as well as the later discovered charm, bottom, and top quarks and the gauge invariant derivative $\slashed{D}$ is given by

$$\slashed{D} = \gamma^\mu \left(\partial_\mu + ig_0 t^a A_{0,\mu}^a \right) \tag{2.2}$$

and the gluonic field strength tensor reads

$$F_{0,\mu\nu}^a = \partial_\mu A_{0,\nu}^a - \partial_\nu A_{0,\mu}^a - g_0 f_{abc} A_{0,\mu}^b A_{0,\nu}^c , \tag{2.3}$$

where the ψ_0 and $A_{0,\mu}^a$ are the bare quark and gluon fields, respectively, g_0 and m_0 the bare coupling constant and quark masses, t^a are the generators of the SU(3), and f_{abc} are the groups' totally anti-symmetric structure constants. In practice additional terms have to be added to the Lagrangian in equation (2.1) according to the Fadeev-Popov procedure in order to fix the gauge and then subsequently compensate for the gauge freedom. However, as these terms are not relevant for the arguments in the following discussion they have been neglected here. So far the Lagrangian has been defined in terms of so called bare quantities as indicated by the subscript 0 and in the following subsection the implications of this will be discussed.

2.1.2. Renormalisation and the running coupling

Taking the theory of QCD as it has been introduced until now and calculating Feynman diagrams one will encounter severe problems as for diagrams containing closed loops the results are divergent due to the behaviour of the integrand when these loop momenta become large, that means in the UV region, and the corresponding divergences are therefore termed UV-divergences. Even though these UV-divergences are an intrinsic feature of the theory described by the Lagrangian in equation (2.1) it is still possible to construct a theory with physically meaningful quantities and predictions from it using the fact that non-abelian gauge theories are renormalisable as shown in reference [54].

As this is a crucial step in any calculation in perturbative QCD a short review of how this works will be presented here. The basic idea behind renormalisation of quantum field theories is to define the theory with a UV regulator and make the parameters, like for example masses and coupling constants, of the theory functions of this regulator with their dependence chosen such that in the limit where this regulator is removed the UV divergences cancel. In order to do this the bare fields in the Lagrangian are expressed in terms of renormalised fields using inverse renormalisation factors[1], for example for the quark and gluon fields

$$\psi_0 \longrightarrow Z_\psi^{-\frac{1}{2}} \psi \,,$$

$$A_{0,\mu}^a \longrightarrow Z_A^{-\frac{1}{2}} A_\mu^a \,. \tag{2.4}$$

These renormalisation factors are – up to finite contributions – fixed by the requirement that the quantities calculated in terms of the renormalised fields should be finite. Implementing the consequences of this procedure in perturbation theory is most conveniently done using a counterterm approach. For this one first has to make the replacements introduced in equation (2.4) in the bare Lagrangian (2.1) and subsequently rewrite the resulting renormalised Lagrangian by introducing renormalised masses and couplings, m and g, and rearrange the terms in such a way that the structure of the original, bare, Lagrangian is recovered with additional terms identified as counterterms. Consider as an example the term in the first part of the bare Lagrangian giving rise to the quark-gluon vertex, that means

$$Z_\psi^{-1} Z_A^{-\frac{1}{2}} g_0 \overline{\psi} t^a \slashed{A}^a \psi \longrightarrow g\mu^\varepsilon \overline{\psi} t^a \slashed{A}^a \psi + \overline{\psi} t^a \slashed{A}^a \psi \left(Z_\psi^{-1} Z_A^{-\frac{1}{2}} g_0 - g\mu^\varepsilon \right) \,. \tag{2.5}$$

Here one now has a part containing only the UV-finite renormalised coupling and fields and the additional counterterm which can be calculated in perturbation theory.

---

[1]Some authors use a different convention where the bare fields are given by the renormalised ones times a renormalisation factor, rather than an inverse renormalisation factor

In equation (2.5) there is, in addition to the dimensionless renormalised coupling, also a factor μ^ε which is a characteristic – the renormalisation scale – of dimensional regularisation, the most used regularisation method in perturbative QCD calculations and also the one employed in this thesis. The idea behind this regulator is that divergent loop integrals are continued to non-integer dimension $D = 4 - 2\varepsilon$, where the integrations can be performed. The dimensional parameter ε then takes on the role of the actual UV regulator as UV divergences manifest themselves as poles in ε. The pole structure of the renormalisation factors is fixed by the requirement that they cancel the poles corresponding to the UV divergences of the bare theory, whereas the finite part of these factors is fixed by the choice of a so called renormalisation prescription. One of the most straight-forward choices is the so called minimal subtraction scheme (MS) where the renormalisation factors cancel only the poles and have no additional finite parts. The most common scheme used in QCD calculations is however the modified minimal subtraction scheme ($\overline{\text{MS}}$) [63] in which compared to the MS scheme counterterms contain an additional factor S_ε for each loop such that a perturbative expansion of the bare coupling, the renormalisation factors, and so on have the following form

$$g_0 = g\mu^\varepsilon \left[1 + \sum_{n=1}^\infty g^{2n} S_\varepsilon^n \sum_{m=1}^n \frac{B_{nm}}{\varepsilon^m} \right], \tag{2.6}$$

$$Z = 1 + \sum_{n=1}^\infty g^{2n} S_\varepsilon^n \sum_{m=1}^{M(n)} \frac{Z_{nm}}{\varepsilon^m}, \tag{2.7}$$

where the order $M(n)$ of the highest pole depends on the quantity being renormalised. The reason for introducing the factor S_ε is that there are terms from the angular integration in $D = 4 - 2\varepsilon$ dimensions which universally appear in renormalised quantities in the MS scheme and can be removed by a suitable choice of the factor S_ε. The standard choice is

$$S_\varepsilon = \left(4\pi e^{-\gamma_{\text{E}}} \right)^\varepsilon, \tag{2.8}$$

where γ_{E} is the Euler-Mascheroni constant. An alternative definition was proposed by Collins in reference [47] as

$$S_\varepsilon = \frac{(4\pi)^\varepsilon}{\Gamma(1 - \varepsilon)}, \tag{2.9}$$

which gives the same renormalised expressions for quantities with at most one ε pole per loop, as will be explicitly verified in section 5.3.2 up to two loop order.

A remarkable feature of renormalised non-abelian gauge theories is that their renormalised coupling runs end exhibits asymptotic freedom, ultimately allowing a perturbative expansion of hard QCD processes. Consider to this end the definition of the bare coupling in the $\overline{\text{MS}}$ scheme, equation (2.6), which at leading order (LO) is given by

$$g_0 = g\mu^\varepsilon \left[1 - \frac{g^2 S_\varepsilon}{16\pi^2 \varepsilon} \left(\frac{11}{6} C_A - \frac{2}{3} T_F n_f \right) + \mathcal{O}(g^4) \right]. \tag{2.10}$$

2. Theory

The bare coupling is naturally independent of the renormalisation scale, such that from equation (2.6) one can deduce the following renormalisation group (RG) equation for the renormalised coupling

$$\frac{dg}{d \ln \mu^2} = -\frac{\varepsilon g_0}{2 \frac{\partial g_0}{\partial g}} . \tag{2.11}$$

Introducing the abbreviation $a_s = \frac{g^2}{16\pi^2} = \frac{\alpha_s}{4\pi}$ which is the standard convention[2] in the literature on the topic (see for example reference [64]) one thus finds the following

$$\frac{da_s}{d \ln \mu^2} = -\frac{\varepsilon g_0 g}{16\pi^2 \frac{\partial g_0}{\partial g}} , \tag{2.12}$$

which, using the LO result for g_0, equation (2.10), then yields the LO RG equation for a_s

$$\frac{da_s}{d \ln \mu^2} = -a_s^2 \left(\frac{11}{3} C_A - \frac{4}{3} T_F n_f \right) \overset{N=3}{=} -a_s^2 \left(11 - \frac{2}{3} n_f \right) = -a_s^2 \beta_0 . \tag{2.13}$$

Here β_0 is the LO QCD β function first calculated by Gross, Wilczek, and Politzer in references [58, 60], which is negative if the theory does not include too many matter fields ($n_f \leq 16$) which is the case for the strong interaction with its six known quark flavours. Solving this renormalisation group equation then yields the running strong coupling constant a_s

$$a_s(\mu) = \frac{1}{\beta_0 \ln \frac{\mu^2}{\Lambda_{\text{QCD}}^2}} . \tag{2.14}$$

Solving the RG equation gave rise to the QCD mass scale Λ_{QCD} below which QCD is strongly coupled, with an experimentally determined value of around $200\,\text{MeV}$. It is quite remarkable that even in massless QCD this physically meaningful, dimensionful quantity emerges. The way the strong coupling runs – that means the fact that it exhibits asymptotic freedom for large energies – can be explained by the non-abelian nature of QCD which results in gluon self-interaction. Looking at the QCD Lagrangian (2.1) and the gluonic field strength tensor (2.3) one immediately can conceive that the additional f_{abc} term with two gluon fields not present in abelian gauge theories results in 3- and 4-gluon vertices. As a result of this, a colour charge is surrounded by virtual gluon fluctuations giving rise to an anti-screening effect in contrast to the screening effect due to virtual fermion-antifermion pairs. If the number of fermions in the theory is not too large the anti-screening effect due to gluons outweighs the screening effect of the fermion-anti-fermion pairs, leading to the observed behaviour.

---

[2]Note that in the remainder of this thesis a different definition of a_s will be used, namely $a_s = \frac{\alpha_s}{2\pi}$

2.1.3. Factorisation theorems: the backbone of perturbative QCD

It is the property of asymptotic freedom which allows for a perturbative expansion of cross sections and Greens' functions in the strong coupling when the associated energy scales become large enough. However, in a scattering event typically not all momenta are large enough for this to be the case, since there are always also interactions between the quarks and gluons inside the probed hadrons where the exchanged momenta are generally of a hadronic scale where QCD is strongly coupled and thus non-perturbative.

In order to see how one can nevertheless use perturbation theory to obtain predictions from first principles in QCD it is useful to look at the parton model. One of the assumptions in the parton model of DIS is that the constituents of the probed hadron, the partons, can be treated as quasi-free particles which do not interact strongly on the timescale of the parton-photon scattering. The reasoning behind this approximation is that as the hadron is strongly Lorentz contracted in the centre-of-mass frame of the scattering and the duration of the scattering is negligible compared to the distance between the individual partons in the transverse direction where the hadron is not contracted such that they can not interact during the scattering. This makes it possible to "factorise" the cross section of this process into a product of a "partonic" QED parton-photon scattering cross section and a parton distribution function (PDF) describing the probability to find a parton of a given flavour inside the probed hadron with a given fraction x of its longitudinal momentum. A similar picture applies also to the case of hadron-hadron collisions where it is again possible to treat the constituent partons of each hadron as quasi-free based on the arguments given above with the difference that now the hard interaction is between individual partons from each of the colliding hadrons scattering off each other. Following the DIS picture the cross section can then again be factorised into two PDFs – one for each colliding hadron – and a partonic QCD cross section for the parton-parton scattering which can be calculated in perturbation theory. While the parton model is of course not full QCD this picture is physically intuitive and provides the basis for what is referred to as factorisation theorems in QCD which are a very important tool forming the foundation of most perturbative QCD cross section calculations.

In a full QCD treatment the situation is naturally more complicated than in the naïve parton model as now there are several aspects that have to be taken into account, most prominently the exchange of additional collinear and soft gluons exchanged between the hard scatterings and the colliding hadrons and between the colliding hadrons, respectively. How these complications are tackled in deriving a factorisation theorem will now be illustrated for the example of the Drell-Yan process, that means the production of a neutral electroweak gauge boson – a photon or a Z boson to be more precise – from a quark-antiquark scattering as illustrated in figure 2.1, with measured transverse momentum of the final states. The first step towards a factorisation theorem for a given process is always to find its leading regions, that means those regions of
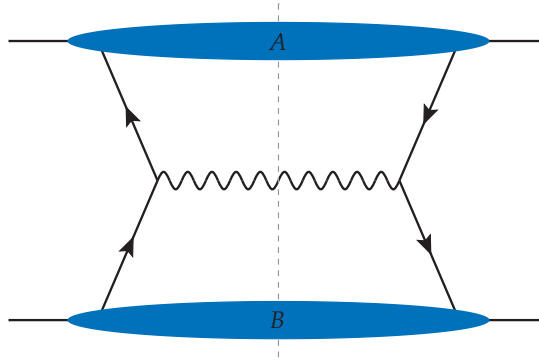
Figure 2.1.: Graphical illustration of the Drell-Yan process. The two large extended blobs symbolise the two colliding hadrons, the lower blob the right moving hadron and the upper blob the left moving hadron respectively. Here and in all following figures of this kind the dashed line represents the final state cut. On each side of the final state cut a quark from one colliding hadron annihilates with an antiquark from the other hadron to produce a neutral electroweak gauge boson indicated by the wavy line. This gauge boson subsequently decays into a dilepton which is not shown here.

loop momenta which give the leading contribution to the cross section. To this end the method by Libby and Sterman [65, 66] is employed which makes use of the fact that, up to normalisation, the cross section depends only on the ratio of the energy and the masses such that there exists a one-to-one correspondence between the limits of high energies and vanishing masses. This implies that in order to obtain the leading behaviour for large energies it suffices to consider the limit of vanishing masses and – in the case of transverse momentum dependent factorisation – also vanishing transverse momenta. The leading regions of a process are then those where the loop momenta are such that the massless propagators become singular resulting in large integrands. However, the existence of such a massless propagator pole is not a sufficient criterion for a momentum region to give a leading contribution to the cross section as it may still be possible to deform the integration contour away from this region which is always the case unless it is pinched between two adjacent poles on opposite sides of the real axis such that this would imply picking up the residue of an additional pole. Finding these leading regions is possible by either using the so called Landau criterion [67] or using a graphical method by Coleman and Norton [68] which makes use of the fact that pinch singular points (or in the case of multidimensional loop integrals pinch singular surfaces) correspond to regions of momentum space where on-shell propagators correspond to classically allowed scattering processes in position space. Even the existence of a pinch singularity does not guarantee a leading contribution from the corresponding momentum region as so far the treatment considered only the denominator structure of the integrand, while neglecting the numerator which may, however, compensate the smallness of the denominator in proximity of a pinch

singularity. Therefore, in order to find the actual leading regions of a process, it is necessary to perform a power counting analysis for every pinch singularity. Following this procedure one finds for the Drell-Yan process the following leading subgraphs:

- One hard subgraph producing the electroweak gauge boson on each side of the final state cut,
- one collinear subgraph for each colliding hadron,
- and finally a soft subgraph,

where individual hard and collinear subgraphs are connected to each other by exactly one fermion line. In addition to this additional exchange – without power suppression – of an arbitrary number of longitudinally polarised collinear gluons is possible between the hard and collinear subgraphs. Gluon exchange between the hard and soft subgraphs is power suppressed and thus can be neglected, in contrast to the exchange of longitudinally polarised soft gluons between the collinear and soft subgraphs which is leading power. Pictorially this structure can be illustrated as shown in figure 2.2. As
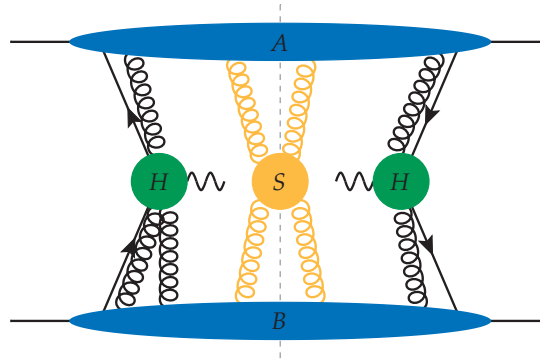
Figure 2.2.: Illustration of the leading subgraphs of the Drell-Yan process with measured transverse momenta of the final states (TMD) as found following the procedure outlined above. The structure corresponds to the list of leading subgraphs above. These subgraphs may – in addition to the quarks and antiquarks connecting the hard (H) and collinear (A and B) subgraphs – be connected by an arbitrary number of longitudinally polarised collinear (black) and soft (yellow) gluons as indicated in the figure.

the name suggests a factorisation theorem makes it possible to factorise, that means separate, perturbative and non-perturbative contributions to a given process while still reproducing the overall cross section up to power suppressed corrections. Intuitively it makes sense to associate the leading subgraphs of a process as the building blocks of such a factorised form of the cross section and indeed the structure of the leading regions for the Drell-Yan process is already rather similar to the one suggested by the parton model picture: The hard subgraphs can be identified as the partonic cross section while the two collinear subgraphs are naturally interpreted as the PDFs. However, this still leaves the unanswered question of how to interpret the soft subgraph and the

arbitrary number of soft and collinear longitudinally polarised gluons which have no equivalent in the parton model. In the following it will be discussed how these gluons which obstruct a direct interpretation of the leading subgraphs in vein of the parton model can be absorbed into the collinear and soft subgraphs, finally resulting in a factorised expression for the cross section.

In order to detach the collinear gluons from the hard scattering subgraphs the fact that their momenta are collinear to the incoming hadrons is used. As a consequence of this, their momentum components exhibit a strong ordering which makes the application of the so called collinear approximation possible. The result of this approximation is that the propagators of these gluons are replaced by so called eikonal propagators as illustrated for the more complicated case of the double parton scattering equivalent of the Drell-Yan process, referred to as the double Drell-Yan process, in section 3.2.1 of reference [26]. Ultimately this makes it possible to absorb the collinear gluons into so called Wilson lines attaching to the quarks and antiquarks entering the hard scattering subgraphs from the collinear subgraphs as illustrated in figure 2.3. These Wilson lines are defined as path ordered exponentials of gluon fields, equation (2.23), and serve an important purpose in the final definition of a parton distribution as they act as gauge links between the fields in the amplitude and the conjugate amplitude, making the PDFs gauge invariant as will be discussed in some more detail in section 2.2.2 when a field theoretic definition of single and double parton distributions will be provided.

Decoupling soft gluons from the collinear subgraphs requires the application of the so called soft or Grammer-Yennie approximation [69] in combination with appropriate Ward identities. As outlined in section 3.2.2 of [26] for the double Drell-Yan process this procedure transforms the soft subgraph with the additional soft gluons into a vacuum expectation value of Wilson line operators as depicted in figure 2.3. A crucial requirement for this step is that contributions from gluons in the so called Glauber momentum region – a subset of the soft momentum region with a momentum scaling dominated by its transverse component – do not give a leading contribution, that means that they cancel in the complete cross section up to power suppressed remainders. This is necessary as in the Glauber region the Grammer-Yennie approximation needed to decouple the soft gluons and transform them into Wilson lines is not valid.

After these steps the cross section is said to be factorised and its structure can be illustrated as in figure 2.3 using the notation introduced in [26] for presenting the properties of Wilson lines. Compared to the parton model picture this factorised expression still contains an explicit soft factor void of a real physical interpretation in terms of the parton model and not accessible in experiments. Therefore it would be desirable to absorb the soft factor into the definitions of parton distributions making it possible to reconcile the full QCD factorisation theorem with intuitive structure of the parton model. As discussed in references [47, 70] this is indeed possible by splitting the soft factor between the two collinear subgraphs in a defined manner which also yields rapidity finite distributions, an issue neglected , but which will briefly be discussed in section 2.2.2.

Figure 2.3.: Factorised cross section for the TMD Drell-Yan process. The collinear and soft approximations – in combination with appropriate Ward identities and a proof that the Glauber momentum region can be neglected – make it possible to absorb the arbitrary number of longitudinally polarised soft and collinear gluons into Wilson lines forming the so called soft factor and acting as gauge links in the PDFs, respectively.

For the SPS Drell-Yan process and its cross-channel equivalents a full proof of the TMD factorisation theorem exists, see for example the detailed discussion in reference [47]. However, the situation is less straight-forward in the presence of coloured final states as this in some cases makes it impossible to factorise the colour structure of a given process, as shown in reference [71]. Fortunately this issue only affects TMD factorisation and does not arise in collinear factorisation where the cross section is integrated over the transverse momenta of the final states.

2.2. General double parton scattering theory

Having laid out the basics of QCD in the prior section where a spotlight has been put on the importance of factorisation theorems for perturbative QCD calculations, paved the way to delve into the specific theory for double parton scattering. As discussed in some detail in the introductory chapter multiple partonic interactions (MPIs) – and in particular double parton scattering (DPS) – may give sizeable contributions to the overall cross section in some cases such that a sound theoretical treatment of DPS is needed. How such a theoretical framework can be established in close analogy to the SPS case will be outlined in the following subsections.

2.2.1. Factorisation for double parton scattering

Naturally, it makes sense to try and extend the well known factorisation theorems introduced before to the case of DPS which in fact has been done already in some of the earliest work on DPS [32]. However, it was only recently that many of the subtleties in the proof of a factorisation theorem which have been glossed over in the early works have been addressed. Following the steps outlined in the review of SPS factorisation – but this time for the double Drell-Yan process (dDY) – one finds basically the same structure as in the SPS case but now with two hard subgraphs on each side of the final state cut as illustrated in figure 2.4. Factorisation of the collinear gluons follows the
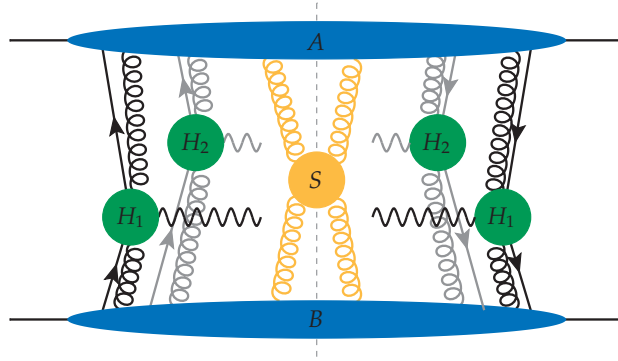
Figure 2.4.: Leading structure of the double Drell-Yan process in analogy obtained using the methods outlined in section 2.1.3. Note that while the general structure remains similar to the SPS case illustrated in figure 2.2 now there are two hard subgraphs on each side of the final state cut.

method outlined before and is in some detail discussed in section 3.2.1 of reference [26]. However, actually proving that the dDY cross section can be written in a factorised form requires some work in the soft gluon sector as it has to be shown that just like in the SPS case the soft gluons can be decoupled using appropriate Ward identities which was shown only very recently in reference [36]. In addition to this it also has to be established that contributions from soft gluons in the Glauber momentum region cancel in the complete cross section for which the arguments from SPS using light-cone perturbation theory (LCPT) have to be extended to the situation of double parton scattering in reference [34]. The result of these steps is that the dDY cross section can again be factorised as depicted in figure 2.5. Even in the case of colour singlet production considered here the colour structure of DPS is quite a bit more complicated than in the SPS case. The reason for this is that for a single parton distribution the parton on the left-hand side and the one on the right-hand side have to be coupled to a colour singlet state, whereas in double parton distributions corresponding partons on the left-hand side and right-hand side are not necessarily coupled to a colour singlet. While it remains true that overall the left-hand side and the right-hand side of the final state cut have to combine to a colour singlet state this is no longer true for the
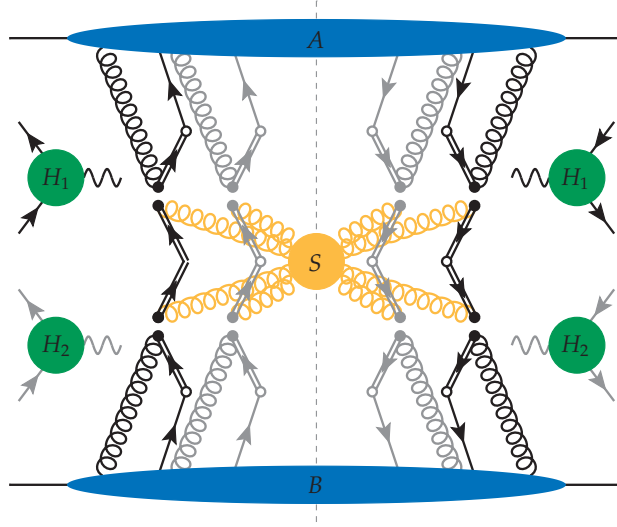
Figure 2.5.: Factorised cross section for the double Drell-Yan process. The structure is again very similar to the SPS case with the main difference being the two hard subgraphs on each side and the fact that instead of collinear subgraphs with one parton leg on each side of the final state cut identified with a PDF one now has collinear subgraphs with two parton legs on each side of the case corresponding to DPDs.

individual partons which can now be in higher colour representations, leading to colour interference distributions as will be discussed in some more detail below.

Even though so far the more general case of transverse momentum dependent factorisation has been considered most of the remainder of this work will be concerned with collinear factorisation and collinear double parton distributions. However, for large values of the interparton distance y, transverse momentum dependent double parton distributions can be matched onto these collinear distributions as discussed in reference [72]. Since the main topic of this thesis are the double parton distributions – in particular collinear (colour singlet) distributions – it is instructive to give the form of the factorisation formula for this case. At leading order, and for colour singlet DPDs, the factorised collinear cross section is given by

$$\frac{\mathrm{d}\sigma_{\mathrm{DPS}}^{AB}}{\mathrm{d}x_1\,\mathrm{d}x_2\,\mathrm{d}\bar{x}_1\,\mathrm{d}\bar{x}_2} = \frac{1}{C} \sum_{a_1 a_2 b_1 b_2} \hat{\sigma}_{a_1 b_1}^{A}(x_1\bar{x}_1 s, \mu_1^2)\, \hat{\sigma}_{a_2 b_2}^{B}(x_2\bar{x}_2 s, \mu_2^2)$$
$$\times \int \mathrm{d}^2 y\; {}^1F_{b_1 b_2}(\bar{x}_1, \bar{x}_2, y; \mu_1, \mu_2)\, {}^1F_{a_1 a_2}(x_1, x_2, y; \mu_1, \mu_2)\,, \qquad (2.15)$$

with collinear colour singlet DPDs ${}^1F_{a_1 a_2}(x_1, x_2, y; \mu_1, \mu_2)$ and parton level cross sections $\hat{\sigma}_{ab}^{A}(x\bar{x}s, \mu^2)$ where y is the relative transverse distance between partons a_1 and a_2. In the above equation C is a combinatorial factor which is equal to 1 of the two observed final states A and B are different, and equal to 2 if they are indistinguishable. At

higher orders the simple product of DPDs and partonic cross sections turns into multiple convolutions in the momentum fractions as can be seen in equation (2.7) of reference [72]. The reason why here colour singlet DPDs have been chosen is simply that for these the soft factor reduces to unity and thus does not have to be absorbed into the definition of the DPDs[3] such that even without this additional step the final structure of the factorised cross section is already evident.

2.2.2. Double parton distributions

As the main topic of this thesis are the double parton distributions appearing first in equation (2.15) some details about these distributions will be given here, starting with definitions for bare DPDs (and PDFs) in position and subsequently momentum space, before discussing how these bare distributions can be renormalised and how the renormalised distributions then depend on the renormalisation scale.

Definition of bare PDFs and DPDs

Bare, that means unrenormalised, collinear position space DPDs (and PDFs) are most conveniently defined in terms of proton matrix elements with position and momentum assignments as shown in figure 2.6:
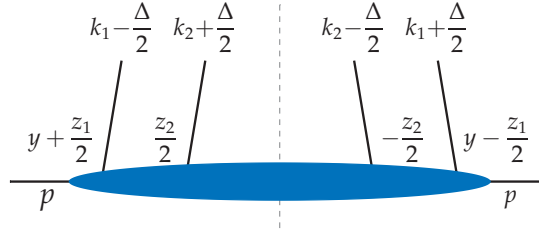
Figure 2.6.: Assignment of position and momentum arguments in DPDs, momenta are written on top of the parton lines whereas positions are written at the bottom. Note the momentum mismatch of Δ between the amplitude and conjugate amplitude, that means to the left and right of the final state cut, indicated by the dashed line. The variables Δ and y are Fourier conjugates just as are the k_i's and z_i's.

$$f_{B,a_1}(x) = (x_1 p^+)^{-n_1} \int \frac{\mathrm{d}z_1^-}{2\pi} \, e^{i x_1 z_1^- p^+} \langle p | \mathcal{O}_{a_1}(0, z_1) | p \rangle \big|_{z_1^+ = 0, z_1 = 0}, \qquad (2.16)$$

$$F_{B,a_1 a_2}^{us,ii'jj'}(x_1, x_2, y) = (x_1 p^+)^{-n_1} (x_2 p^+)^{-n_2} \, 2p^+ \int \mathrm{d}y^- \, \frac{\mathrm{d}z_1^-}{2\pi} \frac{\mathrm{d}z_2^-}{2\pi} \, e^{i(x_1 z_1^- + x_2 z_2^-) p^+}$$

$$\times \langle p | \mathcal{O}_{a_1}^{ii'}(y, z_1) \, \mathcal{O}_{a_2}^{jj'}(0, z_2) | p \rangle \big|_{z_1^+ = z_2^+ = y^+ = 0, z_1 = z_2 = 0}, \qquad (2.17)$$

---

[3]How this is done for the higher colour representations is discussed in reference [72].

where the value of the powers n_i depends on the type of parton a_i and one has $n_i = 1$ for the case that a_i is a gluon while $n_i = 0$ when a_i is a quark or antiquark and $n_i = -1$ if the considered parton is a scalar which will be the case in section 3.3. As is appropriate for reactions with a preferred axis like scattering events at a particle collider so called light-cone coordinates – defined as $v^\pm = (v^0 \pm v^3)/\sqrt{2}$ and $v = (v^1, v^2)$ – have been used here. The superscript us denotes that the DPDs are unsubtracted, implying that the soft factor has not yet been taken into account. When this is not relevant, or in the colour singlet sector where the soft factor is just unity, this superscript will be neglected. In the above definition i, i' and j, j' are the colour indices of the legs in figure 2.6. As mentioned above there is also the possibility that corresponding partons in a DPD on the left- and right-hand side of the final state cut are not coupled to a colour singlet. It is therefore instructive to introduce colour projectors which make it possible to decompose a full DPD into its different colour contributions. Following the discussion in section 2.3 of reference [26] the individual parts are obtained by applying suitable projection operators onto the full DPD, that means

$$^R F_{a_1 a_2} = P_R^{ii'jj'} F_{a_1 a_2}^{ii'jj'} \,. \tag{2.18}$$

In order to distinguish between colour indices in the fundamental and those in the adjoint representation i and j will be used to represent the fundamental representation while for the adjoint representation a and b will be used. For the case when the indices are in the fundamental representation, that means for quark-quark DPDs, the corresponding projectors are

$$P_1^{ii'jj'} = \delta_{ii'}\delta_{jj'} \,,$$
$$P_8^{ii'jj'} = \frac{2N}{\sqrt{N^2 - 1}} t_{ii'}^a t_{jj'}^a \,, \tag{2.19}$$

projecting the pairs ii' and jj' onto colour singlet and octet, respectively. For the case of gluon-gluon distributions where the indices are in the adjoint representation the corresponding projectors read

$$P_1^{aa'bb'} = \delta_{aa'}\delta_{bb'} \,,$$
$$P_A^{aa'bb'} = \frac{\sqrt{N^2 - 1}}{N} f^{aa'c} f^{bb'c} \,,$$
$$P_S^{aa'bb'} = \frac{N\sqrt{N^2 - 1}}{N^2 - 4} d^{aa'c} d^{bb'c} \,,$$
$$P_{10}^{aa'bb'} = \frac{2}{\sqrt{10}} \left(\delta_{ab}\delta_{a'b'} - \delta_{ab'}\delta_{a'b} - \frac{2}{3} f^{aa'c} f^{bb'c} - i \left(d^{abc} f^{a'b'c} + f^{abc} d^{a'b'c} \right) \right) \,,$$
$$P_{27}^{aa'bb'} = \frac{4}{\sqrt{27}} \left(\delta_{ab}\delta_{a'b'} + \delta_{ab'}\delta_{a'b} - \frac{1}{4}\delta_{aa'}\delta_{bb'} - \frac{6}{5} d^{aa'c} d^{bb'c} \right) \,, \tag{2.20}$$

where A and S denote the antisymmetric and symmetric octets, respectively, while 10 and 27 denote the decuplet and 27et, specific to SU(3). Finally one needs in addition to

this projectors for the distributions where both representations are mixed, that means for quark-gluon distributions. In this case the projectors onto colour singlet as well as symmetric and antisymmetric octet are given by

$$
\begin{aligned}
P_1^{ii'bb'} &= \delta_{ii'}\delta_{bb'} \, , \\
P_A^{ii'bb'} &= i\sqrt{2}\, t_{ii'}^c f^{bb'c} \, , \\
P_S^{ii'bb'} &= \sqrt{\frac{2N^2}{N^2-4}} t_{ii'}^c d^{bb'c} \, .
\end{aligned}
\tag{2.21}
$$

The normalisation used here is the one employed in section 2.3 of reference [26] as opposed to the one in section 4 of reference [72]. With this the double parton distributions can be understood as vectors in colour space, while the soft factor which is missing in equation (2.15) is a matrix in colour space, tying the two DPDs together. The reason why the soft factor is absent in the factorisation formula above, equation (2.15), is that for collinear colour singlet distributions the corresponding soft factor simply reduces to unity, which is no longer the case when going to higher colour representations. In order to still obtain a factorisation formula akin to the one presented above for the colour singlet sector it is necessary to absorb the soft factor into the definition of the double parton distributions as illustrated in reference [72]. How exactly this is achieved is not important here as the following discussion is widely independent of this issue as only colour singlet distributions are considered. From now on it will be understood that DPDs have been projected onto a given colour structure using the appropriate projectors such that the colour indices can be neglected. It should also be pointed out that both superscripts present in the definition of the bare DPD are absent in the definition for the collinear PDF as there the two parton legs are always coupled to a colour singlet and the soft factor is just a factor of 1.

In the definitions in equations (2.16) and (2.17) the twist-two operators $\mathcal{O}_a^{ii'}$ are the same for PDFs as they are for DPDs and are for unpolarised partons (which this thesis deals with) given by

$$
\begin{aligned}
\mathcal{O}_q^{ii'}(y,z) &= \frac{1}{2}\bar{q}^{j'}\left(y-\frac{z}{2}\right)\left[W^\dagger\left(y-\frac{z}{2};v\right)\right]_{j'i'}\gamma^+\left[W\left(y+\frac{z}{2};v\right)\right]_{ji}q^j\left(y+\frac{z}{2}\right) , \\
\mathcal{O}_{\bar{q}}^{ii'}(y,z) &= -\frac{1}{2}\bar{q}^{j'}\left(y+\frac{z}{2}\right)\left[W^\dagger\left(y+\frac{z}{2};v\right)\right]_{j'i'}\gamma^+\left[W\left(y-\frac{z}{2};v\right)\right]_{ji}q^j\left(y-\frac{z}{2}\right) , \\
\mathcal{O}_g^{aa'}(y,z) &= G^{+i',b'}\left(y-\frac{z}{2}\right)\left[W^\dagger\left(y-\frac{z}{2};v\right)\right]_{b'a'}\delta^{ii'}\left[W\left(y+\frac{z}{2};v\right)\right]_{ba}G^{+i,b}\left(y+\frac{z}{2}\right) , \\
\mathcal{O}_\phi(y,z) &= \phi\left(y-\frac{z}{2}\right)\phi\left(y+\frac{z}{2}\right) .
\end{aligned}
\tag{2.22}
$$

In the definition of the gluon operator $\mathcal{O}_g^{aa'}$ the superscript indices i and i' are transverse momentum indices and are understood to be summed over in the case of unpolarised distributions considered here. Compared to the most naïve parton model inspired operators containing only quark and gluon field strength operators the definitions of

the twist-two operators above contain so called Wilson lines which are path ordered exponentials of gluon fields A, defined as

$$W(\xi; v) = \mathrm{P} \exp\left[ig \int_0^\infty \mathrm{d}\lambda \, v A^a(\xi - \lambda v)\, t^a \right],$$ (2.23)

where P implies path ordering and v is the direction while ξ is the position at which the Wilson line originates. Without these Wilson lines the twist-two operators and thus also the resulting single and double parton distributions would not be gauge invariant quantities. However, the Wilson lines are not introduced by hand in order to obtain gauge invariant distributions, but rather arise naturally from the factorisation of collinear gluons outlined in section 2.1.3.

In the following chapters mostly momentum space DPDs will be considered which are – at least in the case of unrenormalised distributions – obtained from a $D - 2 = 2 - 2\varepsilon$-dimensional Fourier transformation of the position space distributions, that means

$$F_{B, a_1 a_2}(x_1, x_2, \boldsymbol{\Delta}) = \int \mathrm{d}^{D-2}\boldsymbol{y}\, e^{i\boldsymbol{y}\boldsymbol{\Delta}} F_{B, a_1 a_2}(x_1, x_2, \boldsymbol{y}).$$ (2.24)

In the next subsection where renormalisation of the bare distributions is treated it will become clear why such a simple relation no longer holds for renormalised distributions. The arguments in chapters 3 and 5 rely on the property that bare DPDs as well as bare PDFs can be expressed in terms of bare momentum space Green's functions which in turn can be calculated from Feynman diagrams. To this end one defines the bare momentum space Green's functions as

$$\mathcal{G}_{B, a_1}(k_1) = \int \mathrm{d}^D z_1\, e^{ik_1 z_1} \langle p | \mathcal{O}_{a_1}(z_1) | p \rangle,$$

$$\mathcal{G}_{B, a_1 a_2}^{ii'jj'}(k_1, k_2, \Delta) = \int \mathrm{d}^D z_1\, \mathrm{d}^D z_2\, \mathrm{d}^D y\, e^{i(k_1 z_1 + k_2 z_2 - y\Delta)} \langle p | \mathcal{O}_{a_1}^{ii'}(y, z_1) \mathcal{O}_{a_2}^{jj'}(0, z_2) | p \rangle,$$ (2.25)

From these the bare PDFs and DPDs are then obtained in the following way:

$$f_{B, a_1}(x_1) = (x_1 p^+)^{-n_1} \int \frac{\mathrm{d}k_1^- \, \mathrm{d}^{D-2}\boldsymbol{k}_1}{(2\pi)^D}\, \mathcal{G}_{B, a_1}(k_1),$$ (2.26)

$$F_{B, a_1 a_2}(x_1, x_2, \boldsymbol{\Delta}) = \left[\prod_{i=1}^{2} (x_i p^+)^{-n_i} \int \frac{\mathrm{d}k_i^- \, \mathrm{d}^{D-2}\boldsymbol{k}_i}{(2\pi)^D} \right] 2p^+ \int \frac{\mathrm{d}\Delta^-}{2\pi}\, \mathcal{G}_{B, a_1 a_2}(k_1, k_2, \Delta).$$ (2.27)

Renormalisation and evolution of DPDs

As mentioned already in the previous section the PDFs and DPDs defined so far are UV divergent due to short distance singularities of the twist-two operators. It is thus

necessary to renormalise these divergences in order to obtain UV-finite distributions. Renormalised distributions are obtained from the bare ones as convolutions with appropriate renormalisation factors. To this end it makes sense to introduce shorthand notations for convolutions [73] and discuss some of their properties as some arguments in the upcoming chapters require the use of multiple convolutions which would otherwise introduce quite a clutter of notation.

Convolution integrals. As DPDs are naturally functions of two momentum fraction arguments whereas PDFs, DGLAP splitting kernels, and renormalisation factors are typically functions of a single momentum fraction argument this gives rise to different types of convolutions. Therefore a shorthand notation is introduced which makes it possible to give these different convolutions without having to give explicit momentum fraction arguments. To this end let A, B, and C be functions of a single momentum fraction whereas D depends on two momentum fraction arguments. For the standard convolution of two single argument functions A and B the usual Mellin convolution is used, that means

$$A \otimes B = \int_x^1 \frac{dz}{z} \, A\left(\frac{x}{z}\right) B(z) \, . \tag{2.28}$$

Similarly one can then define the following notation for the convolution of a function A with a function D with respect to the first momentum fraction argument[4]

$$A \underset{1}{\otimes} D = \int_{x_1}^{1-x_2} \frac{dz}{z} \, A\left(\frac{x_1}{z}\right) D(z, x_2) \, . \tag{2.29}$$

Here the integration boundaries are determined by the support properties of the involved functions as for the case that the function A is a PDF (or a single momentum fraction argument splitting kernel or renormalisation factor) one has $A(x) = 0$ for $x < 0$ and $x > 1$. If the two momentum fraction function D is a DPD (or a $1 \rightarrow 2$ splitting kernel or renormalisation factor) then $D(x_1, x_2) = 0$ for $x_1 < 0$, $x_2 < 0$ and $x_1 + x_2 > 1$. The convolution with respect to the second momentum fraction is then defined analogously and denoted by a 2 set under the convolution sign. For subsequent convolutions with respect to the first and second momentum fraction one thus obtains

$$A \underset{1}{\otimes} B \underset{2}{\otimes} D = A \underset{1}{\otimes} \left[B \underset{2}{\otimes} D \right] \, . \tag{2.30}$$

The treatment of the perturbative splitting of one parton inside a hadron into two which gives a contribution to DPDs requires a different type of convolution of a two

---

[4]In inline equations this type of convolution is typeset as $\otimes_1$ rather than $\underset{1}{\otimes}$.

momentum fraction function D with a single momentum fraction function A, namely

$$D \underset{12}{\otimes} A = \int\limits_{x_1+x_2}^{1} \frac{\mathrm{d}z}{z^2} \, D\left(\frac{x_1}{z}, \frac{x_2}{z}\right) A(z) \,. \tag{2.31}$$

For combinations of these different types of convolutions one can easily show the following relations by interchanging the order of integrations

$$[A \underset{1}{\otimes} D] \underset{12}{\otimes} B = A \underset{1}{\otimes} [D \underset{12}{\otimes} B] \,, \qquad [A \underset{1}{\otimes} B \underset{2}{\otimes} D] \underset{12}{\otimes} C = A \underset{1}{\otimes} B \underset{2}{\otimes} [D \underset{12}{\otimes} C] \,, \tag{2.32}$$

so that these convolutions can be written without brackets. In the same manner the following relation for subsequent convolutions of the type introduced in equation (2.31) can be obtained

$$[D \underset{12}{\otimes} A] \underset{12}{\otimes} B = D \underset{12}{\otimes} [A \otimes B] = D \underset{12}{\otimes} A \otimes B \,. \tag{2.33}$$

In section 5.6.6 an alternative version of equation (2.31) will be used, namely

$$D \underset{12}{\otimes} A = \frac{1}{x_1 + x_2} \int\limits_{x_1+x_2}^{1} \mathrm{d}z \, D\left(z\frac{x_1}{x_1 + x_2}, z\frac{x_2}{x_1 + x_2}\right) A\left(\frac{x_1 + x_2}{z}\right) \,. \tag{2.34}$$

Inverse convolution (one variable). For some arguments in chapter 3 the notion of an inverse PDF renormalisation factor Z^{-1} is introduced. For any single momentum fraction function A such an inverse can be defined as the solution of the equation

$$A \otimes A^{-1} = \delta(1 - x) \,. \tag{2.35}$$

Such an inverse is exclusively defined for functions which permit an expansion in the strong coupling a_s as then the equation can be solved order by order in a_s. In particular, if at leading order (LO) one has

$$A(x) = 1 + a_s A^{(1)}(x) + \mathcal{O}(a_s^2) \,, \tag{2.36}$$

then its inverse is at the same order given by

$$A^{-1}(x) = 1 - a_s A^{(1)}(x) + \mathcal{O}(a_s^2) \,. \tag{2.37}$$

Integration over momentum fractions. In order to have a concise way of writing integrals over momentum fraction arguments one can introduce the following shorthand notation for functions of one or two momentum fractions, respectively

$$\int A = \int \mathrm{d}x \, A(x) \,, \qquad\qquad \int\limits_{i} D = \int \mathrm{d}x_i \, D(x_1, x_2) \,, \tag{2.38}$$

with $i = 1, 2$. Further introducing operators X^n and X_i^n that act on a function by multiplying with a power of the appropriate momentum fraction,

$$(X^n A)(x) = x^n A(x), \qquad\qquad (X_i^n D)(x_1, x_2) = x_i^n D(x_1, x_2), \qquad (2.39)$$

makes it possible to use $X^n A$ and $X_2^n D$ in convolution integrals without explicitly giving their momentum arguments. For functions of one argument, one has the well-known rules

$$X^n(A \otimes B) = (X^n A) \otimes (X^n B), \qquad \int X^n (A \otimes B) = \int X^n A \int X^n B, \qquad (2.40)$$

and it is easy to show that for functions of two momentum fractions the following holds

$$\int_2 X_2 (A \underset{2}{\otimes} D) = \int X A \int_2 X_2 D. \qquad (2.41)$$

One can furthermore derive the following identity which will be used in chapter 3

$$\int_2 X_2^n (D \underset{12}{\otimes} A) = \int dx_2 \, x_2^n \int \frac{dz}{z^2} D\left(\frac{x_1}{z}, \frac{x_2}{z}\right) A(z)$$

$$= \int \frac{du_1}{u_1} \int du_2 \, u_2^n \, D(u_1, u_2) \left(\frac{x_1}{u_1}\right)^n A\left(\frac{x_1}{u_1}\right)$$

$$= \left(\int_2 X_2^n D \right) \underset{1}{\otimes} (X^n A), \qquad (2.42)$$

where the subscript on the convolution symbol in the last line indicates that the result depends on the momentum fraction x_1.

Parton indices. In some cases it is instructive to include information about the involved parton types in order to make the structure of an expression clearer for which therefore a compact notation is introduced. For single momentum fraction argument functions $A_{ab}(x), B_{ab}(x)$ and $f_a(x)$ the parton structure is indicated as shown in the following equations

$$[A \otimes B]_{ac} = \sum_b A_{ab} \otimes B_{bc}, \qquad\qquad [A \otimes f]_a = \sum_b A_{ab} \otimes f_b. \qquad (2.43)$$

Here it should be emphasised that summation over repeated parton indices is not implied and that whenever a sum over a parton index is appropriate it is given explicitly. Similar definitions can be given for functions $D_{a_1 a_2, a_0}(x_1, x_2)$ and $F_{a_1 a_2}(x_1, x_2)$

depending on two momentum fraction arguments, namely

$$
\begin{aligned}
[A \underset{1}{\otimes} D]_{a_1 a_2, a_0} &= \sum_b A_{a_1 b} \underset{1}{\otimes} D_{b a_2, a_0}\,, &
[A \underset{1}{\otimes} F]_{a_1 a_2} &= \sum_b A_{a_1 b} \underset{1}{\otimes} F_{b a_2}\,, \\
[A \underset{2}{\otimes} D]_{a_1 a_2, a_0} &= \sum_b A_{a_2 b} \underset{1}{\otimes} D_{a_1 b, a_0}\,, &
[A \underset{2}{\otimes} F]_{a_1 a_2} &= \sum_b A_{a_2 b} \underset{1}{\otimes} F_{a_1 b}\,, \\
[D \underset{12}{\otimes} A]_{a_1 a_2, a_0} &= \sum_b D_{a_1 a_2, b} \underset{12}{\otimes} A_{b a_0}\,, &
[D \underset{12}{\otimes} f]_{a_1 a_2} &= \sum_b D_{a_1 a_2, b} \underset{12}{\otimes} f_b\,.
\end{aligned} \tag{2.44}
$$

Consequently one can also give the parton structure of a combination of convolutions with respect to the first and the second momentum fraction argument in the following way

$$
\begin{aligned}
[A \underset{1}{\otimes} B \underset{2}{\otimes} F]_{a_1 a_2} &= \sum_{b_1, b_2} A_{a_1 b_1} \underset{1}{\otimes} B_{a_2 b_2} \underset{2}{\otimes} F_{b_1 b_2}\,, \\
[A \underset{1}{\otimes} B \underset{2}{\otimes} D]_{a_1 a_2, a_0} &= \sum_{b_1, b_2} A_{a_1 b_1} \underset{1}{\otimes} B_{a_2 b_2} \underset{2}{\otimes} D_{b_1 b_2, a_0}\,.
\end{aligned} \tag{2.45}
$$

Renormalisation and evolution of position space DPDs. With the above definitions for a compact notation of convolutions it is straightforward to give renormalised position space DPDs in terms of the bare distributions in equation (2.17). To this end recall that the UV divergences in the twist-two operators defined in equation (2.22) are renormalised by a convolution with a renormalisation factor $Z(x; \mu, \varepsilon)$, such that for a single PDF one obtains

$$
f_{a_1}(\mu) = [Z(\mu) \otimes f_B]_{a_1}\,, \tag{2.46}
$$

where momentum fraction arguments have been omitted in accordance with the rules introduced before. It should be noted, however, that the dependence on the renormalisation scale μ is given explicitly, as this will make the discussion of the renormalisation scale evolution clearer. In analogy to equation (2.46) a bare position space DPD $F_B(\boldsymbol{y})$ is then renormalised by two of the $Z(\mu)$ factors already known from the PDF case, one for each parton:

$$
F_{a_1 a_2}(\boldsymbol{y}; \mu_1, \mu_2) = [Z(\mu_1) \underset{1}{\otimes} Z(\mu_2) \underset{2}{\otimes} F_B(\boldsymbol{y})]_{a_1 a_2}\,. \tag{2.47}
$$

Here it has been made explicit that the renormalisation scales for the two operators in the definition of the position space DPD may differ from each other as is appropriate when the scales of the two hard processes are different. In order to obtain the renormalisation scale dependence of these renormalised position space DPDs consider again first the familiar case of the single PDFs where the renormalisation scale dependence is governed by the DGLAP equations [74–76].

$$
\frac{\mathrm{d} f_{a_1}(\mu)}{\mathrm{d} \ln \mu^2} = [P(\mu) \otimes f(\mu)]_{a_1}\,, \tag{2.48}
$$

where the DGLAP splitting kernels are defined by the scale dependence of the renormalisation factors Z as

$$\frac{\mathrm{d}Z_{a_1 a_0}(\mu)}{\mathrm{d}\ln\mu^2} = [P(\mu) \otimes Z(\mu)]_{a_1 a_0}. \tag{2.49}$$

With this it is then straightforward to also obtain the renormalisation scale dependence of the renormalised DPD $F_{a_1 a_2}(\boldsymbol{y};\mu_1,\mu_2)$

$$\frac{\mathrm{d}F_{a_1 a_2}(\boldsymbol{y};\mu_1,\mu_2)}{\mathrm{d}\ln\mu_i^2} = [P(\mu_i) \underset{i}{\otimes} F(\boldsymbol{y};\mu_1,\mu_2)]_{a_1 a_2}. \tag{2.50}$$

In the upcoming chapters mostly DPDs at equal renormalisation scales $\mu_1 = \mu_2 = \mu$, denoted by $F_{a_1 a_2}(\boldsymbol{y};\mu)$ will be considered. For these equal scale DPDs the renormalisation scale dependence is thus given by

$$\frac{\mathrm{d}F_{a_1 a_2}(\boldsymbol{y};\mu)}{\mathrm{d}\ln\mu^2} = [P(\mu) \underset{1}{\otimes} P(\mu) \underset{2}{\otimes} F(\boldsymbol{y};\mu)]_{a_1 a_2}. \tag{2.51}$$

Renormalisation and evolution of momentum space DPDs. Given the discussion in the previous paragraph one might be tempted to think that a bare momentum space DPD $F_B(\boldsymbol{\Delta})$ should be renormalised in exactly the same manner. However, this is not entirely true as will be explained now. It has already been pointed out below equation (2.24) – relating bare position and momentum space DPDs via a Fourier transformation – that such a simple relation no longer holds for renormalised distributions. The reason for this is that DPDs contain a contribution from the perturbative splitting of a parton inside the hadron into two partons [25, 26, 28, 35, 37–44, 77]. This splitting contribution is naturally associated with relatively small transverse separation $|\boldsymbol{y}| = y$ of the two partons such that it can be calculated in perturbation theory [26, 35]. In the limit of small $y = |\boldsymbol{y}|$ this even becomes the dominant contribution and the position space DPD can thus be written in a factorized form [72]

$$F_{B,a_1 a_2}(\boldsymbol{y}) = \frac{\Gamma(1-\varepsilon)}{(\pi \boldsymbol{y}^2)^{1-\varepsilon}} [V_B(\boldsymbol{y}) \underset{12}{\otimes} f_B]_{a_1 a_2}, \tag{2.52}$$

with a $1 \to 2$ splitting kernel $V_{B;a_1 a_2,a_0}(x_1,x_2,\boldsymbol{y})$. The structure of this expression elucidates why a simple relation like equation (2.24) no longer holds for the renormalised distributions: DPDs exhibit what is referred to as a $1 \to 2$ splitting singularity for small y or large $\Delta = |\boldsymbol{\Delta}|$ in position and momentum space, respectively. Fourier transforming the bare position space DPD thus leads to an additional singularity in the bare momentum space DPD of equation (2.24) as the $(\boldsymbol{y}^2)^{-1+\varepsilon}$ behaviour of the position space DPD for small y gives a simple pole[5] $1/\varepsilon$. This additional singularity in the bare

---

[5]Notice the difference between this and the UV divergences in the twist-two operators, which lead to higher powers of $1/\varepsilon$ with increasing powers of α_s.

momentum space DPD is renormalised additively with a $1 \rightarrow 2$ renormalisation factor[6] $Z_{a_1 a_2, a_0}(x_1, x_2; \mu, \varepsilon)$, such that the complete renormalised momentum space DPD is given by

$$F_{a_1 a_2}(\boldsymbol{\Delta}; \mu) = [Z(\mu) \underset{1}{\otimes} Z(\mu) \underset{2}{\otimes} F_B(\boldsymbol{\Delta}) + Z_s(\mu) \otimes f_B]_{a_1 a_2}, \tag{2.53}$$

where now the DPDs have been defined at equal scales for both partons from the beginning due to the presence of the additional inhomogeneous term. Introducing single and double Mellin moments by the integrals

$$A(m) = \int \mathrm{d}x \, x^{m-1} A(x), \quad D(m_1, m_2) = \int \mathrm{d}x_1 \, x_1^{m_1-1} \int \mathrm{d}x_2 \, x_2^{m_2-1} D(x_1, x_2), \tag{2.54}$$

one can easily show that (2.53) turns into

$$F^{i_1 i_2}(m_1, m_2, \Delta; \mu) = \sum_{j_1, j_2} Z_{i_1, j_1}(m_1; \mu) Z_{i_2, j_2}(m_2; \mu) F_B^{i_1 i_2}(m_1, m_2, \Delta)$$

$$+ \sum_j Z_{i_1 i_2, j}(m_1, m_2; \mu) f_B^j(m_1 + m_2 - 1), \tag{2.55}$$

in agreement with the leading-order analyses in [78, 79]. As a consequence of this different UV renormalisation the double DGLAP equation for momentum space DPDs also has an inhomogeneous term

$$\frac{\mathrm{d}F_{a_1 a_2}(\boldsymbol{\Delta}; \mu)}{\mathrm{d}\ln \mu^2} = [P(\mu) \underset{1}{\otimes} F(\boldsymbol{\Delta}; \mu) + P(\mu) \underset{2}{\otimes} F(\boldsymbol{\Delta}; \mu) + P_s \underset{12}{\otimes} f(\mu)]_{a_1 a_2}, \tag{2.56}$$

where the $1 \rightarrow 2$ evolution kernel[6] $P_{a_1 a_2, a_0}(x_1, x_2; \mu)$ is given in equation (3.82). With the definitions (2.54) for single and double Mellin moments, one finds the following inhomogeneous evolution equation in Mellin space

$$\frac{\mathrm{d}F^{i_1 i_2}(m_1, m_2; \Delta)}{\mathrm{d}\ln \mu^2} = \sum_{j_1} P_{i_1, j_1}(m_1) F^{j_1 i_2}(m_1, m_2; \Delta) + \sum_{j_2} P_{i_2, j_2}(m_2) F^{i_1 j_2}(m_1, m_2; \Delta)$$

$$+ \sum_j P_{i_1 i_2, j}(m_1, m_2) f^j(m_1 + m_2 - 1), \tag{2.57}$$

in agreement with the LO formulae derived in [78, 79]. More details about the renormalisation and evolution of momentum space DPDs – in particular a derivation of equation (2.56) – will be given in section 3.6.

---

[6]Note that when the parton indices are not given explicitly in convolutions this renormalisation factor is referred to as Z_s to avoid confusion with the regular renormalisation factor Z. The same applies to $P_{a_1 a_2, a_0}$ which is referred to as P_s in order to avoid confusion with P.

2.2.3. A consistent framework for double parton scattering

Unfortunately the factorisation formula given in equation (2.15) is plagued by some issues as will become clear in the remainder of this section. A solution for these problems was proposed in reference [35] by Diehl, Gaunt, and Schönwald (DGS), and will be discussed in some detail in this section. Plugging the small y expression[7] given in equation (2.52) into the expression for the factorised DPS cross section shown in equation (2.15) one directly sees that the integrand exhibits a y^{-4} behaviour which would imply that the DPS cross section diverges, which is certainly not the case. The solution for this issue suggested in reference [35] is to insert a cut-off function $\Phi(u)$ which approaches 1 for $u \gg 1$ and vanishes in the limit $u \to 0$ for each DPD in equation (2.15) which then becomes

$$\frac{\mathrm{d}\sigma_{\mathrm{DPS}}^{AB}}{\mathrm{d}x_1\,\mathrm{d}x_2\,\mathrm{d}\bar{x}_1\,\mathrm{d}\bar{x}_2} = \frac{1}{C} \sum_{a_1 a_2 b_1 b_2} \hat{\sigma}_{a_1 b_1}^A\left(x_1 \bar{x}_1 s, \mu_1^2\right) \hat{\sigma}_{a_2 b_2}^B\left(x_2 \bar{x}_2 s, \mu_2^2\right)$$
$$\times \int \mathrm{d}^2 \boldsymbol{y}\, \Phi^2(y\nu)\, F_{b_1 b_2}\left(\bar{x}_1, \bar{x}_2, \boldsymbol{y}; \mu_1, \mu_2\right) F_{a_1 a_2}\left(x_1, x_2, \boldsymbol{y}; \mu_1, \mu_2\right), \quad (2.58)$$

where the superscripts for the colour channel have been neglected as this structure is assumed to apply for all colour representations (after the soft factor has been absorbed into the DPDs). The exact requirements the cut-off function Φ has to fulfil are discussed in detail in reference [35] and for the remaining discussion a sharp cut-off will be used, namely

$$\Phi(u) = \Theta(u - b_0), \qquad\qquad b_0 = 2e^{-\gamma_{\mathrm{E}}}, \qquad\qquad (2.59)$$

where γ_{E} is the Euler-Mascheroni constant[8]. Restricting the discussion to this choice can be done without a loss of generality as will be shown in chapter 5.

Another issue closely related to the perturbative splitting of one parton into two inside a hadron is the double counting between single and double parton scattering. Consider to this end the two diagrams in figure 2.7. As illustrated by the red boxes in this figure it is possible to associate the diagram in figure 2.7a with SPS as well as with DPS, however, in different kinematic regions. Therefore it is necessary to perform appropriate subtractions when adding σ_{SPS} and σ_{DPS} to obtain the full cross section, that means

$$\sigma = \sigma_{\mathrm{SPS}} - \sigma_{\mathrm{1v1,pt}} + \sigma_{\mathrm{tw4}} - \sigma_{\mathrm{2v1,pt}} + \sigma_{\mathrm{2v1,pt}}, \qquad\qquad (2.60)$$

where $\sigma_{\mathrm{DPS}} = \sigma_{\mathrm{1v1}} + \sigma_{\mathrm{2v1}} + \sigma_{\mathrm{2v2}}$. The twist-four and 2v1 contributions have not been discussed yet as they can be thought of as a mixture of the 1v1 and 2v2 contributions in the sense that in these only the partons in one hadron originate from a $1 \to 2$

---

[7]Even though the expression is for a bare position space DPD this does not alter the argument as the splitting singularity is not affected by renormalisation.

[8]Choosing b_0 in this way makes it possible to simplify certain analytical results in the original paper [35].

(a) (b)
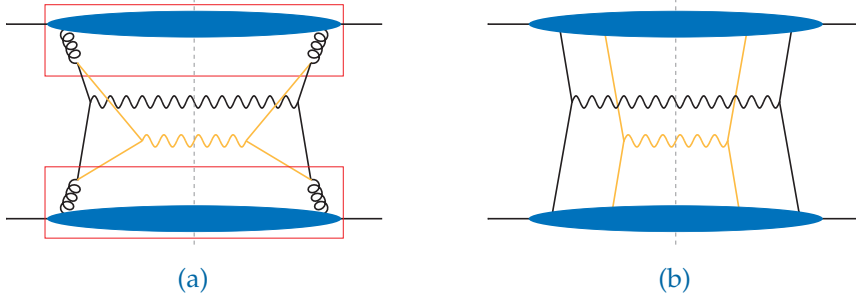
Figure 2.7.: Illustration of different possibilities to produce two final states *A* and *B* that, depending on the kinematics, can be interpreted as SPS or DPS. The fact that the perturbative splitting in these graphs can be interpreted as both, a loop correction to SPS as well as a contribution to DPS, is indicated by boxes representing a perturbative splitting DPD. Subfigure 2.7a represents a loop correction to SPS as well as what is referred to as the 1v1 contribution in [35] to DPS, while in in subfigure 2.7b the genuine – 2v2 – DPS contribution is shown.

splitting. The exact form of the subtraction terms $\sigma_{1v1,pt}$ and $\sigma_{2v1,pt}$ has been derived in reference [35] and is basically obtained from the full 1v1 and 2v1 cross sections by replacing the DPDs which get a contribution from the splitting by their perturbative small y expression. A detailed study of perturbative splitting in DPDs has also been performed in reference [37].

The framework developed in reference [35] forms the basis of most of the work in this thesis and in particular is the reason why an emphasis has been put on the investigation of position space rather than momentum space DPDs. With this framework at hand it is possible to calculate DPS cross sections in a controlled manner with the issue of double counting between SPS and DPS resolved in an elegant way. Regulating the DPS cross section in equation (2.58) using a cut-off rather than a different regulator like for example $\overline{\text{MS}}$ has the advantage that it retains the notion of individual DPDs with a field-theoretic definition for each hadron. This is a definite advantage over a treatment with $\overline{\text{MS}}$ where only the product of two DPDs would be defined, as this makes it possible to study the DPDs using non-perturbative methods like lattice QCD. For progress in this direction see for example reference [80].

3. DPD sum rules in QCD

3.1. Introduction

With the preliminaries laid out in the previous chapter, in particular the DPS framework of reference [35] introduced in section 2.2.3, one might be tempted to think that all necessary ingredients to calculate DPS cross sections are available. However, this is not quite the case as the position space DPDs needed in the factorisation formula given in equation (2.58) are more or less unknown at this point. Due to their genuinely non-perturbative nature DPDs, just like their SPS counterparts, cannot be calculated in perturbation theory and have to be extracted from experimental data or from non-perturbative methods like lattice QCD. While the experimental determination of PDFs has made a lot of progress in recent years such that the accuracy to which PDFs are known continues to improve, the situation is quite different for DPDs as will be discussed now. The by far most important limiting factor is that on one hand compared to SPS cross sections DPS cross sections are quite small, while on the other hand a lot more data is needed to extract a complete set of DPDs with the same precision as a PDF set. To this end consider that for $n_f = 6$ there are 91 distinct collinear DPDs[1], each depending on two momentum fraction arguments x_1 and x_2, the transverse distance y between the two partons, and one (or two) renormalisation scale(s), whereas in the SPS case one has 7 PDFs depending on one momentum fraction x and one renormalisation scale. This illustrates the problem quite nicely: on the one hand gathering experimental data for DPS is hard as the cross sections are small while on the other hand a experimental determination of DPDs requires way more data than that of PDFs to achieve the same precision. A possible alternative to a purely experimental determination of DPDs would be to resort to lattice QCD to calculate the matrix elements in the definitions of DPDs in equation (2.17). While first steps in this direction have already been taken in reference [80] and great advances have also been made for the extraction of PDFs from lattice data as summarised in reference [81], a full extraction of DPDs from lattice data will still take some time (if it is possible at all).

In order to estimate the impact of DPS contributions to the overall cross section it is nevertheless necessary to get at least a rough idea about the shape and size of DPDs. To this end it is useful to construct DPD models based on physical intuition. The most

---

[1]This number can be obtained by considering that for $n_f = 6$ one has 12 distinct quark types and the gluon. Therefore one finds one gg DPD, 12 gq DPDs, 12 qq DPDs, and finally $(12 \cdot 11)/2 = 66$ qq' DPDs with $q \neq q'$.

naïve of these approximates DPDs by a product of impact parameter PDFs, completely neglecting any correlations of the partons inside the hadron, which gives – when one furthermore assumes that the impact parameter PDFs can be factorised into regular PDFs and a Gaussian profile – rise to the well-known DPS pocket formula which factorises the DPS cross section into a product of two SPS cross sections divided by a so called effective cross section. A more sophisticated DPD model – the GS09 DPD set – has been constructed by Gaunt and Stirling in reference [45] using the DPD number and momentum sum rules they introduced. These sum rules are one of the only theoretical constraints known that DPDs have to fulfil (apart from less restrictive ones like positivity). However the GS09 DPD set contains collinear momentum space DPDs at $\Delta = 0$ from which it is not possible to obtain the collinear position space DPDs required for the framework of reference [35] introduced in section 2.2.3. Therefore one project of this dissertation aimed at constructing sum rule improved position space DPDs which can be used in the DGS framework. However, before addressing this issue in chapter 4 in the current chapter a proof for the validity of the DPD sum rules in QCD will be presented. In their original work Gaunt and Stirling [45] pointed out that the sum rules are preserved under LO evolution if they are fulfilled at a starting scale. That the sum rules are indeed fulfilled was shown in appendix C of [46] using the light-cone wave function framework which, however, neglects how the UV singularities associated with the twist-two operators in the definitions of the DPDs in equation (2.17) have to be renormalised.

The aim of this chapter is to fill this gap and prove explicitly that the DPD sum rules are indeed fulfilled at any scale in QCD. To this end a brief review of the sum rules will be given in section 3.2.1 before introducing the framework of light-cone perturbation theory (LCPT) in section 3.2.2. The necessity for using LCPT will be illustrated in section 3.3 by considering how the sum rules arise at the first non-trivial order in covariant perturbation theory in a simple toy model. After this an all-order proof for bare DPDs will be given in section 3.4 with the help of LCPT. In order to complete the proof that the sum rules are valid to all orders in QCD it will be shown in section 3.5 that the sum rules are valid for renormalised DPDs if UV divergences are subtracted in a suitable scheme. In section 3.6 the behaviour of the sum rules under evolution is discussed, in particular the all-order form of the inhomogeneous dDGLAP equation (2.56) is derived, as well as sum rules for the $1 \to 2$ evolution kernels appearing in the inhomogeneous part of the evolution equation. The results presented in this chapter have been published in the European Physics Journal C [73].

3.2. Specific Theory

Before moving on to proving that the sum rules are actually fulfilled to all orders in the strong coupling it makes sense to discuss some of the properties of the sum rules and their interpretation and introduce the framework of light-cone perturbation theory.

3.2.1. The DPD sum rules

In close analogy to the well-known PDF sum rules similar sum rules can also be introduced for unpolarised collinear colour singlet momentum space DPDs at $\mathbf{\Delta} = 0$, abbreviated as

$$F_{a_1 a_2}(x_1, x_2; \mu) = F_{a_1 a_2}(x_1, x_2, \mathbf{\Delta} = \mathbf{0}; \mu) , \tag{3.1}$$

which are – up to the additional renormalisation of the splitting singularity – obtained from the position space DPDs $F_{a_1 a_2}(x_1, x_2; \mu)$ by integrating over $\mathbf{y}$. Just as for PDFs one again finds for DPDs momentum and number sum rules. The former of these reads

$$\sum_{a_2} \int_0^{1-x_1} \mathrm{d}x_2 \, x_2 \, F_{a_1 a_2}(x_1, x_2; \mu) = (1 - x_1) f_{a_1}(x_1; \mu) , \tag{3.2}$$

corresponding to the conservation of the overall hadron momentum under evolution. The conservation of quark flavour on the other hand is described by the DPD number sum rule, given by

$$\int_0^{1-x_1} \mathrm{d}x_2 \, F_{a_1 a_{2,v}}(x_1, x_2; \mu) = \left(N_{a_{2,v}} + \delta_{a_1, \overline{a_2}} - \delta_{a_1, a_2} \right) f_{a_1}(x_1; \mu) , \tag{3.3}$$

where a_2 denotes either a quark or an antiquark and the subscript v on the second parton index of the DPD indicates a valence distribution, meaning the difference of parton and antiparton distributions

$$F_{a_1 a_{2,v}} = F_{a_1 a_2} - F_{a_1 \overline{a_2}} . \tag{3.4}$$

The number of a_v valence partons inside the considered hadron is denoted by N_{a_v}, for example in the case of the proton one would have $N_{u_v} = 2$.

Both of the DPD sum rules permit a probabilistic interpretation in terms of the parton model. For the momentum sum rule one can easily interpret equation (3.2) in the following way: momentum conservation of the overall hadron momentum implies that the sum over all possible partons a_2 of the x_2 integral of a DPD $F_{a_1 a_2}(x_1, x_2; \mu)$ weighted with the momentum fraction x_2 should equal the a_1 PDF $f_{a_1}(x_1; \mu)$ times a factor of 1 minus the momentum fraction of parton a_1, x_1. This will become a bit clearer in section 3.4.4. In a similar manner one can interpret the structure of the DPD number sum rule. For the case that a_1 and a_2 are different (meaning not of the same flavour) it seems to be a natural generalisation of the PDF number sum rule that the x_2 integral over the $F_{a_1 a_{2,v}}$ distribution should equal the number of a_2 valence partons times the f_{a_1} PDF. The additional Kronecker deltas in the prefactor of the PDF in equation (3.3) can be understood following the discussion in section 3.4.3.

3.2.2. Light-cone perturbation theory

As mentioned before the all-order proof of the sum rules for bare DPDs will rely on the framework of light-cone perturbation theory (LCPT, also called light-front perturbation theory) which is quite similar to old-fashioned time ordered perturbation theory, with the difference that the vertices of a graph are ordered in "light-cone time" $x^+ = (x^0 + x^3)/\sqrt{2}$ rather than "ordinary time" x^0. In order to derive the rules of LCPT from regular covariant perturbation theory one has to perform the integrations over all internal minus momenta, thus setting all internal lines on-shell. How exactly this works is for instance shown in chapter 7.2.3 of reference [47], whose normalisation conventions is adopted in the following. For a more in depth discussion of LCPT the reader is referred to the literature, for example references [82–89].

For brevity only the basic rules of LCPT will be given here and details and subtleties are discussed when they are encountered. As in the rest of this chapter, light-cone gauge $n \cdot A = A^+ = 0$ (where n is the light-like vector projecting on plus components[2]) for the gluon will be used since this has the advantage that one does not have to take Wilson lines into account.

1. Starting from a given Feynman graph, each vertex is assigned a light-cone time x_j^+ and all possible orderings of the x_j^+ are considered, giving rise to a number of LCPT graphs. For LCPT graphs the convention is that x^+ increases from left to right on the left-hand side of the final state cut, while on the right-hand side it increases from right to left.

2. Coupling constants and vertex factors are identical to the ones known from covariant perturbation theory with momentum dependent vertices being an exception which will be discussed below.

3. Plus and transverse momentum components, k_l^+ and $\boldsymbol{k}_l$, of a line l are conserved at the vertices.

4. A factor of $1/(2k_l^+)$ has to be included for each propagating line l in a graph, together with a Heaviside step function $\Theta(k_l^+)$ if the routing of k_l is such that it runs from smaller to larger values of x^+.

5. Each loop momentum ℓ has to be integrated over its plus and transverse components with the following integration measure

$$\int \frac{\mathrm{d}\ell^+ \mathrm{d}^{D-2}\boldsymbol{\ell}}{(2\pi)^{D-1}} . \tag{3.5}$$

6. For each state i between two vertices at consecutive light-cone times x_i^+ and x_{i+1}^+ the following factor has to be included

$$\frac{1}{P_i^- - \sum_{l \in i} k_{l,\mathrm{os}}^- + i\epsilon} , \tag{3.6}$$

---

[2] In particular $n = (1, 0, 0, -1)/\sqrt{2}$.

where P_i^- is the sum of the minus components of all external momenta entering the graph before x_i^+. The sum is over the on-shell values of the minus components

$$k_{l,\text{os}}^- = \frac{k_l^2 + m_l^2}{2k_l^+} \tag{3.7}$$

of all lines l running between x_i^+ and x_{i+1}^+.

The dependence of the propagator numerators on the particles minus momenta leads to a separation into propagating and instantaneous contributions. Decomposing a covariant four-momentum k as

$$k = k_{\text{os}} + (k - k_{\text{os}}) \, , \tag{3.8}$$

where by definition k and k_{os} only differ in their minus components, makes it possible to rewrite the covariant fermion propagator as

$$G_f(k) = \frac{\Theta(k^+)}{2k^+} \frac{i(\slashed{k}_{\text{os}}) + m}{k^- - \frac{k^2 + m^2}{2k^+} + i\epsilon} + \frac{\Theta(-k^+)}{-2k^+} \frac{i(\slashed{k}_{\text{os}}) + m}{-k^- - \frac{k^2 + m^2}{-2k^+} + i\epsilon} + \frac{i\gamma^+}{2k^+} \, . \tag{3.9}$$

In this expression the first term describes the propagation of a fermion while the second term describes the propagation of an antifermion, both with positive plus momentum according to point 4 above. The third term which is independent of k^- is thus associated with an instantaneous propagation. In LCPT graphs it is illustrated by a vertical fermion line whose ends are associated with the same light-cone time x^+. Using again the decomposition of equation (3.8) one finds for the gluon propagator in light-cone gauge the following expression

$$G_g^{\mu\nu}(k) = \frac{i}{k^2 + i\epsilon} \left(-g^{\mu\nu} + \frac{n^\mu k_{\text{os}}^\nu + k_{\text{os}}^\nu n^\mu}{k^+} \right) + \frac{in^\mu n^\nu}{(k^+)^2} \, . \tag{3.10}$$

In analogy with (3.9), the first term in (3.10) can be further decomposed into parts with $\Theta(k^+)$ or $\Theta(-k^+)$ while the last term in (3.10) again describes an instantaneous propagation.

Similar decompositions using equation (3.8) have to be made for all Feynman rules in covariant perturbation theory that have a dependence on minus momenta in the numerator, in particular for the three-gluon vertex. Here one can however make use of the fact that all gluon lines that will be considered in section 3.4 are either internal or associated wit the twist-two operators[3] (2.22) for the observed partons. Any gluon vertex in a graph then has all its Lorentz indices contracted with a gluon propagator. The difference between a covariant momentum and its on-shell value is proportional to the light-cone vector n, this means $(k - k_{\text{os}})^\mu \propto n^\mu$, such that it gives zero when contracted with a gluon propagator numerator $G_g^{\mu\nu}$. One can thus simply replace k with k_{os} in the numerator factor of the three-gluon vertex.

---

[3]Note that the Wilson line operators in these definitions reduce to unity in light-cone gauge.

3.3. Analysis of low-order graphs and its limitations

In this section a simple toy model with scalar "quarks" is considered in order to illustrate how the DPD sum rules for bare distributions arise from Feynman diagrams in covariant perturbation theory at the lowest order in α_s. However, it will also be shown in a second example that this is not always quite straightforward, making a generalisation to higher orders more than cumbersome. This serves as a motivation for the use of light-cone perturbation theory in section 3.4, which makes it possible to formulate a proof that is valid at all orders in the strong coupling. It should be pointed out that of course neither covariant nor light-cone perturbation theory are suitable for actually computing parton distributions, which are genuine non-perturbative quantities. The assumption made in this chapter is that general properties of Green functions – in this case the sum rules – remain valid beyond perturbation theory, which is similar to the spirit of perturbative proofs of factorisation in QCD, for example in references [47, 90].

The toy model considered in this section consists of a scalar "hadron" with point-like coupling to scalar "quarks" of two flavours, namely u and $\bar{d}$, with identical masses. The coupling between these quarks and the gluons is as required by gauge invariance. Within this model (double) parton distributions are calculated to the lowest order in α_s using equations (2.26) and (2.27) and the fact that momentum space Green's functions can be expressed in terms of Feynman diagrams. For brevity, the subscript B for bare distributions will be omitted throughout this section.

3.3.1. Sum rules with a gluon PDF

Consider first the case in which parton 1 in the sum rules is a gluon. At lowest order, the gluon PDF appearing on the right-hand side of the sum rules is given by four graphs, two of which are depicted in figure 3.1. The remaining two graphs are obtained

(a) $\mathcal{G}^g_{PDF\,1}$ (b) $\mathcal{G}^g_{PDF\,2}$
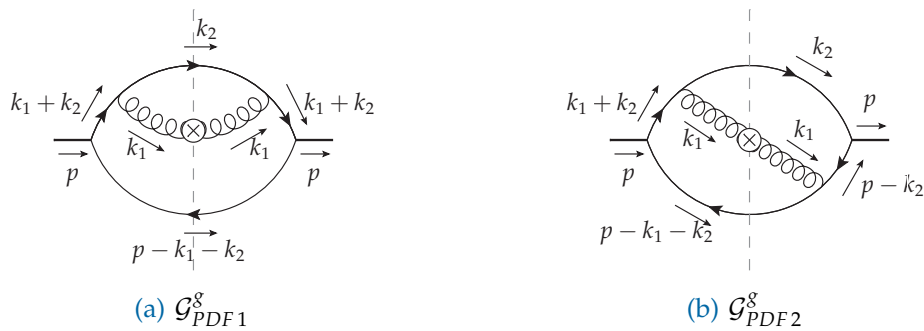
Figure 3.1.: Two graphs contributing to the gluon PDF at order $\mathcal{O}(\alpha_s)$ in the model. Two more graphs are obtained by reversing the arrows that indicate the flow of quark number.

by reversing the arrows on the quark lines (so that in graph 3.1a the gluon couples

to the $\bar{d}$ instead of the u and similarly in graph 3.1b). These additional graphs yield identical expressions due to the symmetries of the model, namely charge conjugation and the identical masses of the two quark flavours. The contributions of these graphs to the gluon PDF are given by

$$f_{g,1}(x_1) = 4 \int d\Gamma_{PDF} (x_1 \mathbf{k}_2 - x_2 \mathbf{k}_1)^2$$
$$\times \left[((k_1 + k_2)^2 - m^2 + i\epsilon)(k_1^2 + i\epsilon)(k_1^2 - i\epsilon)((k_1 + k_2)^2 - m^2 - i\epsilon) \right]^{-1},$$
(3.11)

$$f_{g,2}(x_1) = 4 \int d\Gamma_{PDF} (x_1 \mathbf{k}_2 - x_2 \mathbf{k}_1)(x_2 \mathbf{k}_1 - x_1 \mathbf{k}_2 - \mathbf{k}_1)$$
$$\times \left[((k_1 + k_2)^2 - m^2 + i\epsilon)(k_1^2 + i\epsilon)(k_1^2 - i\epsilon)((p - k_2)^2 - m^2 - i\epsilon) \right]^{-1}.$$
(3.12)

The integration element $d\Gamma_{PDF}$ is given by

$$d\Gamma_{PDF} = \frac{g^2 \mu^{D-4} C_F p^+}{x_1} \frac{dk_1^- d^{D-2} \mathbf{k}_1}{(2\pi)^D} \frac{d^D k_2}{(2\pi)^D}$$
$$\times 2\pi \delta(k_2^2 - m^2) \, 2\pi \delta((p - k_1 - k_2)^2 - m^2),$$
(3.13)

where g denotes the strong coupling and m the quark mass which as already mentioned above is identical for the two flavours. For simplicity the coupling between the hadron and the quarks has been set to 1. In the above expressions a factor of two has been included in order to take into account the contributions from the diagrams with reversed arrows on the quark lines not shown in figure 3.1. The graphs corresponding to the

(a) Graph for a PDF   (b) Graph for a corresponding DPD
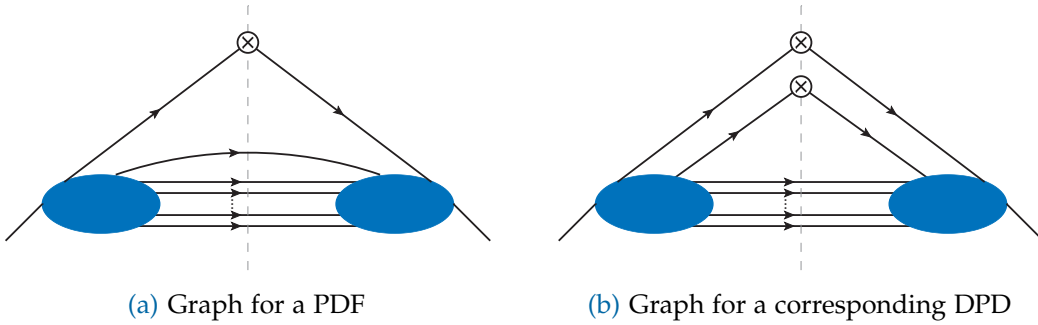
Figure 3.2.: Transition from a given PDF graph to a corresponding DPD graph.

DPDs appearing in the sum rules can be obtained from the PDF graphs by inserting the appropriate operator for parton 2 onto one of the lines crossing the final state cut in the PDF, as illustrated in figure 3.2. For the case at hand – this means for the PDF graphs illustrated in figure 3.1 – the result of this procedure is shown in figure 3.3. The appropriate operator for scalar quarks or antiquarks (the last one in equation (2.22))

(a) $\mathcal{G}^{gu}_{DPD\,1.1}$

(b) $\mathcal{G}^{g\bar{d}}_{DPD\,1.2}$

(c) $\mathcal{G}^{g\bar{d}}_{DPD\,2.1}$

(d) $\mathcal{G}^{g\bar{d}}_{DPD\,2.2}$
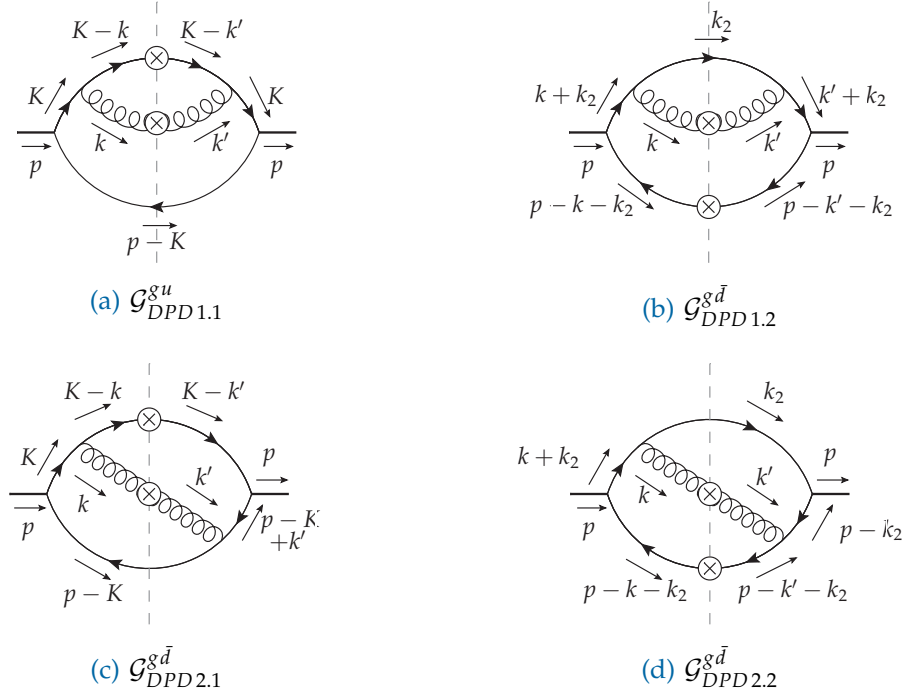
Figure 3.3.: Graphs for gluon-quark or gluon-antiquark DPDs corresponding to the gluon PDF graphs in figure 3.1. The loop momenta are defined in (3.19) and (3.20), and each graph is for the momentum fractions specified in (3.15) to (3.17). Four more graphs are obtained by reversing the direction of arrows on the quark lines.

simply provides a factor 1 in the graphs, such that the expressions for the corresponding DPDs are given by

$$F^{gu}_{1.1}(x_1, x_2) = 4 \int d\Gamma_{DPD,1}\, x_2 (x_1 \mathbf{k}_2 - x_2 \mathbf{k}_1)^2$$

$$\times \left[\left((k_1 + k_2)^2 - m^2 + i\epsilon\right) \left((k_2 + \Delta/2)^2 - m^2 + i\epsilon\right) \left((k_1 - \Delta/2)^2 + i\epsilon\right) \right]^{-1}$$

$$\times \left[\left((k_1 + \Delta/2)^2 - i\epsilon\right) \left((k_2 - \Delta/2)^2 - m^2 - i\epsilon\right) \left((k_1 + k_2)^2 - m^2 - i\epsilon\right) \right]^{-1}, \qquad (3.14)$$

$$F^{g\bar{d}}_{1.2}(x_1, 1 - x_1 - x_2) = 4 \int d\Gamma_{DPD,2}\, (1 - x_1 - x_2)(x_1 \mathbf{k}_2 - x_2 \mathbf{k}_1)^2$$

$$\times \left[\left((k_1 + k_2)^2 - m^2 + i\epsilon\right) \left((p - k_1 - k_2 + \Delta/2)^2 - m^2 + i\epsilon\right) \left((k_1 - \Delta/2)^2 + i\epsilon\right) \right]^{-1}$$

$$\times \left[\left((k_1 + \Delta/2)^2 - i\epsilon\right) \left((p - k_1 - k_2 - \Delta/2)^2 - m^2 - i\epsilon\right) \left((k_1 + k_2)^2 - m^2 - i\epsilon\right) \right]^{-1}, \qquad (3.15)$$

$$F^{gu}_{2.1}(x_1, x_2) = 4 \int d\Gamma_{DPD,1}\, x_2 (x_1 \mathbf{k}_2 - x_2 \mathbf{k}_{)}(x_2 \mathbf{k}_1 - x_1 \mathbf{k}_2 - \mathbf{k}_1)$$

$$\times \left[\left((k_1 + k_2)^2 - m^2 + i\epsilon\right) \left((k_2 + \Delta/2)^2 - m^2 + i\epsilon\right) \left((k_1 - \Delta/2)^2 + i\epsilon\right) \right]^{-1}$$

$$\times \left[\left((k_1 + \Delta/2)^2 - i\epsilon \right) \left((k_2 - \Delta/2)^2 - m^2 - i\epsilon \right) \left((p - k_2)^2 - m^2 - i\epsilon \right) \right]^{-1}, \quad (3.16)$$

$$F_{2.2}^{g\bar{d}}(x_1, 1 - x_1 - x_2) = 4 \int d\Gamma_{DPD,2} (1 - x_1 - x_2)(x_1 k_2 - x_2 k_1)(x_2 k_1 - x_1 k_2 - k_1)$$

$$\times \left[\left((k_1 + k_2)^2 - m^2 + i\epsilon \right) \left((p - k_1 - k_2 + \Delta/2)^2 - m^2 + i\epsilon \right) \left((k_1 - \Delta/2)^2 + i\epsilon \right) \right]^{-1}$$

$$\times \left[\left((k_1 + \Delta/2)^2 - i\epsilon \right) \left((p - k_1 - k_2 - \Delta/2)^2 - m^2 - i\epsilon \right) \left((p - k_2)^2 - m^2 - i\epsilon \right) \right]^{-1}.$$
$$(3.17)$$

Here the integration elements $d\Gamma_{DPD,i}$ ($i = 1, 2$) are given by

$$d\Gamma_{DPD,i} = \frac{2g^2 \mu^{D-4} C_F (p^+)^3}{x_1} \frac{dk_1^- d^{D-2}k_1}{(2\pi)^D} \frac{dk_2^- d^{D-2}k_2}{(2\pi)^D} \frac{d\Delta^-}{2\pi} 2\pi \delta \left(\ell_i^2 - m^2 \right), \quad (3.18)$$

where $\ell_1 = p - k_1 - k_2$ and $\ell_2 = k_2$. In the expressions for $F^{g\bar{d}}$ the second momentum fraction argument has been chosen in a quite counterintuitive way which however will prove useful for deriving the sum rules. The remaining one-loop graphs for DPDs for which parton 1 is a gluon are obtained from the graphs in figure 3.3 by reversing the arrows on the quark lines. Due to the symmetries of the toy model these contributions are related to the ones in equations (3.14) to (3.17) by $F_{1.1}^{gu}(x_1, x_2) = F_{1.1}^{g\bar{d}}(x_1, x_2)$ and analogously for the other three graphs.

Comparing the expressions for the PDF graphs with those for the corresponding DPD graphs one finds that they are already quite similar. In these expressions the momentum dependent numerators agree exactly, such that the main difference are the two additional propagator denominator factors in the DPD, which arise due to the fact that a operator is inserted on a line that runs across the final state cut in the PDF. In order to make the resemblance between the PDF and DPD graphs even more obvious one can get rid of these additional propagator denominator factors by performing the integrations over their minus momentum components using the theorem of residues. Using the variable substitutions of equations (3.19) and (3.20) it is possible to close the integration contours in such a way that only the propagator poles of the two lines corresponding to parton 2 get picked up, setting these lines on-shell. Not only does this remove the additional denominator factors but it also sets the corresponding momenta in the remaining propagator denominators to their on-shell value, just like it is the case in the PDF. The relevant substitutions read

$$k_1^- - \Delta^-/2 = k^-, \qquad k_1^- + \Delta^-/2 = k'^-, \qquad k_1^- + k_2^- = K^- \qquad (3.19)$$

for $F_{1.1}^{gu}$ and $F_{2.1}^{gu}$, and

$$k_1^- - \Delta^-/2 = k^-, \qquad k_1^- + \Delta^-/2 = k'^- \qquad (3.20)$$

for $F_{1.2}^{g\bar{d}}$ and $F_{2.2}^{g\bar{d}}$, where k_2^- is kept as an integration variable. The integration over k^- sets the line corresponding to parton 2 on the left-hand side of the cut to its on-shell

value, while the same is achieved on the right-hand side of the cut by integrating over k'^-. After performing the integrations over all minus components, one obtains for the expressions in (3.11) to (3.17)

$$f_{g,1}(x_1) = \int\limits_0^{1-x_1} dx_2 \, x_2(1 - x_1 - x_2)^3 \int d\Gamma \, \frac{(x_1 k_2 - x_2 k_1)^2}{\left((k_1 + k_2)^2 + m^2\right)^2 \mathcal{D}^2} \,, \tag{3.21}$$

$$f_{g,2}(x_1) = \frac{1}{2} \int\limits_0^{1-x_1} dx_2 \, x_2^2(1 - x_1 - x_2)^2 \int d\Gamma \, \frac{(x_1 k_2 - x_2 k_1)^2 - x_2 k_1^2 + x_1 k_1 k_2}{\left(k_2^2 + m^2\right)\left((k_1 + k_2)^2 + m^2\right)\mathcal{D}^2} \,, \tag{3.22}$$

and

$$F_{1.1}^{gu}(x_1, x_2) = F_{1.2}^{g\bar{d}}(x_1, 1 - x_1 - x_2)$$

$$= \frac{1}{2} \int\limits_0^{1-x_1} dx_2 \, x_2(1 - x_1 - x_2)^3 \int d\Gamma \, \frac{(x_1 k_2 - x_2 k_1)^2}{\left((k_1 + k_2)^2 + m^2\right)^2 \mathcal{D}^2} \,, \tag{3.23}$$

$$F_{2.1}^{gu}(x_1, x_2) = F_{2.2}^{g\bar{d}}(x_1, 1 - x_1 - x_2)$$

$$= \frac{1}{4} x_2^2(1 - x_1 - x_2)^2 \int d\Gamma \, \frac{(x_1 k_2 - x_2 k_1)^2 - x_2 k_1^2 + x_1 k_1 k_2}{\left(k_2^2 + m^2\right)\left((k_1 + k_2)^2 + m^2\right)\mathcal{D}^2} \,, \tag{3.24}$$

where the following abbreviation has been used

$$\mathcal{D} = x_1 k_2^2 + x_2 k_1^2 - (x_1 k_2 - x_2 k_1)^2 + x_1 (1 - x_1) m^2 \,, \tag{3.25}$$

and the measure for the remaining integrations is

$$d\Gamma = \frac{g^2 \mu^{D-4} C_F}{x_1} \frac{d^{D-2} k_1}{(2\pi)^{D-1}} \frac{d^{D-2} k_2}{(2\pi)^{D-1}} \,. \tag{3.26}$$

At this point the similarity between the PDF and corresponding DPD expressions is already very close. In order to show how the sum rules arise from these expressions it should be noted that at the considered order in α_s the only DPDs involving a gluon are the ones given above, and in particular $F^{g\bar{u}}$, F^{gd} and F^{gg} only appear at order α_s^2.

Combining all contributions from graphs 1.1 and 1.2 for the u number sum rule then yields

$$\int\limits_0^{1-x_1} dx_2 \left[F_{1.1}^{gu}(x_1, x_2) + F_{1.2}^{gu}(x_1, x_2)\right] = \int\limits_0^{1-x_1} dx_2 \left[F_{1.1}^{gu}(x_1, x_2) + F_{1.2}^{g\bar{d}}(x_1, x_2)\right]$$

$$= \int\limits_0^{1-x_1} dx_2 \left[F_{1.1}^{gu}(x_1, x_2) + F_{1.2}^{g\bar{d}}(x_1, 1 - x_1 - x_2)\right] = f_1^g(x_1) \,, \tag{3.27}$$

where in the first step the symmetry between u and $\bar{d}$ implicit in the model has been used. In the second step a change of variables in $F^{g\bar{d}}$ has been performed which makes it possible to easily see the last equality from the explicit expressions in (3.21) and (3.23). For the contributions from graphs 2.1 and 2.2 – and hence for the sum over all graphs – one readily derives the analogue of (3.27). Since $N_{u_v} = 1$ in the toy model, this shows that the number sum rule for u quarks is fulfilled. In the same manner, one can show the number sum rule for $\bar{d}$ quarks.

In a similar manner one can show that the DPDs fulfil the momentum sum rule, starting again with the contributions from graphs 1.1 and 1.2:

$$
\int_0^{1-x_1} dx_2 \, x_2 \left[F_{1.1}^{gu}((x_1, x_2) + F_{1.2}^{gu}(x_1, x_2) + F_{1.1}^{g\bar{d}}((x_1, x_2) + F_{1.2}^{g\bar{d}}(x_1, x_2) \right]
$$

$$
= 2 \int_0^{1-x_1} dx_2 \left[x_2 \, F_{1.1}^{gu}((x_1, x_2) + x_2 \, F_{1.2}^{g\bar{d}}(x_1, x_2) \right]
$$

$$
= 2 \int_0^{1-x_1} dx_2 \left[x_2 \, F_{1.1}^{gu}((x_1, x_2) + (1 - x_1 - x_2) \, F_{1.2}^{g\bar{d}}(x_1, 1 - x_1 - x_2) \right]
$$

$$
= 2 \int_0^{1-x_1} dx_2 \left[x_2 \, F_{1.1}^{gu}((x_1, x_2) + (1 - x_1 - x_2) \, F_{1.1}^{gu}(x_1, x_2) \right] = (1 - x_1) \, f_1^g(x_1) .
$$

$$(3.28)$$

Here the first two steps are just the analogues of the same steps in (3.27), while in the last two steps again the explicit expressions of equations (3.21) and (3.23) have been used. An analogous relation can be derived for graphs 2.1 and 2.2 and thus for the sum over all graphs, which confirms the validity of the momentum sum rule.

An interesting observation is that the number as well as the momentum sum rule are fulfilled individually for each PDF graph and its corresponding DPD graphs. Such a one-to-one relation is already suggested by figure 3.2 and will remain true in the all-order proof in section 3.4. However, a crucial step in the preceding derivation was that for each DPD graph it was possible to perform the integrations over minus momenta in such a way that after applying the theorem of residues, the momentum of parton 2 to the left and to the right of the final state cut was set on shell. This is not readily possible for other graphs, as the following example will illustrate.

3.3.2. Sum rules with a quark PDF

Consider now the case in which parton 1 in the sum rules is a u quark (again the expressions for $\bar{d}$ quarks are identical due to the symmetries of the model). In this

case already at leading order in α_s the number of graphs contributing to each PDF is much greater than for the g PDF considered in the previous section. Here one now finds in addition to the real emission graphs in figure 3.4 graphs with a cut quark loop and a vertex or propagator correction to the left or to the right of the cut. For the graph in figure 3.4a and the corresponding DPD graphs, one can again establish the validity of the sum rules exactly as in the previous section. This situation is, however, different for the remaining graphs of figure 3.4 as the following example will illustrate. To this end, consider the graph in figure 3.4b and the corresponding DPD graphs in

(a) $\mathcal{G}^u_{PDF\,1}$

(b) $\mathcal{G}^u_{PDF\,2}$

(c) $\mathcal{G}^{\bar{d}}_{PDF\,3}$

(d) $\mathcal{G}^{\bar{d}}_{PDF\,4}$
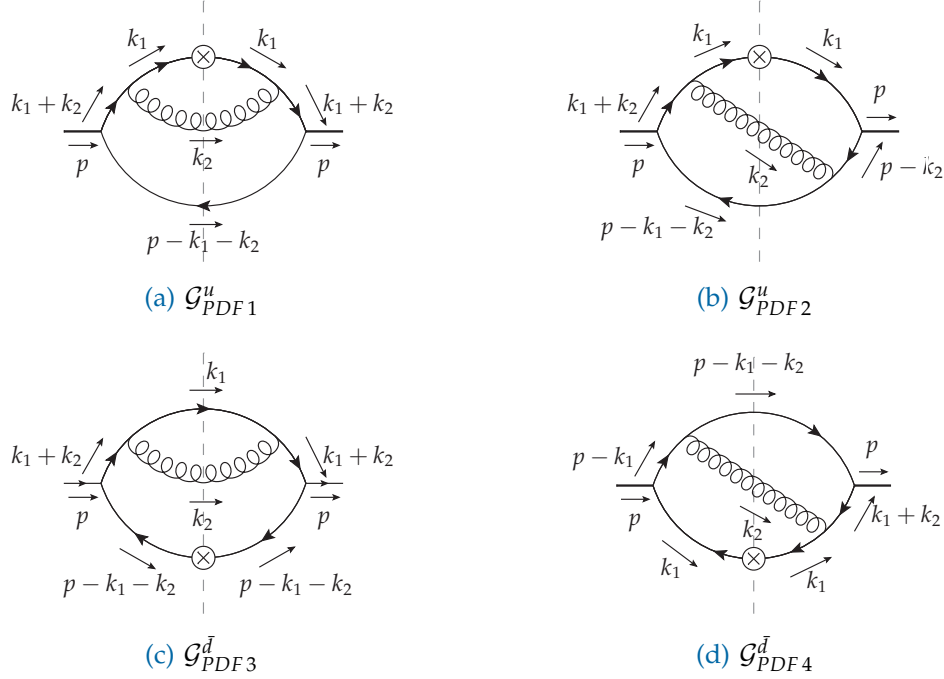
Figure 3.4.: Real emission graphs contributing to quark or antiquark distributions at $\mathcal{O}(\alpha_s)$. Four more graphs are obtained by reversing the arrow on the quark line.

figure 3.5. In order to perform the integrations over minus momenta the same change

(a) $\mathcal{G}^{ug}_{DPD\,2.1}$

(b) $\mathcal{G}^{u\bar{d}}_{DPD\,2.2}$
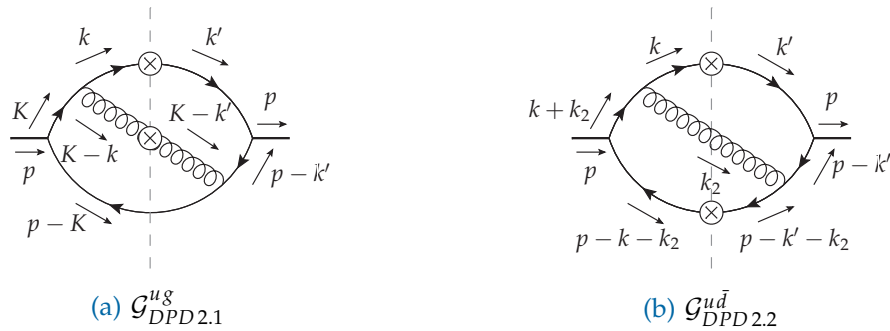
Figure 3.5.: DPD graphs corresponding to the PDF graph in figure 3.4b.

of variables as before is made, namely (3.19) for $F_{2.1}^{ug}$ and (3.20) for $F_{2.1}^{u\bar{d}}$. However, even with these substitutions one finds that in both graphs is is not possible to close the integration contour in such a way that one picks up only the poles corresponding to the propagators associated with parton 2, given that on the right-hand side of the cut their pole in k'^- is on the same side of the real axis as the propagator pole of the $\bar{d}$ that directly couples to the hadron[4]. Performing the integrations over the minus momenta, one then finds

$$f_2^u(x_1) = x_1^2 \int\limits_0^{1-x_1} dx_2 (1 - x_1 - x_2)^3 \int d\Gamma \frac{(x_1 k_2 - x_2 k_1)^2 - x_1 k_2^2 + x_2 k_1 k_2}{\left((k_1 + k_2)^2 + m^2\right) \mathcal{D}_1^2 \mathcal{D}_2} , \qquad (3.29)$$

and

$$F_{2.1}^{ug}(x_1, x_2) = F_{2.2}^{u\bar{d}}(x_1, 1 - x_1 - x_2)$$

$$= x_1^2 (1 - x_1 - x_2)^3 \int d\Gamma \frac{(x_1 k_2 - x_2 k_1)^2 - x_1 k_2^2 + x_2 k_1 k_2}{\left((k_1 + k_2)^2 + m^2\right) \mathcal{D}_1^2 \mathcal{D}_2}$$

$$- \frac{x_1^2 (1 - x_1 - x_2)^2 (1 - x_1)}{x_2} \int d\Gamma \frac{(x_1 k_2 - x_2 k_1)^2 - x_1 k_2^2 + x_2 k_1 k_2}{\left((k_1 + k_2)^2 + m^2\right) \left(k_1^2 + m^2\right) \mathcal{D}_1 \mathcal{D}_2} ,$$

$$(3.30)$$

where

$$\mathcal{D}_1 = x_1 k_2^2 + x_2 k_1^2 - (x_1 k_2 - x_2 k_1)^2 + x_2 (1 - x_2) m^2 ,$$
$$\mathcal{D}_2 = (x_1 k_2 - x_2 k_1)^2 + (1 - 2x_1) k_2^2 + 2x_2 k_1 k_2 + x_2^2 m^2 , \qquad (3.31)$$

and $d\Gamma$ is defined as before in (3.26). Here the first term in equation (3.30) has the same structure as the PDF in equation (3.29) which would be required to show the validity of the sum rules in the same way as in the previous section. However, due to the second term in equation (3.30) originating from the "unwanted" propagator pole when the minus momentum integrals are performed using residues the simple proof used in the previous section no longer works. It has been explicitly checked that this extra term disappears when one sums over all contributing graphs, and the sum rules remain valid also in this example.

A similar situation is encountered in the proof of cancellation of Glauber gluons in single [47, 90] or double hard scattering [34]. While for simple cases covariant perturbation theory suffices to show that this cancellation can be established using the theorem of residues for integrations over minus momenta in a similar way as here, this is no longer the case for more complicated graphs, where this method turns out to be cumbersome [34]. Whether a proof that is valid to all orders in the strong coupling

---

[4]Note that this is not a issue that could be solved by choosing a different momentum routing.

could be performed at all in covariant perturbation theory is unclear, such that in the next section light-cone perturbation theory will be used, which provides a powerful tool for proving the sum rules at all orders, as it is for establishing Glauber gluon cancellation [34, 47, 90] .

3.4. All order proof for bare distributions using LCPT

Following the analysis in the previous section now LCPT is used to derive the DPD sum rules for bare distributions at all orders in the strong coupling. To this end graphs in LCPT at arbitrary fixed order in α_s are considered, using perturbation theory in the same spirit as discussed at the beginning of section 3.3. Having established the validity of the sum rules for any fixed order in α_s, one immediately obtains their validity for the sum over all perturbative orders.

3.4.1. Representation of PDFs and DPDs in LCPT

As a first step the representations of PDFs and DPDs in terms of Green's functions given in equations (2.26) and (2.27) have to be adapted to the LCPT formalism. To this end one finds for the bare PDF

$$f_B^{a_1}(x_1) = \sum_g \left(x_1 p^+\right)^{-n_1} \left(p^+\right)^{N(g)-2} \int \frac{\mathrm{d}k_1^- \mathrm{d}^{D-2}\mathbf{k}_1}{(2\pi)^D} \left(\prod_{i=2}^{N(g)} \frac{\mathrm{d}x_i \, \mathrm{d}^{D-2}\mathbf{k}_i}{(2\pi)^{D-1}}\right)$$

$$\times \, \mathcal{G}_g^{a_1}\left(\{x\}, \{\mathbf{k}\}\right) 2\pi\delta\left(p^- - k_1^- - \sum_{i=2}^{M(g)} k_{i,\mathrm{os}}^-\right) \delta\left(1 - \sum_{i=1}^{M(g)} x_i\right), \qquad (3.32)$$

where

$$x_i = k_i^+ / p^+ . \qquad (3.33)$$

In equation (3.32) the index g now specifies a given cut LCPT graph with a definite x^+ light-cone time ordering of its vertices. The independent momenta of a graph are denoted by k_i, where k_1 always is the momentum of the observed parton. The total number of independent momenta for a given graph is $N(g) - 1$, of which $M(g) - 1$ run across the final state cut. The complete set of light-cone momentum fractions and transverse momentum arguments of a graph is collectively labelled as $\{x\}$ and $\{\mathbf{k}\}$ in equation (3.32) and in corresponding equations.

Just like in the simple toy model considered in section 3.3 $a_1 a$ DPD graphs can be obtained from PDF graphs for a a_1 PDF by inserting the appropriate operator for the

second parton a on one of the final state parton lines of flavour a. The result is

$$F_B^{a_1 a}(x_1, z) = \sum_g \sum_l \delta_{a,f(l)} \left(x_1 p^+\right)^{-n_1} \left(x_l p^+\right)^{-n_l} 2 \left(p^+\right)^{N(g)-2}$$

$$\times \int dx_l \, \delta\left(x_l - z\right) \int \frac{dK^- d^{D-2}\mathbf{k}_1 \, d^{D-2}\mathbf{k}_l}{(2\pi)^{2D-1}} \left(\prod_{\substack{i=2 \\ i \neq l}}^{N(g)} \frac{dx_i \, d^{D-2}\mathbf{k}_i}{(2\pi)^{D-1}}\right)$$

$$\times \mathcal{G}_{g,l}^{a_1 f(l)}\left(\{x\}, \{\mathbf{k}\}\right) 2\pi\delta\left(p^- - K^- - \sum_{\substack{i=2 \\ i \neq l}}^{M(g)} k_{i,\text{os}}^-\right) \delta\left(1 - \sum_{i=1}^{M(g)} x_i\right), \quad (3.34)$$

where the sum over l runs over all parton lines crossing the final state cut on which the operator for parton a can be inserted, with $\delta_{a,f(l)}$ selecting only those lines for which the flavour $f(l) = a$ and $\delta(x_l - z)$ setting the plus momentum fraction x_l of the line l to z. Here it should be pointed out that both the plus momentum and the transverse momentum components of the two observed partons are equal on both sides of the final state cut. While the former is always the case for a DPD, the latter holds only because the sum rules are supposed to be valid only for the case that $\Delta = 0$.

In order to arrive at the expression for the LCPT DPD in equation (3.34) the following variable substitutions have been made in equation (2.27)

$$K^- = (k_1 + k_l)^-, \qquad k^- = (k_l - \Delta)^-/2, \qquad k'^- = (k_l + \Delta)^-/2, \qquad (3.35)$$

before performing the integrations over k^- and k'^-. As a result of the integrations over these minus components the two vertices corresponding to the operator insertions for the observed partons a_1 and a are associated with the *same* light-cone time x^+ on each side of the final state cut, as explained in Appendix B of reference [34]. Considering the definition of a DPD in equation (2.17) this is not surprising, because the two operators $\mathcal{O}_{a_1}$ and $\mathcal{O}_{a_2}$ there are taken at the same light-cone time.

A crucial step to show the equivalence of PDF and DPD expressions in the following section is to show that only such light-cone time orderings contribute to the PDFs and DPDs where the operator insertions are "latest", meaning that there are no vertices with larger x^+. To this end the integration over k_1^- is performed in the expression (3.32) of the PDF, following a simplified version of the argument in chapter 14.4.3 of reference [47]. A general LCPT graph for a PDF, as illustrated in figure 3.6, can be written in the following way

$$\mathcal{G}_g^{a_1} = I F\left(F_A\right) I' \times \{\text{numerator}\}, \qquad (3.36)$$

with

$$I = \prod_{\substack{\text{states } \xi \\ \xi < H}} \frac{1}{p^- - \sum_{l \in \xi} k_{l,\text{os}}^- + i\epsilon}, \qquad I' = \prod_{\substack{\text{states } \xi \\ \xi < H'}} \frac{1}{p^- - \sum_{l \in \xi} k_{l,\text{os}}^- - i\epsilon}, \qquad (3.37)$$
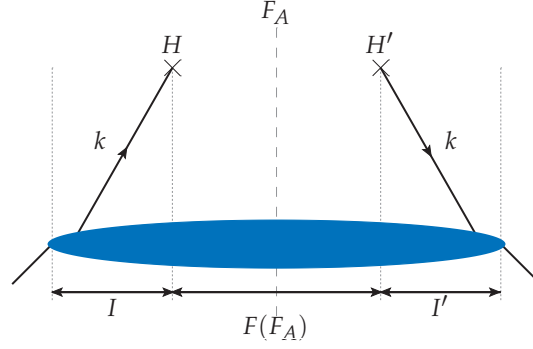
Figure 3.6.: Schematic illustration of an LCPT graph for a PDF. H (H') denotes the light-cone time of the vertex for the insertion of the twist-two operator on the left (right) of the final-state cut. Since the order of vertices matters for evaluating LCPT graphs, one cannot place that operator insertion on the line indicating the final state cut, as was done for the Feynman graphs in section 3.3.

and

$$F(F_A) = \prod_{\substack{\text{states } \xi \\ H < \xi < F_A}} \frac{1}{p^- - k_1^- - \sum_{l \in \xi} k_{l,\text{os}}^- + i\epsilon} \, 2\pi\delta\left(p^- - k_1^- - \sum_{l \in F_A} k_{l,\text{os}}^-\right)$$

$$\times \prod_{\substack{\text{states } \xi \\ H' < \xi < F_A}} \frac{1}{p^- - k_1^- - \sum_{l \in \xi} k_{l,\text{os}}^- - i\epsilon} . \tag{3.38}$$

Since the detailed numerator structure is not relevant for the present argument all vertex factors, propagator numerators and factors of $\pm i$ have been absorbed into the {numerator} factor in (3.36). As illustrated in figure 3.6 the PDF graph is cut across the final state F_A, and the sums in I, I' and F are over intermediate states ξ either before or after the light-cone time of the operator insertion H and H'. Consider now the sum over all graphs g that differ only by the state F_A where the cut is made but are otherwise identical. Numbering the states in $F(F_A)$ from 1 to N, one can thus write

$$\sum_{F_A} F(F_A) = \sum_{c=1}^{N} \left[\prod_{f=1}^{c-1} \frac{1}{p^- - k_1^- - D_f + i\epsilon} \, 2\pi\delta\left(p^- - k_1^- - D_c\right) \prod_{f=c+1}^{N} \frac{1}{p^- - k_1^- - D_f - i\epsilon} \right], \tag{3.39}$$

where the abbreviation $D_f = \sum_{l \in f} k_{l,\text{os}}^-$ has been used. Rewriting the δ function in equation (3.39) as

$$2\pi\delta(x) = i\left[\frac{1}{x + i\epsilon} - \frac{1}{x - i\epsilon}\right], \tag{3.40}$$

then yields the following expression

$$\sum_{F_A} F(F_A) = i\left[\prod_{f=1}^{N} \frac{1}{p^- - k_1^- - D_f + i\epsilon} - \prod_{f=1}^{N} \frac{1}{p^- - k_1^- - D_f - i\epsilon}\right]. \tag{3.41}$$

In this form one can easily see that this expression vanishes for $N \geq 2$ when one integrates over k_1^- using the theorem of residues. For $N = 1$ on the other hand, the initial δ function in (3.32) is reproduced. One can thus conclude that for a PDF only those x^+ orderings of the vertices have to be considered for which there are no states "later" than the operator insertion vertices H and H' on each side of the final state cut.

In a completely analogous manner one can repeat the discussion above for the K^- integration in the expression for a DPD given in equation (3.34), yielding again that only time orderings with no intermediate state after the operator insertions contribute. With this insight the expressions for PDFs and DPDs (equations (3.32) and (3.34), respectively) can be rewritten as

$$
f_B^{a_1}(x_1) = \sum_g (x_1 p^+)^{-n_1} (p^+)^{N(g)-2} \int \frac{\mathrm{d}^{D-2}\boldsymbol{k}_1}{(2\pi)^{D-1}}
$$

$$
\times \left(\prod_{i=2}^{N(g)} \frac{\mathrm{d}x_i \, \mathrm{d}^{D-2}\boldsymbol{k}_i}{(2\pi)^{D-1}} \right) \mathcal{G}_g^{a_1}(\{x\},\{\boldsymbol{k}\}) \, \delta\left(1 - \sum_{i=1}^{M(g)} x_i\right), \tag{3.42}
$$

$$
\int_0^{1-x_1} \mathrm{d}z \, z^m \, F_B^{a_1 a}(x_1, z) = \sum_g \sum_l \delta_{a,f(l)} (x_1 p^+)^{-n_1} (p^+)^{N(g)-2} \int \frac{\mathrm{d}^{D-2}\boldsymbol{k}_1}{(2\pi)^{D-1}}
$$

$$
\times \left(\prod_{i=2}^{N(g)} \frac{\mathrm{d}x_i \, \mathrm{d}^{D-2}\boldsymbol{k}_i}{(2\pi)^{D-1}} \right) 2 x_l^m (x_l p^+)^{-n_l} \mathcal{G}_{g,l}^{a_1 f(l)}(\{x\},\{\boldsymbol{k}\}) \, \delta\left(1 - \sum_{i=1}^{M(g)} x_i\right), \tag{3.43}
$$

where the sum over all graphs g can be restricted to the time orderings just discussed. The DPD has been integrated over its second momentum fraction z with weight z^m, as is required for the sum rules (where $m = 0$ or $m = 1$ for the number and momentum sum rules, respectively).

3.4.2. All order correspondence between PDF and DPD graphs

The last missing step before being able to complete the proof is to establish the following equality

$$
2 (x_l p^+)^{-n_l} \mathcal{G}_{g,l}^{a_1 f(l)} \stackrel{!}{=} \mathcal{G}_g^{a_1} \tag{3.44}
$$

for all graphs g and all partons l that contribute in equations (3.42) and (3.43). This equality implies a unique correspondence between the LCPT graphs g that contribute to f^{a_1} and those that contribute to $F^{a_1 a}$, as indicated in figure 3.7. In the previous section it has already been shown that in a given PDF graph no vertex can be later in light-cone time than the vertex H of the twist-two operator insertion, including the vertex V_2 where the final state line l leaves the graph. It will now be shown that there can also be no instantaneous propagator attached to a twist-two operator insertion. The vertex

(a) LCPT graph for a PDF

(b) LCPT graph for a corresponding DPD
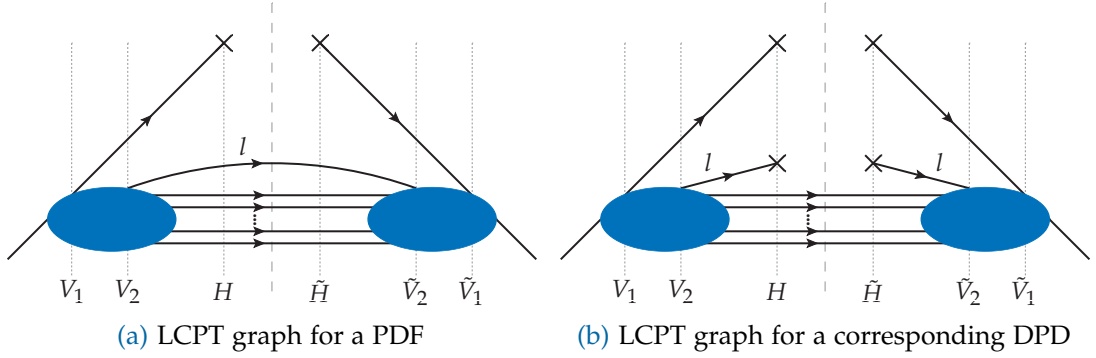
Figure 3.7.: LCPT graphs for a PDF or a DPD. It is understood that the subgraphs denoted by blobs are identical in panels (a) and (b). One may interchange the time ordering between the vertices V_1 and V_2, and independently the time ordering between the vertices $\tilde{V}_1$ and $\tilde{V}_2$.

V_1 where parton 1 leaves the graph must then come before H as well, and in a DPD graph both V_1 and V_2 must come before H. In both PDF and DPD graphs, V_1 may come before or after V_2. Corresponding statements hold for $\tilde{V}_1$, $\tilde{V}_2$ and $\tilde{H}$ to the right of the cut.

In order to show this, consider the vertex rules (in momentum space) associated with the unpolarised twist-two operators given in equation (2.22). For quarks one gets a factor $\gamma^+/2$ tying together the Dirac indices of the parton to the left and the right of the cut, while for antiquarks one gets a factor $-\gamma^+/2$. Multiplying these expressions with the instantaneous part of the fermion propagator (3.9) yields zero since $(\gamma^+)^2 = 0$. For gluons one finds that the twist-two operator gives a factor $(k^+)^2 \delta^{ii'}$ in light-cone gauge, where k^+ denotes plus momentum component of the gluon, which is equal on both sides of the cut. As mentioned below equation (2.22) the indices i and i' are transverse momentum indices denoting the gluon polarisation to the left and right of the cut, respectively. Contracting this with the instantaneous part of the LCPT gluon propagator in equation (3.10) gives zero.

One thus finds that LCPT graphs contributing to a PDF are related to those contributing to a corresponding DPD by inserting the operator for the second parton on a final state line in the PDF graph in analogy to the statement used for Feynman graphs in section 3.3 but now including the statement about the relative time orderings between vertices. With PDF and DPD graphs having the same time ordering of vertices, they have identical light-cone energy denominators (3.6) due to the fact that in LCPT PDF and DPD graphs with identical x^+ ordering of vertices automatically have the same denominator structure since all internal lines are treated as on-shell.

The final step to show the equality in equation (3.44) is to show that the numerator structure in corresponding graphs is also identical. To this end the numerator factor associated with the line l selected by the operator for parton 2 in the DPD is compared to the factor associated with the corresponding final state line in the PDF. In the DPD,

the momenta k and k' carried by l to the left and the right of the cut have the same plus and transverse components, as already noted after equation (3.34). Their on-shell values are hence identical as well, this means

$$k_{\mathrm{os}} = k'_{\mathrm{os}}. \tag{3.45}$$

As a result of the identical structure of PDF and DPD graphs established above, k is furthermore equal to the momentum of the corresponding final state line in the PDF. For the case that l is a quark, one thus finds

$$2 \frac{\not{k}_{\mathrm{os}} + m}{2k^+} \frac{\gamma^+}{2} \frac{\not{k}_{\mathrm{os}} + m}{2k^+} = \frac{\not{k}_{\mathrm{os}} + m}{2k^+} \tag{3.46}$$

for the corresponding numerator in the DPD graph. Here the factor 2 on the left-hand side is taken from the left-hand side of equation (3.44) while the factor $\gamma^+/2$ corresponds to the twist-two operator for quarks as discussed above and a factor $(\not{k}_{\mathrm{os}} + m)/(2k^+)$ amounts for each propagating quark line in accordance with equation (3.9). On the right-hand side of equation (3.46) one easily recognises the factor for the final state line l in the PDF graph, which proves equation (3.44) for quarks. The same argument is easily repeated for antiquarks. If l is a gluon, one finds the following numerator

$$\frac{2}{k^+} \frac{1}{2k^+} \left(-g^{\mu i} + \frac{n^\mu k_{\mathrm{os}}^i + n^i k_{\mathrm{os}}^\mu}{k^+} \right) (k^+)^2 \, \delta^{ii'} \frac{1}{2k^+} \left(-g^{\mu' i'} + \frac{n^{\mu'} k_{\mathrm{os}}^{i'} + n^{i'} k_{\mathrm{os}}^{\mu'}}{k^+} \right)$$

$$= \frac{1}{2k^+} \left(-g^{\mu\mu'} + \frac{n^\mu k_{\mathrm{os}}^{\mu'} + n^{\mu'} k_{\mathrm{os}}^\mu}{k^+} \right) \tag{3.47}$$

in the DPD graph, where the factor $2/k^+ = 2(x_l p^+)^{-1}$ on the left-hand side is again taken from the left-hand side of equation (3.44). The right-hand side of equation (3.47) is the factor for a final state gluon in the PDF graph, completing the proof of equation (3.44).

3.4.3. Number sum rule

With the prerequisites discussed above it is now rather straightforward to show the validity of the number sum rule for bare distributions. To this end one can insert the relation (3.44) into equation (3.43) for the integral of the DPD over its second momentum argument and set the power $m = 0$. The validity of the number sum rule

given in equation (3.3) for a bare DPD then requires that

$$
\sum_g \sum_l \left(\delta_{a_2, f(l)} - \delta_{\overline{a_2}, f(l)} \right) \left(x_1 p^+ \right)^{-n_1} \left(p^+ \right)^{N(g)-2} \int \frac{\mathrm{d}^{D-2}k_1}{(2\pi)^{D-1}} \left(\prod_{i=2}^{N(g)} \frac{\mathrm{d}x_i\, \mathrm{d}^{D-2}k_i}{(2\pi)^{D-1}} \right)
$$

$$
\times \mathcal{G}_g^{a_1} (\{x\}, \{k\})\, \delta \left(1 - \sum_{i=1}^{M(g)} x_i \right)
$$

$$
\stackrel{!}{=} \left(N_{a_{2,v}} + \delta_{a_1, \overline{a_2}} - \delta_{a_1, a_2} \right) \sum_g \left(x_1 p^+ \right)^{-n_1} \left(p^+ \right)^{N(g)-2} \int \frac{\mathrm{d}^{D-2}k_1}{(2\pi)^{D-1}} \left(\prod_{i=2}^{N(g)} \frac{\mathrm{d}x_i\, \mathrm{d}^{D-2}k_i}{(2\pi)^{D-1}} \right)
$$

$$
\times \mathcal{G}_g^{a_1} (\{x\}, \{k\})\, \delta \left(1 - \sum_{i=1}^{M(g)} x_i \right) . \tag{3.48}
$$

This equality holds if it can be shown that

$$
\delta_{a_1, a_2} - \delta_{a_1, \overline{a_2}} + \sum_l \left(\delta_{a_2, f(l)} - \delta_{\overline{a_2}, f(l)} \right) \stackrel{!}{=} N_{a_{2,v}} , \tag{3.49}
$$

where a_2 denotes either a quark or an antiquark (such that $\overline{a_2}$ denotes either an antiquark or a quark, respectively). Here the sum over l on the left-hand side gives the number of partons with flavour a_2 crossing the final state cut in the PDF graph, minus the corresponding number of partons with flavour $\overline{a_2}$. If the observed parton a_1 in the PDF has flavour a_2 ($\overline{a_2}$), that number is increased (decreased) by 1. The result is obviously equal to the difference of partons with flavour a_2 and those with flavour $\overline{a_2}$ in the hadron, which is indeed $N_{a_{2,v}}$, concluding the proof for the number sum rule for bare distributions.

3.4.4. Momentum sum rule

In quite a similar manner as the number sum rule one can proceed in proving the momentum sum rule (3.2) for bare distributions by inserting the relation (3.44) into equation (3.43) with $m = 1$. One then finds that the momentum sum rule holds if

$$
\sum_g \sum_l \left(x_1 p^+ \right)^{-n_1} \left(p^+ \right)^{N(g)-2} \int \frac{\mathrm{d}^{D-2}k_1}{(2\pi)^{D-1}} \left(\prod_{i=2}^{N(g)} \frac{\mathrm{d}x_i\, \mathrm{d}^{D-2}k_i}{(2\pi)^{D-1}} \right)
$$

$$
\times x_l\, \mathcal{G}_g^{a_1} (\{x\}, \{k\})\, \delta \left(1 - \sum_{i=1}^{M(g)} x_i \right)
$$

$$
\stackrel{!}{=} (1 - x_1) \sum_g \left(x_1 p^+ \right)^{-n_1} \left(p^+ \right)^{N(g)-2} \int \frac{\mathrm{d}^{D-2}k_1}{(2\pi)^{D-1}} \left(\prod_{i=2}^{N(g)} \frac{\mathrm{d}x_i\, \mathrm{d}^{D-2}k_i}{(2\pi)^{D-1}} \right)
$$

$$
\times \mathcal{G}_g^{a_1} (\{x\}, \{k\})\, \delta \left(1 - \sum_{i=1}^{M(g)} x_i \right) . \tag{3.50}
$$

However, this just implies that the sum over the momentum fractions x_l of all partons crossing the final state cut in a PDF graph must be equal to $1 - x_1$, which is a direct consequence of momentum conservation such that also the momentum sum rule holds for bare distributions.

3.5. Validity of the sum rules after renormalisation

So far the considerations in this chapter have been limited to proving that the DPD sum rules are fulfilled by bare distributions obtained from the appropriate graphs, confirming the parton model interpretation of the DPD sum rules. However, this is not yet a complete proof, quite the contrary is actually the case, as the important issue of renormalisation has been neglected so far. As the twist-two operators in the PDFs and DPDs considered in the previous section contain short distance singularities which have to be renormalised, it is not directly clear that the sum rules are also fulfilled by renormalised distributions since it is known that the literal interpretation of PDFs as probability densities can be invalidated by renormalisation. This is most obvious for the positivity of the distributions, because one has to subtract terms that become infinite if the UV regulator is removed. In this section it will therefore be shown that renormalisation does not invalidate the sum rules if an appropriate renormalisation scheme – namely the $\overline{\text{MS}}$ scheme – is used.

3.5.1. Implementation of the $\overline{\text{MS}}$ scheme.

The derivations in the remainder of this chapter will be significantly simplified by using a particular implementation of the $\overline{\text{MS}}$ renormalisation scheme. Consider to this end first the definition of this scheme given in section 2.1.2 in close analogy to the presentation in section 3.2.6 of reference [47]. Using for the strong coupling $\alpha_s = g^2/(4\pi)$ rather than g, the relation between the bare and renormalised coupling given in equation (2.6) reads

$$\alpha_0 = \alpha_s \, \mu^{2\varepsilon} \left[1 + \sum_{n=1}^{\infty} \alpha_s^n \, S_\varepsilon^n \sum_{m=1}^{n} \frac{B_{nm}}{\varepsilon^m} \right] , \tag{3.51}$$

while a generic renormalisation factor as given in equation (2.7) is given by

$$Z = Z^{(0)} + \sum_{n=1}^{\infty} \alpha_s^n \, S_\varepsilon^n \sum_{m=1}^{M(n)} \frac{Z_{nm}}{\varepsilon^m} , \tag{3.52}$$

where the tree-level value $Z^{(0)}$ of the renormalisation factor is not important for the argument at hand. In the above equations the coefficients B_{nm} and Z_{nm} are naturally independent of ε. Note however, that Z and thus also $Z^{(0)}$ and Z_{nm} may depend

on additional variables like momentum fractions. The following arguments are valid regardless which of the two definitions of S_ε in equations (2.8) and (2.9) is chosen. In the implementation of the $\overline{\text{MS}}$ scheme defined above the counterterms in equations (3.51) and (3.52) contain finite parts that result from multiplying powers of $1/\varepsilon$ with matching powers of the expansion of S_ε.

As this is an undesirable feature in the discussion of the next two sections, a second renormalisation scheme is defined by

$$\alpha_0 = \alpha_s' \frac{\mu^{2\varepsilon}}{S_\varepsilon} \left[1 + \sum_{n=1}^{\infty} \alpha_s'^n \sum_{m=1}^{n} \frac{B_{nm}'}{\varepsilon^m} \right], \tag{3.53}$$

and

$$Z = Z^{(0)} + \sum_{n=1}^{\infty} \alpha_s'^n \sum_{m=1}^{M(n)} \frac{Z_{nm}'}{\varepsilon^m}, \tag{3.54}$$

where B_{nm}' and Z_{nm}' are again independent of ε. The counterterms in this scheme are pure poles in ε which will prove to be essential for the arguments in the following sections.

It will now be shown that the two schemes defined by equations (3.51), (3.52) and by equations (3.53), (3.54) give the same renormalised quantities at $\varepsilon = 0$. To this end a rescaled strong coupling is introduced as

$$\overline{\alpha}_s(\varepsilon) = \alpha_s'/S_\varepsilon, \tag{3.55}$$

such that equations (3.53) and (3.54) become

$$\alpha_0 = \overline{\alpha}_s(\varepsilon) \mu^{2\varepsilon} \left[1 + \sum_{n=1}^{\infty} \overline{\alpha}_s^n(\varepsilon) S_\varepsilon^n \sum_{m=1}^{n} \frac{B_{nm}'}{\varepsilon^m} \right], \tag{3.56}$$

and

$$Z = Z^{(0)} + \sum_{n=1}^{\infty} \overline{\alpha}_s^n(\varepsilon) S_\varepsilon^n \sum_{m=1}^{M(n)} \frac{Z_{nm}'}{\varepsilon^m}. \tag{3.57}$$

Consider now a renormalised quantity $R(\alpha_s, \varepsilon, B_{nm}, Z_{nm})$ in the first scheme and its counterpart $R'(\overline{\alpha}_s(\varepsilon), \varepsilon, B_{nm}', Z_{nm}')$ in the second scheme. The fact that equations (3.51) and (3.52) have the same functional form as equations (3.56) and (3.57) implies that the renormalised quantities in both schemes also have the same functional form

$$R'(\overline{\alpha}_s, \varepsilon, B_{nm}', Z_{nm}') = R(\overline{\alpha}_s, \varepsilon, B_{nm}', Z_{nm}'). \tag{3.58}$$

The counter term coefficients B_{nm} and Z_{nm} (B_{nm}' and Z_{nm}') are uniquely fixed by the requirement that renormalised quantities have no poles in ε when expanded in α_s and ε

(α_s' and ε). Since $\overline{\alpha}_s(\varepsilon)$ only differs from α_s' by terms of order $\mathcal{O}(\varepsilon)$, one must also obtain an expression without poles in ε when expanding R' in $\overline{\alpha}_s$ – rather than α_s' – and ε. One can thus conclude that the renormalisation coefficients in the two schemes are identical, this means $B_{nm} = B_{nm}'$ and $Z_{nm} = Z_{nm}'$, so that equation (3.58) implies

$$R'(\overline{\alpha}_s, \varepsilon, B_{nm}', Z_{nm}') = R(\overline{\alpha}_s, \varepsilon, B_{nm}, Z_{nm}) . \tag{3.59}$$

With $\overline{\alpha}_s(\varepsilon = 0) = \alpha_s'$ one thus finds that in the primed scheme the value of R' at the physical point is

$$\lim_{\varepsilon \to 0} R'(\overline{\alpha}_s, \varepsilon, B_{nm}', Z_{nm}') = R(\alpha_s', 0, B_{nm}, Z_{nm}) , \tag{3.60}$$

while in the original scheme, the value of R is

$$\lim_{\varepsilon \to 0} R(\alpha_s, \varepsilon, B_{nm}, Z_{nm}) = R(\alpha_s, 0, B_{nm}, Z_{nm}) \tag{3.61}$$

at the physical point. In order to show the equivalence of the two schemes consider now a case in which the renormalised quantity is an observable (for example the hadronic vacuum polarisation). In this case it must have the same value in the two schemes, and one can conclude that $\alpha_s' = \alpha_s$. From this observation follows that for any other quantity, including quantities that are not observables (such as renormalised PDFs or DPDs), the two schemes give the same result at the physical point $\varepsilon = 0$.

For the standard choice $S_\varepsilon = (4\pi e^{-\gamma_E})^\varepsilon$, the relation (3.53) takes the form of a minimal subtraction scheme with $\overline{\mu}^2 = \mu^2/(S_\varepsilon)^{1/\varepsilon} = \mu^2 e^{\gamma_E}/(4\pi)$. This way of implementing $\overline{\text{MS}}$ subtraction is in fact well known in the literature. The argument above illustrates that one can also use the implementation of (3.53) and (3.54) for different choices of S_ε. In the remainder of this work, this implementation will be used, omitting the primes on α_s, B_{nm} and Z_{nm}.

3.5.2. Number sum rule

With the preliminary work of the previous section it is now possible to prove that the DPD sum rules remain valid for renormalised distributions, starting with the DPD number sum rule. To this end one has to show that the difference

$$\Delta_{a_1 a_2} = \int_2 F_{a_1 a_{2,v}} - \left(N_{a_{2,v}} + \delta_{a_1, \overline{a_2}} - \delta_{a_1, a_2} \right) f_{a_1} \tag{3.62}$$

is zero. Here the shorthand notation for integrals over momentum fraction arguments introduced in section 2.2.2 has been used. Using the expression for the renormalised DPD given in equation (2.53) and the rules of computation from section 2.2.2, one can

express the first term on the right-hand side of the above equation in the following way

$$\int\limits_{2} F_{a_1 a_{2,v}} = \sum_{b_1, b_2} Z_{a_1, b_1} \otimes \int\limits_{1} \Big(Z_{a_{2,v}, b_2} \otimes \int\limits_{2} F_{B, b_1 b_2} \Big) + \sum_{b} \int\limits_{2} \Big(Z_{a_1 a_{2,v}, b} \otimes f_{B,b} \Big)$$

$$= \sum_{b_1, b_2} Z_{a_1, b_1} \otimes \int\limits_{1} Z_{a_{2,v}, b_2} \int\limits_{2} F_{B, b_1 b_2} + \sum_{b} \Big(\int\limits_{2} Z_{a_1 a_{2,v}, b} \Big) \otimes f_{B,b} , \qquad (3.63)$$

where parton indices and sums over parton indices have been kept explicit rather than using the shorthand notation of section 2.2.2 as this would make the following arguments unnecessarily complicated. The number sum rule for renormalised PDFs implies a sum rule for their renormalisation factors, which reads

$$\int Z_{a_{1,v}, a_0} = \int \Big(Z_{a_1, a_0} - Z_{\overline{a_1}, a_0} \Big) = \delta_{a_1, a_0} - \delta_{a_1, \overline{a_0}} , \qquad (3.64)$$

and for which a proof can for example be found in section 8.6 of reference [47]. Defining $\overline{a_1} = a_1$ for the case that $a_1 = g$ makes the above relation valid for all parton labels. Using the number sum rule for the PDF renormalisation factors introduced above and the number sum rule for the bare DPDs, the first term in equation (3.63) can thus be rewritten in the following manner

$$\sum_{b_1, b_2} Z_{a_1, b_1} \otimes \int\limits_{1} Z_{a_{2,v}, b_2} \int\limits_{2} F_{B, b_1 b_2} = \sum_{b_1} Z_{a_1, b_1} \otimes \int\limits_{1} \int\limits_{2} F_{B, b_1 a_{2,v}}$$

$$= \sum_{b_1} Z_{a_1, b_1} \otimes \Big(N_{a_{2,v}} + \delta_{b_1, \overline{a_2}} - \delta_{b_1, a_2} \Big) f_{B, b_1}$$

$$= N_{a_{2,v}} f_{a_1} + \sum_{b} \big(\delta_{b, \overline{a_2}} - \delta_{b, a_2} \big) Z_{a_1, b} \otimes f_{B,b} , \qquad (3.65)$$

where in the term proportional to $N_{i_{2,v}}$ the relation between bare and renormalised PDFs introduced in equation (2.46) has been used. Plugging the expressions from equations (3.63) and (3.65) into equation (3.62), this thus becomes

$$\Delta_{a_1 a_2} = \sum_{b} \Big(\int\limits_{2} Z_{a_1 a_{2,v}, b} \Big) \otimes f_{B,b} + \sum_{b} \big(\delta_{b, \overline{a_2}} - \delta_{b, a_2} \big) Z_{a_1, b} \otimes f_{B,b} - \big(\delta_{a_1, \overline{a_2}} - \delta_{a_1, a_2} \big) f_{a_1}$$

$$= \sum_{c} R_{a_1 a_2, c} \otimes f_c \qquad (3.66)$$

with

$$R_{a_1 a_2, c} = \sum_{b} \Big(\int\limits_{2} Z_{a_1 a_{2,v}, b} \Big) \otimes Z^{-1}_{b,k} - \sum_{b} \big(\delta_{a_1, \overline{a_2}} - \delta_{a_1, a_2} - \delta_{b, \overline{a_2}} + \delta_{b, a_2} \big) Z_{a_1, b} \otimes Z^{-1}_{b,c} . \quad (3.67)$$

In the last step of (3.66) the bare PDF has been expressed in terms of the renormalised one, using a inverse renormalisation factor as defined by equation (2.35). In the $\overline{\text{MS}}$

scheme as implemented in section 3.5.1, the perturbative expansions of Z_s and Z involve only pole terms in ε, and subsequently the same holds also for the inverse PDF renormalisation factor Z^{-1}. The tree-level part of $Z_{a_1,b}$ in (3.67) is proportional to $\delta_{a_1,b}$ such that it vanishes when multiplied with the combination of Kronecker symbols in parentheses. Therefore $R_k^{i_1 i_2}$ is a sum of pure pole terms in ε. On the other hand $\Delta^{i_1 i_2}$ is finite at $\varepsilon = 0$ by definition as on the right-hand side of equation (3.62) all quantities are already UV finite. From this one can conclude that all poles in $R_{a_1 a_2,c}$ have to cancel which means that $R_{a_1 a_2,c} = 0$ and consequently $\Delta^{i_1 i_2} = 0$, proving the number sum rule for renormalised DPDs.

The discussion above also implies that

$$\sum_c R_{a_1 a_2,c} \otimes Z_{c,b} = 0 \,, \tag{3.68}$$

which together with equation (3.67) yields the following number sum rule

$$\int_2 Z_{a_1 a_2,v,a_0} = \left(\delta_{a_1,\overline{a_2}} - \delta_{a_1,a_2} - \delta_{a_0,\overline{a_2}} + \delta_{a_0,a_2} \right) Z_{a_1,a_0} \tag{3.69}$$

for the $1 \to 2$ renormalisation factor of the splitting singularity.

3.5.3. Momentum sum rule

Using the same line of arguments as for the number sum rule one can proceed to show that also the momentum sum rule retains its validity for renormalised distributions. In this case one thus has to show that

$$\Delta^{a_1} = \sum_{a_2} \int_2 X_2 \, F_{a_1 a_2} - (1 - X_1) \, f_{a_1} \tag{3.70}$$

is zero. Here the first term on the right-hand side of this expression can again be rewritten using equation (2.53) and the rules for manipulating convolutions introduced in section 2.2.2, yielding

$$\sum_{a_2} \int_2 X_2 \, F_{a_1 a_2} = \sum_{a_2,b_1,b_2} Z_{a_1,b_1} \otimes_1 \int_2 X_2 \left(Z_{a_2,b_2} \otimes_2 F_{B,b_1 b_2} \right) + \sum_{a_2,b} \int_2 X_2 \left(Z_{a_1 a_2,b} \otimes_{12} f_{B,b} \right)$$

$$= \sum_{a_2,b_1,b_2} Z_{a_1,b_1} \otimes_1 \int X Z_{a_2,b_2} \int_2 X_2 \, F_{B,b_1 b_2}$$

$$+ \sum_{a_2,b} \left(\int_2 X_2 \, Z_{a_1 a_2,b} \right) \otimes_1 \left(X f_{B,b} \right) . \tag{3.71}$$

Just like in the case of the number sum rule discussed above one can again use that one can derive a momentum sum rule for the PDF renormalisation factors from the momentum sum rule for renormalised single-parton distributions, which reads

$$\sum_{a_1} \int X Z_{a_1,a_0} = 1 \tag{3.72}$$

for any a_0, as again shown for example in section 8.6 of Collins' book [47]. Using this and the momentum sum rule for bare DPDs, one can rewrite the first term in equation (3.71) in the following way

$$\sum_{a_2,b_1,b_2} Z_{a_1,b_1} \underset{1}{\otimes} \int X Z_{a_2,b_2} \int_2 X_2 F_{B,b_1 b_2} = \sum_{b_1,b_2} Z_{a_1,b_1} \underset{1}{\otimes} \int_2 X_2 F_{B,b_1 b_2}$$

$$= \sum_{b_1} Z_{a_1,b_1} \underset{1}{\otimes} \left[(1 - X) f_{B,b_1} \right] = f^{a_1} - \sum_{b} Z_{a_1,b} \underset{1}{\otimes} (X f_{B,b}) . \tag{3.73}$$

With these manipulations equation (3.70) then is given by

$$\Delta^{a_1} = \sum_{a_2,b} \left(\int_2 X_2 Z_{a_1 a_2,b} \right) \underset{1}{\otimes} (X f_{B,b}) - \sum_{b} Z_{a_1,b} \underset{1}{\otimes} (X f_{B,b}) + X_1 f_{a_1} . \tag{3.74}$$

Here the $X f_{B,b}$ terms can be rewritten as

$$X f_{B,b} = \sum_{c} X \left(Z_{b,c}^{-1} \otimes f_c \right) = \sum_{c} (X Z_{b,c}^{-1}) \otimes (X f_c) \tag{3.75}$$

using equation (2.40). Multiplying equation (2.35) with x and again using equation (2.40), one can easily see that $x Z_{a,b}^{-1}(x)$ is the inverse of $x Z_{a,b}(x)$ with respect to Mellin convolution and matrix multiplication. With this insight equation (3.70) can finally be written as

$$\Delta^{a_1} = \sum_{c} R_{a_1,c} \underset{1}{\otimes} (X f_c) \tag{3.76}$$

with

$$R_{a_1,c} = \sum_{b} \left[\sum_{a_2} \left(\int_2 X_2 Z_{a_1 a_2,b} \right) - (1 - X) Z_{a_1,b} \right] \underset{1}{\otimes} (X Z_{b,c}^{-1}) . \tag{3.77}$$

In this expression the the tree-level part of terms involving $Z_{a_1,b}(x)$ multiplied by $(1 - X)$ vanishes as $Z_{a_1,b}^{(0)}(x)$ is proportional to $\delta(1 - x)$, such that in the implementation of the $\overline{\text{MS}}$ scheme discussed in section 3.5.1 $R_{a_1,c}$ is again a sum of pure pole terms in ε. Since Δ^{a_1} is finite at $\varepsilon = 0$, one must then have $R_{a_1,c} = 0$ and hence $\Delta^{a_1} = 0$, implying that also the momentum sum rule remains valid for renormalised distributions.

Here one can again derive a momentum sum rule for the $1 \to 2$ renormalisation factors using

$$\sum_{c} R_{a_1,c} \otimes (X Z_{c,b}) = 0 \tag{3.78}$$

and equation (3.77), which then reads

$$\sum_{a_2} \int_2 X_2 Z_{a_1 a_2,b} = (1 - X_1) Z_{a_1,b}. \tag{3.79}$$

3.6. DPD evolution and its consequences

As seen already in section 2.2.2 the renormalisation of the splitting singularity results in an additional inhomogeneous term in the evolution equation for renormalised momentum space DPDs – as can be seen in equation (2.56) – which at leading order in α_s has been known for a long time, see for example references [78, 79]. Using the all-order formulation of DPD renormalisation worked out in the previous section 3.5 one can show how the all-order form of the inhomogeneous evolution equation presented in equation (2.56) can be derived. Differentiating equation (2.53) with respect to the renormalisation scale and making use of the fact that bare distributions are independent of the renormalisation scale μ, one obtains

$$\frac{\mathrm{d}F_{a_1 a_2}(\Delta; \mu)}{\mathrm{d}\ln \mu^2} = \left[\left(\frac{\mathrm{d}Z(\mu)}{\mathrm{d}\ln \mu^2} \underset{1}{\otimes} Z(\mu) + Z(\mu) \underset{1}{\otimes} \frac{\mathrm{d}Z(\mu)}{\mathrm{d}\ln \mu^2} \right) \underset{2}{\otimes} F_B(\Delta) \right]_{a_1 a_2}$$
$$+ \left[\frac{\mathrm{d}Z_s(\mu)}{\mathrm{d}\ln \mu^2} \underset{12}{\otimes} f_B \right]_{a_1 a_2}, \tag{3.80}$$

where the shorthand notation for parton indices introduced in section 2.2.2 has been used in order to keep the presentation as concise as possible. Using the renormalisation scale dependence of the PDF renormalisation factors given in equation (2.49) the above equation can be rewritten in the following form

$$\frac{\mathrm{d}F_{a_1 a_2}(\Delta; \mu)}{\mathrm{d}\ln \mu^2} = \left[\left(P(\mu) \underset{1}{\otimes} Z(\mu) \underset{1}{\otimes} Z(\mu) + Z(\mu) \underset{1}{\otimes} P(\mu) \underset{2}{\otimes} Z(\mu) \right) \underset{2}{\otimes} F_B(\Delta) \right]_{a_1 a_2}$$
$$+ \left[\frac{\mathrm{d}Z_s(\mu)}{\mathrm{d}\ln \mu^2} \underset{12}{\otimes} f_B \right]_{a_1 a_2}$$
$$= \left[P(\mu) \underset{1}{\otimes} F(\Delta; \mu) + P(\mu) \underset{2}{\otimes} F(\Delta; \mu) \right]_{a_1 a_2}$$
$$+ \left[\left(\frac{\mathrm{d}Z_s(\mu)}{\mathrm{d}\ln \mu^2} - P(\mu) \underset{1}{\otimes} Z_s(\mu) - P(\mu) \underset{2}{\otimes} Z_s(\mu) \right) \underset{12}{\otimes} f_B \right]_{a_1 a_2}. \tag{3.81}$$

In order to transform the expression in the last line into the the form presented in equation (2.56) a $1 \to 2$ evolution kernels $P_{a_1 a_2,a_0}(x_1, x_2; \mu)$ associated with the splitting singularity in DPDs is defined:

$$P_{a_1 a_2,a_0} = \left[\left(\frac{\mathrm{d}Z_s(\mu)}{\mathrm{d}\ln \mu^2} - P(\mu) \underset{1}{\otimes} Z_s(\mu) - P(\mu) \underset{2}{\otimes} Z_s(\mu) \right) \underset{12}{\otimes} Z^{-1} \right]_{a_1 a_2,a_0}, \tag{3.82}$$

which is equivalent to

$$\frac{dZ_{a_1 a_2, a_0}(\mu)}{d\ln\mu^2} = [P(\mu) \underset{1}{\otimes} Z_s(\mu) + P(\mu) \underset{2}{\otimes} Z_s(\mu) + P_s(\mu) \underset{12}{\otimes} Z(\mu)]_{a_1 a_2, a_0}, \qquad (3.83)$$

which finally yields the following all-order form of the inhomogeneous double DGLAP equation for renormalised momentum space DPDs at arbitrary order in perturbation theory

$$\frac{dF_{a_1 a_2}(\Delta;\mu)}{d\ln\mu^2} = [P(\mu) \underset{1}{\otimes} F(\Delta;\mu) + P(\mu) \underset{2}{\otimes} F(\Delta;\mu) + P_s(\mu) \underset{12}{\otimes} f(\mu)]_{a_1 a_2}, \qquad (3.84)$$

which was already presented in section 2.2.2 as equation (2.56). The above result confirms the form given for NLO evolution in equation (16) of reference [91]. Comparing equation (3.83) to equation (3.84) one easily sees that the renormalisation factor for the splitting singularity satisfies the same form of evolution equation as the renormalised DPD, in analogy to the situation for PDFs and PDF renormalisation factors for which the renormalisation scale dependence is given by equations (2.48) and (2.49), respectively.

Equations (3.80) to (3.84) are valid in $D = 4 - 2\varepsilon$ dimensions, and whenever the left-hand side of an equation is finite for $\varepsilon \to 0$ it is understood that this limit is taken. With the implementation of the $\overline{\text{MS}}$ scheme introduced in section 3.5.1, renormalisation factors contain only pure pole terms in ε, plus an ε independent tree-level term in the case of Z (but not of Z_s). As a result of this the evolution kernels P and P_s do not depend on ε. These evolution kernels must be finite for $\varepsilon \to 0$ which implies that they cannot contain any poles in ε and any terms with a positive power of ε would induce positive powers of ε on the right-hand side of equation (2.49) or equation (3.83). It can be shown that such terms cannot appear by considering the renormalisation scale derivative in D dimensions, given by

$$\frac{d}{d\ln\mu^2} = \left[\beta(\alpha_s(\mu)) - \varepsilon\alpha_s(\mu)\right]\frac{\partial}{\partial\alpha_s(\mu)}, \qquad (3.85)$$

which implies that there are only terms of order ε^n with $n \le 0$ on the left-hand side (and thus also on the right-hand side) of equations (2.49) and (3.83).

It is thus possible to extract the kernel P_s from equation (3.82) by isolating the term of order ε^0 on the right-hand side of said equation. The only term of this order in ε is contained within the renormalisation scale derivative of the Z_s renormalisation factor (convoluted with the tree-level term of Z^{-1}) and arises from the ε dependent part of the renormalisation scale derivative given above multiplying the ε^{-1} pole of $\partial_{\alpha_s} Z_s$. One thus finds that P_s is given by

$$P_{a_1 a_2, a_0}(x_1, x_2; \alpha_s(\mu)) = -\alpha_s(\mu)\frac{\partial}{\partial\alpha_s(\mu)}\left[Z_{a_1 a_2, a_0}(x_1, x_2; \alpha_s(\mu), \varepsilon)\right]_{-1}, \qquad (3.86)$$

where $[\ldots]_k$ denotes coefficient of the ε^k term of the Laurent series of the quantity enclosed in square brackets. Using the same line of arguments one can also express P in terms of the PDF renormalisation factor Z

$$P_{a_1 a_0}\left(x; \alpha_s(\mu)\right) = -\alpha_s(\mu)\, \frac{\partial}{\partial \alpha_s(\mu)} \left[Z_{a_1 a_0}\left(x; \alpha_s(\mu), \varepsilon\right)\right]_{-1}. \tag{3.87}$$

Combining these relations with the number and momentum[5] sum rules for the $1 \to 2$ renormalisation factor Z_s given in equations (3.69) and (3.79), one readily obtains corresponding sum rules

$$\int\limits_0^{1-x_1} \mathrm{d}x_2\, P_{a_1 a_{2,v}, a_0}(x_1, x_2) = \left(\delta_{a_1, \overline{a_2}} - \delta_{a_1, a_2} - \delta_{a_0, \overline{a_2}} + \delta_{a_0, a_2}\right) P_{a_1 a_0}(x_1), \tag{3.88}$$

$$\sum_{a_2} \int\limits_0^{1-x_1} \mathrm{d}x_2\, x_2\, P_{a_1 a_2, a_0}(x_1, x_2) = (1 - x_1) P_{a_1 a_0}(x_1) \tag{3.89}$$

for the $1 \to 2$ evolution kernels, where momentum fractions have been given explicitly instead of using the compact notation of section 2.2.2, making the similarity with the sum rules for DPDs and $1 \to 2$ renormalisation factors more obvious.

Since the derivation of the sum rules for renormalised DPDs in section 3.5 did not depend on any particular value of the renormalisation scale μ it is valid independently of the renormalisation scale. One can thus – as a consistency check – use the all-order form of DPD evolution given in equation (3.84) and the sum rules stated above to verify that the DPD sum rules of equations (3.2) and (3.3) are stable under a change of the renormalisation scale, implying that the renormalisation scale derivative of their left-hand side is equal to the renormalisation scale derivative of their right-hand side.

Consider to this end first the DPD number sum rule. Using again the compact notation introduced in section 2.2.2, the renormalisation scale derivative of the left-hand side of equation (3.3) can be written as

$$\frac{\mathrm{d}}{\mathrm{d} \ln \mu^2} \int_2 F_{a_1 a_{2,v}}(\mathbf{\Delta}; \mu) = \sum_{b_1} P_{a_1 b_1}(\mu) \underset{1}{\otimes} \int_2 F_{b_1 a_{2,v}}(\mathbf{\Delta}; \mu) + \sum_{b_2} \int_2 P_{a_{2,v} b_2}(\mu) \int_2 F_{a_1 b_2}(\mathbf{\Delta}; \mu)$$

$$+ \sum_b \left(\int_2 P_{a_1 a_{2,v}, b}(\mu)\right) \underset{1}{\otimes} f_b(\mu). \tag{3.90}$$

Note that the shorthand notation for parton indices has not been used in order to keep the arguments as clear as possible. Here one can perform further simplifications by

---

[5] We note that the momentum sum rule given in equation (3.89) has the same form as a corresponding sum rule derived in [92, 93] for "two-body inclusive decay probabilities", see equation (49) in reference [93]. These quantities were introduced to describe the evolution of hadronic jets. From the results presented in chapter 5 one can see that the two types of functions start to differ at order α_s^2.

applying the DPD sum rule at scale μ to the first term and the number sum rule of equation (3.88) for the $1 \to 2$ evolution kernel to the last term. The second term in the above expression is zero due to the number sum rule

$$\int P_{a_1,v a_0} = 0 \tag{3.91}$$

for the DGLAP evolution kernels, which readily follows from equations (3.64) and (3.87). With this equation (3.90) can be rewritten as follows

$$\frac{d}{d \ln \mu^2} \int_2 F_{a_1 a_{2,v}}(\boldsymbol{\Delta}; \mu) = \sum_{b_1} P_{a_1 b_1} \underset{1}{\otimes} \left(N_{a_{2,v}} + \delta_{b_1,\overline{a_2}} - \delta_{b_1,a_2} \right) f_{b_1}$$

$$+ \sum_{b} \left(\delta_{a_1,\overline{a_2}} - \delta_{a_1,a_2} - \delta_{b,\overline{a_2}} + \delta_{b,a_2} \right) P_{a_1 b} \underset{1}{\otimes} f_b$$

$$= \left(N_{a_{2,v}} + \delta_{a_1,\overline{a_2}} - \delta_{a_1,a_2} \right) \sum_{b} P_{a_1 b} \underset{1}{\otimes} f_b , \tag{3.92}$$

where on the right-hand side one immediately recognises the sum multiplying the parentheses as the derivative $df_{a_1}/d \ln \mu^2$ and thus the appropriate derivative of the right-hand side of the DPD number sum rule given in equation (3.3). This nicely illustrates the stability of the number sum rule under a change of the renormalisation scale μ.

In order to show the same for the momentum sum rule, one can proceed in full analogy, starting with

$$\frac{d}{d \ln \mu^2} \sum_{a_2} \int_2 X_2 F a_1 a_2(\boldsymbol{\Delta}; \mu) = \sum_{b_1} P_{a_1 b_1}(\mu) \underset{1}{\otimes} \sum_{a_2} \int_2 X_2 F_{b_1 a_2}(\boldsymbol{\Delta}; \mu)$$

$$+ \sum_{b_2,a_2} \int_2 X P_{a_2 b_2}(\mu) \int_2 X_2 F_{a_1 b_2}(\boldsymbol{\Delta}; \mu)$$

$$+ \sum_{b,a_2} \left(\int_2 X_2 P_{a_1 a_2,b}(\mu) \right) \underset{1}{\otimes} \left(X f_b(\mu) \right) . \tag{3.93}$$

Here the second term on the right-hand side is zero due to the momentum sum rule

$$\sum_{a_1} \int X P_{a_1 a_0} = 0 \tag{3.94}$$

for the DGLAP kernels, which can be derived from equations (3.64) and (3.87). Equation (3.93) can be simplified by applying the DPD momentum sum rule at scale μ to the first term on its right-hand side and the relation from equation (3.89) to the last

term such that one obtains the following expression

$$
\frac{\mathrm{d}}{\mathrm{d}\ln\mu^2} \sum_{a_2} \int_2 X_2\, F_{a_1 a_2}(\boldsymbol{\Delta};\mu) = \sum_{b_1} P_{a_1 b_1}(\mu) \underset{1}{\otimes} \left[(1-X)\, f_{b_1}(\mu)\right]
$$
$$
+ \sum_{b} \left[(1-X)\, P_{a_1 b}(\mu)\right] \underset{1}{\otimes} \left(X f_b(\mu)\right)
$$
$$
= \sum_{b} P_{a_1 b}(\mu) \underset{1}{\otimes} f_b(\mu) - \sum_{b} \left(X P_{a_1 b}(\mu)\right) \underset{1}{\otimes} \left(X f_b(\mu)\right)
$$
$$
= (1-X_1) \sum_{b} P_{a_1 b}(\mu) \underset{1}{\otimes} f_b(\mu)\,, \tag{3.95}
$$

where in the last step the relation given in equation (2.40) has been used. Here the last line of the above equation can again be identified as is the renormalisation scale derivative of the right-hand side of the DPD momentum sum rule given in equation (3.2), as required. It should be pointed out that the inhomogeneous term in the double DGLAP equation is essential for the preceding arguments to work. For leading-order evolution, this was already emphasised in references [40, 94].

4. Sum rule improved position space DPD models

4.1. Introduction

As stated already in the introduction of chapter 3, what motivated the proof that the DPD sum rules are valid in full QCD was the idea to use them to construct improved position space DPD models which can be used within the DGS framework to calculate DPS cross sections. The necessity for this arises due to the fact that the original GS09 DPDs are $\boldsymbol{\Delta} = 0$ momentum space distributions which cannot be transformed to position space as this would require the complete $\boldsymbol{\Delta}$ dependence to be known yet. The reason why the GS09 DPDs are defined at $\boldsymbol{\Delta} = 0$ is simply the fact that this is where the sum rules are valid. Using the DPD sum rules as a guidance to improve position space DPDs is thus not a straightforward task as it requires a connection between position space DPDs and their momentum space counterpart at $\boldsymbol{\Delta} = 0$. For the bare distributions such a relation is already given in equation (2.24) which however no longer holds for renormalised DPDs as discussed in some detail in section 2.2.2 and in particular is divergent in $D = 4$ dimensions where one would naturally define a DPD model. A possible solution to this issue is to absorb the cut-off function $\Phi(y\nu)$ introduced in the factorised cross section in equation (2.58) into the definition of the individual DPDs $F_\Phi(y)$ as indicated by the subscript Φ. With this cut-off Fourier transforming momentum space DPDs to position space is straightforward, especially for $\boldsymbol{\Delta} = 0$ where it is tantamount to integrating the position space distributions over y. However, these position space DPDs $F_\Phi(\boldsymbol{\Delta} = 0)$ are not quite the distributions for which the validity of the DPD sum rules has been shown in the previous chapter due to different regularisation of the splitting singularity. Fortunately the differences between distributions where the splitting singularity is treated using the $\overline{\text{MS}}$ scheme, denoted by $F_{\overline{\text{MS}}}(\boldsymbol{\Delta} = 0)$ and those where the cut-off $\Phi(y\nu)$ is used to this end arises only from the region of very small y where the DPDs can be calculated perturbatively as shown in equation (2.52). This makes it possible to derive a matching equation between $F_{\overline{\text{MS}}}(\boldsymbol{\Delta} = 0)$ on one hand and $F_\Phi(\boldsymbol{\Delta} = 0)$ on the other hand.

In this chapter it will be shown how the DPD sum rules can be used to construct a sum rule improved position space DPD model at leading order in the strong coupling. The general procedure employed here applies also for higher order DPD models. However, at the time this project was started the NLO kernel of the perturbative

splitting contribution in equation (2.52) (which will be presented in chapter 5) has not been known, restricting the analysis to LO. As a first step in this direction a discussion of the matching relation mentioned above will be given in section 4.2.1. Before actually using the sum rules to construct improved DPDs, some requirements a DPD model should fulfil are discussed in section 4.2.2 where also the explicit form of the DPD model used as a starting point in the following sections is presented and motivated. Some technical details – in particular about the implementation of numerics – are given in section 4.2.3 before finally moving on to the stepwise improvement of the initial model in section 4.3. Following this the impact of renormalisation scale evolution and of the choice of the cut-off scale ν on the degree to which the sum rules are fulfilled is examined in section 4.4. The results of the project discussed in this chapter are currently being prepared for publication [95].

4.2. Specific theory

Some preliminary considerations are in place before moving on to the actual task of constructing sum rule improved DPD models. In particular the matching between the F_Φ and $F_{\overline{\text{MS}}}$ DPDs has to be considered as well as the general ansatz for a position space DPD model. Furthermore details about the numerical implementation of the evolution of DPDs as well as of the Fourier transformation to position space and the subsequent matching will be discussed in this subsection.

4.2.1. From position space DPD models to $\Delta = 0$ momentum space DPDs

As mentioned already in the introduction of this chapter it is necessary to perform a matching between the momentum space DPDs obtained from the DPD model by integrating over the whole y range with a cut-off function $\Phi(y\nu)$ and the ones where the splitting singularity is regularised using dimensional regularisation and renormalised using the $\overline{\text{MS}}$ scheme. To this end one makes use of the fact that the two schemes differ only in the treatment of the splitting singularity such that differences between $F_\Phi(\Delta = 0)$ and $F_{\overline{\text{MS}}}(\Delta = 0)$ arise only from the region of very small transverse distances y. In this regime the position space DPDs are dominated by the perturbative splitting contribution introduced in equation (2.52) and can be calculated in perturbation theory. At leading order – to which the analysis in this chapter is restricted – this has been calculated in section 3.2 of reference [35] and is given by

$$
\begin{aligned}
&F_{a_1 a_2, \text{spl,pt}}(x_1, x_2, \boldsymbol{y}; \mu) \\
&= \frac{\mu^{2\varepsilon}}{y^{2-4\varepsilon}} \frac{\Gamma^2(1-\varepsilon)}{\pi^{1-2\varepsilon}} \frac{f_{a_0}(x_1 + x_2; \mu)}{x_1 + x_2} \frac{\alpha_s(\mu)}{2\pi} P_{a_1 a_2, a_0}\left(\frac{x_1}{x_1 + x_2}, \varepsilon\right),
\end{aligned}
\tag{4.1}
$$

where the $P_{a_1 a_2, a_0}$ are the $D = 4 - 2\varepsilon$ dimensional generalisation of the kernels computed in section 5.2.2 of reference [26] which agree with the expressions for $P^{n \neq 4}$ in section 3 of reference [96] and read:

$$P_{gg,g}(x, \varepsilon) = 2C_A \left[\frac{x}{1-x} + \frac{1-x}{x} + x(1-x) \right],$$

$$P_{q\bar{q},g}(x, \varepsilon) = T_F \frac{x^2 + (1-x)^2 - \varepsilon}{1 - \varepsilon},$$

$$P_{qg,q}(x, \varepsilon) = C_F \left[\frac{1 + x^2}{1-x} - \varepsilon(1-x) \right]. \tag{4.2}$$

Note that at LO the splitting contribution is a simple product of a PDF and a $1 \to 2$ splitting kernel rather than a convolution as indicated in equation (2.52). This is due to the fact that at LO the $1 \to 2$ splitting kernels contain a delta function which renders the convolution integral trivial. Since in the small y regime the perturbative splitting is the dominant contribution to the position space DPDs the matching between $F_\Phi(\Delta = 0)$ and $F_{\overline{\text{MS}}}(\Delta = 0)$ can be calculated using equation (4.1) and yields

$$F_{\overline{\text{MS}}, a_1 a_2}(x_1, x_2, \Delta; \mu) - F_{\Phi, a_1 a_2}(x_1, x_2, \Delta; \mu, \nu)$$
$$= \left[\ln \frac{\mu^2}{\nu^2} + \frac{P'_{a_1 a_2, a_0}(v, 0)}{P_{a_1 a_2, a_0}(v, 0)} \right] \frac{f^{a_0}(x; \mu)}{x} \frac{\alpha_s(\mu)}{2\pi} P_{a_1 a_2, a_0}(v, 0) + \mathcal{O}\left(\frac{\Delta^2}{\nu^2} \right) + \mathcal{O}(\alpha_s^2), \tag{4.3}$$

where $P'_{a_1 a_2, a_0}(v, 0)$ denotes the partial derivative of $P_{a_1 a_2, a_0}(v, \varepsilon)$ with respect to ε, evaluated at $\varepsilon = 0$ and furthermore the variables $x = x_1 + x_2$ and $v = x_1/(x_1 + x_2)$ have been used to keep the presentation concise. In section 5.4 this matching equation will be generalised to higher orders and the NLO matching kernels can be derived from the results in section 5.6.

As the $\overline{\text{MS}}$ momentum space DPDs do not depend on the cut-off scale ν the matching term should exactly cancel the ν dependence of the cut-off momentum space DPDs which is however not the case for the LO matching as this still leaves higher order terms that are uncancelled. In section 4.4 this remnant ν dependence will be discussed in some detail as this contains valuable information on the size of the higher order contributions neglected in equation (4.3).

4.2.2. Initial DPD model

With these preliminaries sorted out it is time to consider which requirements a first ansatz for a position space DPD model should fulfil and how this can be used to motivate what will finally be used as a starting point from which a sum rule improved DPD model can be constructed.

The analysis in reference [35] suggests that it is reasonable to divide a DPD into an "intrinsic" non-perturbative part and a perturbative "splitting" part, the latter of

which can be calculated in perturbation theory for small y as mentioned already in the discussion around equation (2.52). While for the splitting contribution this gives a pretty precise idea already how this part could be modelled, the situation is much less clear for the intrinsic part where such perturbative input is missing. It therefore makes sense to retreat for this intrinsic part to a model that in similar form has been used in many prior works on DPDs and in particular in the original work on the DPD sum rules by Gaunt and Stirling [45]:

$$F_{a_1 a_2, \text{int}}(x_1, x_2, \boldsymbol{y}; \mu_0, \mu_0) = \frac{1}{4\pi h_{a_1 a_2}} \exp\left[-\frac{y^2}{4h_{a_1 a_2}}\right] f_{a_1}(x_1; \mu_0) f_{a_2}(x_2; \mu_0)$$
$$\times (1 - x_1 - x_2)^2 (1 - x_1)^{-2} (1 - x_2)^{-2}. \quad (4.4)$$

The basic idea that a collinear DPD can be approximated by a product of two collinear PDFs and a spatial profile function is commonly used, and in fact also leads to the well known – but also controversial – pocket formula for the DPS cross section of references [97, 98]. In order to arrive at such a factorised form one assumes that the partons inside a hadron are completely uncorrelated which would allow to express a DPD as a convolution of two impact parameter PDFs (GPDs) as discussed in section 2.1.5 of reference [26]:

$$F_{a_1 a_2}(x_1, x_2, \boldsymbol{y}; \mu_1, \mu_2) = \int d^2\boldsymbol{b}\, f_{a_1}(x_1, \boldsymbol{b} + \boldsymbol{y}; \mu_1) f_{a_2}(x_2, \boldsymbol{b}; \mu_2). \quad (4.5)$$

Furthermore assuming that these impact parameter PDFs also factorise and can be expressed in terms of collinear single parton distributions and a Gaussian impact parameter profile in the following way

$$f_a(x, \boldsymbol{b}; \mu) = \frac{1}{4\pi h_a} f_a(x; \mu) \exp\left[-\frac{b^2}{4h_a}\right], \quad (4.6)$$

the convolution integral in equation (4.5) can be calculated analytically and results in a Gaussian with a width that is the sum of the single particle widths, $h_{a_1 a_2} = h_{a_1} + h_{a_2}$ with the appropriate normalisation of equation (4.4). For the single particle widths the expression from section 4.1 of reference [99] evaluated at a fixed x value of 10^{-3} is used which gives the following values

$$h_g = 2.33\,\text{GeV}^{-2}, \qquad\qquad h_q = h_{\bar{q}} = 3.53\,\text{GeV}^{-2}. \quad (4.7)$$

In addition to this simple product of PDFs and a $\boldsymbol{y}$ profile function furthermore a so called phase-space factor is introduced in accordance with reference [45]. Here the factor $(1 - x_1 - x_2)^2$ guarantees that the DPD smoothly vanishes as $x_1 + x_2 \to 1$ as is required for physical DPDs. Furthermore this also mirrors the fact that finding a parton with momentum fraction x_1 reduces the probability to find a second one with momentum fraction $x_2 \sim 1 - x_1$. However, as this suppresses the DPD rather too strongly along the lines where one of the momentum fractions approaches zero this factor is again divided by $(1 - x_1)^2(1 - x_2)^2$ in order to achieve that in the vicinity of

these lines the the phase-space factor reduces to 1. Such a behaviour is desirable as in the case where only one momentum fraction is large, while the other one is small one expects a smaller suppression than in the case where both momentum fractions become large. As already mentioned above the perturbative result for the splitting contribution given in equation (4.1) and to which the DPD should reduce for small values of y can be used as guidance for modelling the splitting contribution and one can thus make the following ansatz

$$F_{a_1 a_2, \text{spl}}(x_1, x_2, \boldsymbol{y}; \mu_y, \mu_y)$$
$$= \frac{1}{\pi y^2} \exp\left[-\frac{y^2}{4h_{a_1 a_2}}\right] \frac{f_{a_0}(x_1 + x_2; \mu_y)}{x_1 + x_2} \frac{\alpha_s(\mu_y)}{2\pi} P_{a_1 a_2, a_0}\left(\frac{x_1}{x_1 + x_2}\right), \qquad (4.8)$$

which is basically just the perturbative result multiplied by a damping term to suppress the large y region where the splitting can be expected to be negligible. Out of convenience and for a lack of a more intuitive choice the same Gaussian y profile used already in the ansatz for the intrinsic part in equation (4.4) has been used here. A particularly important detail here is that the PDF has to be evaluated at a y-dependent scale $\mu_y \sim 1/y$ to ensure that the scale is appropriate for the splitting considered. In particular the specific y dependence of μ which is used in the following is given by

$$\mu_y = \frac{b_0}{y^*}, \qquad\qquad y^* = \frac{y}{\sqrt{1 + y^2/y_{\text{max}}^2}}. \qquad (4.9)$$

where the y^* prescription ensures that the PDF in the splitting part is never evaluated at too low scales, even for very large values of y where a perturbative description is no longer reliable. The transition between the regime where $\mu_y \sim 1/y$ and the one where it tends towards a value μ_{min} is governed by the value of the parameter y_{max} for which a value of $0.5 \, \text{GeV}^{-1}$ has been chosen according to a study of TMDs in reference [100] where the similar b^* prescription is used.

As this is only an initial ansatz which shall be improved using the DPD sum rules in section 4.3 one has to ask in which ways the initial model can be modified in order to achieve a better agreement with the sum rules. As mentioned before the initial choice for the intrinsic part is motivated by the assumption of completely uncorrelated partons, which is of course a rather strong assumption that may be valid at very low momentum fractions x_1 and x_2 but certainly should be doubted for larger values. These assumptions have already been relaxed a bit by introducing the phase-space factor and in theory nothing forbids to completely disregard the factorized ansatz for the intrinsic part for something else. In practice, however, it is rather difficult to find other, more appropriate, models as unfortunately the genuine non-perturbative nature of the intrinsic part means that unlike for the splitting part one cannot gain any knowledge about it from perturbation theory. In the future one might hope to be able to use results from lattice QCD as a guidance to model the intrinsic part but at present this is not yet possible such that it is most reasonable to stick with the factorized ansatz presented in equation (4.4). Of course this does not mean that there are no modifications of the

current model for the intrinsic part possible – quite the contrary is the case, one is free to modify it at will, the non-trivial part is only finding the correct, or suitable, modifications. As the PDFs used as building blocks are basically the only experimental input in the model introduced above it makes sense to refrain from modifying these and rather focus on the phase-space factor and the y profile.

For the splitting contribution, the situation is, as indicated earlier, quite different, as there one can actually calculate the small y form in perturbation theory, which imposes the constraint that any ansatz for the splitting part should for small y, meaning for $y \ll 1/\Lambda$, where Λ is a generic hadronic scale, recover the perturbative result. For large values of y deviations from this perturbative result are of course allowed as perturbation theory, which comes with uncertainties of order $\mathcal{O}(y\Lambda)$ fails to converge for large y. Within these uncertainties the ansatz for the splitting contribution can be modified at will which was already used in the initial ansatz where the Gaussian damping factor has been introduced and it will be used again to show how one can in a systematic manner achieve a better agreement with the sum rules.

Having laid out what can actually be modified about the model introduced above leads to the important question which requirements a sensible DPD model should fulfil. Of course the main aim is to construct DPDs fulfilling the sum rules to the best degree possible, however, this should not be forced at any price as it would also be preferable that the modifications should be physically motivated. Besides this an analytical expression for the final model is desirable.

4.2.3. Technical details and numerics

Before actually studying the proposed DPD model with the help of the sum rules and modifying it in order to achieve a better agreement with said sum rules, a brief discussion of some of the more technical details is in place. In order to check how well the sum rules are fulfilled for a given DPD model one first has to produce a grid containing the values of the DPDs for discrete values of the momentum fractions x_1 and x_2, the interparton distance y, as well as the renormalisation scale μ. The next step is then to Fourier transform to $\Delta = 0$ momentum space DPDs which is tantamount to integrating over y. As the splitting singularity in such a numerical integration is most straightforwardly regularized using a cut-off one then has to, as discussed in section 4.2.1, match onto $\overline{\text{MS}}$ momentum space DPDs according to equation (4.3). For these $\overline{\text{MS}}$ momentum space DPDs one can then finally perform the sum rule integrals to check how well the sum rules are fulfilled for the model under consideration.

For the PDFs in equations (4.4) and (4.8) a slightly modified version of the LO MSTW08 PDF set introduced in reference [101] is used. In particular the initial s_v distribution is set to zero and a modification term given in equation (3.11) of reference [45] is added to the $\bar{d}$ distribution. The reason for this is that for some values of the momentum fraction x the $\bar{s}$ and $\bar{d}$ distributions in the MSTW08 PDF set become very slightly negative, which

is in principle not allowed for LO PDFs which can be interpreted as probability densities. In the case of SPS calculations, however, this may be neglected, as the absolute size of the distributions is only very small when they become negative – namely $\bar{s}, \bar{d} \geq -0.00005$. For LO DPDs, which also admit an interpretation as probability densities, on the other hand this is not acceptable. This can be understood when one considers the case that one parton in equation (4.4) is $\bar{s}$ or $\bar{d}$ with a momentum fraction such that the corresponding PDF is slightly negative. If now the PDF corresponding to the second parton becomes large, for example for small momentum fractions, the resulting DPD may also become of non-negligible size *and* negative. Since this has to be avoided the above modifications were suggested in reference [45].

As the sum rules have to be evaluated at a fixed scale μ one thus also has to to evolve the splitting DPDs at each value of y in the grid to this fixed scale which requires a numerical implementation of the homogeneous double DGLAP equation which is furthermore also needed to check how well the sum rules are fulfilled at higher scales, away from the starting scale. The production of the DPD grids is performed using a version of the code first used in the original work on the DPD sum rules [45] which has been modified in reference [35] to incorporate the y dependence which is missing in the original GS09 DPD set and where the the appropriate homogeneous dDGLAP evolution has been implemented. With this code DPD grids in the momentum fractions x_1 and x_2, the interparton distance y, and the renormalisation scale μ are produced. Note again that equal scale DPDs are used as is appropriate for the evaluation of the sum rules. This also has the pleasant side effect that one has to deal with lower dimensional and thus substantially smaller grid files. For this study the number of flavours has been restricted to $n_f = 3$ as this leads to substantially smaller DPD grids compared to $n_f = 5$, while still being able to study the general features of the DPDs.

Rather than producing grids that are equally spaced in the momentum fractions x_1 and x_2 following the example of references [35, 45] grids equidistant in the variables $u_i = \ln(x_i/(1 - x_i))$ are produced resulting in a grid that is evenly spaced in $\ln x_i$ for small values of x_i where the DPDs grow rapidly and approximately equally spaced in x_i for larger values of the momentum fractions where the DPDs are generally smaller and vary slower with changes in the momentum fractions x_i. The produced grids consist of 89 grid points in each x_i direction with the smallest and largest x_i values being $x_{\min} = 5 \times 10^{-5}$ and $x_{\max} = 1 - x_{\min}$. As the evolution equation (2.51) is a differential equation in $t = \ln \mu^2$ it is a natural choice to make the grid equidistant in t rather than μ such that one can avoid dealing with varying step sizes during the evolution. In the μ direction the grids contain 51 points. Note that the smallest μ value in the grids is furthermore fixed by the value of the parameter $y_{\max}$ used in the y^* prescription of equation (4.9) as $\mu_{\min}$ has to be slightly larger than $\mu_{y \to \infty} = \frac{b_0}{y_{\max}}$. This is due to technical limitations since it is not possible to evolve from lower scales with the DPD evolution code. The largest value for the renormalisation scale in the grid has been chosen as $\mu_{\max} = 172 \, \text{GeV}$, which is large but not too large. The points in y space are chosen such that they correspond to grid points in μ as this makes the evaluation of

the splitting part simpler and faster by avoiding the need for additional evolution. In addition to the grid points corresponding to the μ grid points the grid furthermore contains additional points for small y values, and in the case of the splitting part also for large values, resulting in 60 points in the y direction for the intrinsic part and 90 points for the splitting part. The actual evolution to different scales is performed using a fourth-order Runge-Kutta algorithm and the evolution basis, described for example in section 4.3 of reference [102]. For more detail about the numerical evolution see also section 4.1 and Appendix A of the original sum rule paper [45].

In order to arrive at the $\Delta = 0$ momentum space DPDs one has to integrate the DPDs numerically over y with the splitting singularity regulated using the cut-off function $\Phi(\nu y)$ introduced in reference [35] and discussed in some detail in section 2.2.3. For convenience and in order to avoid large logarithms in the matching equation (4.3) the cut-off scale ν is set equal to the renormalisation scale μ with the exception of section 4.4 where the dependence of the $\overline{\text{MS}}$ momentum space DPDs on the cut-off scale is analysed. At this point it is instructive to consider briefly how the actual y integration for the intrinsic and splitting contributions is performed as the situation is quite different in these two cases. In the intrinsic model the y dependence is strictly multiplicative in the sense that the only dependence on y is due to the Gaussian profile function, and while under evolution DPDs mix with other DPDs due to successive parton splittings, the final profile is still reasonably well approximated by a superposition of Gaussians of different widths. Thus the y integration can for the intrinsic part be performed in a way that may be described as "semi-analytically" by fitting the y grid points to a superposition of three Gaussians with widths h_{qq}, h_{qg}, and h_{gg}. For these Gaussians it is then straightforward to perform the integration from ν^{-1} to ∞ analytically. Unfortunately the situation is not as favourable for the splitting part as there the initialisation scale μ_y depends on y. In order to arrive at a given fixed renormalisation scale μ at which the y integration and subsequently also the sum rule integrals shall be performed the splitting DPD has to be evolved from μ_y to μ for each y grid point. As this means that for every point in y one has to evolve for a different amount to arrive at μ the y dependence is thus no longer strictly multiplicative and the y integration has to be performed numerically as the approach used for the intrinsic part is bound to fail here. However, this is not totally straightforward either, as the grid is rather coarsely spaced for large y which leads to a decrease in accuracy. Therefore the production code has been modified as mentioned before to increase the number of grid points for large values of y making it possible to perform the y integration also in this case with sufficient precision.

After this the next step is the matching onto $\overline{\text{MS}}$ $\Delta = 0$ momentum space DPDs according to equation (4.3) which is however straightforward to implement. It should be noted here that even at this point the intrinsic and splitting part, as well as the matching part, are kept separate in order to be able to keep track of how much each individual part contributes to the overall DPD. The actual sum rule integrals of equations (3.3) and (3.2) are then also straightforward to perform numerically and at this point it makes sense to briefly comment on how the results are visualised.

Following the example of reference [45] the results are presented as what is there referred to as sum rule ratios, meaning the sum rule integral divided by the PDF quantity it should equal, namely

$$\rho(x_1) = \frac{\int dx_2\, F_{a_1 a_{2,v}}(x_1, x_2; \mu)}{\left(N_{a_{2,v}} + \delta_{a_1, \overline{a_2}} - \delta_{a_1, a_2}\right) f_{a_1}(x_1; \mu)}\,, \quad \rho(x_1) = \frac{\sum_{a_2} \int dx_2\, x_2\, F_{a_1 a_2}(x_1, x_2; \mu)}{(1 - x_1) f_{a_1}(x_1; \mu)}\,, \quad (4.10)$$

for the number sum rule and momentum sum rules, respectively. Note that the integration boundaries omitted here are understood to be as in equations (3.2) and (3.3). The reason for plotting this ratio rather than the difference between the two is that it has the major advantage that it makes it possible to easily read of the relative deviations which are more interesting than absolute deviations. This is due to the fact that for small momentum fraction x_1 even huge absolute deviations may amount for only minor relative deviations as in this regime DPDs tend to be very large. On the other hand, however, this also means that very small absolute deviations may lead to huge relative deviations for large x_1 which is why large relative deviations for $x_1 \gtrsim 0.8$ are of no great concern. In the following section these sum rule ratios will be plotted for the lowest scale in the grid as there one can naturally expect the sum rules to be most sensitive to changes in the model. To be able to read of how much each part – intrinsic, splitting, and matching – contributes to a given sum rule these parts will be plotted separately, along with their sum, in a single plot, as seen for example in figure 4.1. This makes it possible to extract valuable information about which part one needs to modify in which way in order to achieve a better agreement with the sum rules. In section 4.4.1 the sum rule ratios will also be plotted for different scales in order to study how the agreement with the sum rules changes under evolution. Finally in section 4.4.2 it will be studied how well the ν dependence of the DPDs cancels at the considered order in perturbation theory.

4.3. Refining the DPD model

Having discussed the theoretical background and technical details in the previous section one now has everything at hand to actually study how well the sum rules are fulfilled for different modifications of the initial DPD model and how exactly these changes impact the agreement with the sum rules.

4.3.1. Initial DPD model

Consider first the initial DPD model suggested in equations (4.4) and (4.8). As this ansatz is only a first – although physically motivated – guess it is not expected to fulfil the sum rules all too well and it will now be discussed which features of this initial model are already as desired and where there are still deficiencies. The most striking

result is certainly that the momentum sum rules are already surprisingly well fulfilled as can be seen from the plots in figure 4.1. Here it should be noted that not the full

(a) u momentum sum rule

(b) g momentum sum rule
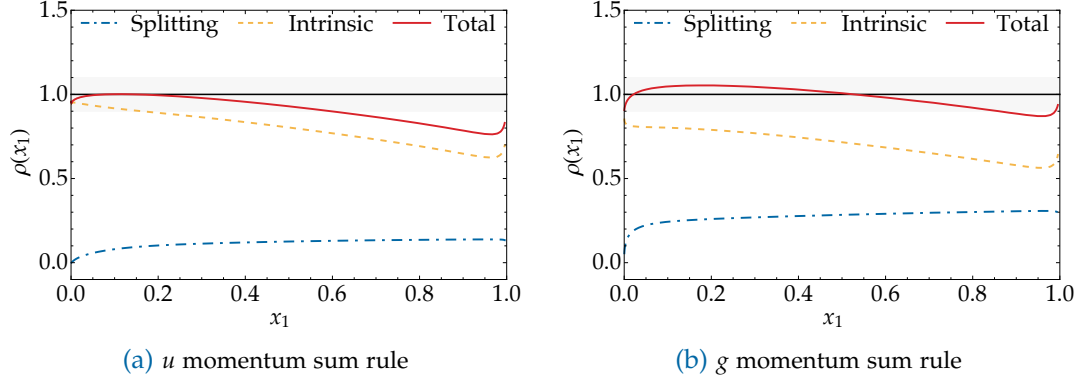
Figure 4.1.: g and u momentum sum rule ratios for the initial, unmodified, model at the scale $\mu_{\min} = 2.25\,\text{GeV}$. In these plots the individual contributions from the intrinsic and splitting parts, as well as their sum have been plotted. For convenience the $\pm 10\%$ deviations are indicated by a light grey band. When not shown explicitly the contribution from the matching term is negligible such that it is not shown in order to avoid cluttering the plots. The remaining plots in this section will follow this example unless explicitly stated otherwise.

set of plots is shown but rather only a few representative ones which nicely illustrate general features, and if this is not possible the plots with the best and worst agreements with the sum rules will be presented. An interesting feature of the momentum sum rules is the large contribution they get from the splitting part as illustrated in figure 4.1. The different size of the splitting contribution is rather easily explained if one considers which DPDs can be produced by LO splittings, namely $q\bar{q}$, qg, $\bar{q}g$ (and of course gq and $g\bar{q}$), and gg. There are thus $2n_f + 1$ different DPDs in the g momentum sum rule which get a sizeable splitting contribution while for the u momentum sum rule there are just 2 DPDs with a large splitting contribution, $u\bar{u}$ and ug. This explains why the splitting contribution to the g sum rule is rather large compared to the one for the u sum rule. However, there are furthermore also differences between the impact of the splitting contributions for different quark momentum sum rules, for example the $\bar{u}$ and $\bar{d}$ momentum sum rules have larger contributions from splitting than the ones for u and d for which splitting contributions are comparable in size. This is can be explained by the fact that u and d PDFs are large compared to $\bar{u}$ and $\bar{d}$ PDFs, such that for the former the intrinsic part is larger, also in comparison to the splitting contribution. Another rather interesting feature of figure 4.1 is the relatively small size of the matching contribution which can be explained by the choice $\nu = \mu$ which will be discussed more thoroughly in section 4.4.2.

At this point a comment on the power that has been chosen for the phase space factor introduced in equation (4.4) is appropriate as this may up to now seem rather ad hoc. In some of the earlier works on DPDs, for example in references [103–106], a simple $(1 - x_1 - x_2)$ factor has been suggested, motivated using the Kutti-Weiskopf model of

reference [107] and the recombination model discussed in reference [108], and more recent works, in particular reference [109], suggested that a $(1 - x_1 - x_2)^2$ factor is appropriate while even higher powers of this suppression factor should be appropriate according to a generalisation of the Brodsky-Farrar quark counting rules, discussed in references [110, 111], to DPDs. The powers of $(1 - x_1)$ and $(1 - x_2)$ of course have to be chosen to match that of $(1 - x_1 - x_2)$ for the phase space factor to exhibit the desire behaviour as discussed below equation (4.7). In order to figure out which choice actually leads to the best agreement with the sum rules it has been studied how well the sum rules are fulfilled for different powers n which leads to the conclusion that the best agreement is achieved for $n = 2$ as can be seen in figures 4.1b and 4.2.

(a) $n = 1$ g momentum sum rule
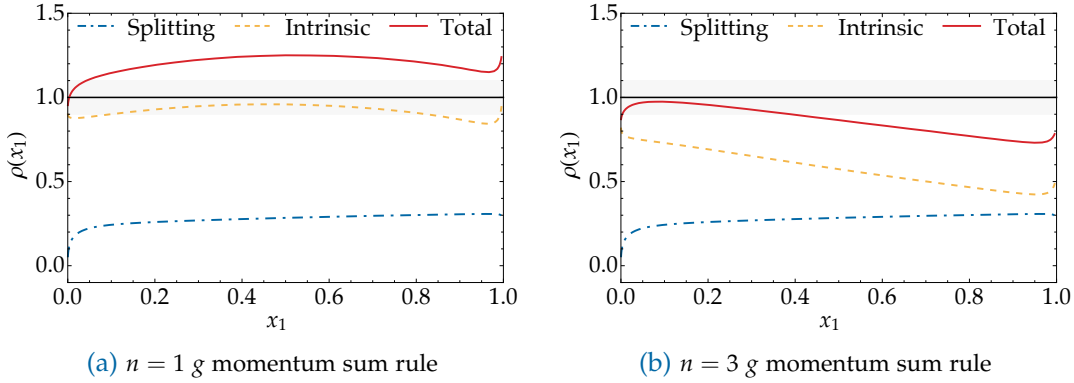
(b) $n = 3$ g momentum sum rule

Figure 4.2.: Sum rule ratio plots of the g momentum sum rule ratio for different powers of the phase space factor in the intrinsic part of the initial model in equation (4.4). The sum rule ratio for $n = 2$ is shown in figure 4.1b.

The reason why the number sum rules have not been taken into consideration for this evaluation is that they are badly violated regardless which power of the phase space factor is used, the reasons for which as well as possible solutions will now be elaborated on. As can be seen in figure 4.3 the sum rule ratio drops significantly below 1 with increasing x_1 for u_v and d_v number sum rules hinting at a rather too strong suppression due to the phase space factor for large momentum fractions. This deficiency of the phase space factor was already noted in reference [45] where also a possible solution to this issue was suggested which will be discussed – and implemented – in the next iteration of the DPD model in the following subsection. Even though the number sum rules are badly violated it is still a positive sign that already without this modification the sum rule ratios are close to one for small values of x_1 where the DPDs tend to be largest. However, there is unfortunately also an exception to this rule in the case of the uu_v number sum rule for which the sum rule ratio is close to two for small x_1 which can be explained by the fact that so far what has been referred to as number effects in the original sum rule paper [45] have not been taken into account. It is only natural to expect that finding a valence quark of a given flavour reduces the probability to find a second valence quark of the same flavour. For example in the proton finding a u

(a) du_v number sum rule

(b) gd_v number sum rule
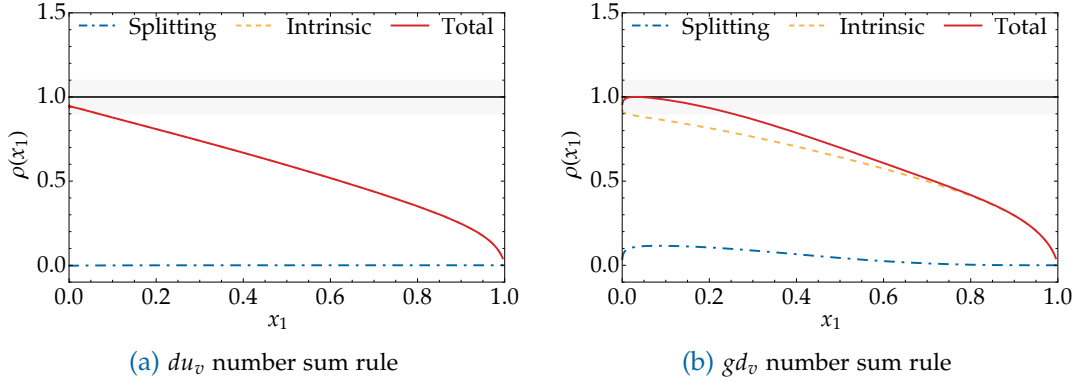
Figure 4.3.: Mixed flavour number sum rules ratios for the initial model exhibiting a strong decrease with increasing momentum fraction x_1. A possible solution to this is to modify the phase space factor in the intrinsic part of the model.

valence quark reduces the probability to find a second one by 50% while finding a d valence quark means that the probability to find a second one vanishes.

An exception to the aforementioned strong decrease for larger momentum fractions x_1 pose the equal flavour number sum rules, meaning uu_v, $\bar{u}u_v$, $\bar{d}d_v$, ss_v, which get a large contribution from the splitting part as can be seen in figure 4.4 and will be discussed now.

(a) uu_v number sum rule

(b) $\bar{d}d_v$ number sum rule
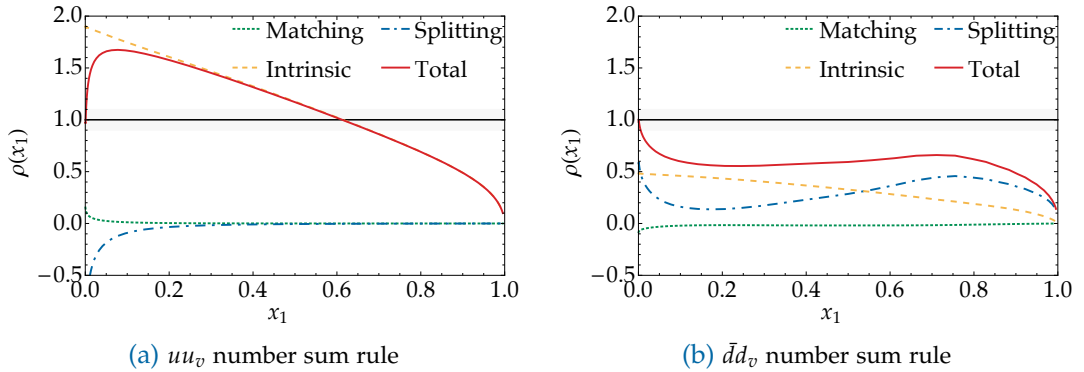
Figure 4.4.: Equal flavour number sum rules ratios for the initial model for which the decrease with increasing momentum fraction x_1 is less pronounced as in the mixed flavour case as these DPDs get a non-negligible splitting contribution.

The reason why these sum rules do get a comparatively large contribution becomes clear when one looks at how splitting valence DPDs are defined

$$F_{qq_v,\text{spl}} = F_{qq,\text{spl}} - F_{q\bar{q},\text{spl}} \approx -F_{q\bar{q},\text{spl}} .\tag{4.11}$$

The approximation in the last step is justified as $q\bar{q}$ DPDs are directly produced at LO via $g \to q\bar{q}$ splitting whereas qq DPDs are not directly produced by LO splitting but

rather emerge in the splitting sector only due to mixing under evolution. Due to this sizeable contribution from the splitting part the sum rule ratios for the equal flavour number sum rules exhibit a noticeably weaker decrease with increasing momentum fraction x_1 as the splitting part is not affected by the phase space factor. This effect is most pronounced for the ss_v number sum rule where the intrinsic contribution vanishes completely as in the modified LO MSTW08 PDF set used for the PDFs in equations (4.4) and (4.8) the s and $\bar{s}$ PDFs are identical. Another rather distinct feature of these equal flavour number sum rule is that the corresponding sum rule ratios exhibit a rather "curvy" behaviour compared to the ones that get no large contribution from the splitting part which is something that will be revisited in subsection 4.3.4.

4.3.2. Modified phase space factor and number effect subtractions

In the first iteration of the DPD model introduced in section 4.2.2 and studied in the previous section the main concern is the bad agreement with the number sum rules discussed above. In this section it will be shown how these deficiencies can be improved by implementing the modifications hinted at in the prior subsection. First of all appropriate subtractions are performed to take into account the aforementioned number affects which is rather straightforward. The stark decrease of the number sum rule rations for larger x_1 values was already encountered in reference [45] where a – unfortunately not physically motivated – solution to this issue has been proposed by making the global phase space factor $\rho(x_1, x_2)$ parton species dependent in the following way

$$\rho^{a_1 a_2}(x_1, x_2) = (1 - x_1 - x_2)^2 (1 - x_1)^{-2 - \alpha(a_2)} (1 - x_2)^{-2 - \alpha(a_1)}, \qquad (4.12)$$

with

$$\alpha(a) = \begin{cases} 0 & \text{if } a \text{ is a sea parton,} \\ 0.5 & \text{if } a \text{ is a valence parton.} \end{cases} \qquad (4.13)$$

After these modifications have been implemented in equation (4.4) one finds that the agreement of the DPD model with the momentum sum rules – which was already pretty good to begin with – has further improved such that for most of the x_1 range the relative deviations are less then 10% as illustrated in figure 4.5 The by far more interesting question, however, is how much these modifications of the phase space factor and the number effect subtractions effect the agreement with the number sum rules. Looking at the uu_v number sum rule in figure 4.6a one immediately sees that both the number effect subtractions and the modified phase space factor had the desired effect even though the suppression is still rather too strong for increasing x_1. This behaviour can also be observed for all other u_v number sum rules whereas the situation is significantly better for the d_v number sum rules, suggesting that maybe a further modification of the phase space factor with different powers $\alpha(u_v)$ and $\alpha(d_v)$ might lead

(a) u momentum sum rule

(b) g momentum sum rule
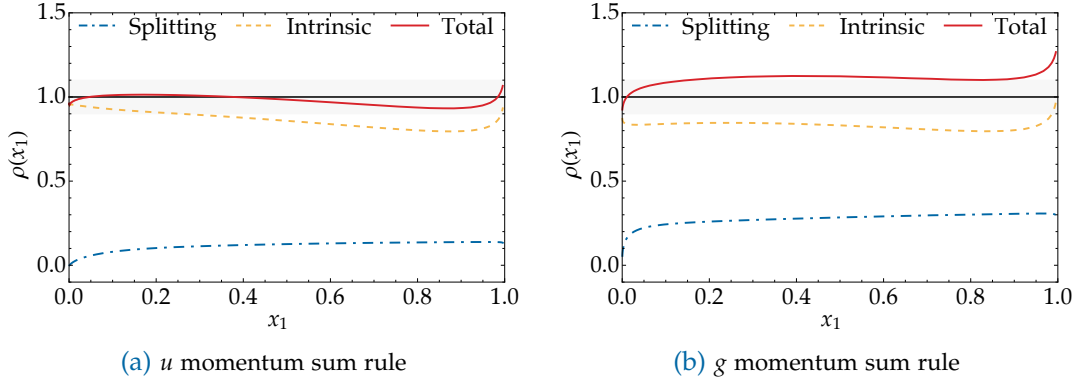
Figure 4.5.: Momentum sum rule ratios for the first iteration of the model with a modified phase space factor. With this modification the suppression for large x_1 has successfully been decreased.

(a) uu_v number sum rule

(b) gd_v number sum rule
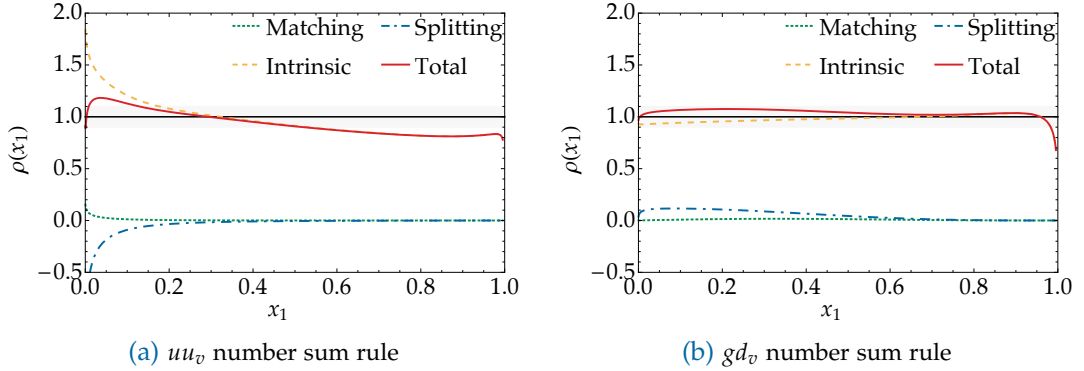
Figure 4.6.: Equal and mixed flavour number sum rule ratio plots for the first iteration of the initial model. Comparing these to figures 4.3 and 4.4 it is obvious that the modifications of the phase space factor as well as the number effect subtractions had the desired effect.

to an even better agreement with the number sum rules. With the modified phase space factor the shortcomings associated with the equal flavour number sum rules become even more apparent and it will shortly be discussed how these may be addressed. While the number effect subtractions are indeed physically motivated the only motivation for the modified phase space factor was that it achieves the intended goal, namely improve the agreement with the number sum rules. One is thus free to choose these modified powers at will and this has been done in the next iteration of the model in the following section.

4.3.3. Fine tuning the modified phase space factor

As a next step a parameter scan over $\alpha(u_v)$ and $\alpha(d_v)$ around their initial value of 0.5 has been performed in order to determine the ideal combination of modified powers for which the best possible agreement with the sum rules is achieved. Since this leads

to a rather large number of different DPD sets one has to compare in order to find the one with the best agreement with the sum rules this raises the interesting question whether one can define a measure that makes it possible to objectively compare how well different DPD models fulfil the sum rules. While this may sound like a rather simple question with a seemingly obvious answer this issue is unfortunately not as straightforward as as it seems. For example, one has to make a decision whether one wants to reduce absolute or relative deviations which would probably lead to quite different results as absolute deviations are generically largest for small x_1 values while they become comparably small for larger x_1 values. As the aim is that the final DPD models fulfil the sum rules reasonably well for all but the largest x_1 values it makes most sense to minimize relative deviations rather than absolute ones.

In order to define a measure for the relative deviations one can then take the following:

$$\delta = \int\limits_{x_{\min}}^{0.8} \mathrm{d}x_1 \, |\rho(x_1) - 1| \, , \tag{4.14}$$

where ρ is the sum rule ratio under consideration, defined in equation (4.10). This measures the average deviation of the sum rule ratio from its ideal value of 1 between $x_{\min}$ and 0.8. Here 0.8 has been chosen as the upper boundary instead of $x_{\max}$ since – as mentioned earlier – large relative deviations for large x_1 values are no major concern. With this measure one can then in an automated way pick out the combination of powers $\alpha(u_v)$ and $\alpha(d_v)$ which minimizes the total relative deviation of all sum rules. Another possible approach to define such a measure would be to take again the absolute value of the difference between the actual value of the sum rule ratio and its ideal value of one but instead of integrating it over x_1 sum the value of it at each x_1 grid point again up to $x_1 = 0.8$. As the DPD grid introduced in section 4.2.3 is rather dense for small x_1 values this results in a measure that puts more emphasis on the small x_1 region where DPDs are naturally expected to be large, making this method somewhat intermediate between the previous one and a measure which reduces the absolute deviations. Both of the measures defined above have been used to analyse the data from the parameter scan and both approaches returned the same values for the modified powers $\alpha(u_v)$ and $\alpha(d_v)$. While this may seem surprising at first this could actually be anticipated as for small x_1 the differences between the models with different powers are not very pronounced such that even for the measure putting emphasis on the small x_1 region the actual difference between different models arises from the medium to large x_1 regime. The results of this parameter scan are illustrated in figure 4.7 which yields the following modified powers:

$$\alpha(a) = \begin{cases} 0 & \text{if } a \text{ is a sea parton,} \\ 0.63 & \text{if } a \text{ is a } u_v \text{ parton,} \\ 0.49 & \text{if } a \text{ is a } d_v \text{ parton.} \end{cases} \tag{4.15}$$
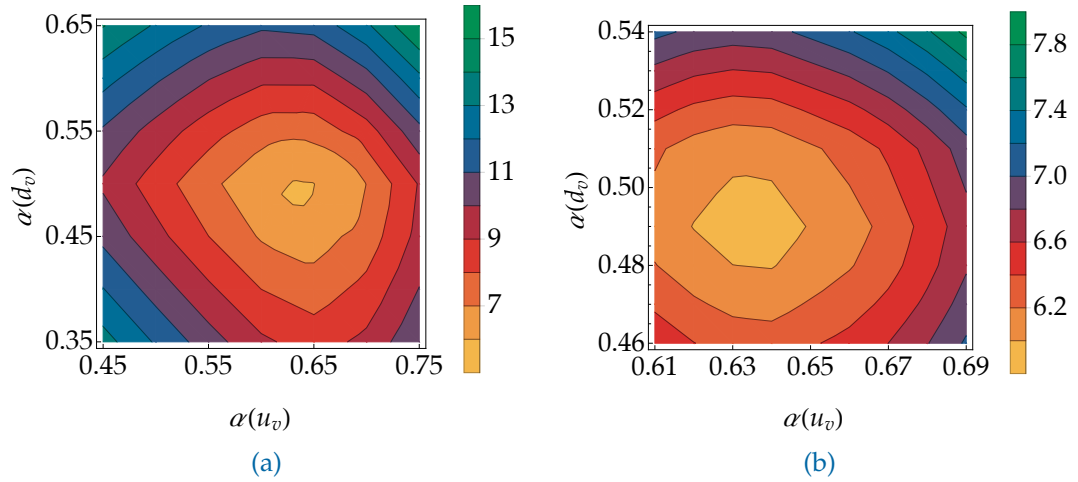
Figure 4.7.: Illustration of the average deviations per sum rule in per cent, depending on the combination of modified powers $\alpha(u_v)$ and $\alpha(d_v)$. The values in this plot correspond to the first measure defined above. In subfigure 4.7a the complete range over which the powers were modified is shown, whereas in subfigure 4.7b a small subset of this where the deviations are smallest is presented.

In what follows it will be discussed how this effects the sum rule ratios and as in the previous sections again the momentum sum rules are considered first, which remain largely unchanged as can be seen by comparing figures 4.5 and 4.8 which are very similar with only a slightly worse agreement in figure 4.8. For the number sum rules,
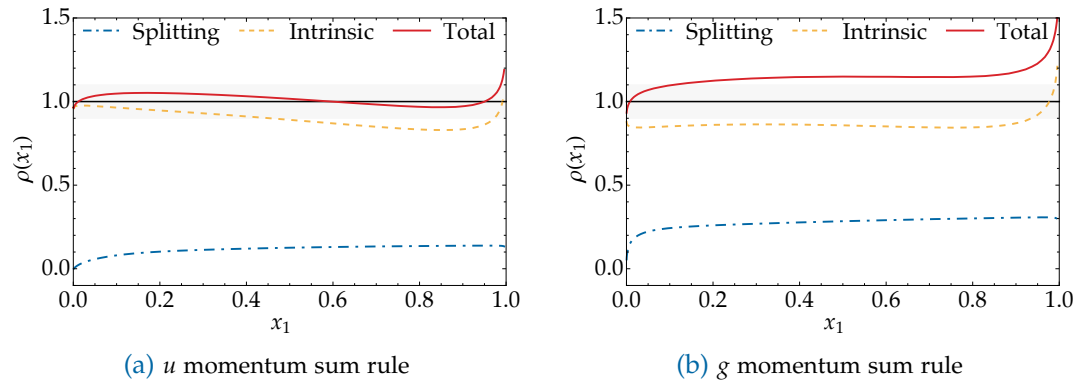
Figure 4.8.: Sum rule ratio plots for the g and u momentum sum rules after the second iteration of the phase space factor.

however, the situation is of course different and one finds a definite improvement for the u_v sum rules, as can be seen in figure 4.9a, while the d_v sum rules remain basically unchanged which comes as no surprise as the ideal value of $\alpha(d_v) = 0.49$ is very close to the initial value of 0.5 used before. Here it should be pointed out that the agreement

(a) uu_v number sum rule

(b) du_v number sum rule
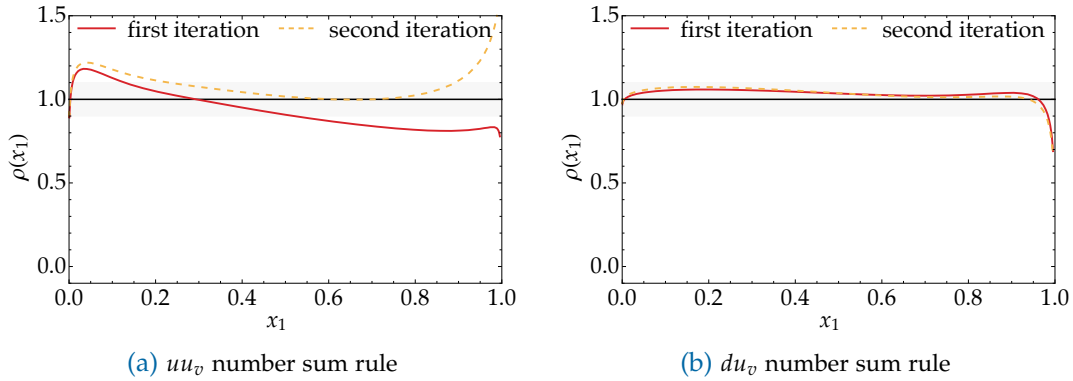
Figure 4.9.: Illustration of the difference between the number sum rule ratios for the first and second iteration of the phase space factor. Here the individual contributions have not been plotted since this is not needed, as the only part that changes compared to figure 4.6 is the intrinsic contribution, and this would just clutter the plots.

actually gets significantly worse for the u_v number sum rules for $x_1 \gtrsim 0.9$, but as mentioned earlier already this is not too great of a concern and can be accepted in return for a better agreement at smaller x_1 values.

The experience with the parameter scan over the powers of the modified phase space factor raised the question as to whether it is possible to find other parameters in the DPD model which could be tuned in much the same way. Possible candidates for such an endeavour are the parameter y_{max} regulating the transition from the $1/y$ behaviour of μ_y to a constant value as well as the widths of the Gaussian damping factor, $h_{a_1 a_2}$. While the initial values for these parameters may be physically motivated they are nevertheless not set in stone as they are used in a context which is not exactly the same as the one for which these values have been originally derived. Therefore parameter scans have been performed also for these parameters, varying them about their initial values, with the result that the sum rules are not very sensitive to changes of these parameters unless one goes far away from their initial, physically motivated, values and even then the agreement with the sum rules worsens rather than improves. The values that give the best agreement with the sum rules according to these parameter scans are in close vicinity of the ones used initially such that it makes most sense to stick with these as they are at least vaguely physically motivated. It is actually not too surprising that the agreement with the sum rules is not too strongly dependent on the widths of the Gaussian damping term. For the intrinsic part the y integration is actually normalised to 1 if one integrates over all of y and does not impose a lower cut-off, such that there – even when using a cut-off – one should not expect a very strong dependence on the choice of the widths $h_{a_1 a_2}$. For the splitting contribution the situation is a bit less straightforward as there the y integration is not normalised to 1, but there one can argue that the damping affects mostly the large y contribution whereas due to the splitting singularity the major contribution to the integral comes from the region of small y such that one again can expect that the dependence on the

exact choice of $h_{a_1 a_2}$ is not too pronounced. In the next step the large y behaviour of the splitting part will be modified which will put more emphasis on this region, such that this statement is no longer strictly valid. Nevertheless these initial values for the parton widths will be used also there, as they provides a reasonable starting point.

4.3.4. Modifying the splitting contribution

At this point the only sum rules still not fulfilled to a decent degree are the equal flavour number sum rules which – as already mentioned before – receive a large contribution from the $g \to q\bar{q}$ splitting. So far the modifications only affected the intrinsic part, leaving the splitting part untouched. However, at this point one has to start thinking about modifying the ansatz for the splitting part, as any modification to the intrinsic part that would improve the situation with the equal flavour number sum rules would most likely lead to a decreased agreement with all other sum rules. To this end one first has to consider what exactly can be modified about the splitting ansatz and what features are fixed by the result from perturbation theory. As mentioned in earlier in section 4.2.2 the small y behaviour of the splitting can be calculated in perturbation theory, with the LO result given in equation (4.1) and the NLO results presented in chapter 5, reliably for $y \ll \frac{1}{\Lambda}$ with deviations of order $\mathcal{O}(y\Lambda)$ where Λ is a generic hadronic scale. Therefore in the small y region the ansatz for the splitting part has to approach the perturbative result and consequently the only thing that can be modified about the splitting ansatz is its large y behaviour – within the accuracy of perturbation theory, of course. While it is thus obviously possible to modify the splitting part, this actually raises more questions than it answers as now one has to figure out which modifications lead to the desired result. The most straightforward option is probably to add a modification term to the initial ansatz that only contributes for large values of y which is for example achieved by the following approach

$$\tilde{F}_{a_1 a_2, \mathrm{spl}}(x_1, x_2, \boldsymbol{y}; \mu_y, \mu_y) = F_{a_1 a_2, \mathrm{spl,pt}}(x_1, x_2, \boldsymbol{y}; \mu_y, \mu_y) \exp\left[\frac{y^2}{4h_{a_1 a_2}}\right]$$

$$\times \left[1 + \left(\exp\left[\frac{y^2}{4h^*_{a_1 a_2}}\right] - 1\right) g_{a_1 a_2}(x_1, x_2)\right], \quad (4.16)$$

where $h^*_{a_1 a_2} > h_{a_1 a_2}$ which results in a weakened damping in the modification term and $g_{a_1 a_2}(x_1, x_2)$ is an a priori unknown function for which the only constraint is that it should be symmetric under exchange of partons 1 and 2 in order to guarantee that

$$F_{a_1 a_2}(x_1, x_2, \boldsymbol{y}; \mu) = F_{a_2 a_1}(x_2, x_1, \boldsymbol{y}; \mu). \quad (4.17)$$

The widths $h^*_{a_1 a_2}$ are chosen such that the deviations from the perturbative result stay within the perturbative uncertainties and also such that the double particle widths can again be written as the sum of single particle widths. To ensure positivity of the resulting modified DPD model one has to require $g > 0$. Whenever the approach

outlined below returned non-positive functions g it has been checked explicitly that this does not violate positivity. As the main goal at this point is to improve the agreement with the equal flavour number sum rules which requires modifications of the $g \to q\bar{q}$ splitting, all other modification terms are set to zero for now. Note also that in the following different modifications are allowed for the splitting to different quark flavours in order to be able to fulfil the different equal flavour number sum rules to the best degree possible.

The reason why such a factorized form of the x_1, x_2, and y dependence has been chosen for the modification term is that this is the only way in which one can determine at least the function $g_{a_1 a_2}(x_1, x_2)$ in a systematic manner as will discussed now. As the final goal is to fulfil the sum rules to the best degree possible one can require that the sum rules should be fulfilled by the modified model and subsequently solve the sum rules for $g_{a_1 a_2}(x_1, x_2)$. What makes this rather non-trivial is again the fact that the splitting part is initialised at a y dependent scale which means that in order to actually use the DPDs with the sum rules one first has to evolve for each y grid point for a different amount to arrive at a given fixed scale μ at which the sum rules are evaluated. However, this unfortunately destroys the factorized form of the modification term in equation (4.16) as evolution mixes $g_{a_1 a_2}(x_1, x_2)$ with the splitting kernel $P_{a_1 a_2, a_0}$ and the PDF f_{a_0} in equation (4.8) (which also depend on the momentum fractions) as the evolution necessarily involves integration over momentum fractions x_1 and x_2. One therefore needs to avoid the necessity of evolution at all costs if the sum rules are to be solved for $g_{a_1 a_2}(x_1, x_2)$. Consider therefore – for now – the equal flavour number sum rules at the scale $\mu_{\min} = \mu_{y \to \infty}$

$$\int\limits_{0}^{1-x_1} \mathrm{d}x_2 \left[\int \mathrm{d}^2 y\, \tilde{F}_{q q_v}(x_1, x_2, y, \mu_{\min}) \right] = (N_{q_v} - 1) f_q(x_1, \mu_{\min}). \qquad (4.18)$$

In order to solve this for $g_{a_1 a_2}(x_1, x_2)$ one first has to decompose $\tilde{F}_{q q_v}$ on the left-hand side of the above equation into its individual contributions

$$\int\limits_{0}^{1-x_1} \mathrm{d}x_2 \left[\int \mathrm{d}^2 y \left(F_{q q_v, \mathrm{int}}(x_1, x_2, y, \mu_{\min}) + F_{q q_v, \mathrm{match}}(x_1, x_2, y, \mu_{\min}) \right) \right.$$
$$\left. + \tilde{F}_{q q_v, \mathrm{spl}}(x_1, x_2, y, \mu_{\min}) \right], \qquad (4.19)$$

where it has already been taken into account that the only part affected by the modifications is the splitting part. As evolution is needed to obtain the modified splitting part at the scale $\mu_{\min}$ one cannot write the splitting part in a way that explicitly contains the function $g_{a_1 a_2}(x_1, x_2)$. Since this is, however, exactly what would be needed to extract this function from the sum rules the following two approximations have to be introduced:

Firstly one can make use of the fact that for small y the initial and modified splitting model do not differ significantly such that the following holds approximately

$$\tilde{F}_{qq_v,\text{spl}}(x_1, x_2, y, \mu_{\min}) \approx F_{qq_v,\text{spl}}(x_1, x_2, y, \mu_{\min}). \tag{4.20}$$

In a moment it will be discussed what is meant here by small y, but first a second approximation that will be made use of in the following is introduced, namely that by construction μ_y approaches $\mu_{\min}$ for large values of y such that in this case one approximately finds

$$\tilde{F}_{qq_v,\text{spl}}(x_1, x_2, y, \mu_{\min}) \approx \tilde{F}_{qq_v,\text{spl}}(x_1, x_2, y, \mu_y). \tag{4.21}$$

Combining these approximations then yields

$$\int \mathrm{d}^2y\, \tilde{F}_{qq_v,\text{spl}}(x_1, x_2, y, \mu_{\min}) \approx \int \mathrm{d}^2y\, F_{qq_v,\text{spl}}(x_1, x_2, y, \mu_{\min})\Theta(y_{\text{sep}} - y)$$
$$+ \int \mathrm{d}^2y\, \tilde{F}_{qq_v,\text{spl}}(x_1, x_2, y, \mu_y)\Theta(y - y_{\text{sep}}), \tag{4.22}$$

where it has been assumed that the approximation in equation (4.20) is valid below a value y_{sep} while the one in equation (4.21) is valid above this threshold. For $y_{\text{sep}} = 1\,\text{GeV}^{-1}$ equation (4.21) is reasonably well fulfilled as $\mu_{\min}$ and μ_y differ only by approximately 12% such that for the remainder of this work this value for y_{sep} will be used. After having obtained the modification function g the validity of the approximation introduced in equation (4.20) which is used for small values of y will be discussed. Rewriting equation (4.22) using equation (4.16) to express the modified splitting part in terms of the unmodified one equation (4.19) can be written as

$$\int\limits_0^{1-x_1} \mathrm{d}x_2 \left[\int \mathrm{d}^2y\, \left(F_{qq_v}(x_1, x_2, y, \mu_{\min}) - F_{q\bar{q},\text{spl}}(x_1, x_2, y, \mu_y)h(y)g_{q\bar{q}}(x_1, x_2)\Theta(y - y_{\text{sep}}) \right) \right],$$
$$\tag{4.23}$$

where

$$h(y) = \exp\left[\frac{y^2}{4h_{q\bar{q}}^*} \right] - 1, \tag{4.24}$$

and it has furthermore been used that at $\mu = \mu_y$ the following holds

$$F_{qq_v,\text{spl}}(x_1, x_2, y, \mu_y) = -F_{q\bar{q},\text{spl}}(x_1, x_2, y, \mu_y). \tag{4.25}$$

such that one can finally rewrite equation (4.18) as

$$\int\limits_0^{1-x_1} \mathrm{d}x_2 \left[\int \mathrm{d}^2y\, \left(F_{q\bar{q},\text{spl}}(x_1, x_2, y, \mu_y)g(y)\Theta(y - y_{\text{sep}}) \right) \right] g_{q\bar{q}}(x_1, x_2)$$
$$\approx \underbrace{\int\limits_0^{1-x_1} \mathrm{d}x_2 \left[\int \mathrm{d}^2y\, F_{qq_v}(x_1, x_2, y, \mu_{\min}) \right] - (N_{q_v} - 1)f_q(x_1, \mu_{\min})}_{-k_q(x_1)}. \tag{4.26}$$

After these steps one can rewrite this as a so called Volterra equation of the first kind introduced in reference [112] and which can be solved for $g_{q\bar{q}}(x_1, x_2)$ numerically. The general form of a Volterra equation of the first kind is the following

$$\int_a^{x_1} dx_2 K(x_1, x_2) g(x_2) = k(x_1). \tag{4.27}$$

In order to bring equation (4.26) to this form one needs to make the assumption that

$$g_{q\bar{q}}(x_1, x_2) = g_{q\bar{q}}(x_1 + x_2). \tag{4.28}$$

Then, shifting $x_1 + x_2 \to x_2$, the left-hand side of equation (4.26) takes the following form

$$\int_{x_1}^{1-x_{\min}} dx_2 \underbrace{\left[\int d^2 y \left(F_{q\bar{q},\mathrm{spl}}(x_1, x_2 - x_1, y, \mu_y) g(y) \Theta(y - y_{\mathrm{sep}}) \right) \right]}_{K_{q\bar{q}}(x_1, x_2)} g_{q\bar{q}}(x_2) \tag{4.29}$$

where the upper boundary which would normally be equal to 1 has been replaced by $1 - x_{\min}$ as this is the largest x value in the grid and one can expect only negligible contributions to the integration from the interval between 1 and $1 - x_{\min}$. Thus one finally ends up with the following equation

$$\int_{1-x_{\min}}^{x_1} dx_2 \, K_{q\bar{q}}(x_1, x_2) g_{q\bar{q}}(x_2) = k_q(x_1), \tag{4.30}$$

which is easily solved numerically for $g_{q\bar{q}}(x_2)$. The most straightforward way to do this is to work in $u = \ln(x/(1-x))$ space using the grid points which are equidistant there such that one can use a simple trapezoidal rule for the u_2 integration – of course in combination with the appropriate Jacobian – which then turns equation (4.30) into a linear system of equations

$$K_{q\bar{q},ij} g_{q\bar{q},j} = k_{q,i}, \tag{4.31}$$

where K_{ij} is an upper diagonal matrix such that the solution of this system of equations is trivially obtained using Gauss-Jordan elimination.

Actually implementing the modifications requires some more work as the functions $g_{q\bar{q}}(x_1, x_2)$ have been obtained numerically while the desired end result is a simple analytical form for the DPD model. Therefore the functions obtained from equation (4.31) have to be fitted to the following general form

$$A + Bx^b + Cx^{c_1}(1-x)^{c_2}, \tag{4.32}$$

(a) $g \to u\bar{u}$

(b) $g \to d\bar{d}$

(c) $g \to s\bar{s}$
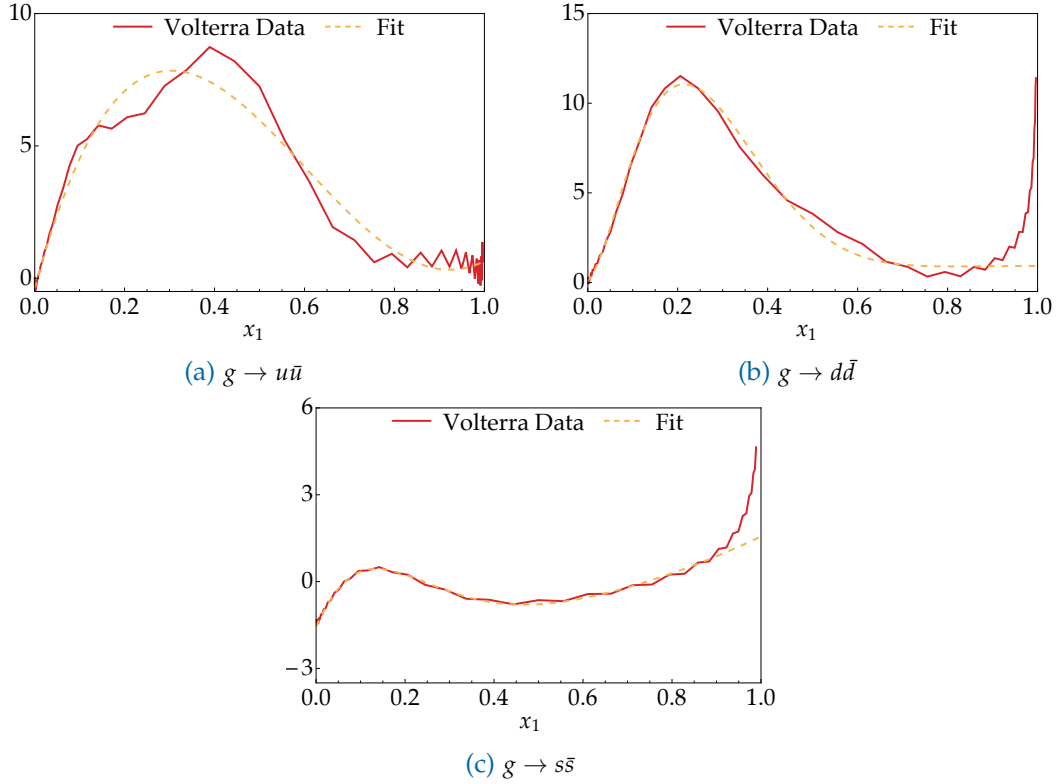
Figure 4.10.: Modification functions $g_{q\bar{q}}$ for the individual $g \to q\bar{q}$ splittings. The plots show both, the actual data points obtained from the solution of the Volterra equation (4.31) as well as the fits to equation (4.32).

which manages to reproduce the general shape of the numerical results but fails to reproduce every detail. As a result the agreement with the sum rules is not as good as it could be which is, however, a price that is acceptable in order to obtain an analytical model. The parameters for the modifying functions are given in table 4.1 and plots are presented in figure 4.10.

Here is now a good point to discuss the validity of the approximation made for small values of y introduced in equation (4.20) and used in equation (4.22). As the deviations are naturally largest for the largest values of y, that means for $y = y_{\text{sep}}$ it is useful to study how large the deviations are at this point given the size of the modifying function $g_{q\bar{q}}(x_1, x_2)$. This can be done by considering the following ratio

$$\left| \frac{\tilde{F}_{qq_v,\text{spl}}(x_1, x_2, y_{\text{sep}}, \mu_{\text{min}}) - F_{qq_v,\text{spl}}(x_1, x_2, y_{\text{sep}}, \mu_{\text{min}})}{F_{qq_v,\text{spl}}(x_1, x_2, y_{\text{sep}}, \mu_{\text{min}})} \right| = \left(\exp\left[\frac{y_{\text{sep}}^2}{h_{q\bar{q}}^*} \right] - 1 \right) \left| g_{q\bar{q}}(x_1, x_2) \right| . \tag{4.33}$$

It is straightforward to see that for fixed y the deviations grow linearly for increasing values of $\left| g_{q\bar{q}}(x_1, x_2) \right|$ reaching up to 25% for $\left| g_{q\bar{q}}(x_1, x_2) \right| = 10$. Therefore the approxi-

mation in eq. (4.20) is not perfect but nevertheless quite reasonable to make as can be seen in a moment.

With these modified $g \to q\bar{q}$ splittings the agreement with the equal flavour number sum rules improves drastically as can be seen in figure 4.11. However, as mentioned before the agreement is not quite perfect, on the one hand due to the approximations which had to be used as well as due to the fact that the analytical model cannot quite reproduce the numerical function returned as the solution of the Volterra equation.

(a) uu_v number sum rule

(b) $\bar{u}u_v$ number sum rule

(c) $\bar{d}d_v$ number sum rule

(d) ss_v number sum rule
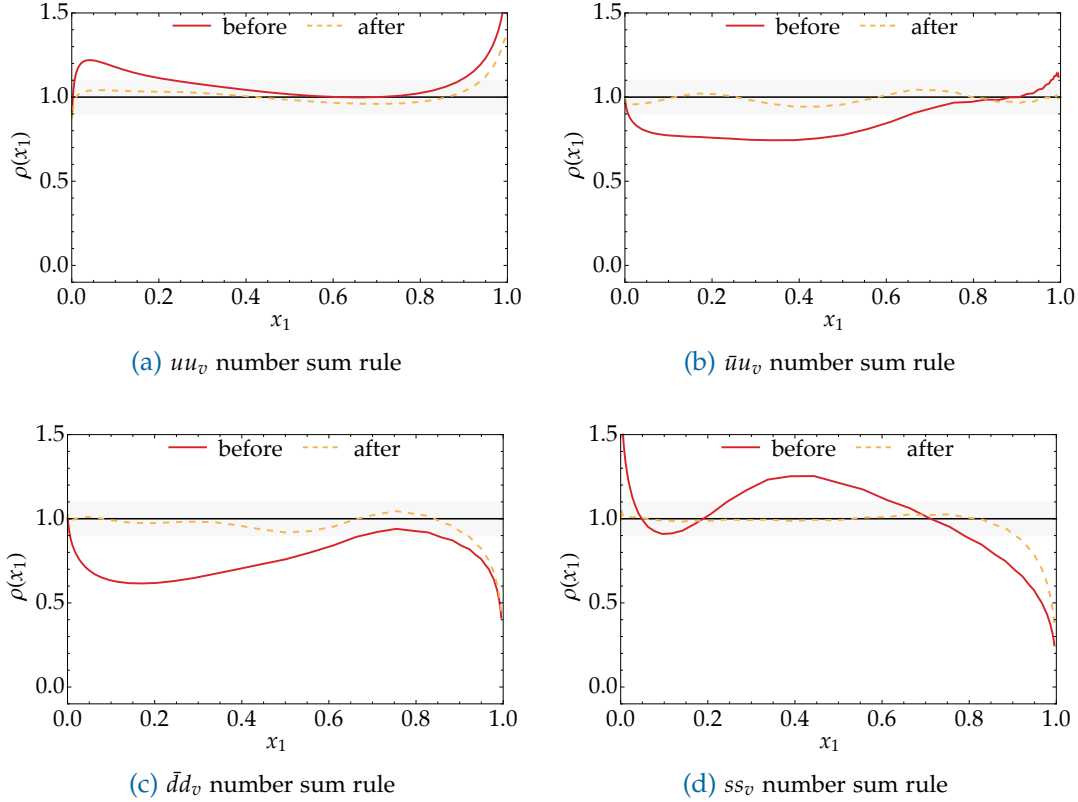
Figure 4.11.: Comparison of the equal flavour number sum rules before and after modification of the splitting part. Here again only the complete sum rule ratio of the two models has been plotted in order to avoid cluttered plots. This can again be done without hiding any information as now only the splitting part changed.

However, these modifications also effect the quark momentum sum rules as illustrated in figure 4.12. The reason for this is obviously that the q momentum sum rule gets non-negligible contributions from the $q\bar{q}$ splitting DPD which has been modified in the last step. Since this change is not too severe and the sum rules are still fulfilled to an approximate accuracy of 10% which – keeping in mind the uncertainties from the matching – is still pretty good, it is not absolutely necessary to modify the $q \to qg$ splitting. Nevertheless the approach described in this subsection has been adapted

(a) u momentum sum rule

(b) $\bar{u}$ momentum sum rule
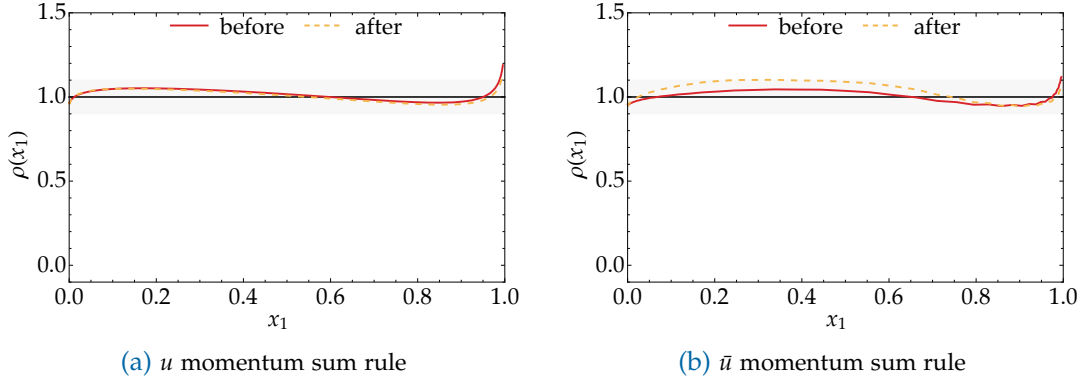
Figure 4.12.: Illustration of the differences between the q sum rule ratios before and after modification of the $g \to q\bar{q}$ splittings. The most pronounced difference is observed for the $\bar{u}$ and $\bar{d}$ momentum sum rules, the former of which is shown in figure 4.12b.

to the momentum sum rules (which is rather straightforward) and used to obtain modification functions for the individual $q \to qg$ splittings. This made it possible to

(a) u momentum sum rule

(b) $\bar{u}$ momentum sum rule
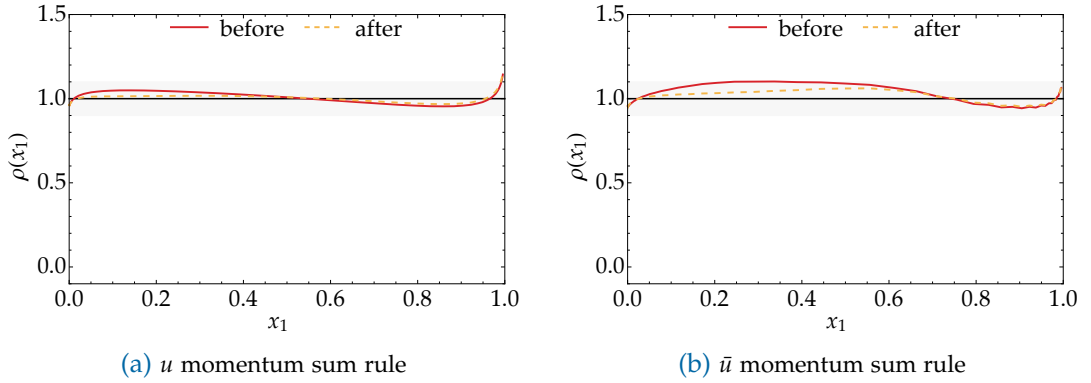
Figure 4.13.: Comparison of the q momentum sum rule ratios before and after modification of the $q \to gq$ splittings.

achieve an even better agreement with the momentum sum rules, as illustrated in figure 4.13 where the momentum sum rules before and after modification of the $q \to qg$ splittings have been compared. As in the case of the $g \to q\bar{q}$ splitting, the parameters of the g_{qg} modification functions are given in table 4.1.

While these modifications indeed lead to a better agreement with the quark momentum sum rules they unfortunately – but not unexpectedly – lead to a rather strong change of the gluon momentum sum rule ratio as the modifications of the $q \to qg$ splitting of course also affect the $q \to gq$ splitting in the same way. In order to fulfil also this sum rule to a decent degree the $g \to gg$ splitting has been modified analogously to the $g \to q\bar{q}$ and $q \to gq$ splittings which makes it possible to achieve a good agreement also with this last sum rule as can be seen in figure 4.14, with the parameters of g_{gg}

also given in table 4.1.

After all these different modifications one can finally again use the measure defined in equation (4.14) to evaluate how well the sum rules are fulfilled for the final DPD model. Doing this one finds that for the momentum sum rules the average deviation is around 1.6%, whereas for the number sum rules the situation is still slightly worse with average deviations of approximately 2.7%. In total this means that the average deviation per sum rule is approximately 2.4%. In order to see how good or bad this is – especially compared to the initial model – the same analysis can be performed in that case, yielding an average deviation of 6.9% for the momentum sum rules and 24.3% for the number sum rules. This nicely illustrates the greatly improved agreement with the DPD sum rules achieved by the modifications of the initial DPD model which have been presented here. The largest part of the improvements in the sum rule sector can be traced back to the first modifications of the phase space factor in section 4.3.2.
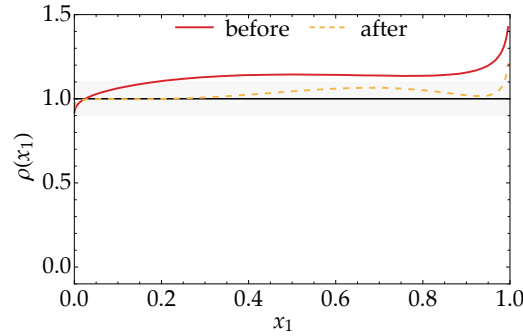
Figure 4.14.: Improvement of the g momentum sum rule ratio after modification of the $g \to gg$ splitting.

$a_0 \to a_1 a_2$	A	B	b	C	c_1	c_2	$h^*_{a_1 a_2}$
$g \to u\bar{u}$	-0.4193	1.0627	7.7448	60.8558	0.9881	2.2641	$10.75\,\mathrm{GeV}^{-2}$
$g \to d\bar{d}$	-0.8020	1.7291	0.0988	932.0289	1.8515	6.8244	$10.75\,\mathrm{GeV}^{-2}$
$g \to s\bar{s}$	-1.5409	3.0985	2.3609	49.8862	1.0964	7.2093	$10.75\,\mathrm{GeV}^{-2}$
$u \to ug$	-1.0184	0.7163	0.1720	6.9015	0.2841	3.3067	$8.39\,\mathrm{GeV}^{-2}$
$d \to dg$	-2.1122	1.5734	0.1889	22.1328	0.3991	4.5915	$8.39\,\mathrm{GeV}^{-2}$
$s \to sg$	-10.2384	10.7879	0.3489	184.0777	1.3930	6.6420	$8.39\,\mathrm{GeV}^{-2}$
$\bar{u} \to \bar{u}g$	-10.1906	10.1898	0.3742	25.6616	0.3928	2.2418	$8.39\,\mathrm{GeV}^{-2}$
$\bar{d} \to \bar{d}g$	-10.1582	10.9392	1.8228	29.0261	0.2952	1.4520	$8.39\,\mathrm{GeV}^{-2}$
$\bar{s} \to \bar{s}g$	-10.2384	10.7879	0.3489	184.0777	1.3930	6.6420	$8.39\,\mathrm{GeV}^{-2}$
$g \to gg$	-25.5496	26.8106	0.2967	16.3186	0.0612	1.6386	$6.03\,\mathrm{GeV}^{-2}$

Table 4.1.: Parameters of the modification functions $g_{a_1 a_2}$ according to eq. (4.32) and the "widths" $h^*_{a_1 a_2}$.

4.4. Scale dependence of the sum rules

In this section it will be investigated how the DPDs – and in particular their agreement with the sum rules – change once one goes from μ_{min} to higher scales and also in the case that the cut-off scale ν is varied.

4.4.1. Renormalisation scale dependence

So far the sum rules have been considered only for the scale μ_{min} such that at this point one should consider how the agreement changes with increasing scale. A general observation one can make is that there is a tendency towards a better agreement with the sum rules for higher scales and that the curves of the sum rule plots tend to become smoother with increasing scale.

The more interesting question, however, is how the individual contributions are affected by evolution to higher scales. In order to discuss this consider again first the quark momentum sum rules, taking the u momentum sum rule as an representative example, illustrated in figure 4.15. Here one clearly sees that the relative size of the splitting

(a) u momentum sum rule at $\mu = 2.25\,\mathrm{GeV}$ (b) u momentum sum rule at $\mu = 144.60\,\mathrm{GeV}$
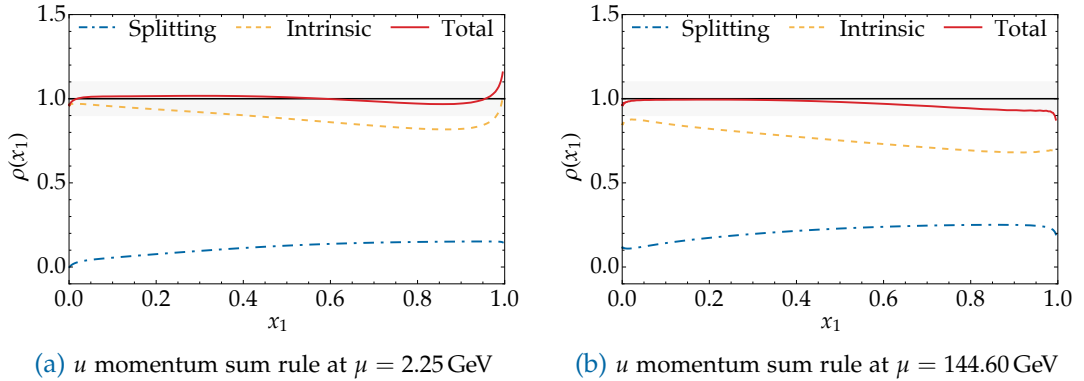
Figure 4.15.: Side-by-side comparison of the quark momentum sum rule ratios for the final iteration of the models at different scales. The somewhat odd values of the scales are due to the fact that the values used are already in the grid which makes it possible to avoid interpolation.

contribution compared to that of the intrinsic part grows with increasing scale while their sum nicely adds up in such a way that the sum rule ratios are remarkably similar in both cases. In reference [45] it was noted that the sum rules remain exact under evolution if they are fulfilled exactly at the starting scale. As in the case at hand the sum rules are fulfilled only approximately at the starting scale one can thus also expect that this remains true under evolution to higher scales which is just what has been found here. In section 3.6 it has been shown that – in position space – this requires a cancellation between the homogeneous and inhomogeneous parts of the momentum space evolution equation (2.56) with similar observations already

made by Ceccopieri and Blok et al. in references [40, 94]. In position space where the evolution equation (2.51) is homogeneous this should amount to cancellations between the splitting and matching parts associated with the inhomogeneous term on the one hand and the intrinsic part associated with the homogeneous term on the other hand.

For the number sum rules one can distinguish three cases, one of which has been discussed in some detail already, namely the equal flavour number sum rules. These equal flavour number sum rules receive – as already mentioned in section 4.3 – a large contribution from the $g \to q\bar{q}$ splitting as can easily be seen in figure 4.16. Here

(a) $\bar{u}u_v$ number sum rule at $\mu = 2.25\,\text{GeV}$ 　　　(b) $\bar{u}u_v$ number sum rule at $\mu = 144.60\,\text{GeV}$
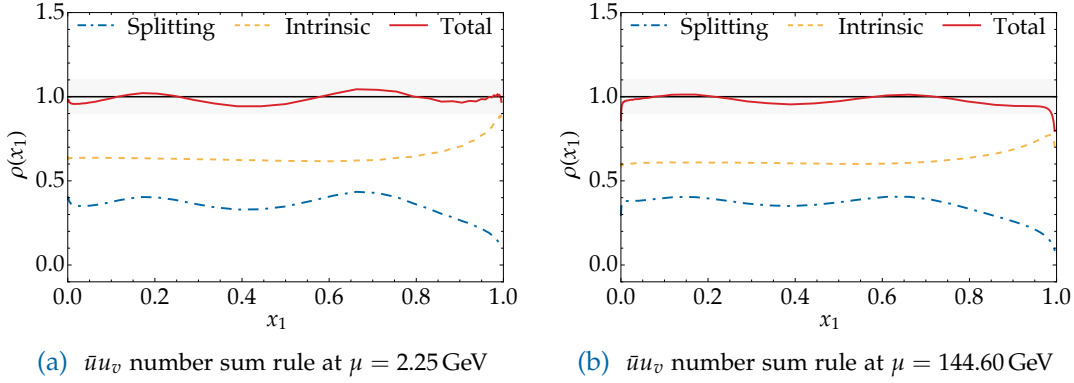
Figure 4.16.: Comparison between the equal flavour number sum rule ratios for the final model at low and high scales. It is evident that for this model the equal flavour number sum rules are not strongly effected by evolution with only a slight smoothing effect noticeable for the splitting part.

it can, however, be noted that the importance of the splitting contribution does not change with increasing scale but rather stays more or less the same with the main difference being that for higher scales the initially rather curvy sum rule ratio plots get smoothed out which is a pretty general feature that can be observed when going to higher scales.

The second kind of number sum rules which get a non-negligible contribution are the gu_v and gd_v ones, for which the splitting part of the DPDs is primarily produced via $q \to gq$ splitting. As the initial u and $\bar{u}$ PDFs, as well as the initial d and $\bar{d}$ PDFs differ this subsequently leads to non-vanishing splitting contributions to the gu_v and gd_v DPDS. In this case evolution has a more pronounced effect on the relative sizes of the splitting and intrinsic contributions as can be seen in figure 4.17. Just like in the case of the momentum sum rules discussed above one now finds that the relative size of the intrinsic part decreases by more or less the same amount as that of the splitting contribution increases such that overall the agreement with the sum rule becomes slightly better at higher scales even though in total it remains pretty much the same.

Finally there is a last kind of number sum rules to be considered here, namely mixed flavour number sum rules, for example du_v or ud_v, for which the valence DPDs involved get no direct contribution from the LO splitting but are only produced due

(a) gu_v number sum rule at $\mu = 2.25\,\mathrm{GeV}$ (b) gu_v number sum rule at $\mu = 144.60\,\mathrm{GeV}$
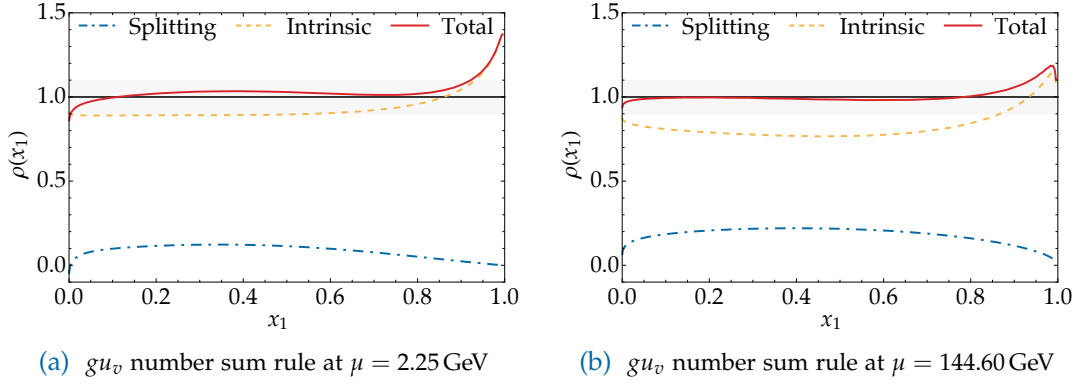
Figure 4.17.: Comparison of the gq_v number sum rule ratios for the final iteration of the model. In this case again a increased contribution of the splitting part at higher scales can be observed.

to consecutive splittings under evolution. The du_v DPD for example arises from the difference of $u \to gu$ and $\bar{u} \to g\bar{u}$ splitting DPDs in which the gluon successively splits into a $d\bar{d}$ pair of which the d quark is observed. It thus comes as no surprise that at low scales the splitting contribution is basically negligible in this case and only becomes remotely important at higher scales as can be seen in figure 4.18.

(a) du_v number sum rule at $\mu = 2.25\,\mathrm{GeV}$ (b) du_v number sum rule at $\mu = 144.60\,\mathrm{GeV}$
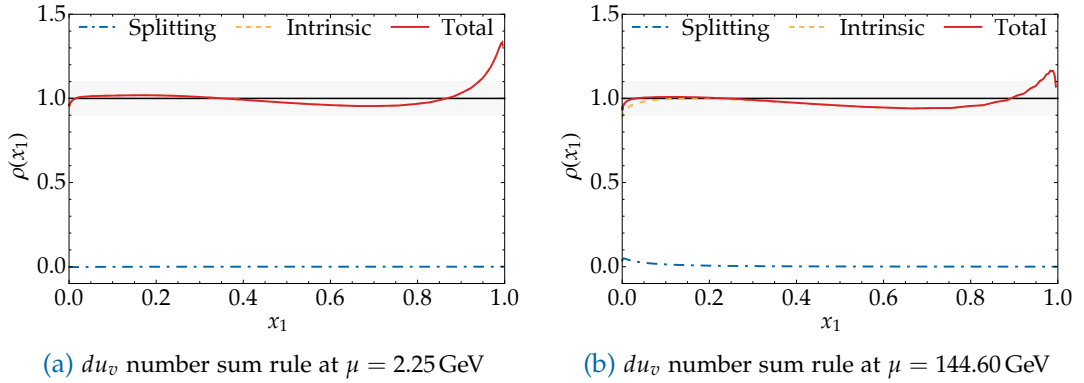
Figure 4.18.: Illustration of the differences between the mixed flavour number sum rule ratios at different scales. A very slight difference of the splitting contribution at higher scales is readily explained by evolution effects.

4.4.2. Cut-off scale dependence

Having discussed the renormalisation scale dependence of the degree to which the sum rules are fulfilled and thus also of the DPDs one can now move on to consider the effect a variation of the cut-off scale ν has on the agreement with the sum rules. If the cancellation of the ν dependence between the cut-off momentum space DPD and the matching term were exact the sum rule ratios should not depend on ν at all. However,

as mentioned already in section 4.2.1 when the matching between the cut-off and $\overline{\text{MS}}$ momentum space DPDs has been discussed the ν dependence cancels between the cut-off momentum space DPD and the matching term only up to higher order terms as the perturbative expansion of the matching has been truncated at LO. Varying the cut-off scale ν thus gives valuable information about the precision of the perturbative matching at the considered order as this is a handle on the size of the neglected higher order terms. In order to get an idea how well the LO matching can be trusted the cut-off scale ν has been varied around its initial value of $\mu_{\min}$ by a factor of two for the initial model[1]. Even though the initial model could not really be expected to fulfil the sum rules too well this nevertheless makes it possible to gain some insight about the accuracy to which the sum rules can be fulfilled. If already at this point it would have been found that the sum rule ratios vary by a substantial amount when ν is varied by a factor of two this would have suggested that there is little use in trying to fulfil the sum rules to a better degree than this uncertainty. However, this is not the case as varying the cut-off scale by a factor of two resulted in changes of at most 10% of the sum rule ratios as illustrated in figure 4.19 for the g and u momentum sum rules and in 4.20 for the $\bar{u}u_v$ and ss_v number sum rules. The only case for which one finds

(a) g momentum sum rule   (b) u momentum sum rule
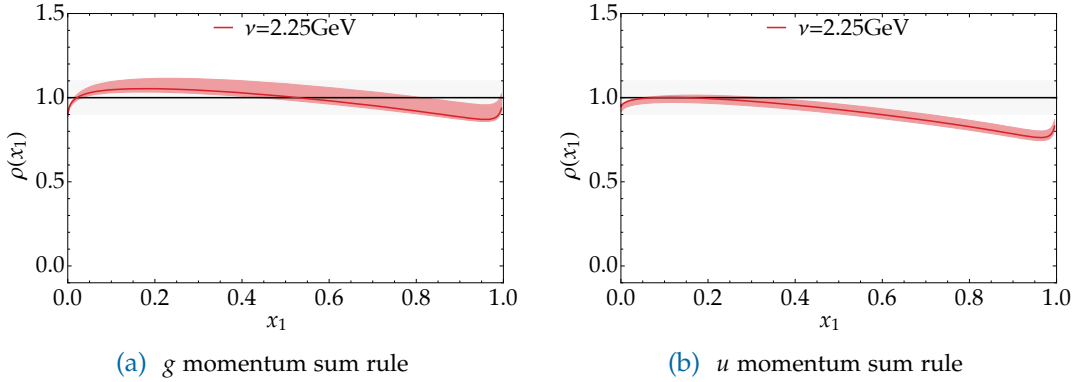
Figure 4.19.: Cut-off scale dependence of the momentum sum rules in the initial model. The plots show the sum rule ratios for $\mu = \mu_{\min}$ with a variation of the cut-off scale ν by a factor of two around the value $\nu = \mu_{\min}$ as indicated by the bands.

larger uncertainties, up to 20%, is the ss_v equal flavour number sum rule which is not too surprising as in this case there is no intrinsic contribution such that the a relative uncertainty of the splitting part also implies the same uncertainty for the complete DPD whereas in cases with an intrinsic contribution the same level of uncertainty of the splitting part would result in a lower uncertainty of the complete DPD as can be seen in figure 4.20.

As theoretical uncertainties associated with the matching are under control one can

---

[1]The reason why this scale dependence is investigated at the lowest scale rather than at some higher scale is simply that due to the running of the strong coupling α_s this is where higher order terms can be expected to have the largest influence.

(a) $\bar{u}u_v$ number sum rule

(b) ss_v number sum rule

Figure 4.20.: Cut-off scale dependence of the equal flavour number sum rule ratios in the initial unmodified model. The renormalisation scale and cut-off scale are as in figure 4.19 and the latter has again been varied ν by a factor of two.

indeed use the sum rules for the $\overline{\text{MS}}$ DPDs to investigate and refine the position space DPD model suggested in section 4.2.2. Following this insight the intrinsic part has been modified in subsections 4.3.2 and 4.3.3. Since in these two subsections only the intrinsic part has been modified the uncertainties associated with the matching were not expected to change significantly which is in line with what has been found. The situation remains basically the same even after the modifications of the splitting part in subsection 4.3.4 where one again finds that the uncertainties are well within the 10% range with the exception of the ss_v equal flavour number sum rule where again uncertainties up to 20% are encountered, as evidenced by the plots in figures 4.21 and 4.22. This should come as no surprise considering that the modifications of the splitting part were aimed at the large y behaviour while the small y behaviour affected by the cut-off remains basically unchanged.

(a) g momentum sum rule

(b) u momentum sum rule
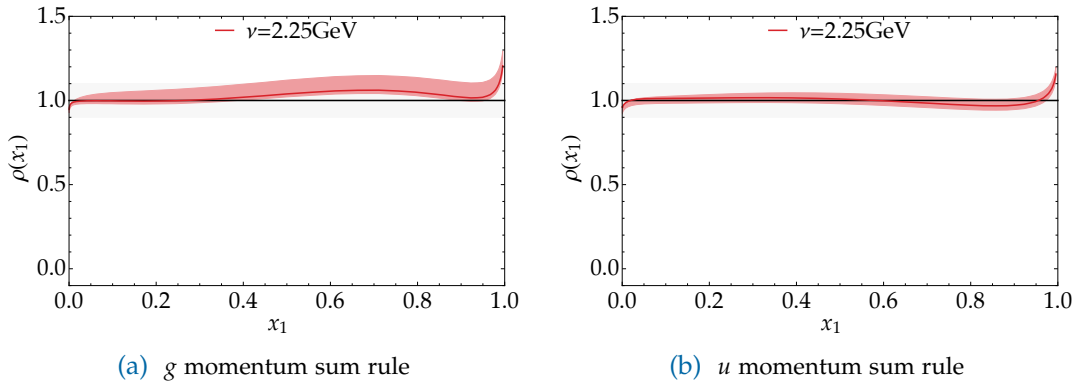
Figure 4.21.: Cut-off scale dependence of the momentum sum rules in the final iteration of the DPD model. Here the cut-off scale is again varied by a factor of two around $\nu = \mu_{\text{min}}$ and the amount by which this alters the agreement with the sum rules is again very similar as in the case of the unmodified model.
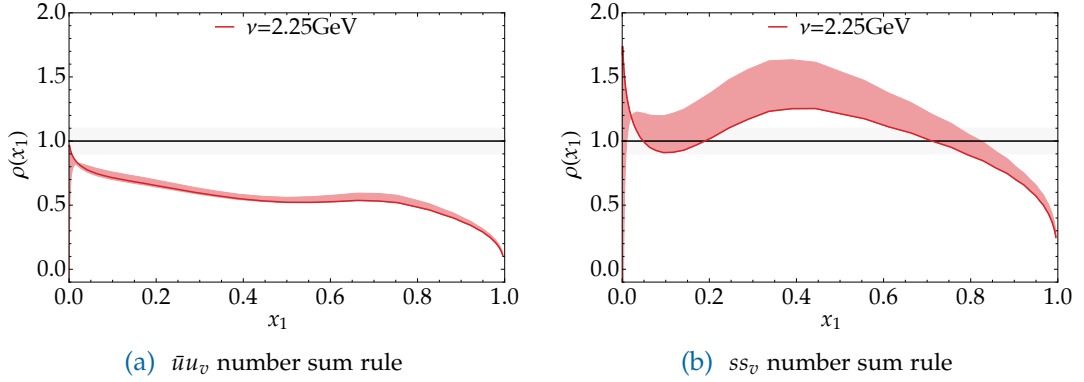
(a) $\bar{u}u_v$ number sum rule

(b) ss_v number sum rule
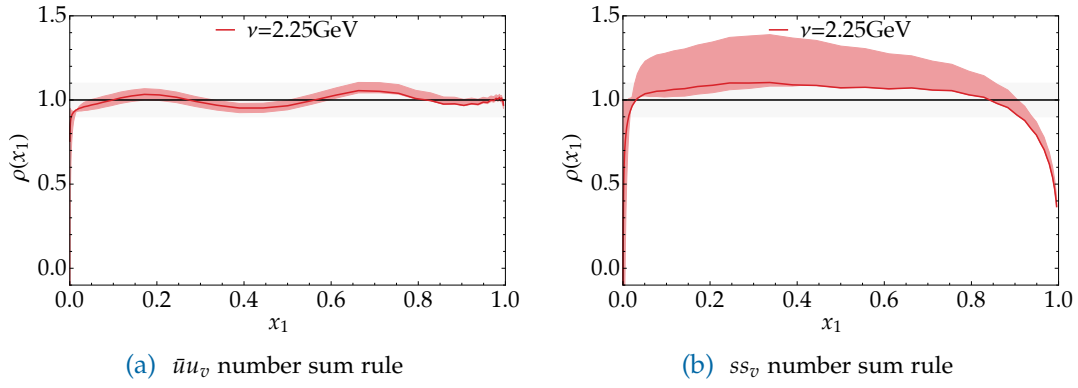
Figure 4.22.: Cut-off scale dependence of the equal flavour number sum rule ratios in the final modified DPD model. The variation of the cut-off scale ν is again as in figure 4.19 and its effects are also comparable in size to the case shown there. In particular the variation of the ss_v number sum rule is again largest.

5. Two-loop splitting in double parton distributions

5.1. Introduction

With the sum rule improved position space DPD model derived in the previous chapter an important component for the calculation of LO DPS cross sections within the framework briefly introduced in section 2.2.3 has been established. At this point one may already wonder what the situation would look like if one wanted to go ahead and calculate DPS cross sections at higher orders. To this end the DGS framework has been designed in a way that can be formulated at arbitrary order in the strong coupling making maximum re-use of known SPS quantities. In order to calculate DPS cross sections at NLO the only missing component is thus the NLO expression for the small y splitting contribution introduced in equation (2.52) which on one hand is needed to obtain the subtraction terms for the double counting between DPS and SPS. Another reason why this $1 \to 2$ splitting contribution is needed for NLO DPS calculations is that this requires also NLO DPDs, or to be more precise, NLO DPD models[1], as an experimental determination of NLO DPDs is at this point basically impossible. This may bring up the question why – with such a lack of information about the non-perturbative input – one should still consider DPS at NLO and it turns out that there are in fact quite a few reasons why this can nevertheless prove instructive. The main motivation for studying DPS beyond leading order is that this provides valuable information about the convergence of the perturbative expansion. As already mentioned in the introduction, DPS is generally expected to give comparatively large contributions when the momentum fractions of the probed partons become small. When the momentum fractions x are very small this may give rise to large logarithms $\ln x$ which may significantly impact the perturbative convergence. As the possible effect of these small x logarithms is hard to estimate a priori it is necessary to study the effect of NLO corrections on the small y DPDs of equation (2.52) and thus also on DPS cross sections. Another reason why a determination of the small y splitting DPD at NLO is quite interesting is that in reference [35] it has been pointed out that at LO evolution effects quite drastically alter the initial $1/y^2$ behaviour of equation (4.1) towards a much less steep decrease with increasing y with these changes also attributed to small x logarithms. As this shifts emphasis away from the small y region where SPS and

---

[1]In analogy to the LO case discussed in chapter 4 this requires the NLO expression for the perturbative $1 \to 2$ splitting.

DPS overlap the dependence of theoretical predictions on the precise way in which SPS and DPS are separated is hence reduced. Considering how important a consistent separation of SPS and DPS is when calculating the overall cross section including DPS contributions it is important to understand how this situation changes when higher order corrections are included. Furthermore, it is interesting how the agreement with the sum rules changes when the NLO correction to the splitting contribution is included. Considering how the major deficiencies with the LO DPD model introduced in the previous chapter were associated with the splitting contribution one might hope that the situation becomes better – maybe even to the point that modifications in the vein of section 4.3.4 are no longer necessary – when the NLO corrections are taken into account.

The missing NLO splitting contribution for small y – and also large Δ in momentum space – will be presented in detail in this chapter. To this end a brief review of state of the art techniques used in the calculation of multi-loop Feynman integrals will be presented in section 5.2 before discussing how the renormalised position and momentum space splitting kernels can be extracted from the bare Feynman diagrams in section 5.3. As a generalisation of the procedure introduced in the previous chapter to higher orders requires also the higher order form of the matching equation (4.3) this will be derived in section 5.4. The actual calculation of the Feynman diagrams needed to obtain the $1 \rightarrow 2$ splitting, evolution, and matching kernels will in detail be discussed in section 5.5 with the results of this calculation presented in section 5.6 where a in depth discussion will be presented. The contents of this chapter are under review for publication in SciPost [113].

5.2. Specific Theory

In recent years a lot of progress has been made in developing sophisticated methods for the calculation of multi-loop Feynman diagrams and some of these methods were used in the calculation of the NLO $1 \rightarrow 2$ splitting DPDs as this involved Feynman integrals that proved to be intractable with standard textbook techniques. The fundamentals of these techniques will be reviewed in this section and references to the original literature will be provided for further reading while mostly following the excellent book on the topic by Smirnov [114] where possible.

5.2.1. Reduction to master integrals: integration by parts reduction

A quite general feature of higher order calculations is that they tend to involve a great number of individual Feynman diagrams, each associated with a corresponding Feynman integral. Even for the calculation at hand which considered only diagrams up to NLO this already meant dealing with up to 100 distinct diagrams. In order not to

have to calculate this huge amount of Feynman integrals the method of integration by parts (IBP) reduction introduced in references [115, 116] has been employed. This made it possible to drastically reduce the computational effort as this way only a small set of so called master integrals had to be calculated, in terms of which all other occurring Feynman integrals could be expressed as will be discussed now. Consider to this end a "family" of scalar Feynman integrals, given by

$$I(p_1, \ldots, p_n; a_1, \ldots a_N) = \int d^D k_1 \ldots d^D k_h \prod_{i=1}^{N} \frac{1}{(q_i^2 + m_i^2)^{a_i}}, \tag{5.1}$$

with $N = n + h$ integer indices a_i, n external momenta p_i, and h loop momenta k_i. Here the q_i are linear combinations of the external and loop momenta p_i and k_i, respectively. It should be noted that the integrals encountered in a calculation are not necessarily in this form in the beginning but can be reduced to such an expression using tensor reduction and expressing scalar products of momenta in the numerators in terms of denominators[2]. Such a family of Feynman integrals – containing in theory an infinite number of different integrals – can then be reduced to a finite number of master integrals using relations between integrals with different powers a_i of denominators. In order to derive these IBP relations one makes use of the following relation

$$\int d^D k_1 \ldots d^D k_h \frac{\partial}{\partial k_j^\mu} \left(r_l^\mu \prod_{i=1}^{N} \frac{1}{(q_i^2 + m_i^2)^{a_i}} \right) \overset{!}{=} 0, \tag{5.2}$$

where $r_l = k_l$ for $1 \leq l \leq h$ and $r_{h+l} = p_l$ for $1 \leq l \leq n$. This relation arises from the properties of dimensionally regularised integrals in $D = 4 - 2\varepsilon$ dimensions for which surface terms can be shown to be negligible when integration by parts is used (the left-hand side of equation (5.2) has just the form of a surface term). Scalar products in the numerator of the left-hand side of the form $k_j \cdot k_i$ and $k_j \cdot p_i$ arising from the differentiation with respect to k_j are subsequently again expressed in terms of the denominators $q_i^2 + m_i^2$ such that one finally obtains the IBP relations as a sum of integrals of a family

$$\sum_i \alpha_i I(p_1, \ldots, p_n; a_1 + b_{i,1}, \ldots a_N + b_{i,N}) = 0. \tag{5.3}$$

From this an infinite number of relations between the integrals in equation (5.1) can be obtained by plugging in all possible values for the indices $a_1, \ldots, a_N$.

In order to illustrate how this works in practice consider the following very simple example of a family of Feynman integrals

$$I(a) = \int d^D k \frac{1}{(k^2 + m^2)^a}, \tag{5.4}$$

---

[2]Note that in some cases the denominators arising in diagrams do not form a complete basis with respect to the external and loop momenta which makes it necessary to introduce additional denominators in order to make such a reduction to scalar integrals of the form in equation (5.1) possible.

with no external momenta and only one loop momentum. Therefore one finds in this case also only one IBP relation, given by

$$
\int \mathrm{d}^D k \, \frac{\partial}{\partial k^\mu} \frac{k^\mu}{(k^2 + m^2)^a} = \int \mathrm{d}^D k \left(\frac{D}{(k^2 + m^2)^a} - \frac{2ak^2}{(k^2 + m^2)^{a+1}} \right)
$$

$$
= \int \mathrm{d}^D k \left(\frac{D - 2a}{(k^2 + m^2)^a} + \frac{2am^2}{(k^2 + m^2)^{a+1}} \right) \overset{!}{=} 0 \,. \tag{5.5}
$$

From this condition one easily derives a relation between the integrals of the family with different indices a, namely

$$
I(a) = \frac{2(a-1) - D}{2(a-1)m^2} I(a-1) \,, \tag{5.6}
$$

which makes it possible to express all integrals of the family in equation (5.4) with $a > 1$ recursively in terms of just one master integral, namely $I(1)$.

Naturally the situation is more complicated in cases with more external and loop momenta such that IBP relations become increasingly tedious to solve by hand. Nevertheless some of the most famous implementations of this technique use exactly this kind of approach, for example `MINCER` introduced in references [117, 118]. A more modern approach was suggested by Laporta in references [119, 120] which does not aim to solve the of IBP relations of equation (5.3) in full generality but rather only for the limited subset of indices $a_1, \ldots, a_N$ needed for a given calculation. This procedure then yields a (potentially very large) linear system of integrals which can be solved using straightforward Gauss elimination, yielding as results the integrals in terms of the master integrals. Since this algorithm has first been proposed it has been implemented in a number of publicly available codes, most notably `AIR` [121], `Reduze` [122, 123], and `FIRE` [124–127]. However, Laporta's algorithm has the downside that it produces rather large databases of identities that have to be stored, or calculated on the fly every time they are needed for reduction, both of which can become problematic for complicated systems. Therefore a different approach has been followed in the development of `LiteRed` [128] which uses a heuristic algorithm in order to find symbolic IBP reduction rules. Compared to the Laporta algorithm this has the advantage of being fast and needing very little storage, which, however, comes at the price that due to the heuristic nature of the algorithm it is not guaranteed that this approach works for every imaginable case. Nevertheless `LiteRED` has been used successfully in the calculations presented in this chapter.

5.2.2. Calculating master integrals: method of differential equations and the canonical basis

The reduction to master integrals is of course only the first step in the calculation of a large number of Feynman integrals while the second step is to actually calculate

these master integrals. To this end standard textbook techniques like Feynman or alpha parametrisation can be sufficient for simpler master integrals but one finds that already for four denominators the resulting parameter integrals become intractable. Therefore more sophisticated methods for the evaluation of Feynman integrals have been developed, for example the use of the Mellin-Barnes representation or differential equations, the latter of which has been used to calculate the master integrals in this chapter. The approach to use differential equations in order to solve master integrals was introduced in references [129–132]. In order to solve the master integrals one takes the derivative of the master integrals with respect to kinematic invariants like external momenta or masses and uses IBP reduction to express the resulting expressions again in terms of master integrals. This way one then obtains a system of ordinary first order differential equations for the set of master integrals which has to be solved using appropriate boundary conditions – or more precisely the values of the master integrals for these boundary conditions. One advantage of this approach is that for suitably chosen boundary conditions – for example a particular combination of external momenta – the master integrals may be simplified to the point where they can be calculated using standard methods like Feynman and alpha parameters. The resulting system is then iteratively solved using elementary methods and forward substitution with the values of the master integrals for the aforementioned suitably chosen kinematics as boundary conditions. However, even then one may encounter cases where a solution of these differential equations is quite challenging as they may be coupled such that standard techniques fail to obtain a solution.

Here a method suggested by Henn in reference [133] provides a valuable aid. In this reference it was suggested that a system of differential equations for master integrals could be brought into what is referred to as the canonical form where the solution – order by order in the dimensional parameter ε – is straightforward. Consider to this end the situation of a set of N master integrals denoted by I_i and kinematic variables denoted by x_i such that the differential equation with respect to x_m can be written as

$$\frac{\partial \mathbf{I}(\varepsilon, x_i)}{\partial x_m} = \mathbb{A}_m(\varepsilon, x_i)\mathbf{I}(\varepsilon, x_i)\,, \tag{5.7}$$

where $\mathbf{I}$ is a N dimensional vector with the I_i's as entries and $\mathbb{A}_m$ is a $N \times N$ matrix. Performing a change of basis functions as prescribed by

$$\mathbf{I}(\varepsilon, x_i) = \mathbb{T}(\varepsilon, x_i)\tilde{\mathbf{I}}(\varepsilon, x_i)\,, \tag{5.8}$$

leads to an equivalent system of differential equations for the new functions $\tilde{\mathbf{I}}(\varepsilon, x_i)$, namely

$$\frac{\partial \tilde{\mathbf{I}}(\varepsilon, x_i)}{\partial x_m} = \tilde{\mathbb{A}}_m(\varepsilon, x_i)\tilde{\mathbf{I}}(\varepsilon, x_i)\,, \tag{5.9}$$

where the new matrix $\tilde{\mathbb{A}}_m$ is obtained from $\mathbb{A}_m$ through the following relation

$$\tilde{\mathbb{A}}_m(\varepsilon, x_i) = \mathbb{T}^{-1}(\varepsilon, x_i)\mathbb{A}_m(\varepsilon, x_i)\mathbb{T}(\varepsilon, x_i) - \mathbb{T}^{-1}(\varepsilon, x_i)\frac{\partial}{\partial x_m}\mathbb{T}(\varepsilon, x_i)\,. \tag{5.10}$$

It has then been suggested in reference [133] that by a suitable choice of such a basis transformation equation (5.7) can be transformed to the canonical form where the differential equation takes on the the following form

$$\frac{\partial \tilde{\mathbf{I}}(\varepsilon, x_i)}{\partial x_m} = \varepsilon \, \mathbb{B}_m(\varepsilon, x_i) \tilde{\mathbf{I}}(\varepsilon, x_i) \,, \tag{5.11}$$

such that the solution of the differential equation is – order by order in ε – given by iterated integrals and thus basically trivial. In the original paper on this approach criteria for the choice a suitable basis have been given based on the concept of transcendentality which could be used to determine a new set of basis functions. A more systematic approach to this problem has been suggested by Lee in reference [134] who proposed an algorithm to find the matrix $\mathbb{T}$ which performs the appropriate change of basis. There it has also been pointed out that the matrix $\mathbb{B}$ should be of Fuchsian form, meaning

$$\mathbb{B}_m(\varepsilon, x_i) = \sum_i \frac{\mathbb{B}_{m,k}(\varepsilon, x_i)}{x_m - x_i} \,, \tag{5.12}$$

which makes it possible to express the results in terms of generalised harmonic polylogarithms. Lee's algorithm has been implemented in the publicly available code `Fuchsia` by Gituliar [135] which has been used in the calculations presented in this chapter.

5.3. Renormalisation Group analysis: Splitting kernels at higher orders

Before moving on to the actual calculation of the bare $1 \to 2$ splitting diagrams in figures 5.1, 5.2, and 5.3 in section 5.5 a detailed analysis of how the renormalised splitting, matching, and evolution kernels can be extracted from the bare results will be presented in the present section. Recall to this end that as mentioned earlier the perturbative splitting becomes the prevalent contribution for small y in position space and correspondingly for large Δ in momentum space. In position space the factorised form of the bare splitting DPD has already been given in equation (2.52) and a corresponding factorised expression can also be given in momentum space, namely

$$F_{B,a_1 a_2}(\boldsymbol{\Delta}) = [W_B(\boldsymbol{\Delta}) \underset{12}{\otimes} f_B]_{a_1 a_2} \,, \tag{5.13}$$

with a bare momentum space $1 \to 2$ splitting kernel $W_{B;a_1 a_2, a_0}(x_1, x_2, \boldsymbol{\Delta})$. Following the discussion in section 2.2.2 one can naturally derive the renormalised splitting DPDs in position and momentum space using equations (2.46), (2.47) and (2.53), which are then given by

$$F_{a_1 a_2}(\boldsymbol{y}; \mu) = \frac{\Gamma(1-\varepsilon)}{(\pi \boldsymbol{y}^2)^{1-\varepsilon}} [V(\boldsymbol{y}; \mu) \underset{12}{\otimes} f(\mu)]_{a_1 a_2} \,, \quad F_{a_1 a_2}(\boldsymbol{\Delta}; \mu) = [W(\boldsymbol{\Delta}; \mu) \underset{12}{\otimes} f(\mu)]_{a_1 a_2} \,, \tag{5.14}$$

where the renormalised $1 \to 2$ splitting kernels read

$$V_{a_1 a_2, a_0}(\boldsymbol{y}; \mu) = [Z(\mu) \underset{1}{\otimes} Z(\mu) \underset{2}{\otimes} V_B(\boldsymbol{y}) \underset{12}{\otimes} Z^{-1}(\mu)]_{a_1 a_2, a_0},$$

$$W_{a_1 a_2, a_0}(\boldsymbol{\Delta}; \mu) = [Z(\mu) \underset{1}{\otimes} Z(\mu) \underset{2}{\otimes} W_B(\boldsymbol{\Delta}) \underset{12}{\otimes} Z^{-1}(\mu) + Z_s(\mu) \underset{12}{\otimes} Z^{-1}(\mu)]_{a_1 a_2, a_0}. \quad (5.15)$$

5.3.1. Preliminaries

Since the bare results are most conveniently obtained in momentum space from the calculation of Feynman diagrams the following discussion will be concerned with the renormalisation of the momentum space kernels in terms of which finally the renormalised position space kernels will be derived. Note that in the following discussion of this section parton indices will be omitted as they can be inferred from the structure of the equations.

$\overline{\text{MS}}$ implementation and coupling renormalisation

The first step towards the renormalised momentum space kernels $W(\boldsymbol{\Delta}; \mu)$ is to implement the $\overline{\text{MS}}$ scheme consistently and perform the appropriate renormalisation of the strong coupling. Consider to this end the perturbative expansion of the bare momentum space kernel with bare strong coupling α_0

$$W_B(\boldsymbol{\Delta}) = \sum_n \left(\frac{\alpha_0}{2\pi}\right)^n W_0^{(n)}(\boldsymbol{\Delta}). \quad (5.16)$$

Renormalisation of the bare strong coupling requires the introduction of the coupling renormalisation factor Z_α and the $\overline{\text{MS}}$ scheme is implemented as discussed in section 3.5.1 such that each power of the strong coupling is divided by the corresponding power of the factor S_ε. The bare momentum space kernel is then given by

$$W_B(\boldsymbol{\Delta}) = \sum_n \left(\frac{\mu^{2\varepsilon}}{S_\varepsilon} \frac{\alpha_s(\mu)}{2\pi} Z_\alpha(\mu)\right)^n W_0^{(n)}(\boldsymbol{\Delta})$$

$$= \sum_n a_s^n(\mu) \left(\frac{\mu}{\Delta}\right)^{2\varepsilon n} Z_\alpha^n(\mu) W_B^{(n)}, \quad (5.17)$$

where in the last step the abbreviation a_s from footnote 2 has been used and $\boldsymbol{\Delta}$ independent coefficients $W_B^{(n)}$ have been introduced as

$$W_B^{(n)}(x_1, x_2; \varepsilon) = \boldsymbol{\Delta}^{2\varepsilon n} S_\varepsilon^{-n} W_0^{(n)}(x_1, x_2, \boldsymbol{\Delta}; \varepsilon). \quad (5.18)$$

This could be achieved using the fact that $W_0^{(n)}(\boldsymbol{\Delta}) \propto \boldsymbol{\Delta}^{-2\varepsilon n}$ for dimensional reasons. Up to order a_s one finds for the coupling renormalisation factor

$$Z_\alpha(\mu) = 1 - \frac{a_s(\mu)}{\varepsilon} \frac{\beta_0}{2} + \mathcal{O}(a_s^2(\mu)), \quad (5.19)$$

with β_0 as implicitly defined in equation (2.13). Using equations (5.17) and (5.19) one finds the following expression for the bare momentum space $1 \to 2$ splitting kernel up to order a_s^2

$$W_B(\Delta) = a_s \left(\frac{\mu}{\Delta}\right)^{2\varepsilon} W_B^{(1)} + a_s^2 \left(\frac{\mu}{\Delta}\right)^{4\varepsilon} W_B^{(2)} - a_s^2 \left(\frac{\mu}{\Delta}\right)^{2\varepsilon} \frac{\beta_0}{2\varepsilon} W_B^{(1)} + \mathcal{O}(a_s^3). \qquad (5.20)$$

Renormalisation factors and splitting functions

Just like the momentum space $1 \to 2$ splitting kernels also the renormalisation factors Z and Z_s can be expanded as a perturbative series in a_s which then reads

$$Z(x, \varepsilon; \mu) = \delta(1 - x) + \sum_{n=1}^{\infty} a_s^n(\mu) Z^{(n)}(x, \varepsilon),$$

$$Z_s(x_1, x_2, \varepsilon; \mu) = \sum_{n=1}^{\infty} a_s^n(\mu) Z_s^{(n)}(x_1, x_2, \varepsilon). \qquad (5.21)$$

Note that the $1 \to 2$ renormalisation factor Z_s has no tree level term, corresponding to the fact that the $1 \to 2$ splitting starts only at order $\mathcal{O}(a_s)$. With the implementation of the $\overline{\text{MS}}$ scheme introduced in section 3.5.1 all counterterms are then pure poles in ε. An analogous perturbative expansion can furthermore also be performed for the evolution kernels P and P_s, namely

$$P(x; \mu) = \sum_{n=0}^{\infty} a_s^{n+1}(\mu) P^{(n)}(x), \qquad P_s(x_1, x_2; \mu) = \sum_{n=0}^{\infty} a_s^{n+1}(\mu) P_s^{(n)}(x_1, x_2). \qquad (5.22)$$

In combination with equations (3.86) and (3.87) these expansions give rise to the following relations between the renormalisation factors and the corresponding splitting kernels

$$\left[Z^{(1)}\right]_{-1} = -P^{(0)}, \qquad \left[Z_s^{(1)}\right]_{-1} = -P_s^{(0)}, \qquad \left[Z_s^{(2)}\right]_{-1} = -P_s^{(1)}/2, \qquad (5.23)$$

which will be of crucial importance in the remainder of this section. Going back to equation (3.82) one can then use the above relations to express also the ε^{-2} pole of the splitting renormalisation factor in terms of known quantities. To this end one uses that the ε^{-1} pole on the right-hand side of equation (3.82) has to vanish as P_s is independent of ε. In combination with the D-dimensional renormalisation group derivative in equation (3.85) this makes it possible to derive the following identity

$$\left[Z_s^{(2)}\right]_{-2} = \frac{1}{2}\left(\frac{\beta_0}{2} P_s^{(0)} + P^{(0)} \underset{1}{\otimes} P_s^{(0)} + P^{(0)} \underset{2}{\otimes} P_s^{(0)} + P_s^{(0)} \underset{12}{\otimes} P^{(0)}\right). \qquad (5.24)$$

This can be further simplified by taking into account that at LO the $1 \to 2$ evolution kernel has the form

$$P_s^{(0)}(x_1, x_2) = \delta(1 - x_1 - x_2) P_s^{(0)}(x_1), \qquad (5.25)$$

with a kinematic constraint due to the fact that at this order the splitting process gives exactly two final state partons carrying together the momentum of the initial splitting parton. The one-variable kernel $P_s(x)$ is equal to $P^{(0)}(x)$, except that it has no $\delta(1-x)$ terms and no plus prescription on $1/(1-x)$ factors which arise from virtual diagrams in $P^{(0)}(x)$. Therefore the convolutions in (5.24) turn into ordinary products:

$$
P^{(0)} \underset{1}{\otimes} P_s^{(0)} = P^{(0)}\left(\frac{x_1}{1-x_2}\right) \frac{P_s^{(0)}(1-x_2)}{1-x_2} \, ,
$$

$$
P^{(0)} \underset{2}{\otimes} P_s^{(0)} = P^{(0)}\left(\frac{x_2}{1-x_1}\right) \frac{P_s^{(0)}(x_1)}{1-x_1} \, ,
$$

$$
P_s^{(0)} \underset{12}{\otimes} P^{(0)} = P_s^{(0)}\left(\frac{x_1}{x_1+x_2}\right) \frac{P^{(0)}(x_1+x_2)}{x_1+x_2} \, . \tag{5.26}
$$

Note that for flavour diagonal transitions these expressions still contain δ- and plus-distributions, which will be made explicit in equations (5.125) and (5.126).

5.3.2. Momentum space kernels

Following these preliminaries it is now possible to derive how the renormalised momentum space $1 \to 2$ splitting kernel in equation (5.15) is related to its bare counterpart. Consider therefore the expansion of the renormalised kernel in $D = 4 - 2\varepsilon$ dimensions

$$
W(\boldsymbol{\Delta}, \varepsilon; \mu) = \sum_{n=1}^{\infty} a_s^n(\mu)\, W^{(n)}(\boldsymbol{\Delta}, \varepsilon; \mu) \, , \quad W^{(n)}(\boldsymbol{\Delta}, \varepsilon; \mu) = \sum_{m=0}^{n} \left(\frac{\mu}{\boldsymbol{\Delta}}\right)^{2\varepsilon m} W^{(n,m)}(\varepsilon) \, . \tag{5.27}
$$

Here the coefficient $W^{(n,n)}$ equals the nth order term $W_B^{(n)}$ of the bare kernel W_B in equation (5.17), the coefficients $W^{(n,m)}$ with $0 < m < n$ are products of lower order terms $W_B^{(m)}$ with renormalisation counterterms for the twist-two operators or the strong coupling, while $W^{(n,0)}$ originates from the counterterm for the splitting singularity. The kernel in 4 dimensions is finally obtained by expanding $(\mu/\Delta)^{2\varepsilon m}$ in ε, which yields

$$
W^{(n)}(\boldsymbol{\Delta}; \mu) \underset{\text{def}}{=} W^{(n)}(\boldsymbol{\Delta}, \varepsilon = 0; \mu) = \sum_{k=0}^{n} \left(\ln\frac{\mu^2}{\boldsymbol{\Delta}^2}\right)^k W^{[n,k]} \, , \tag{5.28}
$$

where the coefficients $W^{[n,k]}$ are given by

$$
W^{[n,0]} = \sum_{m=0}^{n} \left[W^{(n,m)}\right]_0 \, , \qquad W^{[n,k]} = \sum_{m=1}^{n} \frac{m^k}{k!} \left[W^{(n,m)}\right]_{-k} \quad \text{for } k \geq 1 \, . \tag{5.29}
$$

From the requirement that poles in ε cancel in the coefficients $W^{(n)}$ one can furthermore derive the following finiteness conditions

$$
0 = \sum_{m=0}^{n} \left[W^{(n,m)}\right]_{-j} \, , \qquad 0 = \sum_{m=1}^{n} m^k \left[W^{(n,m)}\right]_{-k-j} \quad \text{for } k \geq 1 \, , \tag{5.30}
$$

where $j \geq 1$ in all cases.

Following the discussion below equation (5.27) one thus finds that at LO the coefficients $W^{(n,m)}$ in equation (5.27) are given by

$$W^{(1,1)} = W_B^{(1)}, \qquad\qquad W^{(1,0)} = Z_s^{(1)} = -\varepsilon^{-1} P_s^{(0)}, \qquad (5.31)$$

where in the last step equation (5.23) has been used. As $W^{(1)}$ has at most single poles the first condition in equation (5.30) implies

$$\left[W_B^{(1)}\right]_{-1} = P_s^{(0)}. \qquad (5.32)$$

The LO coefficients of the renormalised kernel in 4 dimensions defined in equation (5.28) can thus be extracted as

$$W^{[1,0]} = \left[W^{(1,1)}\right]_0 = \left[W_B^{(1)}\right]_0, \qquad\qquad W^{[1,1]} = \left[W^{(1,1)}\right]_{-1} = P_s^{(0)}. \qquad (5.33)$$

At NLO the situation is naturally more complicated and the coefficients $W^{(n,m)}$ of the renormalised $1 \to 2$ momentum space kernel in $D = 4 - 2\varepsilon$ dimensions given in equation (5.27) are found to be given by the following expressions

$$W^{(2,2)} = W_B^{(2)},$$

$$W^{(2,1)} = -\frac{\beta_0}{2\varepsilon} W_B^{(1)} + Z^{(1)} \underset{1}{\otimes} W_B^{(1)} + Z^{(1)} \underset{2}{\otimes} W_B^{(1)} - W_B^{(1)} \underset{12}{\otimes} Z^{(1)}$$

$$= -\frac{1}{\varepsilon} \left(\frac{\beta_0}{2} W_B^{(1)} + P^{(0)} \underset{1}{\otimes} W_B^{(1)} + P^{(0)} \underset{2}{\otimes} W_B^{(1)} - W_B^{(1)} \underset{12}{\otimes} P^{(0)} \right),$$

$$W^{(2,0)} = Z_s^{(2)} - Z_s^{(1)} \underset{12}{\otimes} Z^{(1)}$$

$$= -\frac{1}{2\varepsilon} P_s^{(1)} + \frac{1}{\varepsilon^2} \left[Z_s^{(2)} \right]_{-2} - \frac{1}{\varepsilon^2} P_s^{(0)} \underset{12}{\otimes} P^{(0)}, \qquad (5.34)$$

where in the second steps use was made of equation (5.23). In this case the finiteness conditions of equation (5.30) now read

$$0 = \left[W^{(2,2)}\right]_{-1} + \left[W^{(2,1)}\right]_{-1} + \left[W^{(2,0)}\right]_{-1},$$

$$0 = \left[W^{(2,2)}\right]_{-2} + \left[W^{(2,1)}\right]_{-2} + \left[W^{(2,0)}\right]_{-2},$$

$$0 = 2\left[W^{(2,2)}\right]_{-2} + \left[W^{(2,1)}\right]_{-2}. \qquad (5.35)$$

Using the relation for the double pole of $Z_s^{(2)}$ derived in equation (5.24) and the fact the double poles in $W^{(2,1)}$ in equation (5.34) are obtained by replacing $W_B^{(1)}$ with $\varepsilon^{-1} P_s^{(0)}$, one can derive the following relation

$$\left[W_B^{(2)}\right]_{-2} = \frac{1}{2} \left(\frac{\beta_0}{2} P_s^{(0)} + P^{(0)} \underset{1}{\otimes} P_s^{(0)} + P^{(0)} \underset{2}{\otimes} P_s^{(0)} - P_s^{(0)} \underset{12}{\otimes} P^{(0)} \right), \qquad (5.36)$$

fixing the double pole of $W_B^{(2)}$ in terms of the LO kernels and thus serving as a valuable cross check of the two-loop calculation in the following sections. For the single poles on the other hand, one obtains from equation (5.34)

$$
\left[W_B^{(2)}\right]_{-1} = \frac{1}{2} P_s^{(1)} + \left(\frac{\beta_0}{2}\left[W_B^{(1)}\right]_0 + P^{(0)} \underset{1}{\otimes} \left[W_B^{(1)}\right]_0 + P^{(0)} \underset{2}{\otimes} \left[W_B^{(1)}\right]_0 - \left[W_B^{(1)}\right]_0 \underset{12}{\otimes} P^{(0)}\right),
$$
(5.37)

from which the NLO $1 \to 2$ evolution kernel $P_s^{(1)}$ can be extracted given the bare NLO splitting kernel $W_B^{(2)}$. Finally, the coefficients of the renormalised kernel in 4 dimensions are obtained by collecting the finite contributions, which yields

$$
W^{[2,0]} = \left[W_B^{(2)}\right]_0 - \left(\frac{\beta_0}{2}\left[W_B^{(1)}\right]_1 + P^{(0)} \underset{1}{\otimes} \left[W_B^{(1)}\right]_1 + P^{(0)} \underset{2}{\otimes} \left[W_B^{(1)}\right]_1 - \left[W_B^{(1)}\right]_1 \underset{12}{\otimes} P^{(0)}\right),
$$

$$
W^{[2,1]} = P_s^{(1)} + \frac{\beta_0}{2} W^{[1,0]} + P^{(0)} \underset{1}{\otimes} W^{[1,0]} + P^{(0)} \underset{2}{\otimes} W^{[1,0]} - W^{[1,0]} \underset{12}{\otimes} P^{(0)},
$$

$$
W^{[2,2]} = \frac{1}{2}\left(\frac{\beta_0}{2} P_s^{(0)} + P^{(0)} \underset{1}{\otimes} P_s^{(0)} + P^{(0)} \underset{2}{\otimes} P_s^{(0)} - P_s^{(0)} \underset{12}{\otimes} P^{(0)}\right),
$$
(5.38)

where equation (5.33) has been used to replace $\left[W_B^{(1)}\right]_0$ by $W^{[1,0]}$. Inserting equations (5.33) and (5.38) into the factorisation formula for $F(\Delta; \mu)$ in equation (5.14) and taking the renormalisation group derivative, one obtains the inhomogeneous double DGLAP equation (2.56) up to order a_s^2 as a cross check.

In order to evaluate equation (5.38) and extract the renormalised NLO $1 \to 2$ momentum space kernel one needs $W_B^{(1)}$ up to $\mathcal{O}(\varepsilon)$. The full expressions for $W_B^{(1)}$ in $D = 4 - 2\varepsilon$ dimensions are easily computed along the lines of section 5 in [26] and read

$$
W_B^{(1)}(x_1, x_2) = \delta(1 - x_1 - x_2)\, W_B^{(1)}(x_1),
$$
(5.39)

with

$$
\varepsilon R_\varepsilon W_B^{(1)}(x) = P(x, \varepsilon),
$$
(5.40)

where the $P(x, \varepsilon)$ are as given in equation (4.2) and the factor

$$
R_\varepsilon = \frac{S_\varepsilon}{(4\pi)^\varepsilon} \frac{\Gamma(1 - 2\varepsilon)}{\Gamma(1 + \varepsilon)\Gamma^2(1 - \varepsilon)} = 1 + \mathcal{O}(\varepsilon^2)
$$
(5.41)

has been introduced with S_ε specified in equations (2.8) or (2.9), respectively. Since $W_B^{(1)}(x_1, x_2)$ has the same kinematic constraint on x_1 and x_2 as $P_s^{(0)}$ in equation (5.25), the convolutions in equation (5.38) again reduce to ordinary products as already in equation (5.26), with $P_s^{(0)}$ replaced as appropriate.

The square of the tree-level graphs for the splitting $a_0 \to a_1 a_2$ that give rise to the expressions in equation (5.39) appears in many higher-order calculations and has been computed in many papers before. Here it should be noted, however, that W_B is computed for transverse momenta of a_1 and a_2 that differ by $\pm\Delta$ between the amplitude and its conjugate as indicated already in figure 2.6. This is typically not the case in other contexts. Nevertheless, the expressions on the right-hand side of equation (5.39) agree with the expressions for $P^{n\neq 4}$ given in section 3 of reference [96].

Equivalence of $\overline{\text{MS}}$ scheme implementations

In section 3.5.1 two different choices for the $\overline{\text{MS}}$ factor S_ε have been introduced along with the statement that for quantities with at most one pole in ε per order in a_s the two yield the same renormalised quantities. Here it will be shown that this is indeed the case and the two different definitions of S_ε yield the same renormalised kernels $W^{[n,k]}$ in 4 dimensions at LO and NLO. Consider to this end the expansion of the standard S_ε and the one suggested by Collins in reference [47], which coincide in the constant and the first-order term $[S_\varepsilon]_1$ of the Taylor expansion of S_ε around $\varepsilon = 0$, but differ in the second-order term $[S_\varepsilon]_2$. Because $W_B^{(1)}$ has only a single pole in ε, it is straightforward to see that the renormalised LO kernels are identical for the two choices, as are the associated renormalisation factors $Z^{(1)}$ and $Z_s^{(1)}$. Since $W_B^{(2)}$ contains at most double poles in ε, the NLO renormalisation factor $Z_s^{(2)}$ is the same for the two choices as well. The only remaining dependence on $[S_\varepsilon]_2$ in the renormalised two loop kernel $W^{(2)}(\Delta;\mu)$ at $\varepsilon = 0$ can thus come from the terms

$$
\left[W^{(2,2)}\right]_{-2}\left[S_\varepsilon^{-2}\right]_2 + \left[W^{(2,1)}\right]_{-2}\left[S_\varepsilon^{-1}\right]_2
$$
$$
= \left(3\left[W^{(2,2)}\right]_{-2} + \left[W^{(2,1)}\right]_{-2}\right)\left(\left[S_\varepsilon\right]_1\right)^2 - \left(2\left[W^{(2,2)}\right]_{-2} + \left[W^{(2,1)}\right]_{-2}\right)\left[S_\varepsilon\right]_2. \quad (5.42)
$$

The expression in the first line of the above equation arises from considering equation (5.34) where the only dependence on S_ε is due to the terms $W_B^{(2)}$ and $W_B^{(1)}$ which contain negative powers of S_ε according to equation equation (5.18) while the renormalisation factors Z and Z_s are independent of S_ε in the implementation of the $\overline{\text{MS}}$ scheme introduced in section 3.5.1. From this the second line is obtained by expressing $[S_\varepsilon^{-2}]_2$ and $[S_\varepsilon^{-1}]_2$ in terms of $[S_\varepsilon]_1$ and $[S_\varepsilon]_2$. Finally, using the last of the NLO finiteness relations in equation (5.35) it can be shown that the remaining dependence on $[S_\varepsilon]_2$ cancels in this expression, which completes the argument.

5.3.3. Position space kernels

In order to obtain the renormalised position space $1 \to 2$ splitting kernel $V(y;\mu)$ consider how the bare kernels $V_B(y)$ and $W_B(\Delta)$ are related. As the bare momentum space DPDs are related to the bare position space DPDs by a Fourier transform as

shown in equation (2.24) the bare position space kernel $V_B(y)$ is naturally obtained from $W_B(\Delta)$ by the inverse Fourier transform. Using equation (E.1) in reference [72], one gets for the a_s^n term in (5.17)

$$\int \frac{\mathrm{d}^{D-2}\Delta}{(2\pi)^{D-2}} e^{-i\Delta y} \left(\frac{\mu}{\Delta}\right)^{2\varepsilon n} W_B^{(n)} = \frac{\Gamma(1-\varepsilon)}{(\pi y^2)^{1-\varepsilon}} \left(\frac{y\mu}{b_0}\right)^{2\varepsilon n} n\varepsilon\, T_{\varepsilon,n}\, W_B^{(n)} , \tag{5.43}$$

with b_0 given in equation (2.59) and

$$T_{\varepsilon,n} = \frac{\Gamma(1-\varepsilon-\varepsilon n)}{\Gamma(1+\varepsilon n)\,\Gamma(1-\varepsilon)} e^{-2n\gamma\varepsilon} = 1 + \zeta_2\, n\varepsilon^2 + \frac{\zeta_3}{3}\left(2n^3 + 3n^2 + 3n\right)\varepsilon^3 + \mathcal{O}(\varepsilon^4), \tag{5.44}$$

where ζ_n denotes the Riemann ζ function evaluated at integer argument n. One can then define[3]

$$V(y,\varepsilon;\mu) = \sum_{n=1}^{\infty} a_s^n(\mu)\, V^{(n)}(y,\varepsilon;\mu), \quad V^{(n)}(y,\varepsilon;\mu) = \sum_{m=1}^{n} \left(\frac{y\mu}{b_0}\right)^{2\varepsilon m} V^{(n,m)}(\varepsilon). \tag{5.45}$$

In contrast to equation (5.27) there is no $m = 0$ term here, since in momentum space this term is associated with the splitting which is absent in y space. The counterterms for the twist-two operators and the QCD coupling, on the other hand, are identical in momentum and position space such that one can derive the following relation between the coefficients of the renormalised position and momentum space kernels in $D = 4 - 2\varepsilon$ dimensions

$$V^{(n,m)}(\varepsilon) = m\varepsilon\, T_{\varepsilon,m}\, W^{(n,m)}(\varepsilon). \tag{5.46}$$

The kernel in physical dimensions can again be obtained in much the same way as the momentum space kernel in the previous section by expanding equation (5.45) around $\varepsilon = 0$

$$V^{(n)}(y,\mu) \underset{\mathrm{def}}{=} V^{(n)}(y,\varepsilon=0;\mu) = \sum_{k=0}^{n-1} \left(\ln\frac{y^2\mu^2}{b_0^2}\right)^k V^{[n,k]}. \tag{5.47}$$

Here the coefficients $V^{[n,k]}$ and $V^{(n,m)}$ obey exactly the same relations as $W^{[n,k]}$ and $W^{(n,m)}$ in equations (5.29) and (5.30), with the difference that as mentioned already above the sum over m always starts at $m = 1$ in this case.

From equation (5.46) one can then – at LO and NLO – derive the following relation between the coefficients $V^{(n,m)}$ and $W^{(n,m)}$

$$\left[V^{(n,m)}\right]_{-k} = \left[m\varepsilon\, W^{(n,m)}\right]_{-k} = m\left[W^{(n,m)}\right]_{-k-1} \qquad \text{for } k \geq 0 \text{ and } n = 1,2. \tag{5.48}$$

---

[3]Note that here and in equation (5.47) a convention that differs from equations (3.15) and (3.16) in reference [35] is used.

From this it follows that the kernel $V^{(1)}$ is finite for $\varepsilon = 0$ while $V^{(2)}$ has at most single poles, resulting in only a single finiteness condition, given by

$$0 = \left[V^{(2,2)}\right]_{-1} + \left[V^{(2,1)}\right]_{-1}, \tag{5.49}$$

which is fulfilled due to equation (5.48) for $k = 1$ and $n = 2$ and the third relation in equation (5.35). For the coefficients $V^{[n,k-1]}$ of the finite part of the kernel, the relations in equation (5.48) thus imply

$$
\begin{aligned}
V^{[n,k-1]} &= \sum_{m=1}^{n} \frac{m^k}{(k-1)!} \left[W^{(n,m)}\right]_{-k} = k \sum_{m=0}^{n} \frac{m^k}{k!} \left[W^{(n,m)}\right]_{-k} \\
&= k\, W^{[n,k]} \qquad\qquad \text{for } 1 \le k \le n \text{ and } n = 1,2,
\end{aligned}
\tag{5.50}
$$

where the relation in equation (5.29) and its counterpart for the position space coefficients $V^{[n,k]}$ have been used. At LO and NLO one can thus derive the following simple relation between the kernels in 4 dimensions:

$$V^{(n)}(\boldsymbol{y}; \mu) = \frac{\partial}{\partial \ln \mu^2} W^{(n)}(\Delta = b_0/y; \mu) \qquad \text{for } n = 1,2. \tag{5.51}$$

Explicitly, the coefficients of the renormalised position space $1 \to 2$ kernel in 4 dimensions are, up to NLO, given by

$$V^{[1,0]} = W^{[1,1]} = P_s^{(0)},$$

$$V^{[2,0]} = W^{[2,1]} = P_s^{(1)} + \frac{\beta_0}{2} \left[W_B^{(1)}\right]_0 + P^{(0)} \underset{1}{\otimes} \left[W_B^{(1)}\right]_0 + P^{(0)} \underset{2}{\otimes} \left[W_B^{(1)}\right]_0 - \left[W_B^{(1)}\right]_0 \underset{12}{\otimes} P^{(0)},$$

$$V^{[2,1]} = 2W^{[2,2]} = \frac{\beta_0}{2} P_s^{(0)} + P^{(0)} \underset{1}{\otimes} P_s^{(0)} + P^{(0)} \underset{2}{\otimes} P_s^{(0)} - P_s^{(0)} \underset{12}{\otimes} P^{(0)}. \tag{5.52}$$

As a cross check these expressions can again be inserted into the factorisation formula of equation (5.14) for $F(\boldsymbol{y}; \mu)$ from which one then correctly obtains the homogeneous double DGLAP equation (2.51) up to order a_s^2 by taking the renormalisation scale derivative.

Higher orders

Keeping in mind the simple relations between the position and momentum space $1 \to 2$ splitting kernels – equations (5.50) and (5.51) – one may wonder whether these remain valid at all orders n. Consider to this end the situation at NNLO, meaning $n = 3$, where the $\mathcal{O}(\varepsilon^2)$ term of $T_{\varepsilon,n}$ contributes for the first time, namely to the finite part of $V^{(3)}$ but not to its poles. Using equations (5.44) and (5.48) one then finds

$$V^{[3,0]} = \sum_{m=1}^{3} \left[V^{(3,m)}\right]_0 = \sum_{m=1}^{3} m \left[W^{(3,m)}\right]_{-1} + \zeta_2 \sum_{m=1}^{3} m^2 \left[W^{(3,m)}\right]_{-3}. \tag{5.53}$$

Here the sum multiplying ζ_2 vanishes due to the finiteness conditions in equation (5.30) for $k = 2, j = 1$, such that equation (5.50) remains valid for $n = 3$. At N^3LO, however, the situation is different, as can be seen by considering $V^{[4,0]}$

$$V^{[4,0]} = \sum_{m=1}^{4} \left[V^{(4,m)} \right]_0 = \sum_{m=1}^{4} m \left[W^{(4,m)} \right]_{-1} + \zeta_2 \sum_{m=1}^{4} m^2 \left[W^{(4,m)} \right]_{-3}$$
$$+ \frac{\zeta_3}{3} \sum_{m=1}^{4} \left(2m^4 + 3m^2 + 3m \right) \left[W^{(4,m)} \right]_{-4}. \tag{5.54}$$

Here the sum over $m^k \left[W^{(4,m)} \right]_{-4}$ vanishes for $k = 1, 2, 3$ but not for $k = 4$ according to the finiteness condition of equation (5.30). Using equation (5.29) one thus obtains

$$V^{[4,0]} = W^{[4,1]} + 16\zeta_3 W^{[4,4]}, \tag{5.55}$$

which illustrates that at this order equation (5.50) and thus also equation (5.51) are no longer valid.

5.4. Matching between momentum and position space DPDs at higher orders

With the results from the preceding section it is now possible to generalise the matching between cut-off and $\overline{\text{MS}}$ momentum space DPDs. Consider to this end again a cut-off regularised momentum space DPD as defined in reference [35]:

$$F_{\Phi, a_1 a_2}(x_1, x_2, \mathbf{\Delta}; \mu, \nu) = \int \mathrm{d}^2 \mathbf{y} \, e^{i \mathbf{y} \mathbf{\Delta}} \, \Phi(y\nu) \, F_{a_1 a_2}(x_1, x_2, \mathbf{y}; \mu), \tag{5.56}$$

where Φ is – without a loss of generality, as will be shown in a moment – the hard cut-off defined already in equation (2.59). The difference between the $\overline{\text{MS}}$ renormalised momentum space DPD defined in equation (2.53) and the cut-off momentum space DPD defined in equation (5.56) is then given by[4]

$$F_{\overline{\text{MS}}}(\mathbf{\Delta}; \mu) - F_{\Phi}(\mathbf{\Delta}; \mu, \nu) = \lim_{\varepsilon \to 0} \left[\int \mathrm{d}^{D-2} \mathbf{y} \, e^{i \mathbf{\Delta} \mathbf{y}} F(\mathbf{y}, \varepsilon; \mu) + Z_s(\varepsilon; \mu) \underset{12}{\otimes} Z^{-1}(\varepsilon; \mu) \otimes f(\varepsilon; \mu) \right]$$
$$= \lim_{\varepsilon \to 0} \left[\int \mathrm{d}^{D-2} \mathbf{y} \, F(\mathbf{y}, \varepsilon; \mu) + Z_s(\varepsilon; \mu) \underset{12}{\otimes} Z^{-1}(\varepsilon; \mu) \otimes f(\mu) \right]$$
$$+ \int \mathrm{d}^2 \mathbf{y} \left[e^{i \mathbf{\Delta} \mathbf{y}} - 1 \right] F(\mathbf{y}; \mu). \tag{5.57}$$

In this equation the splitting counterterm needed to regularise the splitting singularity in equation (2.53) has been written out explicitly. Furthermore all ε dependences have

---

[4]Note that here the integrals are understood to be restricted to values of $y < b_0/\nu$.

been indicated, using the shorthand notation $F(y; \mu) = F(y, \varepsilon = 0; \mu)$ in the last term. Using the above relation the matching may be split up into a part at $\boldsymbol{\Delta} = 0$ involving DPDs in $D = 4 - 2\varepsilon$ dimensions and a $\boldsymbol{\Delta}$ dependent part that involves only DPDs at the physical point $\varepsilon = 0$.

A crucial point for the following arguments is that the the cut-off scale ν is understood to be large enough to justify replacing $F(y; \mu)$ with the perturbative splitting contribution given in equation (5.14), up to corrections in powers of Λ/ν, where Λ is understood to be a generic hadronic scale. Here it should be noted that as discussed in section 3.3 of reference [35], the corrections of order Λ/ν arise from twist-three distributions, which are expected to be small at low x_1 and x_2, where DPDs are naturally large. Therefore the dominant power corrections are expected to be of order Λ^2/ν^2.

At this point it makes sense to show that the choice of the hard cut-off as a regulator function in equation (5.56) really comes without a loss of generality. Consider to this end the difference between two momentum space DPDs defined with different regulator functions Φ_1 and Φ_2, given by

$$F_{\Phi_1}(\boldsymbol{\Delta}; \mu, \nu) - F_{\Phi_2}(\boldsymbol{\Delta}; \mu, \nu) = \int d^2 y \, e^{i\Delta y} \left[\Phi_1(y\nu) - \Phi_2(y\nu)\right] F(y; \mu).$$ (5.58)

In this expression $F(y; \mu)$ can be evaluated at the physical point, as the regulator functions Φ_i guarantee that the integrals over y is finite in the ultraviolet. As the expression in square brackets vanishes for distances y of hadronic size due to the fact that both regulator functions Φ_i approach 1 in this limit, $F(y; \mu)$ can be replaced by its small y perturbative splitting form given in equation (5.14). With the help of equation (5.47) the difference between the momentum space DPDs defined with different regulator functions in equation (5.58) can thus be expressed in terms of $V^{[n,k]}_{12} \otimes f(\mu)$ and the integrals

$$\int \frac{d(y^2)}{y^2} J_0(y\Delta) \left(\ln \frac{y^2\mu^2}{b_0^2}\right)^k \left[\Phi_1(y\nu) - \Phi_2(y\nu)\right],$$ (5.59)

where the Bessel function J_0 arises from performing the angular part of the y integration. Therefore it is straightforward to match between momentum space DPDs F_{Φ_i} defined with different regulator functions Φ_i, justifying limiting the discussion to the hard cut-off of equation (2.59).

5.4.1. Matching at zero Δ

As a first step towards the complete matching formula consider first the matching at $\Delta = 0$, which again can be written as a convolution of a $1 \to 2$ matching kernel U

with a PDF, in close analogy to the factorised expressions for the perturbative splitting contribution in equation (5.14)

$$F_{\overline{\text{MS}}}(\mathbf{\Delta} = 0; \mu) - F_{\Phi}(\mathbf{\Delta} = 0; \mu, \nu) = U(\mu, \nu) \underset{12}{\otimes} f(\mu) + \mathcal{O}(\Lambda/\nu). \tag{5.60}$$

In order to derive the form of the matching kernel $U(x_1, x_2; \mu, \nu)$, in the first term on the right-hand side of equation (5.57) $F(\mathbf{y}, \varepsilon; \mu)$ is replaced by its perturbative splitting form given in equation (5.14), which gives rise to integrals of the following form

$$\int_{y < b_0/\nu} \mathrm{d}^{D-2}\mathbf{y} \, \frac{\Gamma(1-\varepsilon)}{(\pi y^2)^{1-\varepsilon}} \left(\frac{y\mu}{b_0}\right)^{2\varepsilon m} = \frac{1}{m\varepsilon} \left(\frac{\mu}{\nu}\right)^{2\varepsilon m}, \tag{5.61}$$

where the y dependence from equation (5.45) has been used. The matching kernel in $D = 4 - 2\varepsilon$ dimensions, $U(x_1, x_2, \varepsilon; \mu, \nu)$, can again be expanded in a_s in close analogy to equations (5.27) and (5.45) as

$$U(\varepsilon; \mu, \nu) = \sum_{n=1}^{\infty} a_s^n(\mu) \, U^{(n)}(\varepsilon; \mu, \nu), \qquad U^{(n)}(\varepsilon; \mu, \nu) = \sum_{m=0}^{n} \left(\frac{\mu}{\nu}\right)^{2\varepsilon m} U^{(n,m)}(\varepsilon). \tag{5.62}$$

One thus finds that the coefficients $U^{(n,m)}$, $V^{(n,m)}$, and $W^{(n,m)}$ are related as

$$U^{(n,m)} = \frac{1}{m\varepsilon} V^{(n,m)} = T_{\varepsilon,m} W^{(n,m)} \qquad \text{for } m \geq 1, \tag{5.63}$$

with $T_{\varepsilon,m}$ as defined in equation (5.44), where in the last step the relation between $V^{(n,m)}$ and $W^{(n,m)}$ given in equation (5.46) has been used. The $m = 0$ coefficients $U^{(n,0)}$ originate from the splitting counterterm in equation (5.57) and thus read

$$U^{(n,0)} = W^{(n,0)}. \tag{5.64}$$

Making the step to physical dimensions, one finds that the matching kernel can again be written – in analogy to equations (5.28) and (5.47) – as

$$U^{(n)}(\mu, \nu) \underset{\text{def}}{=} U^{(n)}(\varepsilon = 0; \mu, \nu) = \sum_{m=0}^{n} \left(\ln \frac{\mu^2}{\nu^2}\right)^m U^{[n,m]}. \tag{5.65}$$

The coefficients $U^{[n,k]}$ and $U^{(n,m)}$ again follow the same relations as $W^{[n,k]}$ and $W^{(n,m)}$ in equation (5.29) and in particular he coefficients $U^{(n,m)}$ fulfil finiteness relations analogous to those for $W^{(n,m)}$ in equation (5.30).

Considering that $T_{\varepsilon,m} = 1 + \mathcal{O}(\varepsilon^2)$, it is evident from equation (5.63) that the pole terms of $U^{(n)}$ and $W^{(n)}$ coincide at LO and NLO, ensuring the validity of the finiteness conditions for U and consequently fixing all coefficients of the logarithms in equation (5.65). For the non-logarithmic term on the other hand one obtains the following relation

$$U^{[n,0]} = \sum_{m=0}^{n} \left[U^{(n,m)}\right]_0 = \sum_{m=0}^{n} \left[W^{(n,m)}\right]_0 + \zeta_2 \sum_{m=1}^{n} m \left[W^{(n,m)}\right]_{-2} \quad \text{for } n = 1, 2, \tag{5.66}$$

which has been obtained using equations (5.63), (5.64) and (5.44). The sum multiplying ζ_2 vanishes due to the finiteness conditions in equation (5.30) for $k = 1$, $j = 1$. In total on thus finds that at LO and NLO the coefficients for the $1 \to 2$ matching kernel in physical dimensions are identical to those of the renormalised momentum space $1 \to 2$ splitting kernel, namely

$$U^{[n,k]} = W^{[n,k]} \qquad\qquad \text{for } 0 \le k \le n \text{ and } n = 1, 2. \qquad (5.67)$$

Higher orders

Just like in the case of the position space kernel one may again wonder if the simple relation between the $U^{[n,k]}$ and $W^{[n,k]}$ kernels obtained in equation (5.67) remains valid at higher orders. To this end, consider the non-logarithmic NNLO coefficient $U^{[3,0]}$, given by

$$
\begin{aligned}
U^{[3,0]} &= \sum_{m=0}^{3} \left[U^{(3,m)}\right]_0 \\
&= \sum_{m=0}^{3} \left[W^{(3,m)}\right]_0 + \zeta_2 \sum_{m=1}^{3} m \left[W^{(3,m)}\right]_{-2} + \frac{\zeta_3}{3} \sum_{m=1}^{3} \left(2m^3 + 3m + 3\right) \left[W^{(3,m)}\right]_{-3} \\
&= W^{[3,0]} + 4\zeta_3\, W^{[3,3]} \,.
\end{aligned}
\qquad (5.68)
$$

In the first non-trivial step in the above equation relation (5.63) has been used to express the $U^{(n,m)}$ coefficients in terms of the $W^{(n,m)}$ coefficients while in the last step again the finiteness condition given in equation (5.30) has been used. Therefore one finds that already at NNLO the equivalence in equation (5.67) no longer holds. It is, however, possible to derive a relation between the matching kernels and the position space kernels from equation (5.63), that is valid to all orders.

$$\left[U^{(n,m)}\right]_{-k-1} = \frac{1}{m}\left[V^{(n,m)}\right]_{-k} \qquad\qquad \text{for } k \ge 0,\, m \ge 1, \text{ and all } n. \qquad (5.69)$$

From this one can finally derive – in analogy to equation (5.50) – the following relation

$$U^{[n,k]} = \frac{1}{k}\, V^{[n,k-1]} \qquad\qquad \text{for } 1 \le k \le n \text{ and all } n, \qquad (5.70)$$

which for $n = 1, 2$ is of course consistent with equations (5.50) and (5.67).

5.4.2. Matching at non-zero Δ

In order to derive the matching for non-zero Δ now both terms on the right-hand side of equation (5.57) have to be taken into account. To this end one can use the

perturbative splitting form of the position space DPD $F(y; \mu)$ given in equation (5.14) and the expansion of the kernel position space $1 \to 2$ splitting kernel V defined in equation (5.47), to obtain

$$
F_{\overline{\text{MS}}}(\Delta; \mu) - F_{\Phi}(\Delta; \mu, \nu) = U(\mu, \nu) \underset{12}{\otimes} f(\mu) + \sum_{n=1}^{\infty} a_s^n(\mu) \sum_{k=0}^{n-1} I_k(\Delta; \mu, \nu) \, V^{[n,k]} \otimes f(\mu) \,,
$$

$$(5.71)$$

where corrections are again of order $\mathcal{O}(\Lambda/\nu)$ and the coefficients I_k are given by the following integrals

$$
I_k(\Delta; \mu, \nu) = \int_0^{b_0^2/\nu^2} \frac{\mathrm{d}(y^2)}{y^2} \left[J_0(y\Delta) - 1 \right] \left(\ln \frac{y^2 \mu^2}{b_0^2} \right)^k,
$$

$$(5.72)$$

which are obtained after the angular part of the y integration has been performed in analogy to the situation in equation (5.59). Here the renormalisation scale dependence can be made explicit by rewriting the above equation as

$$
I_k(\Delta; \mu, \nu) = \sum_{j=0}^{k} \binom{k}{j} I_j(\Delta; \nu, \nu) \left(\ln \frac{\mu^2}{\nu^2} \right)^j,
$$

$$(5.73)$$

where the coefficients $I_j(\Delta; \nu, \nu)$ are given by

$$
I_j(\Delta; \nu, \nu) = 2 \int_0^a \frac{\mathrm{d}z}{z} \left[J_0(z) - 1 \right] \left(\ln \frac{z^2}{a^2} \right)^j = \frac{1}{j+1} \int_0^a \mathrm{d}z \, J_1(z) \left(\ln \frac{z^2}{a^2} \right)^{j+1},
$$

$$(5.74)$$

with $a = b_0 \Delta/\nu$. The relations given in the equations above can be further simplified when the limits $\Delta \ll \nu$ and $\nu \ll \Delta$ are considered. For the first case the behaviour of equation (5.73) is straightforwardly obtained by Taylor expanding the Bessel function around $\Delta = 0$, yielding

$$
I_k(\Delta; \mu, \nu) \underset{\Delta \ll \nu}{=} -\frac{b_0^2 \Delta^2}{4\mu^2} \int_0^{\mu^2/\nu^2} \mathrm{d}z \, \ln^k z = -\frac{b_0^2 \Delta^2}{4\nu^2} \left[\left(\ln \frac{\mu^2}{\nu^2} \right)^k + \sum_{j=0}^{k-1} c_j \left(\ln \frac{\mu^2}{\nu^2} \right)^j \right], \quad (5.75)
$$

with numerical coefficients c_j. In the case that $\nu \ll \Delta$ on the other hand the limiting behaviour of equation (5.73) is obtained by writing out the polynomial series of $\ln^{k+1}(z^2/a^2) = \left[\ln(\nu^2/\Delta^2) + \ln(z^2/b_0^2) \right]^{k+1}$ and extending the z integration to infinity in equation (5.74) such that one obtains

$$
I_j(\Delta; \nu, \nu) \underset{\nu \ll \Delta}{=} \frac{1}{j+1} \left[\left(\ln \frac{\nu^2}{\Delta^2} \right)^{j+1} + \sum_{i=0}^{j} d_i \left(\ln \frac{\nu^2}{\Delta^2} \right)^i \right],
$$

$$(5.76)$$

where the d_i are again numerical coefficients. In order to finally obtain the large Δ behaviour of $I_k(\Delta; \mu, \nu)$ in equation (5.73) the above expression for $I_j(\Delta; \nu, \nu)$ is used and the binomial sum rearranged, yielding

$$I_k(\Delta; \mu, \nu) \underset{\nu \ll \Delta}{=} \frac{1}{k+1} \left[\left(\ln \frac{\mu^2}{\Delta^2} \right)^{k+1} - \left(\ln \frac{\mu^2}{\nu^2} \right)^{k+1} \right] + \dots, \tag{5.77}$$

where the ellipsis denotes terms with fewer powers of logarithms.

In order to be able to use the matching equation (5.71) truncated in a_s reliably, large logarithms at higher orders must be avoided. This requires to take $\nu \sim \mu$ for the Δ independent term with $U(\mu, \nu)$. However, this leads to the occurrence of large logarithms in equation (5.77), such that the limit $\nu \ll \Delta$ has to be avoided as otherwise the matching relation breaks down when the perturbative series is truncated. On the other hand, no large logarithms appear for $\Delta \ll \nu$ according to equation (5.75), such that fixed order matching is thus possible both for $\Delta \sim \nu$ and for $\Delta \ll \nu$.

For $j = 0, 1, 2$ a closed form of coefficients $I_j(\Delta; \nu, \nu)$ can be obtained in terms of the generalised hypergeometric functions $_pF_q$, namely

$$I_0(\Delta; \nu, \nu) = -\frac{a^2}{4} \, _2F_3\left(1, 1; 2, 2, 2; -\frac{a^2}{4}\right),$$

$$I_1(\Delta; \nu, \nu) = \frac{a^2}{4} \, _3F_4\left(1, 1, 1; 2, 2, 2, 2; -\frac{a^2}{4}\right),$$

$$I_2(\Delta; \nu, \nu) = -\frac{a^2}{2} \, _4F_5\left(1, 1, 1, 1; 2, 2, 2, 2, 2; -\frac{a^2}{4}\right). \tag{5.78}$$

5.4.3. Scale independence of matching

Here the dependence of the matching equation (5.71) on the cut-off scale ν and its behaviour under renormalisation group evolution will be discussed in detail. To this end consider first the ν dependence of the left- and right-hand sides of equation (5.71) which will now be shown to be identical. The logarithmic ν derivative of the left-hand side is given by

$$-\frac{\mathrm{d}}{\mathrm{d}\ln\nu^2} F_\Phi(\Delta = 0; \mu, \nu) = -\frac{\mathrm{d}}{\mathrm{d}\ln\nu^2} \pi \int_{b_0^2/\nu^2}^\infty \mathrm{d}y^2 \, J_0(y\Delta) \, F(\boldsymbol{y}; \mu)$$

$$= -\frac{\pi b_0^2}{\nu^2} J_0\left(\frac{b_0\Delta}{\nu}\right) F\left(y = \frac{b_0}{\nu}; \mu\right)$$

$$= -J_0\left(\frac{b_0\Delta}{\nu}\right) \sum_{n=1}^\infty a_s^n \sum_{k=0}^{n-1} \left(\ln \frac{\mu^2}{\nu^2}\right)^k V^{[n,k]} \underset{12}{\otimes} f(\mu), \tag{5.79}$$

where in the last step once again the perturbative splitting form of $F(y; \mu)$ given in equation (5.14) and equation (5.47) have been, as is appropriate for $y = b_0/\nu$. For the ν dependence of the right-hand side of equation (5.71) on the other hand one gets

$$
\frac{\mathrm{d}}{\mathrm{d}\ln\nu^2} \sum_{n=1}^{\infty} a_s^n \left\{ \sum_{k=0}^{n} \left(\ln\frac{\mu^2}{\nu^2} \right)^k U^{[n,k]} + \sum_{k=0}^{n-1} I_k(\Delta; \mu, \nu)\, V^{[n,k]} \right\} \underset{12}{\otimes} f(\mu)
$$
$$
= - \sum_{n=1}^{\infty} a_s^n \sum_{k=0}^{n-1} \left(\ln\frac{\mu^2}{\nu^2} \right)^k \left\{ (k+1)\, U^{[n,k+1]} + \left[J_0\left(\frac{b_0\Delta}{\nu} \right) - 1 \right] V^{[n,k]} \right\} \underset{12}{\otimes} f(\mu)\,, \quad (5.80)
$$

where the integral representation of I_k given in equation (5.72) has been used. Using the relation between the position space $1 \to 2$ splitting kernel V and the matching kernel U derived in equation (5.70), one easily sees that both sides of the matching equation (5.71) have the same cut-off scale dependence at each fixed order in a_s, as it should be. This statement holds up to power corrections in Λ/ν, which arise from replacing $F(y; \mu)$ with its perturbative splitting form given in equation (5.14).

Consider next the renormalisation scale dependence of the matching equation (5.71). Using the appropriate – homogeneous or inhomogeneous – double DGLAP equations, one obtains for the renormalisation scale derivative of the left-hand side

$$
\frac{\mathrm{d}}{\mathrm{d}\ln\mu^2} \left[F_{\overline{\mathrm{MS}}}(\Delta; \mu) - F_\Phi(\Delta; \mu, \nu) \right] = P_s \underset{12}{\otimes} f(\mu) + P \underset{1}{\otimes} \left[F_{\overline{\mathrm{MS}}}(\Delta; \mu) - F_\Phi(\Delta; \mu, \nu) \right]
$$
$$
+ P \underset{2}{\otimes} \left[F_{\overline{\mathrm{MS}}}(\Delta; \mu) - F_\Phi(\Delta; \mu, \nu) \right]\,, \quad (5.81)
$$

where the term with P_s arises from the $\overline{\mathrm{MS}}$ momentum space DPD where the splitting singularity is renormalised according to equation (2.56). Here one can on the right-hand side replace the difference of DPDs with the matching expression given in equation (5.71). Comparing this to the renormalisation group derivative of the right-hand side of equation (5.71), one finds that the matching equation holds at arbitrary renormalisation scale μ if

- the renormalisation scale dependence of $U(\mu, \nu) \otimes_{12} f(\mu)$ is given by the inhomogeneous double DGLAP equation. That this is indeed the case can, at LO and NLO, be explicitly verified using the inhomogeneous evolution equation for $W(\mu, \nu) \otimes_{12} f(\mu)$ and the equality of the momentum space $1 \to 2$ splitting kernel W and the matching kernel U stated in equation (5.67),
- the Δ dependent term

$$
\sum_{n=1}^{\infty} a_s^n(\mu) \sum_{k=0}^{n-1} I_k(\Delta; \mu, \nu)\, V^{[n,k]} \underset{12}{\otimes} f(\mu) \quad (5.82)
$$

on the other hand satisfies the homogeneous double DGLAP equation. That this is indeed the case can be shown considering that the renormalisation scale

dependence of the splitting form of $F(\boldsymbol{y}; \mu)$

$$\sum_{n=1}^{\infty} a_s^n(\mu) \sum_{k=0}^{n-1} \left(\ln \frac{y^2\mu^2}{b_0^2} \right)^k V^{[n,k]} \underset{12}{\otimes} f(\mu) \tag{5.83}$$

is governed by the homogeneous equation and that $I_k(\Delta; \mu, \nu)$ and $\ln^k(y^2\mu^2/b_0^2)$ satisfy the same differential equation in the renormalisation scale μ.

As these requirements are fulfilled for the perturbative splitting forms of $F(\Delta; \mu)$ and $F(\boldsymbol{y}; \mu)$, the double DGLAP equations are fulfilled only up to order a_s^n if the perturbative series for the splitting or matching kernel is truncated at order a_s^n.

5.5. Two-loop calculation

In this section the actual calculation of the $1 \to 2$ splitting, evolution, and matching kernels V, W, P_s, and U introduced in sections 5.3 and 5.4 will be presented at NLO accuracy. Due to the relations derived in the preceding sections it suffices to this end to calculate only the momentum space $1 \to 2$ splitting kernel W as all other kernels can be expressed in terms of this quantity. In order to illustrate how the momentum space splitting kernel $W_{a_1a_2,a_0}^{(2)}(\Delta)$ can be obtained consider the factorisation formula for the bare position space DPD $F_{B,a_1a_2/a_0}(\Delta)$ of partons a_1 and a_2 in a parton a_0 given in equation (5.13). The NLO term is obtained by expanding this in a_s and reads

$$F_{B,a_1a_2/a_0}^{(2)}(\Delta) = \sum_b \left[W_{B,a_1a_2,b}^{(2)}(\Delta) \underset{12}{\otimes} f_{B,b/a_0}^{(0)} + W_{B,a_1a_2,b}^{(1)}(\Delta) \underset{12}{\otimes} f_{B,b/a_0}^{(1)} \right]$$

$$= W_{B,a_1a_2,a_0}^{(2)}(\Delta), \tag{5.84}$$

where $f_{B,b/a_0}$ denotes the bare PDF of parton b in parton a_0. In order to arrive at the second equality it has been used that the tree-level expression $f_{B,b/a_0}^{(0)}(x) = \delta_{ba_0}\delta(1-x)$ whereas the order $\mathcal{O}(a_s)$ term $f_{B,b/a_0}^{(1)} = 0$ because the corresponding loop integrals do not depend on any dimensionful scale such that they vanish in dimensional regularisation. One can therefore conclude that the bare two loop momentum space kernel $W_{B,a_1a_2,a_0}^{(2)}$ is obtained directly from the two-loop graphs for the bare DPD of partons a_1 and a_2 in an on-shell parton a_0. The computation of these graphs is performed with massless quarks and gluons, such that the relevant graphs exhibit both infrared and ultraviolet divergences, both of which are being treated using dimensional regularisation.

5.5.1. Channels and graphs

Consider now at which order in a_s a kernel $W_{a_1a_2,a_0}$ is first non-zero. Due to the conservation of quark and antiquark flavour one finds that the splitting $a_0 \to a_1a_2$ starts at

1. LO for $g \to gg$, $g \to q\bar{q}$ and $q \to qg$,
2. NLO for $g \to qg$, $q \to gg$ and $q_j \to q_j q_k$, $q_j \to q_j \bar{q}_k$, $q_j \to q_k \bar{q}_k$,

where the indices j and k label quark flavours and may be equal or different. In the following these two different cases will be referred to as "LO channels" and "NLO channels", respectively. The remaining channels at the same orders can be obtained by interchanging partons a_1 and a_2 or by charge conjugation, where the kernels for charge conjugated channels are identical. All other splitting processes start either at NNLO or N³LO.

Real emission graphs (or "real graphs" for short) are shown in figures 5.1 and 5.2 for LO and NLO channels, respectively. In addition to the graphs shown in these figures further graphs for the same channels are related to the ones shown by complex conjugation and by interchanging the lines for partons a_1 and a_2 if $a_1 = a_2$ and are understood to be taken into account. Note that the unobserved parton radiated into the final state is uniquely determined for given a_0, a_1, and a_2: it is a gluon for the LO channels and a quark or antiquark for the NLO channels.

In addition to the real emission graphs discussed above one has for the LO channels also virtual loop graphs (or "virtual graphs" for short). These virtual graphs are obtained from LO splitting graphs by adding a vertex correction to the splitting vertex or a propagator correction for one of the lines of parton a_1 or a_2 (propagator corrections for the massless on-shell parton a_0 are zero in dimensional regularisation), as illustrated in figure 5.3.

In order to avoid confusion a brief comment about the flavour structure for channels where a_0, a_1 and a_2 are only quarks or antiquarks is in order at this point. Consider to this end the graphs 5.2k, 5.2l and 5.2n in which there are separate fermion lines for quarks q and q', which may or may not be of the same flavour. The kernels $W_{a_1 a_2, a_0}$ corresponding to these graphs are denoted as specified in figure 5.2. The situation is, however, different for graphs 5.2m and 5.2o which involve only a single quark flavour and are thus considered to be of a valence type denoted by a superscript v on the corresponding kernels. From these kernels the complete kernels for a specific flavour transition are thus obtained as

$$W_{q_j \bar{q}_k, q_i} = \delta_{jk} W_{q'\bar{q}',q} + \delta_{ij} W_{q\bar{q}',q} + \delta_{ij}\delta_{jk} W^v_{q\bar{q},q} \, ,$$
$$W_{q_j q_k, q_j} = \delta_{jk} W_{q'q,q} + W_{qq',q} + \delta_{jk} W^v_{qq,q} \, , \qquad (5.85)$$

where $W_{q'q,q}(x_1, x_2) = W_{qq',q}(x_2, x_1)$.

Feynman versus light-cone gauge. In order to ensure that mistakes during the lengthy calculations could be ruled out all graphs making up the bare partonic DPDs have been calculated independently twice – once in covariant Feynman gauge, and once in $A^+ = 0$ light-cone gauge. The Feynman rules used in these calculations are for convenience reviewed in Appendix A.

(a) LD   (b) UD   (c) UND   (d) T2B

(e)   (f)   (g)

(h)   (i)   (j)   (k)

(l)   (m)   (n)   (o)

(p)   (q)
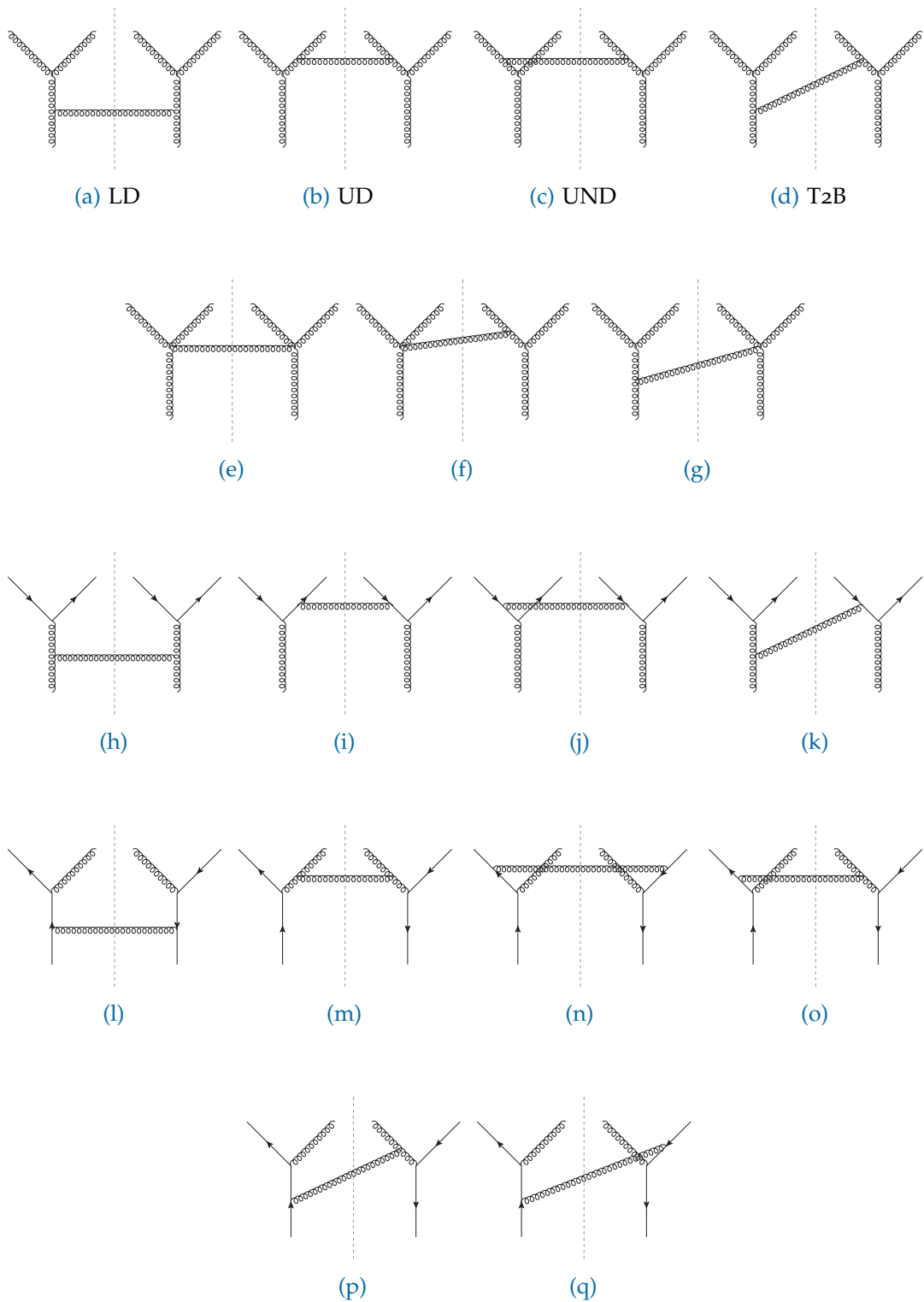
Figure 5.1.: Real graphs for LO channels. The parton lines at the bottom of the graph correspond to a_0, and those on top to a_1, a_2, a_2 and a_1 from left to right. The topologies "LD", "UD" etcetera are explained in section 5.5.2.

(a) (b) (c) (d)

(e) (f)

(g) (h) (i) (j)

(k) $W_{q'\bar{q}',q}$ (l) $W_{q\bar{q}',q}$ (m) $W_{q\bar{q},q}^{v}$

(n) $W_{qq',q}$ (o) $W_{qq,q}^{v}$

Figure 5.2.: Real graphs for NLO channels. The association of parton lines is as in figure 5.1.

Figure 5.3.: Virtual graphs for the amplitude in LO channels. The tree graphs in the complex conjugate amplitude are not shown.

One of the main differences between Feynman and light-cone gauge is that in addition[5] to the graphs shown in figures 5.1, 5.2, and 5.3 (which have to be calculated in both gauges), one gets in Feynman gauge also graphs with Wilson lines attaching to the active partons, as already discussed in section 2.2.2. Following the prescription illustrated in figure 5.4 the corresponding Wilson line graphs are rea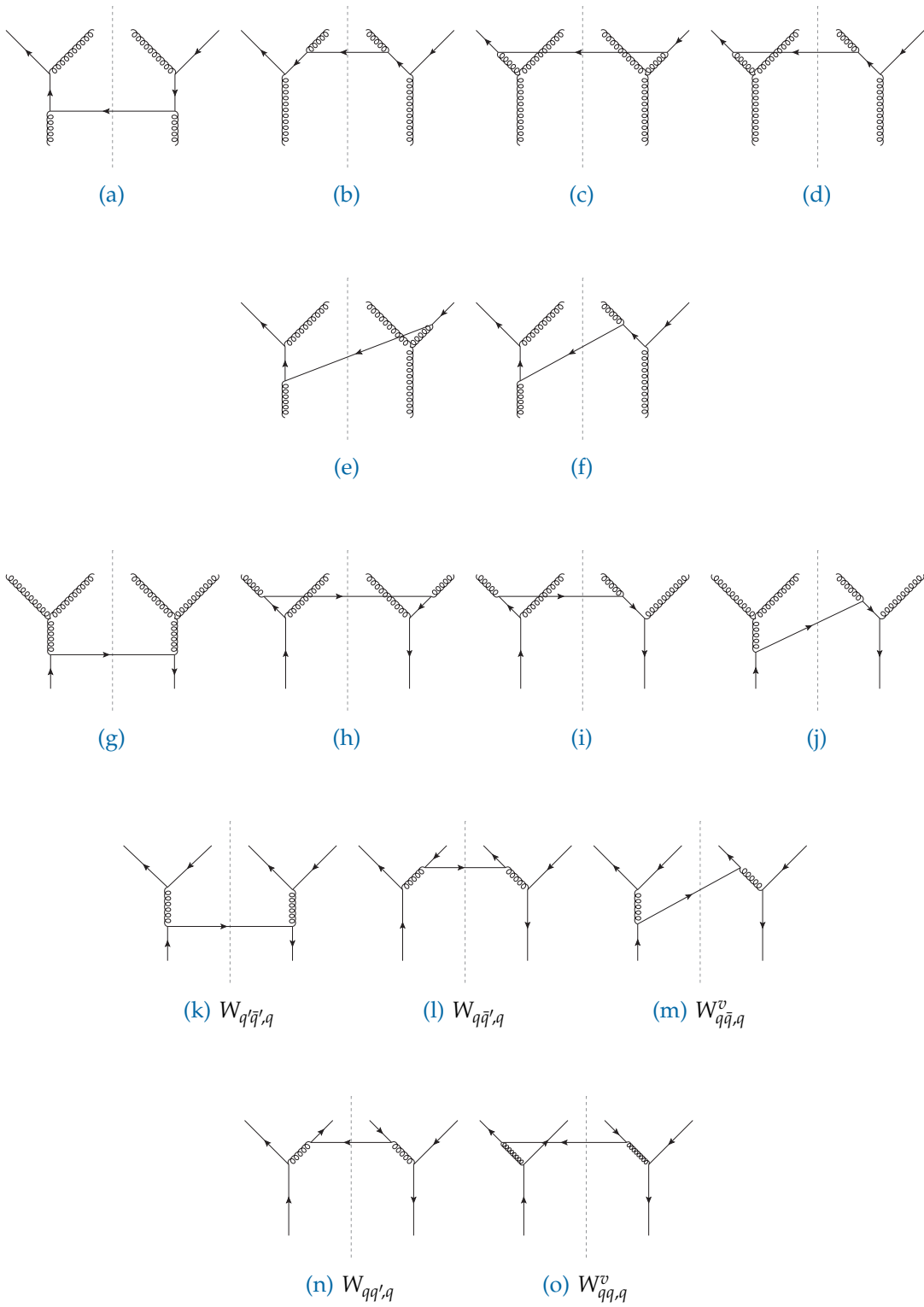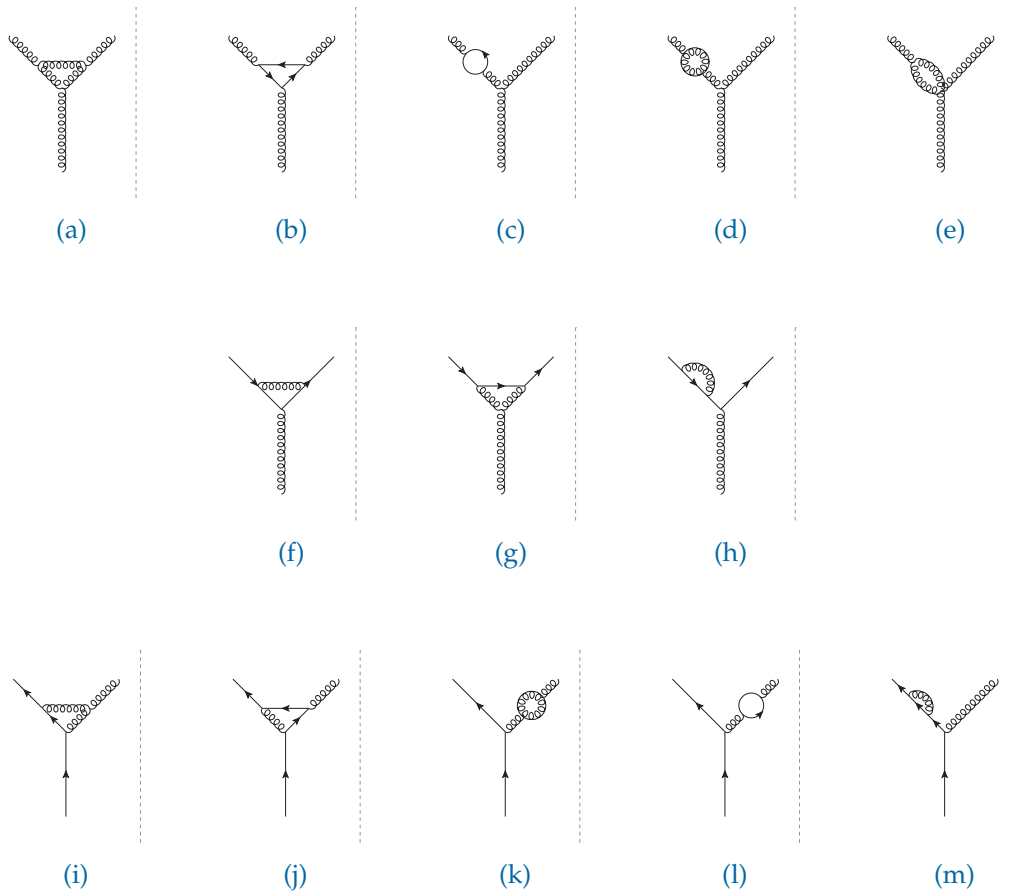dily obtained from the graphs in figures 5.1, 5.2, and 5.3. One can observe that Wilson line graphs arise in two cases, the first of which is when an active parton, a_1 or a_2, is a gluon emerging from a three-gluon vertex on one of the upper legs, as is for instance the case in figures 5.1a, 5.1b, and 5.3a. As shown in figure 5.4a and 5.4b graphs of this kind give rise to two kinds of Wilson line graphs. In the case that the active parton is a quark or antiquark originating from a quark-gluon vertex on one of the upper legs on the other hand, as is for example the case in figures 5.1h, 5.1l, 5.3f, and 5.3g, this leads to only one corresponding Wilson

---

[5]This is due to the fact that the Wilson lines reduce to unity in $A^+ = 0$ light-cone gauge as is readily seen from equation (2.23).
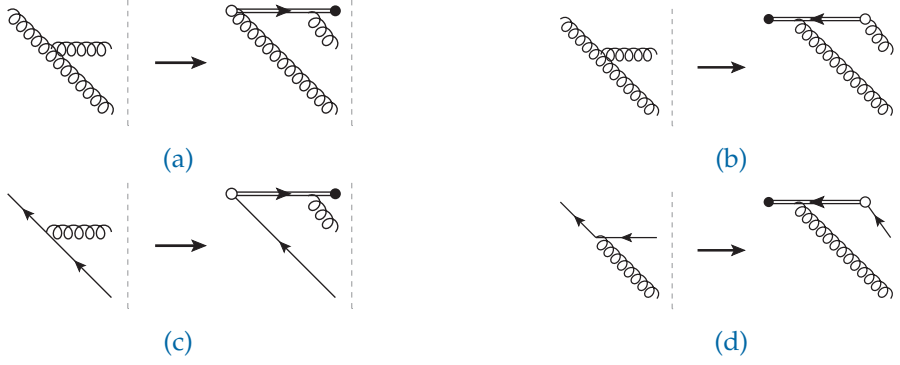
Figure 5.4.: Rules for obtaining the Wilson line graphs needed in Feynman gauge from graphs without Wilson lines. In each of the four panels, the top left parton is an active one (a_1 or a_2). These rules apply to both real and virtual graphs, and corresponding rules hold on the right of the final state cut. Note that the three-gluon vertex in the upper panels gives rise to two different graphs.

line graph with a gluon attaching to a quark Wilson line, visualised in figures 5.4c and 5.4d.

Another type of graphs that have to be calculated in Feynman gauge while they are absent in light-cone gauge are the Fadeev-Popov ghost versions of all graphs containing closed gluon loops, such as for example in figures 5.3a and 5.3d.

Kinematics. The general kinematic structure for real graphs – both in LO and NLO channels – is depicted in figure 5.5. All calculations are performed in a frame where the incoming parton a_0 has plus momentum p^+ while its transverse and minus momentum components vanish. For the active partons a_1 and a_2 the plus momenta $x_1 p^+$ and $x_2 p^+$ are equal in the amplitude and its conjugate, whereas their transverse momenta differ by $\pm\Delta$ as shown in figure 5.5 which differs from the momentum assignment in figure 2.6[6]. An analogous shift is also performed for the minus momentum components. For the parton a_3 which goes across the final state cut with plus momentum $x_3 p^+$ the momentum components are uniquely fixed by the momenta of the active partons a_1 and a_2 due to momentum conservation, namely

$$x_3 = 1 - x_1 - x_2, \qquad k_3^- = -k_1^- - k_2^-, \qquad \boldsymbol{k}_3 = -\boldsymbol{k}_1 - \boldsymbol{k}_2. \qquad (5.86)$$

In order to obtain DPDs from the real graphs in figures 5.1 and 5.2 the expressions corresponding to these graphs have to be integrated over k_1^-, k_2^-, and Δ^-, which corresponds to having $z_1^+ = 0$, $z_2^+ = 0$, and $y^+ = 0$, respectively, in the matrix element in equation (2.17). As the splitting kernels are derived from collinear DPDs furthermore

[6]This is achieved by shifting $k_1 \to k_1 + \frac{\Delta}{2}$ and $k_2 \to k_2 - \frac{\Delta}{2}$ and is done as this leads to a simpler denominator structure in the corresponding Feynman integrals.
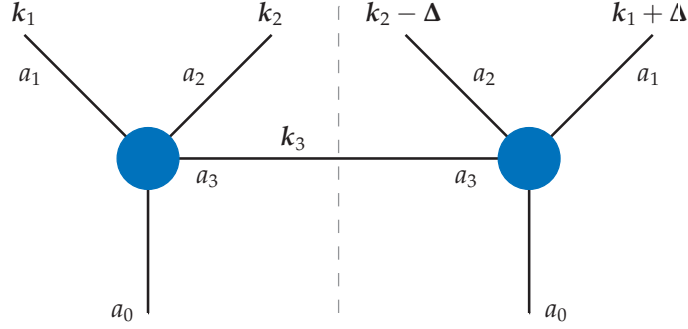
Figure 5.5.: Assignment of transverse momenta in a real graph. Note that compared with the symmetric assignment in [35] the integration variables k_1 and k_2 have been shifted such that $\mathbf{\Delta}$ appears only on the right-hand side of the cut.

(a) vertex correction

(b) propagator correction
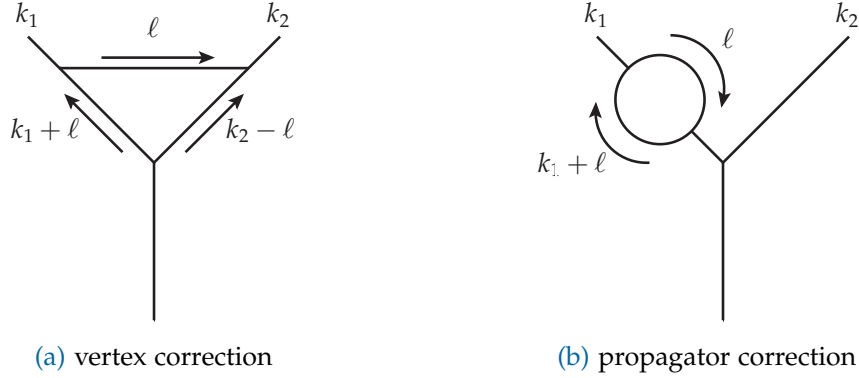
Figure 5.6.: Assignment of momenta in generic virtual graphs to the left of the cut. An analogous assignment holds for loops to the right of the cut, with k_1 and k_2 shifted by $+\Delta$ and $-\Delta$, respectively.

integrations over the transverse momenta k_1 and k_2 have to be performed, which is tantamount to setting $z_1 = 0$ and $z_2 = 0$, respectively, in equation (2.17).

For the virtual graphs encountered in the LO channels the generic kinematic structure is exemplified in figure 5.6. Here one now finds that due to momentum conservation one has $k_2^- = -k_1^-$ and $\mathbf{k}_2 = -\mathbf{k}_1$, as a result of which the integrations over k_2^- and $\mathbf{k}_2$ become redundant. Instead one now finds an additional loop momentum ℓ, over which one has to integrate.

5.5.2. Performing the calculation

At this point all preliminaries which are required for the actual calculation of the bare momentum space $1 \to 2$ splitting kernel $W^{(2)}_{a_1 a_2, a_0}(\mathbf{\Delta})$ have been worked out. The

initial expressions corresponding to each graph are obtained using the Feynman rules given in appendix A and subsequently performing the Dirac and colour algebra using FORM [136] or FeynCalc [137][7]. After this has been taken care of the phase space and loop integrals have to be performed, which is where the calculations for real graphs with a parton emitted into the final state and virtual graphs containing closed loops start to differ. As a result of this the the methodology for performing the integrations in these two cases will be discussed separately.

Real emission diagrams

In the case of the real emission graphs one can distinguish four different so called topologies which are exemplified by figures 5.1a, 5.1b, 5.1c, and 5.1d, and referred to as LD (lower diagonal), UD (upper diagonal), UND (upper non-diagonal) and T2B (top to bottom), respectively. The four-gluon graphs in figures 5.1e, 5.1f, and 5.1g can be considered to fit into the T2B topology, as all the denominator factors in these diagrams are covered by those in the T2B topology.

After the Dirac indices in the numerator have been contracted the next step in the calculation is to perform the integrations over the minus components of momenta k_1, k_2, and Δ. To this end a change of variables is performed which makes this task as simple as possible. In particular this is achieved using again the variable transformation introduced in equation (3.19). Following this change of variables the K^- integration can be performed using the on-shell delta function, whereas the integrals over k^- and k'^- can be performed using the theorem of residues. The above change of variables made this "simple" in the sense that now for all topologies, one is able to close the integration contour on only one pole, both in the k^- and in the k'^- integration.

The remaining step in the calculation of the individual graphs is then – as all plus components are fixed by the operators in equation (2.17) – to integrate over k_1 and k_2 at fixed Δ. To this end it is used that every graph may be written in a form where its denominator factors are contained within the following finite set[8]:

$$D_1 = \frac{(k_1 + \Delta)^2}{x_1} + \frac{(k_2 - \Delta)^2}{x_2} + \frac{(k_1 + k_2)^2}{x_3}, \qquad D_2 = \frac{k_1^2}{x_1} + \frac{k_2^2}{x_2} + \frac{(k_1 + k_2)^2}{x_3},$$

$$D_3 = (k_1 + \Delta)^2, \qquad\qquad\qquad D_4 = k_2^2,$$

$$\tilde{D}_4 = k_1^2, \qquad\qquad\qquad\qquad \tilde{D}_5 = (k_1 + k_2)^2. \qquad (5.87)$$

One can observe that graphs of all topologies have denominators D_1 and D_2 in common. In addition to these common denominator factors LD graphs furthermore have $\tilde{D}_5$,

---

[7]In practice, FORM was used in the light-cone gauge calculation, whilst FeynCalc was used for the Feynman gauge calculation. Of course, either code could have been used for both computations.

[8]This may require shifting of integration momenta, and use of the fact that the integrals are invariant under the substitution $\Delta \to -\Delta$

whereas UD graphs have D_3 and $\tilde{D}_4$, T2B graphs have D_3 and $\tilde{D}_5$, and UND graphs have D_3 and D_4.

As discussed already in section 5.2.1 the large set of Feynman integrals corresponding to all graphs can be reduced to a small set of master integrals. To this end first all numerator factors in the graphs are expressed in terms of the denominator factors D_i and $\tilde{D}_i$, before integration by parts identities, as implemented in LiteRed [128], are used to reduce the results for all graphs to master integrals. For graphs with the topology UND the master integrals have the general form

$$I_1(\alpha_1, \alpha_2, \alpha_3, \alpha_4) = \int \frac{\mathrm{d}^{D-2}k_1\, \mathrm{d}^{D-2}k_2}{\prod_{i=1..4} D_i^{\alpha_i}} \,. \tag{5.88}$$

And in particular the actual master integrals are given by the following set

$$\begin{aligned}
&I_1(1,1,0,0), \quad I_1(0,1,1,0), \quad I_1(1,1,1,0), \\
&I_1(1,0,1,1), \quad I_1(1,1,1,1), \quad I_1(2,1,1,1),
\end{aligned} \tag{5.89}$$

as well as integrals related to these by the simple transformation $x_1 \leftrightarrow x_2$.

In the case of graphs belonging to the remaining topologies – LD, UD, and T2B – the master integrals are parametrised by

$$I_2(\alpha_1, \alpha_2, \alpha_3, \alpha_4, \alpha_5) = \int \frac{\mathrm{d}^{D-2}k_1\, \mathrm{d}^{D-2}k_2}{\prod_{i=1...3} D_i^{\alpha_i} \prod_{i=4...5} \tilde{D}_i^{\alpha_i}} \,, \tag{5.90}$$

and specifically the finite set of master integrals to which all of the graphs fitting into these topologies may be reduced are given by

$$\begin{aligned}
&I_2(1,1,0,0,0), \quad I_2(0,1,1,0,0), \quad I_2(1,1,1,0,0), \\
&I_2(0,1,1,0,1), \quad I_2(1,1,1,1,0),
\end{aligned} \tag{5.91}$$

and integrals related to these by the substitution $x_1 \leftrightarrow x_2$. Note that the here master integrals in the first line coincide with the ones in the first line of equation (5.89) such that these only have to be calculated once.

In order to calculate the master integrals the method of differential equations introduced in section 5.2.2 is used. In the case at hand the only external variables on which the master integrals depend are x_1, x_2 and Δ^2. However, differential equations in Δ^2 only provide trivial information and are thus not suitable to obtain the master integrals. This is due to the fact that Δ^2 is the only dimensionful external quantity, such that each master integral only depends on Δ^2 via an overall prefactor of a power of Δ^2 that is easily determined by dimensional analysis. Therefore differential equations in x_1 are used to calculate the master integrals. As outlined in section 5.2.2 appropriate boundary conditions have to be imposed in order to fix the "constants" of integration arising when the differential equations are solved, which in this case are actually functions

of x_2. These constants can be obtained from the calculation the leading behaviour of the master integrals in the limit that $x_3 \to 0$ where the master integrals simplify to a point where they can be calculated analytically using standard textbook techniques. A valuable cross check is provided by the differential equations in x_2 which have to be satisfied by the final solutions of the x_1 differential equations.

How the actual solution of the differential equations for the master integrals is most instructively illustrated for the UND case. There the system of differential equations has an almost entirely triangular matrix structure and is schematically given by:

$$
\frac{\partial}{\partial x_1}
\begin{bmatrix}
I_1(1,1,0,0) \\
I_1(0,1,1,0) \\
I_1(1,1,1,0) \\
I_1(1,0,1,1) \\
I_1(1,1,1,1) \\
I_1(2,1,1,1)
\end{bmatrix}
=
\begin{bmatrix}
\blacksquare & 0 & 0 & 0 & 0 & 0 \\
0 & \blacksquare & 0 & 0 & 0 & 0 \\
\blacklozenge & \blacklozenge & \blacksquare & 0 & 0 & 0 \\
0 & \blacklozenge & 0 & \blacksquare & 0 & 0 \\
\blacklozenge & \blacklozenge & \blacklozenge & \blacklozenge & \blacksquare & \blacksquare \\
\blacklozenge & \blacklozenge & \blacklozenge & \blacklozenge & \blacksquare & \blacksquare
\end{bmatrix}
\begin{bmatrix}
I_1(1,1,0,0) \\
I_1(0,1,1,0) \\
I_1(1,1,1,0) \\
I_1(1,0,1,1) \\
I_1(1,1,1,1) \\
I_1(2,1,1,1)
\end{bmatrix} ,
\tag{5.92}
$$

where black squares $\blacksquare$ denote entries of the form $c(x_1, x_2)$ while black diamonds $\blacklozenge$ denote entries of the form $c_1(x_1, x_2) + c_2(x_1, x_2) P_{x_1 \leftrightarrow x_2}$. Here $P_{x_1 \leftrightarrow x_2}$ is the operator transforming a given master integral $I_1(\alpha_1, \alpha_2, \alpha_3, \alpha_4)$ to the corresponding master integral with $x_1 \leftrightarrow x_2$. Due to this rather simple structure most master integrals can be computed using elementary methods for first-order differential equations and forward substitution, starting from $I_1(1,1,0,0)$ and $I_1(0,1,1,0)$ and working downwards. In the case of the two-denominator master integrals $I_1(1,1,0,0)$ and $I_1(0,1,1,0)$ an exact analytical solution in $D = 4 - 2\varepsilon$ dimensions is possible, whereas for the more complicated master integrals the results are obtained as a series in ε up to the required order. For the two four-denominator master integrals $I_1(1,1,1,1)$ and $I_1(2,1,1,1)$ elementary methods are, however, not sufficient as for these two master integrals one finds a coupled system of equations. As already discussed in section 5.2.2 the solution of these differential equations is greatly simplified by a change of basis to the so called canonical basis. To this end the coupled 2×2 system is transformed to the canonical basis with a transformation matrix obtained using `Fuchsia`. In this form it is then straightforward to obtain a solution for these two integrals as a series in ε. For the second family of master integrals the situation is less complicated as there the system of differential equations for the I_2 integrals is fully triangular, such that in this case elementary methods for differential equations plus forward substitution are sufficient to obtain the master integrals.

Consider now how the leading behaviour of the integrals for $x_3 \to 0$ – which serves as a boundary condition in the solution of the differential equations – is computed. To this end the method of regions introduced in reference [138] is used. In order to determine the leading momentum regions of the integrations a scaling parameter $\lambda \ll 1$ is introduced, with $x_3 \sim \lambda$. One then finds that for all master integrals the following region gives a leading contribution in λ:

$$
R_1: \quad x_3 \sim \lambda, \quad x_1, x_2 \sim 1, \quad k_1^2, k_2^2, (k_1 + \Delta)^2 \sim \Delta^2, \quad (k_1 + k_2)^2 \sim \lambda \Delta^2. \tag{5.93}
$$

In the case of the four-denominator master integral $I_1(1,0,1,1)$ of the UND topology one can in addition to this identify a further leading region, namely

$$R_2: \quad x_3 \sim \lambda, \quad x_1, x_2 \sim 1, \quad k_1^2, k_2^2, (k_1 + \Delta)^2, (k_1 + k_2)^2 \sim \Delta^2. \tag{5.94}$$

In order to derive the form of the approximated integrands in these regions the appropriate scaling of momenta is used and subleading terms in λ are neglected in the denominators, resulting in expressions that are homogeneous in λ. At this point every master integral has a sufficiently simple form to be solved to all orders in ε using the standard method of Feynman parameters. In order to obtain the full leading behaviour in the limit $x_3 \to 0$ the contributions from the two leading regions have to be added together. As mentioned above, every master integral gets a leading contribution from the region R_1 specified in equation (5.93) which is multiplied by an overall non-integer power of x_3 for $\varepsilon \neq 0$, namely $x_3^{1-\varepsilon}$. The occurrence of this global x_3 dependence can be explained by the fact that all denominators behave like λ^0, whereas the phase space contributes $\lambda^{1-\varepsilon}$. In the region R_2 detailed in equation (5.94) from which only the master integral $I_1(1,0,1,1)$ gets a leading contribution the situation is different as there one finds that the overall result is multiplied by an integer power of x_3, namely x_3^1, because D_1 behaves like λ^{-1}, whilst all other denominators and the phase space behave like λ^0.

In order to check that the results obtained for the master integrals are indeed correct the analytic results have been checked against a numerical computation of the integrals performed using the program FIESTA 2 [139] at 10 randomly chosen (x_1, x_2) points, which were found to agree within the precision of the numerical computation.

However, the calculation of the bare graphs is not finished at this point as careful consideration of the limit $x_3 \to 0$ is needed. This is due to the fact that some graphs exhibit singular behaviour in this limit. To this end it comes in handy that the full (all-order in ε) behaviour of the graphs for $x_3 \to 0$ is known from the boundary condition computation for the master integrals. For graphs associated with the non-UND topologies, this singularity is always regulated by the dimensional regularisation parameter ε, since the non-UND master integrals only have the leading region R_1 for $x_3 \to 0$, coming with an overall factor of $x_3^{-1-n\varepsilon}$. This factor can be expanded in the following way:

$$\theta(x_3)\, x_3^{-1-n\varepsilon} = -\frac{1}{n\varepsilon}\, \delta(x_3) + \mathcal{L}_0(x_3) - n\varepsilon\, \mathcal{L}_1(x_3) + \frac{n^2\varepsilon^2}{2}\, \mathcal{L}_2(x_3) + \mathcal{O}(\varepsilon^3), \tag{5.95}$$

with plus distributions denoted as

$$\mathcal{L}_n(x) = \left[\frac{\theta(x)\, \ln^n(x)}{x} \right]_+. \tag{5.96}$$

Useful relations for these distributions are given in reference [140]. Here it can be noted that the final results turn out to involve only $\mathcal{L}_0$ while all terms containing $\mathcal{L}_n$ with $n > 0$ cancel after a sum over graphs.

A different situation is encountered for graphs of the UND topologies, in particular those which get a contribution from the master integral $I_1(1,0,1,1)$, as there one can have terms which just go as $1/x_3$ and are not regulated by ε. While the singularities discussed above are soft singularities this corresponds to a rapidity divergence which is (in covariant gauges) associated with light-like Wilson lines and has to be regulated somehow. To this end a regulator is typically inserted via some modification of the Wilson line propagator in covariant gauges, whereas in light-cone gauge the gluon propagator has to be modified appropriately. One possible choice of regulator is the so called δ regulator which – in covariant Feynman gauge – introduces a small additional term in the denominator of a Wilson line propagator. Consider to this end the Wilson line propagator as given in figure A.4, and in particular only its denominator $\ell v \pm i\varepsilon$ which for light-like Wilson lines reduces to $1/(\ell^+ \pm i\varepsilon)$. Here one can furthermore drop the $\pm i\varepsilon$ term as this is not needed here since only the integrations over the minus momentum components are performed using complex contour integration techniques. In order to regulate the singularity $\ell^+ \to 0$ one then introduces the δ regulator in the following way

$$\frac{1}{\ell^+} \to \frac{1}{\ell^+ + i\delta}\,. \tag{5.97}$$

For the calculation at hand it suffices to take only the real part of this modified Wilson line propagator as the imaginary part cancels when complex conjugated graphs are added such that one can furthermore make the following replacement

$$\frac{1}{\ell^+ + i\delta} \to \frac{\ell^+}{(\ell^+)^2 + \delta^2}\,. \tag{5.98}$$

In this form one can then again perform a distributional expansion in the vein of equation (5.95), namely

$$\frac{\ell^+}{(\ell^+)^2 + \delta^2} = -\delta(\ell^+)\ln\delta + \mathcal{L}_0(\ell^+)\,, \tag{5.99}$$

where the rapidity divergences are now manifest as $\ln\delta$ terms. Since colour singlet DPDs do not suffer from rapidity divergences[9] – as noted for example in section 3.5 of reference [26] or in reference [142] – the divergences associated with $I_1(1,0,1,1)$ must cancel after a sum over graphs, including the virtual loop graphs. As discussed in section 2.2.2 the situation is different in the colour interference case where these rapidity divergences cancel only when the appropriate soft factor has been taken into account.

How exactly these rapidity divergences are regulated depends on the used regulator for which there are various possible choices, such as the analytic regulator of reference [143], the exponential regulator of reference [144], the "pure rapidity regulator" of

---

[9]This is analogous to what happens in the single scattering sector, where for the collinear PDFs no rapidity divergences occur, see for example reference [141].

reference [145], the δ regulator of reference [146] used above, the CMU η regulator of references [147, 148], or the use of Wilson lines slightly tilted away from the light cone as described in reference [47]. In the calculations presented in this chapter each of the latter three options have been tried, and one finds that when consistently implementing the regulator in all real emission and virtual loop graphs (and the appropriate contribution from the soft factor in the colour interference case), the sum over graphs yields the same rapidity-divergence-free result for all regulators. Here it is important to point out that the rapidity regulator always has to be removed before ultraviolet renormalisation is performed and ε is set to zero, as is prescribed when using such regulators.

Virtual diagrams

Consider now the virtual loop graphs where the calculation differs in some points from the one of the real emission graphs just discussed. In this case the integrations over minus momenta (including ℓ^-) can again be performed using contour integration techniques which now places restrictions on the plus component ℓ^+ of the loop momentum as will be seen in a moment. The integrations over the transverse momenta k_1 and ℓ were also again performed using integration by parts reduction which yielded, after some relabelling of integration momenta, two master integrals encountered already in the real emission sector, namely $I_1(0, 1, 1, 0)$ and $I_1(0, 1, 1, 1)$, where the latter is obtained from $I_1(1, 0, 1, 1)$ by interchanging $x_1 \leftrightarrow x_2$.

The main difference between the calculations of real emission and virtual loop graphs is certainly that in the latter case one has an additional integration over the plus component of the loop momentum. This integration is restricted to a finite range as a result of the earlier integrations over minus components: when ℓ^+ is outside a certain range, all poles move into one half-plane for one of these integrations, and the result is zero. In most cases the ℓ^+ integration can be performed straightforwardly using standard integration techniques. However, in some cases, in particular in Wilson line graphs in Feynman gauge, one again encounters endpoint singularities for $\ell^+ \to 0$ which have to be treated consistently. To this end one again performs distributional expansions analogous to the ones in equation (5.95) in cases where these singularities are regulated by ε, and when this is not the case again an appropriate rapidity regulators has to be introduced. While in the real emission sector rapidity divergences are associated with the UND topology in the virtual loop sector the graphs containing such a rapidity divergence are vertex correction graphs in which the line with momentum ℓ is a gluon, such as figure 5.3f.

5.6. Results

Now that the calculation of the bare momentum space $1 \to 2$ splitting kernels has been discussed in the previous section 5.5 and the extraction of the renormalised kernels

from these bare results has been described in section 5.3 the next step is to present these renormalised kernels up to NLO and discuss some of their properties. Here it is sufficient to limit the discussion to the $1 \to 2$ evolution kernel P_s and the momentum space $1 \to 2$ splitting kernel W as results for the kernels V and U can readily be obtained from W using the relations given in equations (5.52) and (5.67), respectively.

5.6.1. Support and singularity structure

Before the actual results are presented consider first briefly the singularity structure of the kernels at NLO. This differs between the LO and NLO channels defined at the beginning of section 5.5.1. In the LO channels the kernels have the following general form

$$K(x_1, x_2) = K_{\mathrm{reg}}(x_1, x_2) + \frac{K_p(x_1, x_2)}{[1 - x_1 - x_2]_+} + K_\delta(x_1)\, \delta(1 - x_1 - x_2)\,, \tag{5.100}$$

where K is either $W^{(2)}$ or $P_s^{(1)}$. In contrast to this structure the kernels for NLO channels contain only a term K_{reg}. In the region defined by the conditions $0 < x_1$, $0 < x_2$ and $x_1 + x_2 \leq 1$ the functions K_{reg} and K_p are regular, while K_δ is regular in the region $0 < x_1 < 1$. Here it should be noted that these regions exclude the points $x_1 = 1$ and $x_2 = 1$, where some kernels have power-law divergences of the form $(1 - x_1)^{-n_1}(1 - x_2)^{-n_2}$ with integers n_1 and n_2. The reason why these points may be excluded is that these points are not reached in any physical double parton scattering process, where both x_1 and x_2 must be strictly positive. Note also that the decomposition in equation (5.100) is invariant under the simultaneous replacement

$$\begin{aligned} K_{\mathrm{reg}}(x_1, x_2) &\to K_{\mathrm{reg}}(x_1, x_2) + \varphi(x_1, x_2)\,, \\ K_p(x_1, x_2) &\to K_p(x_1, x_2) - (1 - x_1 - x_2)\, \varphi(x_1, x_2)\,, \end{aligned} \tag{5.101}$$

where $\varphi(x_1, x_2)$ is a regular function, leaving a freedom of choice in the form of K_{reg} and K_p for a given kernel.

Inserting the general form of the NLO $1 \to 2$ kernels given in equation (5.100) into the convolution with a PDF and using the representation (2.34), one obtains one-variable distributions $1/[1 - z]_+$ and $\delta(1 - z)$, so that

$$\left[K \underset{12}{\otimes} f \right](x_1, x_2) = \frac{1}{x_1 + x_2} \int\limits_{x_1 + x_2}^{1} \mathrm{d}z \left\{ K_{\mathrm{reg}}(zu, z\bar{u}) + \frac{K_p(zu, z\bar{u})}{[1 - z]_+} \right\} f\left(\frac{x_1 + x_2}{z} \right)$$

$$+ K_\delta(u)\, \frac{f(x_1 + x_2)}{x_1 + x_2}\,, \tag{5.102}$$

with

$$u = \frac{x_1}{x_1 + x_2}\,, \qquad\qquad \bar{u} = 1 - u\,. \tag{5.103}$$

This particular form of this convolution comes in very handy when the kinematic limits are discussed in section 5.6.6. Note that the term with K_δ in the above equation (5.102) has the same structure as the convolution of the LO kernels $W^{(1)}$ or $P_s^{(0)}$ with a PDF f.

Before presenting the kernels in detail, consider the following symmetries

$$
\begin{aligned}
W_{q\bar{q},g}(x_1, x_2) &= W_{\bar{q}q,g}(x_1, x_2), & W_{gq,g}(x_1, x_2) &= W_{g\bar{q},g}(x_1, x_2), \\
W_{q'\bar{q}',q}(x_1, x_2) &= W_{\bar{q}'q',q}(x_1, x_2), & W_{qq',q}(x_1, x_2) &= W_{q\bar{q}',q}(x_1, x_2),
\end{aligned}
\tag{5.104}
$$

with analogous relations valid also for the kernels $P_{a_1 a_2, a_0}$. The relations in the first line follow from charge conjugation, whereas those in the second line are obtained by reversing the quark line associated with q' (but not the one associated with q). Due to these relations the channels on the right-hand side of equation (5.104) do not need to be discussed further in the following. Recall furthermore that kernels for specific flavour transitions are obtained from (5.85) and its analogue for $P_{a_1 a_2, a_0}$, and that kernels for channels with an initial $\bar{q}$ are equal to the kernels for the charge conjugate channels with an initial q.

Useful building blocks for presenting the explicit kernels $P_s^{(1)}$ are the following functions

$$
\begin{aligned}
p_{gg}(x) &= \frac{x}{1-x} + \frac{1-x}{x} + x(1-x), & p_{qq}(x) &= \frac{1+x^2}{1-x}, \\
p_{qg}(x) &= x^2 + (1-x)^2, & p_{gq}(x) &= \frac{1+(1-x)^2}{x},
\end{aligned}
\tag{5.105}
$$

which are proportional to the LO DGLAP evolution kernels away from the endpoint $x = 1$. Using these functions the LO kernels $P_s^{(0)}$ and $W^{[1,0]}$ read

$$
\begin{aligned}
P_{gg,g}^{(0)}(x) &= 2C_A\, p_{gg}(x) & W_{gg,g}^{[1,0]}(x) &= 0, \\
P_{q\bar{q},g}^{(0)}(x) &= T_F\, p_{qg}(x), & W_{q\bar{q},g}^{[1,0]}(x) &= -2T_F x(1-x) \\
P_{qg,q}^{(0)}(x) &= C_F\, p_{qq}(x), & W_{qg,q}^{[1,0]}(x) &= -C_F(1-x).
\end{aligned}
\tag{5.106}
$$

In the following the NLO kernels will be expressed in terms of a overcomplete set of momentum fractions x_1, x_2 and $x_3 = 1 - x_1 - x_2$. This makes symmetry properties more transparent and often allows for more compact expressions. Furthermore the notation $\bar{x}_i = 1 - x_i$ will be used.

5.6.2. $1 \to 2$ evolution kernels

Consider now the explicit results for the NLO $1 \to 2$ evolution kernels $P_s^{(1)}$, starting with the pure gluon channel $g \to gg$.

$g \to gg$ **channel.** To this end the following auxiliary functions are introduced

$$R_{gg,g}(x_1, x_2, x_3) = C_A^2 \left\{ \frac{\ln(1 + x_1/x_3) + \ln(1 + x_1/x_2)}{x_1} \frac{x_2\, p_{gg}(x_2)}{\bar{x}_3} \right.$$

$$+ 2\left[\frac{x_2^2\,(3 + 4x_2)}{\bar{x}_1^4} - \frac{x_2\,(4 + 9x_2 + x_2^2)}{\bar{x}_1^3} + \frac{1 + 6x_2 + 2x_2^2}{\bar{x}_1^2} - \frac{1 + x_2}{\bar{x}_1} + \frac{1}{2} \right]$$

$$+ \ln x_1 \left[\frac{4x_1^2}{\bar{x}_3^4} - \frac{4x_1(1 + x_1)}{\bar{x}_3^3} + \frac{4(2 + x_1 + 2x_1^2)}{\bar{x}_3^2} - \frac{3 - 3x_1 + x_1^2 + x_1^3}{\bar{x}_1^4} x_2^2 \right.$$

$$\left. + \frac{10 - 25x_1 + 12x_1^2 - 3x_1^3}{2\bar{x}_1^2} - \frac{2 + 7x_1 - 3x_1^2}{\bar{x}_2} - \frac{2}{\bar{x}_1\bar{x}_2\bar{x}_3} \right]$$

$$- \frac{\ln \bar{x}_1}{x_1} \left[\frac{2 + 3x_1 - 9x_1^2 + 9x_1^3 - x_1^4}{\bar{x}_1^4} x_2^2 + \frac{6 + 4x_1 - 5x_1^2 + 10x_1^3 - 3x_1^4}{2\bar{x}_1^2} \right.$$

$$\left. \left. - \frac{4 - 6x_1 + 9x_1^2 - 6x_1^3 + 3x_1^4}{\bar{x}_1\bar{x}_2} \right] \right\},$$

$$D_{gg,g}(x_1) = -C_A^2 \left\{ \frac{3}{4} + 2\,p_{gg}(x_1) \left[\ln x_1 \ln \bar{x}_1 + \frac{\pi^2}{6} - \frac{2}{3} \right] \right\}$$

$$+ \beta_0\, C_A \frac{40 - 27x_1 - 20x_1^3}{12x_1}, \tag{5.107}$$

in terms of which the $1 \to 2$ evolution kernel $P_{gg,g}^{(1)}$ can be written as

$$P_{gg,g}^{(1)}(x_1, x_2, x_3) = R(x_1, x_2, x_3) + R(x_2, x_1, x_3) + R(x_3, x_2, x_1)$$

$$+ R(x_1, x_3, x_2) + R(x_3, x_1, x_2) + R(x_2, x_3, x_1) + \left[D(x_1) + D(x_2) \right] \delta(x_3), \tag{5.108}$$

where the subscripts on R and D have been omitted for brevity. Replacing $x_3 = 1 - x_1 - x_2$ and subsequently expressing R as a function of only x_1 and x_2, this can be rewritten as

$$P_{gg,g}^{(1)}(x_1, x_2) = R(x_1, x_2) + R(x_2, x_1) + R(1 - x_1 - x_2, x_2) + R(x_1, 1 - x_1 - x_2)$$

$$+ R(1 - x_1 - x_2, x_1) + R(x_2, 1 - x_1 - x_2) + \left[D(x_1) + D(x_2) \right] \delta(1 - x_1 - x_2). \tag{5.109}$$

In equation (5.108) one can easily see that, apart from the distribution term involving $\delta(x_3)$, the kernel is fully symmetric in the momentum fractions of the three final-state gluons. While the symmetry under the interchange $x_1 \leftrightarrow x_2$ had to be expected, the symmetry between an observed gluon (a_1 or a_2) and the unobserved one (a_3) may come as a bit of a surprise. This "active-spectator symmetry" (where a_1, a_2 are referred to as active partons and a_3 as the spectator) will be discussed in some detail in section 5.6.5.

5. Two-loop splitting in double parton distributions

$g \to q\bar{q}$ **and related channels.** For the $g \to q\bar{q}$ channel, one can define the following auxiliary functions

$$
\begin{aligned}
R_{q\bar{q},g}(x_1, x_2, x_3) = C_A T_F \bigg\{ & \frac{\ln(1 + x_3/x_2)}{x_3} \frac{p_{qg}(x_1) + p_{qg}(x_2)}{2} \\
& - x_1 x_2 \frac{3 - 10x_3 + 3x_3^2}{\bar{x}_3^4} + \frac{1 - 6x_3 + 5x_3^2 - 2x_3^3}{2\bar{x}_3^2} \\
& - 2\ln x_1 \left[\frac{2x_1^2}{\bar{x}_3^4} - \frac{2x_1(1 + x_1)}{\bar{x}_3^3} + \frac{1 + 2x_1 + 4x_1^2}{\bar{x}_3^2} - \frac{1 + 6x_1 - 2x_1^2}{2\bar{x}_3} + 1 - x_1 - \frac{x_3}{2} \right] \\
& + 2\ln \bar{x}_1 \left[\frac{1 - 2x_1 + 2x_1^2}{2\bar{x}_3} + 1 - x_1 - \frac{x_3}{2} \right] \\
& - 2\ln x_3 \left[x_1 x_2 \frac{2 - 3x_3 + 2x_3^2}{\bar{x}_3^4} - \frac{1 - x_3 + x_3^2}{2\bar{x}_3^2} \right] \\
& - \frac{2\ln \bar{x}_3}{x_3} \left[x_1 x_2 \frac{1 + x_3 - 3x_3^2 + 3x_3^3}{\bar{x}_3^4} - \frac{1 + x_3 - 2x_3^2 + 2x_3^3}{2\bar{x}_3^2} \right] \bigg\} \\
+ C_F T_F \bigg\{ & -\left[\frac{3x_3}{\bar{x}_1^2} - \frac{1 + 5x_3}{\bar{x}_1} + 3 + 2x_3 \right] + 2\ln x_1 \left[\frac{x_3}{2\bar{x}_1^2} - \frac{1 + x_3}{\bar{x}_1} - \frac{x_3}{2\bar{x}_2^2} + \frac{1 + x_3}{\bar{x}_2} \right] \\
& + 2(2\ln \bar{x}_1 - \ln x_3) \left[\frac{x_3}{2\bar{x}_1^2} - \frac{1 + x_3}{\bar{x}_1} + 1 \right] \bigg\},
\end{aligned}
$$

$$
S_{q\bar{q},g}(x_1) = -2(C_A - 2C_F) T_F x_1 \bar{x}_1,
$$

$$
\begin{aligned}
D_{q\bar{q},g}(x_1) = {} & C_A T_F \left\{ x_1^2 - \ln^2 x_1 \, p_{qq}(x_1) \right\} + C_F T_F \bigg\{ \frac{3}{2} - 2x_1 \bar{x}_1 (\ln x_1 + \ln \bar{x}_1) \\
& + \left[\ln^2 x_1 - \ln x_1 \ln \bar{x}_1 - \frac{\pi^2}{6} + \frac{3}{2} \right] p_{qg}(x_1) \bigg\},
\end{aligned}
\tag{5.110}
$$

in terms of which the $1 \to 2$ evolution kernel $P^{(1)}_{q\bar{q},g}$ can be written as

$$
\begin{aligned}
P^{(1)}_{q\bar{q},g}(x_1, x_2, x_3) = {} & R_{q\bar{q},g}(x_1, x_2, x_3) + R_{q\bar{q},g}(x_2, x_1, x_3) + \frac{S_{q\bar{q},g}(x_1) + S_{q\bar{q},g}(x_2)}{[x_3]_+} \\
& + \left[D_{q\bar{q},g}(x_1) + D_{q\bar{q},g}(x_2) \right] \delta(x_3).
\end{aligned}
\tag{5.111}
$$

Here one now finds that the $1 \to 2$ evolution kernel $P^{(1)}_{qg,g}$ for the channel $g \to qg$ can be expressed using the same functions as

$$
P^{(1)}_{qg,g}(x_1, x_2, x_3) = R_{q\bar{q},g}(x_1, x_3, x_2) + R_{q\bar{q},g}(x_3, x_1, x_2) + \frac{S_{q\bar{q},g}(x_1) + S_{q\bar{q},g}(x_3)}{x_2}.
\tag{5.112}
$$

Just like in the case of the pure gluon channel, one can here again observe active-spectator symmetry for the splitting process $g \to q\bar{q}g$. The kernel $P^{(1)}_{qg,g}(x_1, x_2, x_3)$ is

obtained from $P^{(1)}_{q\bar{q},g}(x_1, x_2, x_3)$ by omitting $\delta(x_3)$ and replacing $1/[x_3]_+$ with $1/x_3$, and then interchanging $x_2 \leftrightarrow x_3$.

$q \to qg$ **and related channels.** Consider next the channel $q \to qg$, where one can again define auxiliary functions

$$
\begin{aligned}
R_{qg,q}(x_1, x_2, x_3) = C_A C_F \Bigg\{ &-\frac{\ln(1 + x_3/x_1) + \ln(1 - x_3/\bar{x}_1)}{x_3} \frac{x_2\, p_{gq}(x_2)}{\bar{x}_1} \\
&+ 2\left[\frac{3x_1}{\bar{x}_1^4} x_3^2 - \frac{x_1}{\bar{x}_1^2} - \frac{3}{4}\right] - (\ln x_1 + 2\ln \bar{x}_1)\left[x_1 \frac{2x_2^2}{\bar{x}_1^4} + \frac{3 + x_2^2}{\bar{x}_1^2} - \frac{1}{\bar{x}_1}\right] \\
&+ 2\ln x_2 \left[\frac{2x_2^2}{\bar{x}_1^4} - \frac{2x_2(1 + x_2)}{\bar{x}_1^3} + \frac{4 + 2x_2 + x_2^2}{\bar{x}_1^2} - \frac{2 + x_2}{\bar{x}_1} + \frac{1}{2}\right] \Bigg\} \\
+ C_F^2 \Bigg\{ &\frac{2\ln(1 + x_3/x_1)}{x_3} \frac{x_2\, p_{gq}(x_2)}{\bar{x}_1} - 2\left[\frac{x_3}{\bar{x}_2^2} + \frac{1 + x_3}{2\bar{x}_2} - 1\right] \\
&- \ln x_1 \left[\frac{x_2}{\bar{x}_3^2} - \frac{2 - x_2}{\bar{x}_3} - \frac{4}{\bar{x}_1} + 1\right] - \ln x_2 \left[\frac{x_2}{\bar{x}_3^2} - \frac{2 - x_2}{\bar{x}_3} - \frac{2 - x_2}{\bar{x}_2^2} x_3 + \frac{2}{\bar{x}_2}\right] \\
&+ \frac{2\ln \bar{x}_2}{x_2}\left[\frac{x_3}{\bar{x}_2^2} - \frac{2}{\bar{x}_2} + \frac{x_2\, p_{gq}(x_2)}{\bar{x}_1}\right] \Bigg\},
\end{aligned}
$$

$$
S_{qg,q}(x_1) = 2 C_A C_F\, \bar{x}_1,
$$

$$
\begin{aligned}
D_{qg,q}(x_1) = C_A C_F &\left\{ 1 - 2\bar{x}_1 \ln \bar{x}_1 + \left[\ln^2 x_1 - 2\ln x_1 \ln \bar{x}_1 - 2\operatorname{Li}_2(x_1) + \frac{4}{3}\right] p_{qq}(x_1) \right\} \\
- C_F^2 &\left\{ 1 + 2\bar{x}_1 \ln x_1 + \left[\ln^2 x_1 + 3\ln x_1 - 2\operatorname{Li}_2(x_1) + \frac{\pi^2}{3}\right] p_{qq}(x_1) \right\} \\
+ \beta_0 C_F &\left\{ \bar{x}_1 + \left[\ln x_1 + \frac{5}{3}\right] p_{qq}(x_1) \right\},
\end{aligned}
\tag{5.113}
$$

which make it possible to express the $1 \to 2$ evolution kernel $P^{(1)}_{qg,q}$ as

$$
\begin{aligned}
P^{(1)}_{qg,q}(x_1, x_2, x_3) = R_{qg,q}(x_1, x_2, x_3) + R_{qg,q}(x_1, x_3, x_2) + \frac{S_{qg,q}(x_1)}{[x_3]_+} + \frac{S_{qg,q}(x_1)}{x_2} \\
+ D_{qg,q}(x_1)\, \delta(x_3).
\end{aligned}
\tag{5.114}
$$

In terms of the same auxiliary functions, the evolution kernel for $q \to gg$ can be expressed as

$$
P^{(1)}_{gg,q}(x_1, x_2, x_3) = R_{qg,q}(x_3, x_2, x_1) + R_{qg,q}(x_3, x_1, x_2) + \frac{S_{qg,q}(x_3)}{x_1} + \frac{S_{qg,q}(x_3)}{x_2},
\tag{5.115}
$$

which is symmetric in the arguments x_1 and x_2, as it must be. Here one may again observe active-spectator symmetry, this time under the exchange $x_1 \leftrightarrow x_3$.

$q \to q\bar{q}$ **and related channels.** Finally one finds that the $1 \to 2$ evolution kernels for quark-antiquark transitions can be written as

$$P_{q'\bar{q}',q}^{(1)}(x_1, x_2, x_3) = R_{q'\bar{q}',q}(x_1, x_2, x_3) + R_{q'\bar{q}',q}(x_2, x_1, x_3) \tag{5.116}$$

with an auxiliary function $R_{q'\bar{q}',q}$ given by

$$R_{q'\bar{q}',q} = -C_F T_F \left\{ x_1 x_2 \frac{1 - 6x_3 + x_3^2}{\bar{x}_3^4} + \frac{x_3}{\bar{x}_3^2} \right.$$
$$\left. + \left(2\ln x_1 - \ln x_3 - 2\ln \bar{x}_3 \right) \frac{x_1^2 + x_2^2}{2\bar{x}_3^3} p_{qq}(x_3) \right\}. \tag{5.117}$$

The quark valence kernels on the other hand are given by

$$P_{qq,q}^{v\,(1)}(x_1, x_2, x_3) = R_{qq,q}^{v}(x_1, x_2, x_3) + R_{qq,q}^{v}(x_2, x_1, x_3), \tag{5.118}$$

where the function $R_{qq,q}^{v}$ reads

$$R_{qq,q}^{v}(x_1, x_2, x_3) = -C_F(C_A - 2C_F) \left\{ \frac{2x_3}{\bar{x}_1^2} - \frac{1 + x_3}{\bar{x}_1} + (2\ln \bar{x}_1 - \ln x_3) \frac{1 + x_3^2}{2\bar{x}_1 \bar{x}_2} \right\}. \tag{5.119}$$

The $1 \to 2$ evolution kernels for the remaining channels again obey active-spectator symmetry and are therefore given by

$$P_{qq',q}^{(1)}(x_1, x_2, x_3) = P_{q'q,q}^{(1)}(x_2, x_1, x_3) = P_{q'\bar{q}',q}^{(1)}(x_2, x_3, x_1) \tag{5.120}$$

and

$$P_{q\bar{q},q}^{v\,(1)}(x_1, x_2, x_3) = P_{qq,q}^{v\,(1)}(x_1, x_3, x_2). \tag{5.121}$$

5.6.3. $1 \to 2$ **momentum space splitting kernels**

Consider now the renormalised $1 \to 2$ momentum space kernels $W_{a_1 a_2, a_0}^{(2)}$ as defined in equation (5.28). Here one can make a distinction between the logarithmic coefficients $W^{[2,1]}$ and $W^{[2,2]}$ and the non-logarithmic coefficients $W^{[2,0]}$ as will be seen in a moment.

Terms originating from LO kernels

As specified in equation (5.38), the kernels $W^{[2,1]}$ and $W^{[2,2]}$ can be constructed from $P_s^{(1)}$ – which has been given above already – and from additional terms that originate from convolutions of LO kernels. In the case of the LO channels, one easily finds that these additional terms have the form

$$W_{a_1 a_2, a_0} : \quad \frac{\beta_0}{2} K_{a_1 a_2, a_0} + P_{a_1 a_1}^{(0)} \underset{1}{\otimes} K_{a_1 a_2, a_0} + P_{a_2 a_2}^{(0)} \underset{2}{\otimes} K_{a_1 a_2, a_0} - K_{a_1 a_2, a_0} \underset{12}{\otimes} P_{a_0 a_0}^{(0)}, \qquad (5.122)$$

where $K = W^{[1,0]}$ or $P_s^{(0)}$ [10]. As mentioned already below equation (5.26) the flavour diagonal DGLAP kernels $P_{a_i a_i}^{(0)}$ in equation (5.122) still contain distribution terms, which can be made explicit. To this end, the kernels are written in the following form

$$P_{gg}^{(0)}(x) = P_{gg,\mathrm{reg}}^{(0)}(x) + \frac{2C_A}{[1-x]_+} + \frac{\beta_0}{2} \delta(1-x),$$

$$P_{qq}^{(0)}(x) = P_{qq,\mathrm{reg}}^{(0)}(x) + \frac{2C_F}{[1-x]_+} + \frac{3}{2} C_F \delta(1-x), \qquad (5.123)$$

in close analogy to equation (5.100), where the regular terms read

$$P_{gg,\mathrm{reg}}^{(0)}(x) = 2C_A \left[\frac{1-x}{x} + x(1-x) - 1 \right], \qquad P_{qq,\mathrm{reg}}^{(0)}(x) = -C_F(1+x). \qquad (5.124)$$

With this the convolutions in equation (5.122) can be written as

$$P_{gg}^{(0)} \underset{1}{\otimes} K = P_{gg,\mathrm{reg}}^{(0)}\left(\frac{x_1}{\bar{x}_2}\right) \frac{K(\bar{x}_2)}{\bar{x}_2} + \frac{2C_A}{[x_3]_+} K(\bar{x}_2) + \frac{1}{2}(\beta_0 - 4C_A \ln x_1) K(x_1) \delta(x_3),$$

$$P_{gg}^{(0)} \underset{2}{\otimes} K = P_{gg,\mathrm{reg}}^{(0)}\left(\frac{x_2}{\bar{x}_1}\right) \frac{K(x_1)}{\bar{x}_1} + \frac{2C_A}{[x_3]_+} K(x_1) + \frac{1}{2}(\beta_0 - 4C_A \ln \bar{x}_1) K(x_1) \delta(x_3),$$

$$K \underset{12}{\otimes} P_{gg}^{(0)} = K\left(\frac{x_1}{\bar{x}_3}\right) \frac{P_{gg,\mathrm{reg}}^{(0)}(\bar{x}_3)}{\bar{x}_3} + \frac{2C_A}{[x_3]_+} \frac{1}{\bar{x}_3} K\left(\frac{x_1}{\bar{x}_3}\right) + \frac{\beta_0}{2} K(x_1) \delta(x_3), \qquad (5.125)$$

and

$$P_{qq}^{(0)} \underset{1}{\otimes} K = P_{qq,\mathrm{reg}}^{(0)}\left(\frac{x_1}{\bar{x}_2}\right) \frac{K(\bar{x}_2)}{\bar{x}_2} + \frac{2C_F}{[x_3]_+} K(\bar{x}_2) + \frac{1}{2} C_F (3 - 4\ln x_1) K(x_1) \delta(x_3),$$

$$P_{qq}^{(0)} \underset{2}{\otimes} K = P_{qq,\mathrm{reg}}^{(0)}\left(\frac{x_2}{\bar{x}_1}\right) \frac{K(x_1)}{\bar{x}_1} + \frac{2C_F}{[x_3]_+} K(x_1) + \frac{1}{2} C_F (3 - 4\ln \bar{x}_1) K(x_1) \delta(x_3),$$

$$K \underset{12}{\otimes} P_{qq}^{(0)} = K\left(\frac{x_1}{\bar{x}_3}\right) \frac{P_{qq,\mathrm{reg}}^{(0)}(\bar{x}_3)}{\bar{x}_3} + \frac{2C_F}{[x_3]_+} \frac{1}{\bar{x}_3} K\left(\frac{x_1}{\bar{x}_3}\right) + \frac{3}{2} C_F K(x_1) \delta(x_3), \qquad (5.126)$$

---

[10]Note that repeated parton indices on the right-hand side are *not* summed over.

respectively. Here the parton labels on K have been omitted for brevity. In order to obtain these relations, equation (B13) from reference [140] has been used to bring all plus distribution terms into the form $1/[x_3]_+$.

In the NLO channels on the other hand one finds that the convolution terms in equation (5.38) are given by

$$W_{qg,g} : \quad P_{qg}^{(0)} \underset{1}{\otimes} K_{gg,g} + P_{gq}^{(0)} \underset{2}{\otimes} K_{q\bar{q},g} - K_{qg,q} \underset{12}{\otimes} P_{qg}^{(0)} ,$$

$$W_{gg,q} : \quad P_{gq}^{(0)} \underset{1}{\otimes} K_{qg,q} + P_{gq}^{(0)} \underset{2}{\otimes} K_{gq,q} - K_{gg,g} \underset{12}{\otimes} P_{gq}^{(0)} , \tag{5.127}$$

and

$$W_{q_j\bar{q}_k,q_i} : \qquad\qquad \delta_{ij}\, P_{qg}^{(0)} \underset{2}{\otimes} K_{qg,q} - \delta_{jk} K_{q\bar{q},g} \underset{12}{\otimes} P_{gq}^{(0)} ,$$

$$W_{q_j q_k,q_j} : \delta_{jk}\, P_{qg}^{(0)} \underset{1}{\otimes} K_{gq,q} + P_{qg}^{(0)} \underset{2}{\otimes} K_{qg,q} . \tag{5.128}$$

After charge conjugation symmetry has been used to replace $P_{\bar{q}g}^{(0)}$ and $P_{g\bar{q}}^{(0)}$ one finds that in the above expressions only the flavour non-diagonal DGLAP kernels

$$P_{qg}^{(0)}(x) = P_{q\bar{q},g}^{(0)}(x) , \qquad\qquad P_{gq}^{(0)}(x) = P_{gq,q}^{(0)}(x) , \tag{5.129}$$

appear.

Note that at the considered order in a_s there is exactly one parton combination in each type of convolution term for all LO and NLO channels $a_0 \to a_1 a_2$. At order α_s^3 this will no longer hold, as there is more than one possibility for the spectator partons for given a_0, a_1, and a_2.

The active-spectator symmetry observed for the kernels $P_s^{(1)}$, does no longer hold for the LO induced terms just discussed, and therefore this symmetry does not hold for $W^{[2,1]}$ and $W^{[2,2]}$ either. An example illustrating this feature quite nicely is the $W_{gg,g}^{[2,2]}$ coefficient. Apart from distribution terms, all functions in the convolutions (5.26) are equal to $2C_A\, p_{gg}$ in that case. Consider then the exchange $x_1 \leftrightarrow x_3$ which leaves the first term in equation (5.26) invariant, whilst interchanging the second and third terms. Due to the fact the latter enter $W_{gg,g}^{[2,2]}$ with opposite signs in equation (5.38), active-spectator symmetry is broken.

Non-logarithmic terms

Consider next the coefficients $W^{[2,0]}$ of the renormalised momentum space $1 \to 2$ splitting kernels $W_{a_1 a_2, a_0}^{(2)}$, which are not multiplied by logarithms. As these are rather lengthy, the presentation here will be limited to a discussion of their structure and general features. Their full expressions are given in the ancillary files associated with the paper based on the work in this chapter [113]. Note that while the functions $W^{[2,0]}$

are not needed for the NLO position space $1 \to 2$ splitting kernels $V^{(2)}$, they do appear in the matching kernels $U^{(2)}$ between cut-off and $\overline{\text{MS}}$ momentum space DPDs.

The general structure of the $W^{[2,0]}$ coefficients may be written as

$$W^{[2,0]}_{gg,g} : C_A^2 \left[R^A_{gg,g} + \delta(x_3) D^A_{gg,g} \right] + \beta_0 C_A \delta(x_3) D^\beta_{gg,g},$$

$$W^{[2,0]}_{q\bar{q},g} : C_A T_F \left\{ R^A_{q\bar{q},g} + \delta(x_3) D^A_{q\bar{q},g} + \frac{S^A_{q\bar{q},g}}{[x_3]_+} \right\} + C_F T_F \left\{ R^F_{q\bar{q},g} + \delta(x_3) D^F_{q\bar{q},g} + \frac{S^F_{q\bar{q},g}}{[x_3]_+} \right\},$$

$$W^{[2,0]}_{qg,q} : C_A C_F \left[R^A_{qg,q} + \delta(x_3) D^A_{qg,q} \right] + C_F^2 \left[R^F_{qg,q} + \delta(x_3) D^F_{qg,q} \right] + \beta_0 C_F \delta(x_3) D^\beta_{qg,q},$$

$$W^{[2,0]}_{qg,g} : C_A T_F R^A_{qg,g} + C_F T_F R^F_{qg,g},$$

$$W^{[2,0]}_{gg,q} : C_A C_F R^A_{gg,q} + C_F^2 R^F_{gg,q}, \tag{5.130}$$

and

$$W^{[2,0]}_{qq',q} : C_F T_F R^F_{qq',q}, \qquad\qquad W^{[2,0]}_{q'\bar{q}',q} : C_F T_F R^F_{q'\bar{q}',q},$$

$$W^{v\,[2,0]}_{qq,q} : C_F (C_A - 2C_F) R^F_{qq,q}, \qquad W^{v\,[2,0]}_{q\bar{q},q} : C_F (C_A - 2C_F) R^F_{q\bar{q},q}. \tag{5.131}$$

Here the functions $R^c_{a_1 a_2, a_0}$ with $c = A, F, \beta$ are regular as specified below equation (5.100) and independent of colour factors and of the number n_F of active quark flavours. One can easily see that the colour structure of $W^{[2,0]}_{a_1 a_2, a_0}$ is the same as for the corresponding kernel $P^{(1)}_{a_1 a_2, a_0}$.

In the above expressions in equations (5.130) and (5.131) the regular parts R^c are by far the most lengthy ones, containing rational functions as well as the product of rational functions with logarithms, with products of two logarithms, and with dilogarithms. The logarithms appearing in these functions have arguments $x_1, \bar{x}_1, x_2, \bar{x}_2, x_3$, or $\bar{x}_3$, while the arguments of the dilogarithms can be reduced to the set $x_1, x_2, \bar{x}_3, x_1/\bar{x}_2, x_2/\bar{x}_1$, and $-x_2/x_1$, using the relations given in section II.B of reference [149]. A particularly nice feature of this choice of arguments is that with these arguments, all logarithms and dilogarithms are real valued. In the denominators of rational functions, the highest powers of x_i and $\bar{x}_i$ (with $i = 1, 2, 3$) are the same as in the evolution kernels $P^{(1)}_s$ given earlier.

On the other hand the plus distribution parts S^c of the $W^{[2,0]}$ coefficients are either zero or simple polynomials in x_1 and $\bar{x}_1$. As they determine the leading behaviour in the limit $x_1 + x_2 \to 1$ they will be given explicitly in equation (5.139) below.

Finally the delta distribution parts D^c are in general less lengthy than the regular parts, but they involve rational functions and the product of rational functions with trilogarithms, with products of logarithms and dilogarithms, with dilogarithms, and

with products of up to three logarithms. The arguments of all logarithms and polylogarithms are only x_1 or $\bar{x}_1$. The rational functions often coincide with the corresponding functions in equation (5.105), or at least they have the same denominators as these functions.

5.6.4. Number and momentum sum rules

Proving that the DPD sum rules proposed in reference [45] are valid in QCD in chapter 3 yielded as a by-product corresponding number and momentum sum rules for the $1 \rightarrow 2$ evolution kernels P_s, given in equations (3.91) and (3.94), respectively. Note that in these sum rules the distribution terms in the DGLAP evolution kernels on the right-hand side cancel as can be easily seen: Consider the number sum rule given in equation (3.91), where such terms appear only if $a_0 = a_1$, in which case the sum of Kronecker deltas yields zero. In the case of the momentum sum rule given in equation (3.94) on the other hand, distribution terms are removed by the prefactor $1 - x_1$.

While for the LO kernels, the sum rules in equations (3.91) and (3.94) are readily verified using the relation (5.25) and the list of possible transitions $a_0 \rightarrow a_1 a_2$, the situation is quite different at NLO, where the sum rules provide non-trivial relations between the evolution kernels $P_s^{(1)}$ and the DGLAP splitting functions, which are well known at that order, see for example references [150–158]. These relations serve as a valuable cross check of the results for the $1 \rightarrow 2$ evolution kernels $P_s^{(1)}$ given in section 5.6.2.

Number sum rule

Consider to this end first the number sum rule of equation (3.91) for the different parton combinations, starting with the ones that involve $1 \rightarrow 2$ evolution kernels in LO channels, namely

$$\int \mathrm{d}x_2 \, P_{q\bar{q},g}^{(1)} = P_{qg}^{(1)} \,,$$
$$\int \mathrm{d}x_2 \, P_{gq,q}^{(1)} = P_{gq}^{(1)} \,, \tag{5.132}$$

where the arguments of the kernels and integration boundaries are implicitly understood to be as in equation (3.91) and have been omitted for brevity here and in the following. Furthermore NLO kernels that vanish identically, such as $P_{qq,g}^{(1)}$ and $P_{g\bar{q},q}^{(1)}$ are omitted. In the case of the NLO channels, the following notation introduced for example in reference [102] is used for the DGLAP kernels.

$$P_{q_i q_k} = \delta_{ik} P_{qq}^V + P_{qq}^S \,,$$
$$P_{\bar{q}_i q_k} = \delta_{ik} P_{\bar{q}q}^V + P_{\bar{q}q}^S \,. \tag{5.133}$$

Note that at NLO the relation

$$P_{qq}^S = P_{\bar{q}q}^S \tag{5.134}$$

holds for the flavour singlet parts of the DGLAP kernels. Taking linear combinations of the number sum rules for the different transitions $q_j \to q_j q_k$ and $q_i \to q_j \bar{q}_k$ and using the symmetry relations given in equation (5.104), one obtain the following number sum rules for the $1 \to 2$ evolution kernels in the NLO channels

$$\int \mathrm{d}x_2 \, P_{qq,q}^{(1)\,v} = \int \mathrm{d}x_2 \, P_{q\bar{q},q}^{(1)\,v} \,,$$

$$\int \mathrm{d}x_2 \, P_{\bar{q}q,q}^{(1)\,v} = 2 P_{\bar{q}q}^{V\,(1)} \,,$$

$$\int \mathrm{d}x_2 \, P_{q'q,q}^{(1)} = \int \mathrm{d}x_2 \, P_{q'\bar{q}',q}^{(1)} = P_{qq}^{S\,(1)} \,. \tag{5.135}$$

It has been checked explicitly that the results for the $1 \to 2$ evolution kernels given in section 5.6.2 fulfil all of the number sum rules in equations (5.132) and (5.135).

Momentum sum rule

In the case of the momentum sum rules the situation is straightforward and one finds the following sum rules for the NLO $1 \to 2$ evolution kernels

$$\int \mathrm{d}x_2 \, x_2 \left[P_{gg,g}^{(1)} + 2n_f P_{gq,g}^{(1)} \right] = (1 - x_1) P_{gg}^{(1)} \,,$$

$$\int \mathrm{d}x_2 \, x_2 \left[P_{gq,q}^{(1)} + P_{gg,q}^{(1)} \right] = (1 - x_1) P_{gq}^{(1)} \,,$$

$$\int \mathrm{d}x_2 \, x_2 \left[P_{q\bar{q},g}^{(1)} + P_{qg,g}^{(1)} \right] = (1 - x_1) P_{qg}^{(1)} \,,$$

$$\int \mathrm{d}x_2 \, x_2 \left[P_{qg,q}^{(1)} + P_{qq,q}^{(1)\,v} + P_{q\bar{q},q}^{(1)\,v} + 2n_f P_{qq',q}^{(1)} \right] = (1 - x_1) P_{qq}^{V\,(1)} \,,$$

$$\int \mathrm{d}x_2 \, x_2 \, P_{\bar{q}q,q}^{(1)\,v} = (1 - x_1) P_{\bar{q}q}^{V\,(1)} \,,$$

$$\int \mathrm{d}x_2 \, x_2 \left[P_{q'q,q}^{(1)} + P_{q'\bar{q}',q}^{(1)} \right] = (1 - x_1) P_{qq}^{S\,(1)} \,, \tag{5.136}$$

all of which are fulfilled for the $1 \to 2$ evolution kernels presented in section 5.6.2.

5.6.5. Active-spectator symmetry

In this subsection the "active-spectator" symmetry observed in section 5.6.2 will be discussed in some detail. To this end it makes sense to consider the kernels away from the point $x_3 = 0$, such that only real emission graphs contribute and distribution terms can be neglected. As already mentioned in sections 5.6.2 and 5.6.3 one observes

active-spectator symmetry to hold for the evolution kernels $P_s^{(1)}$ in all parton channels, while it is not obeyed by any of the coefficients $W^{[2,k]}$ that make up the NLO momentum space $1 \to 2$ splitting kernel $W^{(2)}$.

When one considers how the momentum space $1 \to 2$ splitting kernel is renormalised in equation (5.15), the lack of this symmetry for $W^{(2)}$ is not surprising. This is due to the fact that the renormalisation of W clearly treats observed and spectator partons in an asymmetric way. Besides this, the situation with respect to active and spectator partons is quite different already in the bare graphs as for the active partons their transverse momenta differ by $\pm\Delta$ in the amplitude and its conjugate. For unpolarised DPDs this is in fact the only difference between active partons and spectators. To see this, consider the bare DPDs F_B in light-cone perturbation theory, as has been done in chapter 3, where both active and spectator partons are on their mass shell by construction. As shown in section 3.4, for $\Delta = 0$ the numerator factors in light-cone perturbation theory are also identical for active and spectator partons in bare DPDs, provided of course that one considers unpolarised partons.

While the above argument is able to explain why the active-spectator symmetry cannot be observed for $W^{(2)}$ it does little to illustrate why it nevertheless holds for $P_{a_1 a_2, a_0}^{(1)}$. To this end it is important to note that for $x_3 > 0$ the $1 \to 2$ evolution kernels are associated with the ultraviolet divergences of two-loop graphs for the splitting process $a_0 \to a_1 a_2 a_3$, where a_3 is the spectator parton. More precisely, these kernels arise from kinematic configurations in which all three final state partons – a_1, a_2, and a_3 – have large transverse momenta. In particular the finite value of Δ can be neglected in this region of phase space, such that one should have active-spectator symmetry according to the arguments in the previous paragraph. Here it should be noted that divergences from configurations in which only two of the three final state partons have transverse momenta in the ultraviolet are not associated with $P_s^{(1)}$, but rather with the lower-order splitting kernels $P_s^{(0)}$ or $P^{(0)}$.

Another argument that illustrates why active-spectator symmetry holds for the NLO $1 \to 2$ evolution kernels is the following: In the calculation of the bare graphs that were used to extract $P_s^{(1)}$ Δ played the role of a hard scale and could thus not be set to zero. However, $P_s^{(1)}$ naturally appears in the inhomogeneous double DGLAP equation (2.56) for $F(\Delta; \mu)$, which is valid also at $\Delta = 0$. One could hence compute $P_s^{(1)}$ from graphs with $\Delta = 0$, provided that one has a dimensionful infrared regulator for separating infrared and ultraviolet poles in dimensional regularisation. With Δ being set to zero one again can expect active-spectator symmetry to hold.

5.6.6. Kinematic limits

In this subsection various kinematic limits of the NLO $1 \to 2$ evolution and momentum space splitting kernels $P_s^{(1)}$ and $W^{(2)}$ are examined and their behaviour in these

limits discussed. In particular their leading behaviour in these limiting cases will be presented.

Threshold limit: large $x_1 + x_2$

Consider to this end first the kinematic limit $x_1 + x_2 \to 1$ which is analogous to $x_3 \to 0$. In this limit the convolution in equation (5.102) can readily be simplified by explicitly writing out the plus distribution, such that one obtains the following expression

$$K \underset{12}{\otimes} f \underset{x_3 \to 0}{=} -\left[K_p(x_1, x_2) \ln x_3 - K_\delta(x_1) \right] \frac{f(x_1 + x_2)}{x_1 + x_2}. \tag{5.137}$$

As one can see from this expression a logarithm in x_3 is generated by the plus distribution term of the kernel K, dominating the convolution integral in the threshold limit $x_3 \to 0$. No higher powers of $\ln x_3$ are generated in the convolution in equation (5.102), since the kernels do not contain distributions $\mathcal{L}_k(x_3)$ with $k > 0$. A similar situation is known in the case of the convolution of ordinary DGLAP splitting functions with PDFs, where no such distributions appear even at NNLO as can be seen in references [159, 160].

As the plus distribution coefficients of the kernels are relatively short they can be given explicitly at this point. Note that plus distributions are generically only associated with the LO channels. For the $1 \to 2$ evolution kernels the coefficients multiplying the plus distributions are given by

$$P^{(1)}_{q\bar{q},g;\,p} = -2\left(C_A - 2C_F\right) T_F \left(x_1 \bar{x}_1 + x_2 \bar{x}_2\right),$$
$$P^{(1)}_{qg,q;\,p} = 2C_A C_F \bar{x}_1, \tag{5.138}$$

while for the momentum space $1 \to 2$ splitting kernels they read

$$W^{[2,2]}_{gg,g;\,p} = C_A^2 \left[p_{gg}(x_1) + p_{gg}(x_2) \right],$$
$$W^{[2,2]}_{q\bar{q},g;\,p} = -\frac{(C_A - 2C_F) T_F}{2} \left[p_{qg}(x_1) + p_{qg}(x_2) \right], \qquad W^{[2,0]}_{q\bar{q},g;\,p} = \frac{1}{2} P^{(1)}_{q\bar{q},g;\,p},$$
$$W^{[2,2]}_{qg,q;\,p} = C_A C_F \, p_{qq}(x_1), \tag{5.139}$$

where coefficients $P^{(1)}_{a_1 a_2, a_0;\,p}$ and $W^{[2,k]}_{a_1 a_2, a_0;\,p}$ that vanish exactly have been omitted.

As mentioned above the kernels $P_s^{(1)}$ and $W^{(2)}$ for NLO channels have no plus distribution terms, such that their leading threshold behaviour is $\ln^n x_3$ with $n = 0, 1, 2$, which gives a convolution $K \underset{12}{\otimes} f$ of order $x_3 \ln^n x_3$. In particular, one finds the following leading behaviour of the remaining kernels in the limit $x_3 \to 0$

$$P^{(1)}_{gg,g} \sim \mathcal{O}(\ln x_3), \qquad P^{(1)}_{qg,g} \sim \mathcal{O}(\ln x_3), \qquad P^{(1)}_{gg,q} \sim \mathcal{O}(\ln x_3),$$
$$P^{(1)}_{qq',q} \sim \mathcal{O}(\ln x_3), \qquad P^{(1)}_{q\bar{q}',q} \sim \mathcal{O}(\ln x_3), \qquad P^{v\,(1)}_{qq,q} \sim \mathcal{O}(\ln x_3),$$
$$P^{v\,(1)}_{q\bar{q},q} \sim \mathcal{O}(1), \tag{5.140}$$

and

$$
\begin{aligned}
W^{[2,0]}_{\bar{q}g,g} &\sim \mathcal{O}(\ln^2 x_3), & W^{[2,1]}_{\bar{q}g,g} &\sim \mathcal{O}(\ln x_3), & W^{[2,2]}_{\bar{q}g,g} &\sim \mathcal{O}(1), \\
W^{[2,0]}_{gg,q} &\sim \mathcal{O}(\ln^2 x_3), & W^{[2,1]}_{gg,q} &\sim \mathcal{O}(\ln x_3), & W^{[2,2]}_{gg,q} &\sim \mathcal{O}(1), \\
W^{[2,0]}_{qq',q} &\sim \mathcal{O}(\ln^2 x_3), & W^{[2,1]}_{qq',q} &\sim \mathcal{O}(\ln x_3), & W^{[2,2]}_{qq',q} &\sim \mathcal{O}(1), \\
W^{[2,0]}_{q'\bar{q}',q} &\sim \mathcal{O}(\ln^2 x_3), & W^{[2,1]}_{q'\bar{q}',q} &\sim \mathcal{O}(\ln x_3), & W^{[2,2]}_{q'\bar{q}',q} &= 0, \\
W^{v\,[2,0]}_{qq,q} &\sim \mathcal{O}(\ln^2 x_3), & W^{v\,[2,1]}_{qq,q} &\sim \mathcal{O}(\ln x_3), & W^{v\,[2,2]}_{qq,q} &= 0, \\
W^{v\,[2,0]}_{q\bar{q},q} &\sim \mathcal{O}(\ln x_3), & W^{v\,[2,1]}_{q\bar{q},q} &\sim \mathcal{O}(1), & W^{v\,[2,2]}_{q\bar{q},q} &= 0.
\end{aligned}
\tag{5.141}
$$

Small $x_1 + x_2$

The next case of interest is the one in which both momentum fractions x_1 and x_2 are small. When two systems of moderately large invariant mass are produced at high collision energy this is in fact a typical situation. As in the limit $x_1 + x_2 \to 0$ also the lower boundary of the convolution integral in equation (5.102) goes to zero the convolution includes the region $z \to 0$ in the kernel $K(zu, z\bar{u})$, where u is defined in terms of the external momentum fractions x_1 and x_2 by equation (5.103).

Recall to this end the analogous situation for the one-dimensional Mellin convolution of a LO DGLAP kernel and a PDF, given by

$$
P^{(0)} \otimes f = \int_x^1 \frac{\mathrm{d}z}{z} \, P^{(0)}(z) \, f\left(\frac{x}{z}\right).
\tag{5.142}
$$

In the case that $P(x) \propto x^{-1}$ and $f(x) \propto x^{-1} \ln^k x^{-1}$ for $x \ll 1$, the region $x \ll z \ll 1$ in the above equation (5.142) gives a behaviour proportional to

$$
\frac{1}{x} \int \frac{\mathrm{d}z}{z} \ln^k \frac{z}{x} \sim \frac{1}{k+1} \frac{1}{x} \ln^{k+1} \frac{1}{x},
\tag{5.143}
$$

where the leading logarithmic behaviour in x on the right-hand side has been obtained by extending the integration to the full range $x \le z \le 1$. One can easily see that this corresponds to the generation of small-x logarithms in a PDF: starting with k powers of $\ln x^{-1}$ in a PDF, the convolution with a kernel proportional to $1/x$ results in an additional power of that logarithm.

In full analogy one obtains a small-x logarithm in the two-variable convolution of equation (5.102) if $f(x)$ has the same small-x behaviour as above and the kernel K exhibits the following behaviour

$$
K(zu, z\bar{u}) \sim \frac{w(u)}{z^2} \qquad \text{for } z \ll 1.
\tag{5.144}
$$

In this case the region $x_1 + x_2 \ll z \ll 1$ then contributes to the convolution $K \otimes_{12} f$ as

$$\frac{w(u)}{(x_1 + x_2)^2} \int \frac{dz}{z} \ln^k \frac{z}{x_1 + x_2} \sim \frac{w(u)}{k+1} \frac{1}{(x_1 + x_2)^2} \ln^{k+1} \frac{1}{x_1 + x_2}, \tag{5.145}$$

where on the right-hand side the leading logarithmic behaviour has again been extracted by extending the integration to the full range $x_1 + x_2 \leq z \leq 1$. On the other hand, if $K(zu, z\bar{u})$ grows less fast than z^{-2} at small z, then the region $z \ll 1$ is no longer dominant in the convolution integral, and no small-x logarithm arises from integrating over z. Here it should also be pointed out that the u dependence of the kernel in equation (5.144) directly determines the u dependence of the convolution in equation (5.145).

For the $1 \to 2$ evolution kernels $P_s^{(1)}(zu, z\bar{u})$, one finds the following leading behaviour at small z

$$P_{gg,g}^{(1)} \sim \frac{2C_A^2}{z^2} \left[1 - 6u\bar{u} + \frac{2u^3 - 2u^2 + 4u - 1}{u} \ln \bar{u} + \frac{2\bar{u}^3 - 2\bar{u}^2 + 4\bar{u} - 1}{\bar{u}} \ln u \right],$$

$$P_{q\bar{q},g}^{(1)} \sim -\frac{2C_A T_F}{z^2} \left[p_{qg}(u) \ln(u\bar{u}) + (1 - 2u)^2 \right],$$

$$P_{gg,q}^{(1)} \sim \frac{C_F}{C_A} P_{gg,g}^{(1)},$$

$$P_{q'\bar{q}',q}^{(1)} \sim \frac{C_F}{C_A} P_{q\bar{q},g}^{(1)}, \tag{5.146}$$

while for the $P_s^{(1)}$ kernels without a z^{-2} singularity on the other hand, one finds that in the limit $z \to 0$ they behave as

$$P_{qg,q}^{(1)} \sim \mathcal{O}(z^{-1}), \qquad P_{qg,g}^{(1)} \sim \mathcal{O}(z^{-1}),$$

$$P_{qq',q}^{(1)} \sim \mathcal{O}(1), \qquad P_{qq,q}^{v\,(1)} \sim \mathcal{O}(z^2), \qquad P_{q\bar{q},q}^{v\,(1)} \sim \mathcal{O}(z^{-1}). \tag{5.147}$$

In the case of the momentum space $1 \to 2$ splitting kernels one finds the following expressions for the $W^{[2,k]}$ coefficients which exhibit a z^{-2} behaviour at small z

$$W_{gg,g}^{[2,0]} \sim \frac{C_A^2}{z^2} \left[3 - 20u\bar{u} - \frac{2u^3 - 2u^2 + 4u - 3}{6u} \pi^2 + (1 - 6u\bar{u}) \ln(u\bar{u}) \right.$$

$$+ \frac{2u^3 - 2u^2 + 4u - 1}{2u} \ln^2 \bar{u} - \frac{2u^4 - 4u^3 + 6u^2 + 3u - 3}{2u\bar{u}} \ln^2 u$$

$$\left. - \frac{2u^4 - 4u^3 + 6u^2 - 7u + 2}{u\bar{u}} \ln u \ln \bar{u} + \frac{3(1 - 2u)}{u\bar{u}} \mathrm{Li}_2 \frac{u-1}{u} \right],$$

$$W_{gg,g}^{[2,1]} \sim \frac{2C_A^2}{z^2} \left[1 - 6u\bar{u} + \frac{2u^3 - 2u^2 + 4u - 1}{u} \ln \bar{u} + \frac{2\bar{u}^3 - 2\bar{u}^2 + 4\bar{u} - 1}{\bar{u}} \ln u \right],$$

$$W_{gg,g}^{[2,2]} \sim -\frac{2C_A^2}{z^2} \frac{u^4 - 2u^3 + 3u^2 - 2u - 1}{u\bar{u}},$$

$$W_{q\bar{q},g}^{[2,0]} \sim \frac{C_A T_F}{6z^2} \left[p_{qg}(u) \left(\pi^2 - 72 - 3\ln^2(u\bar{u}) - 24\ln(u\bar{u}) \right) + 48 + 18\ln(u\bar{u}) \right],$$

$$W_{q\bar{q},g}^{[2,1]} \sim \frac{2C_A T_F}{z^2} \left[2 - p_{qg}(u)\left(\ln(u\bar{u}) + 3 \right) \right],$$

$$W_{q\bar{q},g}^{[2,2]} \sim -\frac{C_A T_F}{z^2} p_{qg}(u), \tag{5.148}$$

and

$$W_{gg,q}^{[2,0]} \sim \frac{C_F}{C_A} W_{gg,g}^{[2,0]}, \qquad W_{gg,q}^{[2,1]} \sim \frac{C_F}{C_A} W_{gg,g}^{[2,1]}, \qquad W_{gg,q}^{[2,2]} \sim \frac{2}{z^2} \left[\frac{2C_F^2}{u\bar{u}} - C_A C_F p_{gg}(u) \right],$$

$$W_{q'\bar{q}',q}^{[2,0]} \sim \frac{C_F}{C_A} W_{q\bar{q},g}^{[2,0]}, \qquad W_{q'\bar{q}',q}^{[2,1]} \sim \frac{C_F}{C_A} W_{q\bar{q},g}^{[2,1]}, \qquad W_{q'\bar{q}',q}^{[2,2]} = 0, \tag{5.149}$$

while for the coefficients which are less singular one finds that their leading behaviour in the limit $z \to 0$ is given by

$$\begin{aligned}
W_{\bar{q}g,q}^{[2,0]} &\sim \mathcal{O}(z^{-1}), & W_{\bar{q}g,q}^{[2,1]} &\sim \mathcal{O}(z^{-1}), & W_{\bar{q}g,q}^{[2,2]} &\sim \mathcal{O}(z^{-1}), \\
W_{\bar{q}g,g}^{[2,0]} &\sim \mathcal{O}(z^{-1}), & W_{\bar{q}g,g}^{[2,1]} &\sim \mathcal{O}(z^{-1}), & W_{\bar{q}g,g}^{[2,2]} &\sim \mathcal{O}(z^{-1}), \\
W_{q'q,q}^{[2,0]} &\sim \mathcal{O}(1), & W_{q'q,q}^{[2,1]} &\sim \mathcal{O}(1), & W_{q'q,q}^{[2,2]} &\sim \mathcal{O}(1), \\
W_{qq,q}^{v\,[2,0]} &\sim \mathcal{O}(1), & W_{qq,q}^{v\,[2,1]} &\sim \mathcal{O}(z^2), & W_{qq,q}^{v\,[2,2]} &= 0, \\
W_{q\bar{q},q}^{v\,[2,0]} &\sim \mathcal{O}(z^{-1}), & W_{q\bar{q},q}^{v\,[2,1]} &\sim \mathcal{O}(z^{-1}), & W_{q\bar{q},q}^{v\,[2,2]} &= 0. \tag{5.150}
\end{aligned}$$

Looking at the expressions in equations (5.146), (5.148) and (5.149) one finds that for both types of kernels, the channels with a z^{-2} behaviour are $g \to gg$, $g \to q\bar{q}$, $q \to gg$, and $q \to q'\bar{q}'$. Going back to the expressions for the bare graphs one finds that the graphs giving rise to such a behaviour are those in which — on both sides of the final-state cut — the spectator parton is emitted from a three-particle vertex from which also a slow gluon is emitted, where "slow" is understood relative to the incoming parton at that vertex. Examples for such graphs are figures 5.1a to 5.1d and figures 5.2g to 5.2j.

Another interesting feature of the small z expressions of $P_s^{(1)}$, $W^{[2,0]}$, and $W^{[2,1]}$ (but not of $W^{[2,2]}$) worth pointing out here is the Casimir scaling between $q \to gg$ and $g \to gg$, and between $q \to q'\bar{q}'$ and $g \to q\bar{q}$. For these kernels the small z limits in these pairs of channels are simply related by a proportionality factor C_F/C_A as can be seen in equations (5.146) and (5.149).

Triple Regge limit

With the results for the small $x_1 + x_2$ limit just presented at hand it is now possible to analyse the "triple Regge limit" $x_1 \ll x_1 + x_2 \ll 1$ (or analogously $x_2 \ll x_1 + x_2 \ll 1$).

The limiting behaviour of the $P_s^{(1)}$ and $W^{(2)}$ kernels in this case is obtained by simply taking the limit $u \to 0$ in equation (5.145). At this point only the kernels which exhibit a z^{-2} behaviour have to be considered and one finds the following expressions for the $1 \to 2$ evolutions kernels in this limit

$$P_{gg,g}^{(1)} \sim \frac{2C_A^2}{z^2}\left(2 + 3\ln u\right), \qquad\qquad P_{gg,q}^{(1)} \sim \frac{C_F}{C_A}P_{gg,g}^{(1)},$$

$$P_{q\bar{q},g}^{(1)} \sim -\frac{2C_A T_F}{z^2}\left(1 + \ln u\right), \qquad\qquad P_{q'\bar{q}',q}^{(1)} \sim \frac{C_F}{C_A}P_{q\bar{q},g}^{(1)}, \qquad (5.151)$$

while for the coefficients $W^{[2,k]}$ of the NLO momentum space $1 \to 2$ splitting kernels one finds in the LO channels

$$W_{gg,g}^{[2,0]} \sim \frac{C_A^2}{6z^2}\left(36 - \pi^2 + 9\ln^2 u\right),$$

$$W_{gg,g}^{[2,1]} \sim \frac{2C_A^2}{z^2}\left(2 + 3\ln u\right), \qquad\qquad W_{gg,g}^{[2,2]} \sim \frac{2C_A^2}{z^2}\frac{1}{u},$$

$$W_{q\bar{q},g}^{[2,0]} \sim \frac{C_A T_F}{6z^2}\left(\pi^2 - 24 - 6\ln u - 3\ln^2 u\right),$$

$$W_{q\bar{q},g}^{[2,1]} \sim -\frac{2C_A T_F}{z^2}\left(1 + \ln u\right), \qquad\qquad W_{q\bar{q},g}^{[2,2]} \sim -\frac{C_A T_F}{z^2}, \qquad (5.152)$$

and in the NLO channels

$$W_{gg,q}^{[2,0]} \sim \frac{C_F}{C_A}W_{gg,g}^{[2,0]}, \qquad W_{gg,q}^{[2,1]} \sim \frac{C_F}{C_A}W_{gg,g}^{[2,1]}, \qquad W_{gg,q}^{[2,2]} \sim -\frac{2C_F(C_A - 2C_F)}{z^2}\frac{1}{u},$$

$$W_{q'\bar{q}',q}^{[2,0]} \sim \frac{C_F}{C_A}W_{q\bar{q},g}^{[2,0]}, \qquad W_{q'\bar{q}',q}^{[2,1]} \sim \frac{C_F}{C_A}W_{q\bar{q},g}^{[2,1]}, \qquad W_{q'\bar{q}',q}^{[2,2]} = 0. \qquad (5.153)$$

Here one can easily see that in the considered limit $x_1 \ll x_1 + x_2 \ll 1$ the leading singular behaviour of all these kernels involves at most two powers of $\ln u$ which is $\approx \ln(x_1/x_2)$. The only exception to this rule are the case of kernels $W_{gg,a_0}^{[2,2]}$ for the emission of two gluons, in which a power-law behaviour like $u^{-1} \approx x_2/x_1$ of the kernels is observed. This results in a power-law behaviour like $u^{-1}(x_1 + x_2)^{-2} \approx (x_1 x_2)^{-1}$ of the convolution in equation (5.145). One finds that this behaviour comes from the terms $P_{ga_0}^{(0)} \otimes_1 P_{a_0 g,g}^{(0)}$ and $P_{ga_0}^{(0)} \otimes_2 P_{ga_0,g}^{(0)}$ and corresponds to graphs with UD topology as shown in figures 5.1b and 5.2h. In these graphs there are two consecutive three-point vertices at which an observed slow gluon is radiated from a parton carrying the full or almost the full initial plus-momentum. The appearance of a $1/u$ power behaviour only in $W^{[2,2]}$ but not in $W^{[2,1]}$ or $P_s^{(1)}$ means that this behaviour goes along with a double logarithm $\ln^2(\mu^2/\Delta^2)$. This corresponds to strong ordering in the transverse momenta at the two consecutive splitting vertices, which gives two logarithmic transverse-momentum integrals.

Analogous expressions for limit $x_2 \ll x_1 + x_2$ are easy to obtain, as all the channels with a z^{-2} behaviour have kernels $K(u_1, u_2)$ that are symmetric in u_1 and u_2.

Small x_1 or x_2

Consider finally the limit in which $x_1 \ll 1$ whilst x_2 is not. This limit is of importance in cases where two hard systems of vastly different mass are produced via DPS, with one system being very heavy, whereas the other one is light compared with the total collision energy. In this case the lower boundary of the integration in the convolution in equation (5.102) cannot reach the region $z \ll 1$. Due to this limitation the z integration does not give rise to small-x logarithms such that the limit $x_1 \ll 1$ of the convolution is simply obtained from the limit $u \ll 1$ in the kernel $K(zu, z\bar{u})$. Here it should be noted that, unlike in the case $x_1 + x_2 \ll 1$, the distribution parts K_p and K_δ of the kernel can also contribute to the small x_1 behaviour.

In the following the leading behaviour of all kernels for the case in which $x_1 \ll 1$ whilst x_2 remains unconstrained is given. Not only does this cover the limit just discussed, but it will also make it possible to consider the nested limit $x_1 \ll x_2 \ll 1$ later on. An analogous discussion holds of course for the limit $x_2 \ll 1$ at generic values of x_1. For small u and generic z, one finds for the $1 \to 2$ evolution kernels

$$P_{gg,g}^{(1)} \sim \frac{2\delta(1-z)}{3u} \left[C_A^2 \left(4 - \pi^2\right) + 5\beta_0 \, C_A \right],$$

$$P_{gq,q}^{(1)} \sim \frac{2 C_A \, C_F}{3u} \left[\frac{1-z}{z} + \delta(1-z)\left(4 - \pi^2\right) \right] + \frac{10\beta_0 \, C_F \, \delta(1-z)}{3u},$$

$$P_{gq,g}^{(1)} \sim -\frac{4 \left(C_A - 2C_F\right) T_F \left(1-z\right)}{u},$$

$$P_{gg,q}^{(1)} \sim \frac{2 C_A \, C_F}{u}, \tag{5.154}$$

while the kernels which are less singular than u^{-1} go like

$$
\begin{array}{lll}
P_{q\bar{q},g}^{(1)} \sim \mathcal{O}(\ln^2 u), & P_{qg,q}^{(1)} \sim \mathcal{O}(\ln^2 u), & P_{qg,g}^{(1)} \sim \mathcal{O}(\ln u), \\
P_{qq',q}^{(1)} \sim \mathcal{O}(\ln u), & P_{q'q,q}^{(1)} \sim \mathcal{O}(\ln u), & P_{q'\bar{q}',q}^{(1)} \sim \mathcal{O}(\ln u), \\
P_{qq,q}^{v\,(1)} \sim \mathcal{O}(1), & P_{q\bar{q},q}^{v\,(1)} \sim \mathcal{O}(\ln u), & P_{\bar{q}q,q}^{v\,(1)} \sim \mathcal{O}(\ln u).
\end{array} \tag{5.155}
$$

In the LO channels the $W^{[2,k]}$ coefficients with a u^{-1} singularity are in this limit given by

$$W_{gg,g}^{[2,0]} \sim \frac{2\delta(1-z)}{9u} \left[C_A^2 \left(16 - 45\zeta(3)\right) + 14\beta_0 \, C_A \right],$$

$$W_{gg,g}^{[2,1]} \sim \frac{2\delta(1-z)}{3u} \left[C_A^2 \left(4 - \pi^2\right) + 5\beta_0 \, C_A \right],$$

$$W_{gg,g}^{[2,2]} \sim \frac{2 C_A^2}{u} \left\{ \frac{1}{[1-z]_+} + \frac{(1-z)(1+z^2)}{z^2} - \delta(1-z) \ln u \right\} + \frac{\beta_0 \, C_A \, \delta(1-z)}{u},$$

$$W_{gq,q}^{[2,0]} \sim \frac{C_F}{C_A} W_{gg,g}^{[2,0]},$$

$$W_{gq,q}^{[2,1]} \sim \frac{C_F}{C_A} W_{gg,g}^{[2,1]},$$

$$W_{gq,q}^{[2,2]} \sim \frac{2 C_A C_F}{u} \left\{ \frac{1}{[1-z]_+} + \frac{1-z}{2z} - \delta(1-z) \ln u \right\} + \frac{\beta_0 C_F \delta(1-z)}{u}, \qquad (5.156)$$

while the ones in the NLO channels read in this limit

$$W_{gq,g}^{[2,0]} \sim -\frac{2(C_A - 2C_F) T_F}{u} (1-z),$$

$$W_{gq,g}^{[2,1]} \sim -\frac{4(C_A - C_F) T_F}{u} (1-z), \qquad W_{gq,g}^{[2,2]} \sim \frac{C_A T_F}{u} \frac{p_{qg}(z)}{z},$$

$$W_{gg,q}^{[2,0]} \sim \mathcal{O}(\ln^2 u),$$

$$W_{gg,q}^{[2,1]} \sim \frac{2C_F (C_A - C_F)}{u}, \qquad W_{gg,q}^{[2,2]} \sim -\frac{C_F (C_A - 2C_F)}{u} \frac{p_{gq}(z)}{z}. \qquad (5.157)$$

Finally, the limiting behaviour of the subleading kernels is given by

$$
\begin{aligned}
W_{q\bar{q},g}^{[2,0]} &\sim \mathcal{O}(\ln^3 u), & W_{q\bar{q},g}^{[2,1]} &\sim \mathcal{O}(\ln^2 u), & W_{q\bar{q},g}^{[2,2]} &\sim \mathcal{O}(\ln u), \\
W_{qg,q}^{[2,0]} &\sim \mathcal{O}(\ln^3 u), & W_{qg,q}^{[2,1]} &\sim \mathcal{O}(\ln^2 u), & W_{qg,q}^{[2,2]} &\sim \mathcal{O}(\ln u), \\
W_{qg,g}^{[2,0]} &\sim \mathcal{O}(\ln^2 u), & W_{qg,g}^{[2,1]} &\sim \mathcal{O}(\ln u), & W_{qg,g}^{[2,2]} &\sim \mathcal{O}(1). \\
W_{qq',q}^{[2,0]} &\sim \mathcal{O}(\ln^2 u), & W_{qq',q}^{[2,1]} &\sim \mathcal{O}(\ln u), & W_{qq',q}^{[2,2]} &\sim \mathcal{O}(1), \\
W_{q'q,q}^{[2,0]} &\sim \mathcal{O}(\ln^2 u), & W_{q'q,q}^{[2,1]} &\sim \mathcal{O}(\ln u), & W_{q'q,q}^{[2,2]} &\sim \mathcal{O}(1), \\
W_{q'\bar{q}',q}^{[2,0]} &\sim \mathcal{O}(\ln^2 u), & W_{q'\bar{q}',q}^{[2,1]} &\sim \mathcal{O}(\ln u), & W_{q'\bar{q}',q}^{[2,2]} &= 0, \\
W_{qq,q}^{v\,[2,0]} &\sim \mathcal{O}(\ln u), & W_{qq,q}^{v\,[2,1]} &\sim \mathcal{O}(1), & W_{qq,q}^{v\,[2,2]} &= 0, \\
W_{q\bar{q},q}^{v\,[2,0]} &\sim \mathcal{O}(\ln u), & W_{q\bar{q},q}^{v\,[2,1]} &\sim \mathcal{O}(1), & W_{q\bar{q},q}^{v\,[2,2]} &= 0, \\
W_{\bar{q}q,q}^{v\,[2,0]} &\sim \mathcal{O}(\ln u), & W_{\bar{q}q,q}^{v\,[2,1]} &\sim \mathcal{O}(1), & W_{\bar{q}q,q}^{v\,[2,2]} &= 0.
\end{aligned} \qquad (5.158)
$$

Here one can easily see that the channels with a u^{-1} singularity are those in which the parton with momentum fraction x_1 is a gluon. This corresponds to graphs in which a slow gluon is radiated from a parton with momentum fraction much larger than x_1. This is the case when one has a vertex with the emission of a "slow" gluon in the same sense as specified after equation (5.150).

As discussed above the preceding expressions are obtained by approximating the kernels $K(zu, z\bar{u})$ for $u \ll 1$. In the expressions obtained this way one may subsequently take the limit $z \ll 1$, which becomes relevant in the convolution if $x_1 + x_2 \ll 1$. Comparing the results of this procedure with those in equations (5.151) to (5.153), one

finds that in general the limits $u \ll 1$ and $z \ll 1$ do not commute. The only case when they do commute is if a kernel has the maximally singular behaviour $-z^{-2} u^{-1}$ – in both limits. This holds for the kernels $W_{gg,g}^{[2,2]}$ and $W_{gg,q}^{[2,2]}$ already discussed after equation (5.153). In all other cases, the behaviour of the convolution $K \otimes_{12} f$ in the triple Regge limit $x_1 \ll x_1 + x_2 \ll 1$ depends on the direction in which this limit is approached.

6. Summary and Outlook

In this chapter a brief review of the main results of the previous three chapters will be presented along with a discussion of work in progress and an outlook onto future projects.

Chapter 3 was concerned with a proof of the DPD sum rules proposed by Gaunt and Stirling in reference [45] which are one of the only currently known constraints for DPDs. To this end it was first shown in section 3.3 that in a simple toy model with scalar "quarks" a calculation of LO Feynman graphs indeed yields the sum rules at the considered order. However, this LO analysis highlighted the caveats one encounters in covariant perturbation theory which make a generalisation to higher orders very cumbersome, if not not feasible at all. Therefore in section 3.4 a different approach was used to establish that the DPD sum rules are valid at all orders in the strong coupling for unrenormalised DPDs. This could be shown using light-cone perturbation theory which had already been used to show the cancellation of Glauber gluons in SPS and DPS, as described in references [47, 90] and [34], respectively. Following this a detailed study of the UV singularities and their renormalisation in momentum space DPDs was performed in section 3.5. With the help of a particular implementation of the $\overline{\text{MS}}$ scheme it could be shown that the sum rules remain valid even for renormalised momentum space DPDs. In section 3.6 the renormalisation scale dependence of the sum rules was subsequently investigated which made it possible to derive the all-order form of the inhomogeneous double DGLAP equation for momentum space DPDs. As a by-product of this number and momentum sum rules for the $1 \rightarrow 2$ evolution kernels P_s in the inhomogeneous part of the evolution equation could be derived. On the one hand these sum rules can be used to verify that the sum rules remain valid under renormalisation scale evolution at all orders in the strong coupling, and on the other hand they provide a valuable cross-check for the calculation of higher order contributions to the $1 \rightarrow 2$ evolution kernels as they relate the P_s kernels to the regular DGLAP evolution which already have been calculated up to three loops (NNLO) in references [159, 160].

Following this it was shown in chapter 4 how the DPD sum rules can be used to construct improved LO position space models for the framework introduced in reference [35]. As the DPD sum rules are valid for momentum space DPDs at $\mathbf{\Delta} = 0$ it first had to be shown in section 4.2.1 how at LO a position space DPD model can be matched onto $\overline{\text{MS}}$ renormalised momentum space DPDs. In the following section 4.2.2 the initial ansatz for the DPD model borrowed from reference [35] was discussed in some detail, before technical details concerning the numerical implementation were

discussed in section 4.2.3. After these preliminaries had been sorted out, the agreement of the initial DPD model with the DPD sum rules was investigated in section 4.3.1 where the deficiencies of this initial model and possible ways to resolve these also were discussed. As a first step the initial phase space factor of the intrinsic part of the model was modified in accordance with the procedure described in the original sum rule paper [45] and so called number effect subtractions were implemented to take into account that finding a valence parton of a given flavour inside a hadron reduces the probability to find a second valence parton of the same flavour accordingly. With these modifications it was found that the agreement with the number sum rules greatly improved in most cases – with an exception being the equal flavour number sum rules – while the agreement with the momentum sum rules remained widely unchanged. In the next section the phase space factor was modified once more using a parameter scan over the modified powers which resulted in an even better agreement with the number sum rules, again leaving the momentum sum rules mostly unchanged. As a last step the remaining issue with the equal flavour number sum rules was tackled by adding a small modification term to the splitting part which gives a large contribution in the case of these sum rules. The required form of this modification term was obtained by rewriting the appropriate sum rules as a so called Volterra integral equation which could be numerically solved for the modification function. This lead to a greatly improved agreement of the equal flavour number sum rules. However, this came at the cost that as a result of the modified $g \to q\bar{q}$ splitting the agreement with the momentum sum rules became noticeably worse. To counteract this the $q \to qg$ and $g \to gg$ splittings were modified in much the same manner in two consecutive steps, leading to an agreement with basically all sum rules at a level better than $\pm 10\%$. Finally the dependence of the sum rules on the renormalisation scale μ and cut-off scale ν was discussed in section 4.4.

In chapter 5 the NLO expression of the perturbative $1 \to 2$ splitting contribution was the main focus. The reason why this was considered is the fact that this is the last missing ingredient for NLO DPD models and thus also NLO DPS cross section calculations in the colour singlet sector within the framework of reference [35]. The required state of the art methods for the rather complicated calculations presented in this chapter were introduced in section 5.2, followed by a renormalisation group analysis of the $1 \to 2$ splitting at NLO in section 5.3. There it was shown how the renormalised NLO momentum and position space $1 \to 2$ splitting kernels $W^{(2)}_{a_1 a_2, a_0}$ and $V^{(2)}_{a_1 a_2, a_0}$, as well as the NLO $1 \to 2$ evolution kernel $P^{(2)}_{a_1 a_2, a_0}$ can be extracted from the bare NLO results for the NLO $1 \to 2$ momentum space splitting kernel $W^{(2)}_{B, a_1 a_2, a_0}$. In section 5.4 the generalisation of the matching between position space DPDs in 4 dimensions onto $\overline{\text{MS}}$ momentum space DPDs to higher orders was discussed in detail, laying the foundations to the construction of sum rule improved NLO DPD models in close analogy to the procedure illustrated in chapter 4. The actual calculation of the bare NLO $1 \to 2$ momentum space kernel $W^{(2)}_{B, a_1 a_2, a_0}$ was presented in section 5.5 where it was noted that this kernel can be obtained directly from the sum over two-loop graphs for the bare DPD of partons a_1 and a_2 in an on-shell parton a_0. The calculation of

these bare graphs was performed using integration by parts reduction and the resulting master integrals were computed with the help of the method of differential equations with boundary conditions obtained using the method of regions. The correctness of the results for the master integrals was checked at ten randomly chosen (x_1, x_2) values using the program FIESTA 2. In section 5.6.4 it was shown that the NLO $1 \to 2$ evolution kernels fulfil the number and momentum sum rules derived in section 3.6, reaffirming the correctness of the results. Finally the leading behaviour of the $W^{(2)}_{a_1 a_2, a_0}$ and $P^{(1)}_{a_1 a_2, a_0}$ kernels was given in section 5.6.6 in the limits $x_1 + x_2 \to 1$, $x_1 + x_2 \ll 1$, $x_1 \ll 1$, and $x_1 \ll x_1 + x_2 \ll 1$. A detailed comparison of the $1 \to 2$ splitting results presented in this thesis with existing results from the literature has been performed by Jonathan Gaunt in section 5.4 of the corresponding paper [113]. The discussion presented in this chapter was limited to the $1 \to 2$ splitting in the colour singlet sector while the colour interference sector was not treated here as this is still work in progress. What sets apart the colour interference sector from the colour singlet sector is not only the different colour structure, but most importantly the fact that rapidity divergences due to light-like Wilson lines cancel only when the soft factor is taken into account. This requires extra care when handling the rapidity divergences, and it has to be checked that the final results are indeed independent of the choice of rapidity regulator. Note also, that only the case of unpolarised partons was treated in the present work, as the inclusion of polarised splittings requires some more work and is an issue that will be tackled in the near future. The non-trivial part in the polarised case is that this requires not only a tensor reduction of all open indices, but also a consistent implementation of the BMHV scheme of references [54, 161] for γ^5 in $D = 4 - 2\varepsilon$ dimensions which leads to quite non-trivial calculations.

Appendix

Appendix A.

Feynman rules

In this appendix the Feynman rules used in the calculations of chapters 3 and 5 are presented. As the computations there are performed using cut graphs this requires also the Feynman rules for propagators and vertices in the complex conjugate amplitude on the right-hand side of the cut. For clarity the rules for parts of a graph in the amplitude and for those in the complex conjugate amplitude are given individually as well as rules for propagators running across the final state cut. Note also that all Feynman rules are given for massless quarks.

A.1. Scalar Feynman rules in light-cone gauge

The calculations in section 3.3 were performed in a toy model with scalar u and $\bar{d}$ "quarks" in light-cone gauge. In this toy model the pointlike coupling of the scalar quarks to the hadron in which they are contained has been set to one, just like the operator which is inserted for observed partons, as can be seen in equation (2.22). The scalar Feynman rules required for the computations in section 3.3 are given in figure A.1.

A.2. QCD Feynman rules

In contrast to the toy model calculations of section 3.3 the calculations of the NLO $1 \rightarrow 2$ splitting contribution to DPDs at short distances or correspondingly at large momenta in chapter 5 were performed in full QCD. In order to rule out possible errors due to a wrong use of Feynman rules these calculations were performed independently in Feynman and light-cone gauge. These two gauges differ only in the numerator structure of the gluon propagator and the fact that the eikonal lines corresponding to Wilson line operators which are present in Feynman gauge are absent in $A^+ = 0$ light-cone gauge due to the fact that there light-like Wilson lines reduce to unity.

A.2.1. Feynman gauge

The Feynman rules used for the Feynman gauge calculations in chapter 5 follow the conventions in chapters 3 and 7 of reference [47]. In order to be able to give these in a concise way in figure A.2 the following short hand notation for the three and four gluon vertices is used in accordance with reference [72]:

$$V^{\mu\nu\rho}(p,q,r) = (p-q)^{\rho}g^{\mu\nu} + (q-r)^{\mu}g^{\nu\rho} + (r-p)^{\nu}g^{\rho\mu} \tag{A.1}$$

for the three-gluon vertex, and

$$\begin{aligned} W^{\mu\nu\rho\sigma}_{abcd} = &f_{eab}f_{ecd}(g^{\mu\rho}g^{\nu\sigma} - g^{\mu\sigma}g^{\nu\rho}) + f_{eac}f_{ebd}(g^{\mu\nu}g^{\rho\sigma} - g^{\mu\sigma}g^{\nu\rho}) \\ &+ f_{ead}f_{ebc}(g^{\mu\nu}g^{\rho\sigma} - g^{\mu\rho}g^{\nu\sigma}) \end{aligned} \tag{A.2}$$

for the four gluon vertex. The Feynman rules involving only quarks and gluons are presented in figure A.2. As stated in section 5.5.1 in Feynman gauge one needs to calculate Faddeev-Popov ghost versions of all graphs with closed gluon loops with only three-gluon vertices. The appropriate Feynman rules are given in figure A.3.

As in Feynman gauge eikonal lines arising from the expansion of Wilson line operators defined in equation (2.23) have to be taken into account the corresponding Feynman rules for eikonal propagators and gluons attaching to eikonal lines are given in figure A.4. In order to illustrate the Feynman rules for the eikonal propagators the notation introduced in reference [26] was used. To this end full and empty circles are drawn at the ends of each eikonal line, where the full circle denotes the relative past whereas the empty circle indicates the relative future when the path of the Wilson line through space-time is considered. This direction determines the sign of the $i\epsilon$ term in the propagator denominators. Furthermore an arrow drawn over the eikonal line indicates the direction of the momentum flow while the arrow on the eikonal line gives the direction of the colour flow and fixes the overall sign and determines the order in which colour indices are contracted. For the Feynman rules governing the coupling of gluons to eikonal lines in the fundamental or adjoint representation given in the third and fourth lines of figure A.4 it should be noted that in the case of a gluon coupling to eikonal line in the adjoint representation the relative sign between the amplitude and the conjugate amplitude can – just like in the case of the three-gluon vertex – be understood by looking at the relation $f_{cab} = -i(t^a)_{cb}$ from which one immediately sees that a minus sign is obtained by complex conjugation.

Finally, in figure A.5 the rules for gluons entering the operator in a gluon distribution are presented. This particular rule was derived in section 7.6 of reference [47] by expanding the operator $n_{\mu}F^{\mu j}(z)W(z,n)$ in g. However, this Feynman rule is valid only in the case that the Wilson line to which the eikonal line corresponds is light-like, meaning that $v = n$ where n is the light-like vector projecting on the plus components, defined in footnote 2.

A.2.2. Light-cone gauge

The QCD Feynman rules in light-cone gauge correspond largely to the ones used in Feynman gauge with the major difference being that the numerator of the gluon propagator differs from the one used in Feynman gauge. In particular the gluon propagators coincide with those from figure A.1. Furthermore Wilson lines reduce to unity in $A^+ = 0$ light-cone gauge such that they do not have to be considered there. The same is also the case for the rule concerning the gluon operator in figure A.5.
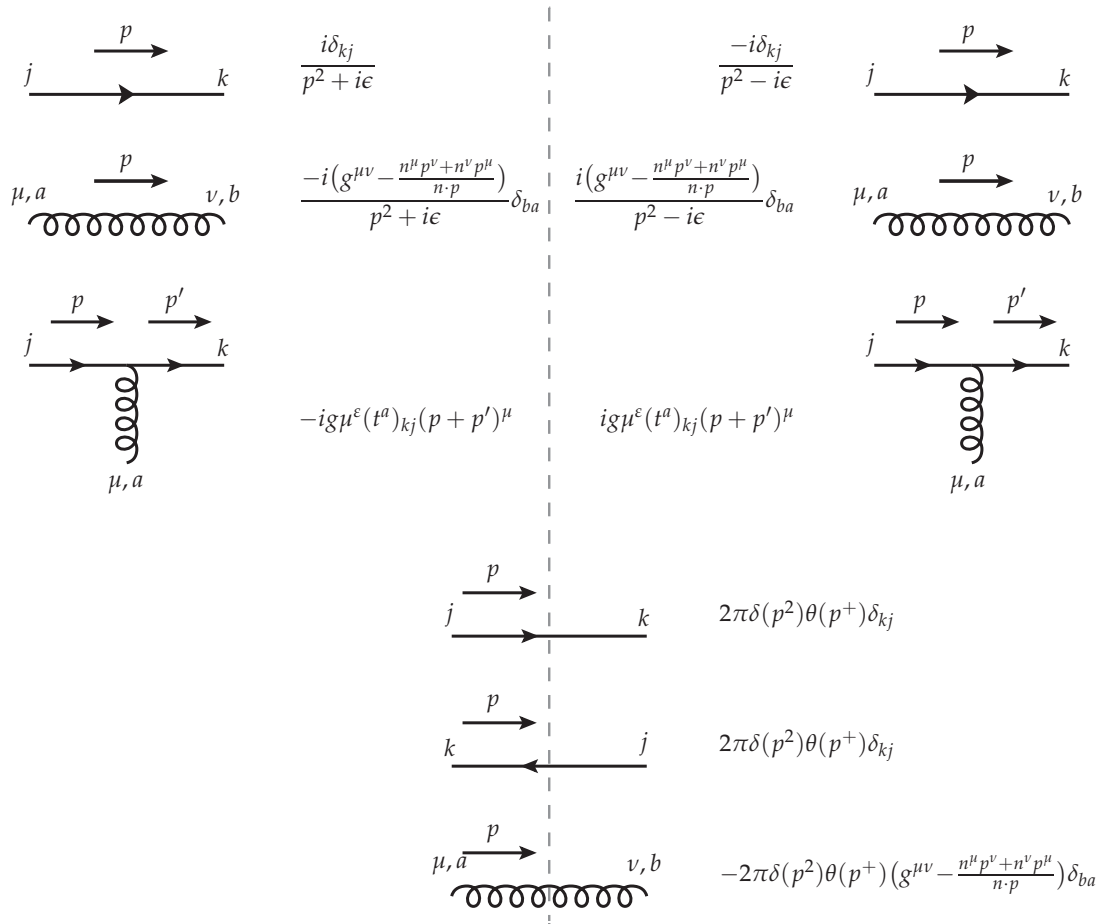
Figure A.1.: Illustration of the scalar Feynman rules in light-cone gauge used in chapter 3. Not shown here are the rules for three- and four-gluon vertices which are not needed in the calculations of section 3.3 and are identical to the ones in full QCD given in figure A.2. In scalar QCD one furthermore encounters a two-gluon-two-scalar vertex which is also not shown here for brevity. Here and in the following j and k are understood to be colour indices in the fundamental representation whereas a and b are in the adjoint representation.
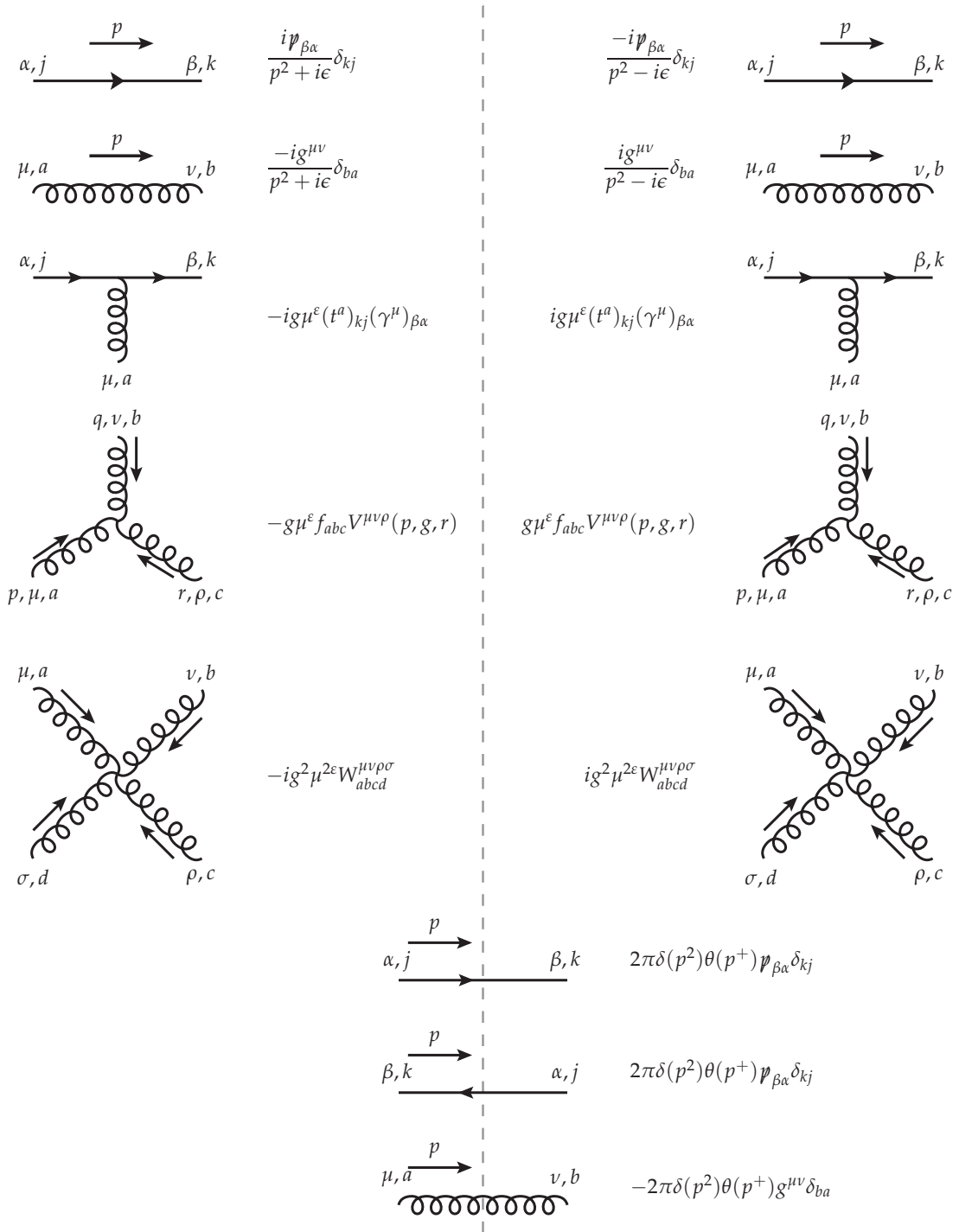
Figure A.2.: Illustration of the QCD Feynman rules in Feynman gauge used in chapter 5. Here $V^{\mu\nu\rho}(p,q,r)$ and $W^{\mu\nu\rho\sigma}_{abcd}$ are as defined in equations (A.1) and (A.2), respectively. With the sign convention for the cut antiquark propagator used here no minus sign is needed for closed quark loops running across the final state cut.
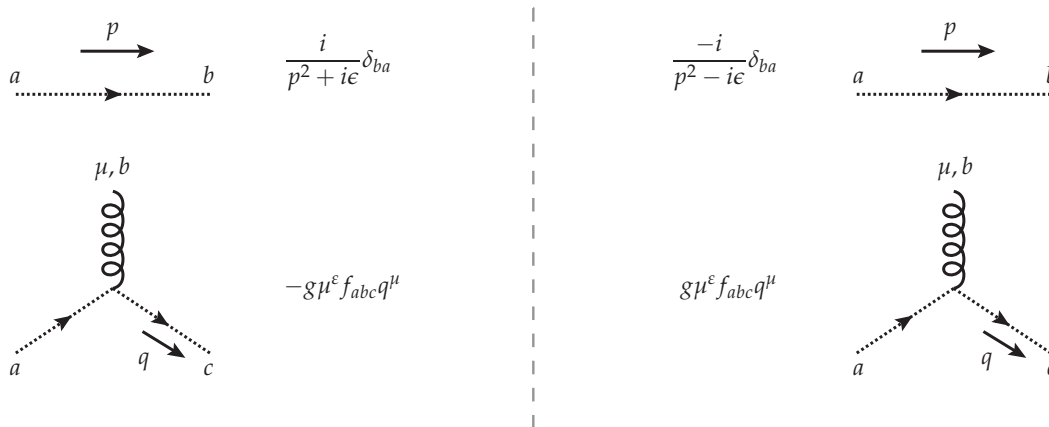
Figure A.3.: Illustration of the ghost Feynman rules in Feynman gauge used in chapter 5.
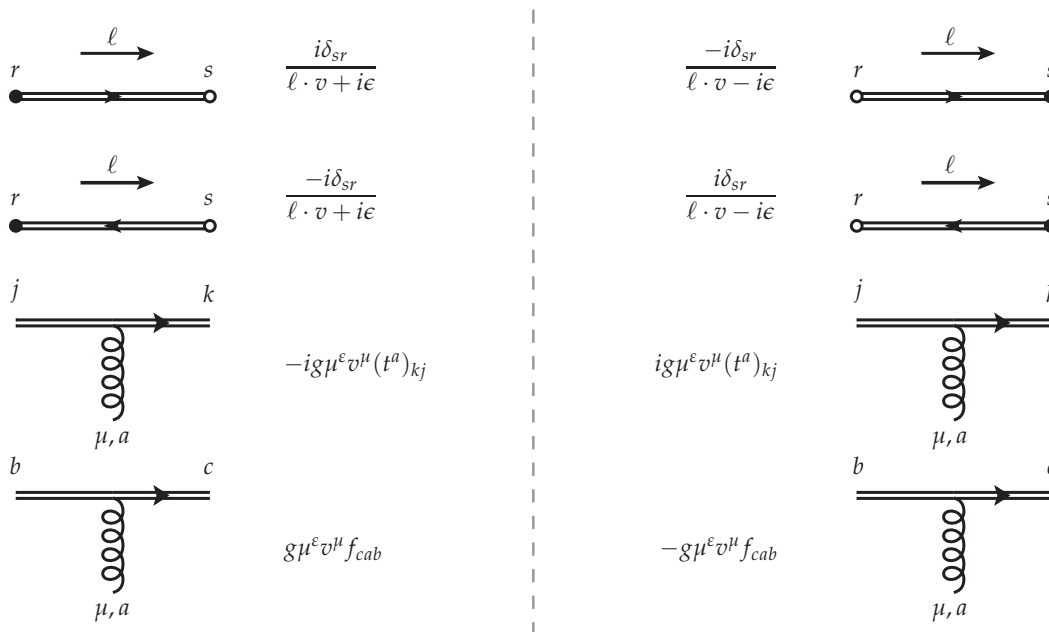
Figure A.4.: Illustration of the QCD Feynman rules in Feynman gauge involving eikonal lines. Here v is the direction of the eikonal lines in spacetime. Note that r and s are understood to be colour indices in either the fundamental or adjoint representation.

$$-i(q \cdot n\, g^{j\mu} - p^j n^\mu)\delta_{ba} \qquad i(q \cdot n\, g^{j\mu} - p^j n^\mu)\delta_{ba}$$
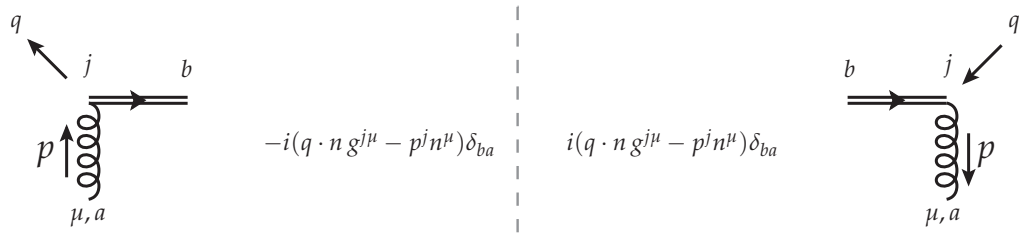
Figure A.5.: Feynman rules for gluons entering the operator in a gluon distribution. Here the index j is understood to be transverse with respect to the light-like vector n and the rule for cases without eikonal attachments is obtained by setting $q = p$.

Bibliography

[1] Axial Field Spectrometer. "Double Parton Scattering in pp Collisions at $\sqrt{s} = 63$-GeV". In: *Z. Phys.* C34 (1987), p. 163. DOI: 10.1007/BF01566757 (cit. on p. 2).

[2] UA2. "A Study of multi - jet events at the CERN anti-p p collider and a search for double parton scattering". In: *Phys. Lett.* B268 (1991), pp. 145–154. DOI: 10.1016/0370-2693(91)90937-L (cit. on p. 2).

[3] CDF. "Study of four jet events and evidence for double parton interactions in $p\bar{p}$ collisions at $\sqrt{s} = 1.8$ TeV". In: *Phys. Rev.* D47 (1993), pp. 4857–4871. DOI: 10.1103/PhysRevD.47.4857 (cit. on p. 2).

[4] CDF. "Measurement of double parton scattering in $\bar{p}p$ collisions at $\sqrt{s} = 1.8$ TeV". In: *Phys. Rev. Lett.* 79 (1997), pp. 584–589. DOI: 10.1103/PhysRevLett.79.584 (cit. on p. 2).

[5] CDF. "Double parton scattering in $\bar{p}p$ collisions at $\sqrt{s} = 1.8$TeV". In: *Phys. Rev.* D56 (1997), pp. 3811–3832. DOI: 10.1103/PhysRevD.56.3811 (cit. on p. 2).

[6] LHCb. "Observation of J/ψ pair production in pp collisions at $\sqrt{s} = 7TeV$". In: *Phys. Lett.* B707 (2012), pp. 52–59. DOI: 10.1016/j.physletb.2011.12.015. arXiv: 1109.0963 [hep-ex] (cit. on p. 2).

[7] LHCb. "Observation of double charm production involving open charm in pp collisions at $\sqrt{s} = 7$ TeV". In: *JHEP* 06 (2012). [Addendum: JHEP03,108(2014)], p. 141. DOI: 10.1007/JHEP03(2014)108, 10.1007/JHEP06(2012)141. arXiv: 1205.0975 [hep-ex] (cit. on p. 2).

[8] LHCb. "Production of associated Y and open charm hadrons in pp collisions at $\sqrt{s} = 7$ and 8 TeV via double parton scattering". In: *JHEP* 07 (2016), p. 052. DOI: 10.1007/JHEP07(2016)052. arXiv: 1510.05949 [hep-ex] (cit. on p. 2).

[9] ATLAS. "Measurement of hard double-parton interactions in $W(\rightarrow l\nu)+$ 2 jet events at $\sqrt{s}$=7 TeV with the ATLAS detector". In: *New J. Phys.* 15 (2013), p. 033038. DOI: 10.1088/1367-2630/15/3/033038. arXiv: 1301.6872 [hep-ex] (cit. on p. 2).

[10] ATLAS. "Measurement of the production cross section of prompt J/ψ mesons in association with a $W^{\pm}$ boson in pp collisions at $\sqrt{s} = 7$ TeV with the ATLAS detector". In: *JHEP* 04 (2014), p. 172. DOI: 10.1007/JHEP04(2014)172. arXiv: 1401.2831 [hep-ex] (cit. on p. 2).

[11]   ATLAS. "Observation and measurements of the production of prompt and non-prompt J/ψ mesons in association with a Z boson in pp collisions at $\sqrt{s}$ = 8 TeV with the ATLAS detector". In: *Eur. Phys. J.* C75.5 (2015), p. 229. DOI: 10.1140/epjc/s10052-015-3406-9. arXiv: 1412.6428 [hep-ex] (cit. on p. 2).

[12]   ATLAS. "Study of hard double-parton scattering in four-jet events in pp collisions at $\sqrt{s}$ = 7 TeV with the ATLAS experiment". In: *JHEP* 11 (2016), p. 110. DOI: 10.1007/JHEP11(2016)110. arXiv: 1608.01857 [hep-ex] (cit. on p. 2).

[13]   ATLAS. "Measurement of the prompt J/ ψ pair production cross-section in pp collisions at $\sqrt{s}$ = 8 TeV with the ATLAS detector". In: *Eur. Phys. J.* C77.2 (2017), p. 76. DOI: 10.1140/epjc/s10052-017-4644-9. arXiv: 1612.02950 [hep-ex] (cit. on p. 2).

[14]   ATLAS. "Study of the hard double-parton scattering contribution to inclusive four-lepton production in pp collisions at $\sqrt{s}$ = 8 TeV with the ATLAS detector". In: *Phys. Lett.* B790 (2019). [Phys. Lett.790,595(2019)], pp. 595–614. DOI: 10.1016/j.physletb.2019.01.062. arXiv: 1811.11094 [hep-ex] (cit. on p. 2).

[15]   ATLAS. "Measurement of the ratio of cross sections for inclusive isolated-photon production in pp collisions at $\sqrt{s}$ = 13 and 8 TeV with the ATLAS detector". In: *JHEP* 04 (2019), p. 093. DOI: 10.1007/JHEP04(2019)093. arXiv: 1901.10075 [hep-ex] (cit. on p. 2).

[16]   CMS. "Study of double parton scattering using W + 2-jet events in proton-proton collisions at $\sqrt{s}$ = 7 TeV". In: *JHEP* 03 (2014), p. 032. DOI: 10.1007/JHEP03(2014)032. arXiv: 1312.5729 [hep-ex] (cit. on p. 2).

[17]   CMS. "Observation of Y(1S) pair production in proton-proton collisions at $\sqrt{s}$ = 8 TeV". In: *JHEP* 05 (2017), p. 013. DOI: 10.1007/JHEP05(2017)013. arXiv: 1610.07095 [hep-ex] (cit. on p. 2).

[18]   J.-P. Lansberg, H.-S. Shao, and N. Yamanaka. "Indication for double parton scatterings in $W+$ prompt J/ψ production at the LHC". In: *Phys. Lett.* B781 (2018), pp. 485–491. DOI: 10.1016/j.physletb.2018.04.020. arXiv: 1707.04350 [hep-ph] (cit. on p. 2).

[19]   A. Kulesza and W. J. Stirling. "Like sign W boson production at the LHC as a probe of double parton scattering". In: *Phys. Lett.* B475 (2000), pp. 168–175. DOI: 10.1016/S0370-2693(99)01512-9. arXiv: hep-ph/9912232 [hep-ph] (cit. on p. 2).

[20]   J. R. Gaunt et al. "Same-sign W pair production as a probe of double parton scattering at the LHC". In: *Eur. Phys. J.* C69 (2010), pp. 53–65. DOI: 10.1140/epjc/s10052-010-1362-y. arXiv: 1003.3953 [hep-ph] (cit. on p. 2).

[21]   CMS. "Double Parton Scattering cross section limit from same-sign W bosons pair production in di-muon final state at LHC". In: (2015). CMS-PAS-FSQ-13-001 (cit. on p. 2).

[22] CMS. "Measurement of double parton scattering in same-sign WW production in p-p collisions at $\sqrt{s} = 13$ TeV with the CMS experiment". In: (2017). CMS-PAS-FSQ-16-009 (cit. on p. 2).

[23] F. A. Ceccopieri, M. Rinaldi, and S. Scopetta. "Parton correlations in same-sign *W* pair production via double parton scattering at the LHC". In: *Phys. Rev.* D95.11 (2017), p. 114030. DOI: 10.1103/PhysRevD.95.114030. arXiv: 1702.05363 [hep-ph] (cit. on p. 2).

[24] S. Cotogno, T. Kasemets, and M. Myska. "A spin on same-sign W-boson pair production". In: (2018). arXiv: 1809.09024 [hep-ph] (cit. on p. 2).

[25] M. Diehl and A. Schäfer. "Theoretical considerations on multiparton interactions in QCD". In: *Phys. Lett.* B698 (2011), pp. 389–402. DOI: 10.1016/j.physletb.2011.03.024. arXiv: 1102.3081 [hep-ph] (cit. on pp. 2, 3, 26).

[26] M. Diehl, D. Ostermeier, and A. Schäfer. "Elements of a theory for multiparton interactions in QCD". In: *JHEP* 03 (2012). [Erratum: JHEP03,001(2016)], p. 089. DOI: 10.1007/JHEP03(2012)089. arXiv: 1111.0910 [hep-ph] (cit. on pp. 2, 3, 14, 16, 19, 20, 26, 65, 66, 105, 127, 156).

[27] B. Blok et al. "The Four jet production at LHC and Tevatron in QCD". In: *Phys. Rev.* D83 (2011), p. 071501. DOI: 10.1103/PhysRevD.83.071501. arXiv: 1009.2714 [hep-ph] (cit. on p. 2).

[28] B. Blok et al. "pQCD physics of multiparton interactions". In: *Eur. Phys. J.* C72 (2012), p. 1963. DOI: 10.1140/epjc/s10052-012-1963-8. arXiv: 1106.5533 [hep-ph] (cit. on pp. 2, 3, 26).

[29] C. H. Kom, A. Kulesza, and W. J. Stirling. "Pair Production of J/psi as a Probe of Double Parton Scattering at LHCb". In: *Phys. Rev. Lett.* 107 (2011), p. 082002. DOI: 10.1103/PhysRevLett.107.082002. arXiv: 1105.4186 [hep-ph] (cit. on p. 2).

[30] C. H. Kom, A. Kulesza, and W. J. Stirling. "Prospects for observation of double parton scattering with four-muon final states at LHCb". In: *Eur. Phys. J.* C71 (2011), p. 1802. DOI: 10.1140/epjc/s10052-011-1802-3. arXiv: 1109.0309 [hep-ph] (cit. on p. 2).

[31] LHCb. "Measurement of the J/ψ pair production cross-section in pp collisions at $\sqrt{s} = 13$ TeV". In: *JHEP* 06 (2017). [Erratum: JHEP10,068(2017)], p. 047. DOI: 10.1007/JHEP06(2017)047. arXiv: 1612.07451 [hep-ex] (cit. on p. 2).

[32] N. Paver and D. Treleani. "Multi - Quark Scattering and Large p_T Jet Production in Hadronic Collisions". In: *Nuovo Cim.* A70 (1982), p. 215. DOI: 10.1007/BF02814035 (cit. on pp. 3, 16).

[33] M. Mekhfi. "MULTIPARTON PROCESSES: AN APPLICATION TO DOUBLE DRELL-YAN". In: *Phys. Rev.* D32 (1985), p. 2371. DOI: 10.1103/PhysRevD.32.2371 (cit. on p. 3).

[34]   M. Diehl et al. "Cancellation of Glauber gluon exchange in the double Drell-Yan process". In: *JHEP* 01 (2016), p. 076. DOI: 10.1007/JHEP01(2016)076. arXiv: 1510.08696 [hep-ph] (cit. on pp. 3, 16, 43–45, 149).

[35]   M. Diehl, J. R. Gaunt, and K. Schönwald. "Double hard scattering without double counting". In: *JHEP* 06 (2017), p. 083. DOI: 10.1007/JHEP06(2017)083. arXiv: 1702.06486 [hep-ph] (cit. on pp. 3, 4, 26, 28, 29, 31, 32, 64, 65, 69, 70, 95, 107, 109, 110, 122, 149, 150).

[36]   M. Diehl and R. Nagar. "Factorisation of soft gluons in multiparton scattering". In: (2018). arXiv: 1812.09509 [hep-ph] (cit. on pp. 3, 16).

[37]   A. V. Manohar and W. J. Waalewijn. "What is Double Parton Scattering?" In: *Phys. Lett.* B713 (2012), pp. 196–201. DOI: 10.1016/j.physletb.2012.05.044. arXiv: 1202.5034 [hep-ph] (cit. on pp. 3, 26, 29).

[38]   M. G. Ryskin and A. M. Snigirev. "Double parton scattering in double logarithm approximation of perturbative QCD". In: *Phys. Rev.* D86 (2012), p. 014018. DOI: 10.1103/PhysRevD.86.014018. arXiv: 1203.2330 [hep-ph] (cit. on pp. 3, 26).

[39]   J. R. Gaunt. "Single Perturbative Splitting Diagrams in Double Parton Scattering". In: *JHEP* 01 (2013), p. 042. DOI: 10.1007/JHEP01(2013)042. arXiv: 1207.0480 [hep-ph] (cit. on pp. 3, 26).

[40]   B. Blok et al. "Perturbative QCD correlations in multi-parton collisions". In: *Eur. Phys. J.* C74 (2014), p. 2926. DOI: 10.1140/epjc/s10052-014-2926-z. arXiv: 1306.3763 [hep-ph] (cit. on pp. 3, 26, 61, 89).

[41]   A. M. Snigirev, N. A. Snigireva, and G. M. Zinovjev. "Perturbative and nonperturbative correlations in double parton distributions". In: *Phys. Rev.* D90.1 (2014), p. 014015. DOI: 10.1103/PhysRevD.90.014015. arXiv: 1403.6947 [hep-ph] (cit. on pp. 3, 26).

[42]   K. Golec-Biernat and E. Lewandowska. "Electroweak boson production in double parton scattering". In: *Phys. Rev.* D90.9 (2014), p. 094032. DOI: 10.1103/PhysRevD.90.094032. arXiv: 1407.4038 [hep-ph] (cit. on pp. 3, 26).

[43]   J. R. Gaunt, R. Maciula, and A. Szczurek. "Conventional versus single-ladder-splitting contributions to double parton scattering production of two quarkonia, two Higgs bosons and $c\bar{c}c\bar{c}$". In: *Phys. Rev.* D90.5 (2014), p. 054017. DOI: 10.1103/PhysRevD.90.054017. arXiv: 1407.5821 [hep-ph] (cit. on pp. 3, 26).

[44]   M. Rinaldi et al. "Correlations in Double Parton Distributions: Perturbative and Non-Perturbative effects". In: *JHEP* 10 (2016), p. 063. DOI: 10.1007/JHEP10(2016)063. arXiv: 1608.02521 [hep-ph] (cit. on pp. 3, 26).

[45]   J. R. Gaunt and W. J. Stirling. "Double Parton Distributions Incorporating Perturbative QCD Evolution and Momentum and Quark Number Sum Rules". In: *JHEP* 03 (2010), p. 005. DOI: 10.1007/JHEP03(2010)005. arXiv: 0910.4347 [hep-ph] (cit. on pp. 3, 32, 66, 68–71, 73, 75, 88, 138, 149, 150).

[46] J. Gaunt. "Double parton scattering in proton-proton collisions". PhD thesis. Cambridge U., 2012-10-09. DOI: 10.17863/CAM.16589. URL: https://www.repository.cam.ac.uk/handle/1810/243945 (cit. on pp. 4, 32).

[47] J. Collins. *Foundations of perturbative QCD*. Vol. 32. Cambridge Monographs on Particle Physics, Nuclear Physics and Cosmology. Cambridge University Press, 2011. DOI: 10.1017/CBO9780511975592 (cit. on pp. 5, 9, 14, 15, 34, 36, 43–45, 51, 54, 56, 106, 128, 149, 156).

[48] M. Gell-Mann. "Symmetries of baryons and mesons". In: *Phys. Rev.* 125 (1962), pp. 1067–1084. DOI: 10.1103/PhysRev.125.1067 (cit. on p. 5).

[49] M. Gell-Mann. "A Schematic Model of Baryons and Mesons". In: *Phys. Lett.* 8 (1964), pp. 214–215. DOI: 10.1016/S0031-9163(64)92001-3 (cit. on p. 5).

[50] G. Zweig. "An SU(3) model for strong interaction symmetry and its breaking. Version 1". In: (1964) (cit. on p. 5).

[51] G. Zweig. "An SU(3) model for strong interaction symmetry and its breaking. Version 2". In: *DEVELOPMENTS IN THE QUARK THEORY OF HADRONS. VOL. 1. 1964 - 1978*. Ed. by D. Lichtenberg and S. P. Rosen. 1964, pp. 22–101 (cit. on p. 5).

[52] C.-N. Yang and R. L. Mills. "Conservation of Isotopic Spin and Isotopic Gauge Invariance". In: *Phys. Rev.* 96 (1954). [,150(1954)], pp. 191–195. DOI: 10.1103/PhysRev.96.191 (cit. on p. 6).

[53] L. D. Faddeev and V. N. Popov. "Feynman Diagrams for the Yang-Mills Field". In: *Phys. Lett.* B25 (1967). [,325(1967)], pp. 29–30. DOI: 10.1016/0370-2693(67)90067-6 (cit. on p. 6).

[54] G. 't Hooft and M. J. G. Veltman. "Regularization and Renormalization of Gauge Fields". In: *Nucl. Phys.* B44 (1972), pp. 189–213. DOI: 10.1016/0550-3213(72)90279-9 (cit. on pp. 6, 8, 151).

[55] S. Weinberg. "A Model of Leptons". In: *Phys. Rev. Lett.* 19 (1967), pp. 1264–1266. DOI: 10.1103/PhysRevLett.19.1264 (cit. on p. 6).

[56] A. Salam. "Weak and Electromagnetic Interactions". In: *Conf. Proc.* C680519 (1968), pp. 367–377 (cit. on p. 6).

[57] R. P. Feynman. "The behavior of hadron collisions at extreme energies". In: *Conf. Proc.* C690905 (1969), pp. 237–258 (cit. on p. 6).

[58] D. J. Gross and F. Wilczek. "Asymptotically Free Gauge Theories - I". In: *Phys. Rev.* D8 (1973), pp. 3633–3652. DOI: 10.1103/PhysRevD.8.3633 (cit. on pp. 7, 10).

[59] D. J. Gross and F. Wilczek. "Ultraviolet Behavior of Nonabelian Gauge Theories". In: *Phys. Rev. Lett.* 30 (1973). [,271(1973)], pp. 1343–1346. DOI: 10.1103/PhysRevLett.30.1343 (cit. on p. 7).

[60] H. D. Politzer. "Reliable Perturbative Results for Strong Interactions?" In: *Phys. Rev. Lett.* 30 (1973). [,274(1973)], pp. 1346–1349. DOI: 10.1103/PhysRevLett.30. 1346 (cit. on pp. 7, 10).

[61] H. Fritzsch and M. Gell-Mann. "Current algebra: Quarks and what else?" In: *eConf* C720906V2 (1972), pp. 135–165. arXiv: hep-ph/0208010 [hep-ph] (cit. on p. 7).

[62] H. Fritzsch, M. Gell-Mann, and H. Leutwyler. "Advantages of the Color Octet Gluon Picture". In: *Phys. Lett.* 47B (1973), pp. 365–368. DOI: 10.1016/0370-2693(73)90625-4 (cit. on p. 7).

[63] W. A. Bardeen et al. "Deep Inelastic Scattering Beyond the Leading Order in Asymptotically Free Gauge Theories". In: *Phys. Rev.* D18 (1978), p. 3998. DOI: 10.1103/PhysRevD.18.3998 (cit. on p. 9).

[64] S. A. Larin and J. A. M. Vermaseren. "The Three loop QCD Beta function and anomalous dimensions". In: *Phys. Lett.* B303 (1993), pp. 334–336. DOI: 10.1016/0370-2693(93)91441-O. arXiv: hep-ph/9302208 [hep-ph] (cit. on p. 10).

[65] G. F. Sterman. "Mass Divergences in Annihilation Processes. 1. Origin and Nature of Divergences in Cut Vacuum Polarization Diagrams". In: *Phys. Rev.* D17 (1978), p. 2773. DOI: 10.1103/PhysRevD.17.2773 (cit. on p. 12).

[66] S. B. Libby and G. F. Sterman. "Mass Divergences in Two Particle Inelastic Scattering". In: *Phys. Rev.* D18 (1978), p. 4737. DOI: 10.1103/PhysRevD.18.4737 (cit. on p. 12).

[67] L. D. Landau. "On analytic properties of vertex parts in quantum field theory". In: *Nucl. Phys.* 13 (1959), pp. 181–192. DOI: 10.1016/0029-5582(59)90154-3 (cit. on p. 12).

[68] S. Coleman and R. E. Norton. "Singularities in the physical region". In: *Nuovo Cim.* 38 (1965), pp. 438–442. DOI: 10.1007/BF02750472 (cit. on p. 12).

[69] G. Grammer Jr. and D. R. Yennie. "Improved treatment for the infrared divergence problem in quantum electrodynamics". In: *Phys. Rev.* D8 (1973), pp. 4332–4344. DOI: 10.1103/PhysRevD.8.4332 (cit. on p. 14).

[70] S. M. Aybat and T. C. Rogers. "TMD Parton Distribution and Fragmentation Functions with QCD Evolution". In: *Phys. Rev.* D83 (2011), p. 114042. DOI: 10.1103/PhysRevD.83.114042. arXiv: 1101.5057 [hep-ph] (cit. on p. 14).

[71] T. C. Rogers and P. J. Mulders. "No Generalized TMD-Factorization in Hadro-Production of High Transverse Momentum Hadrons". In: *Phys. Rev.* D81 (2010), p. 094006. DOI: 10.1103/PhysRevD.81.094006. arXiv: 1001.2977 [hep-ph] (cit. on p. 15).

[72] M. G. A. Buffing, M. Diehl, and T. Kasemets. "Transverse momentum in double parton scattering: factorisation, evolution and matching". In: *JHEP* 01 (2018), p. 044. DOI: 10.1007/JHEP01(2018)044. arXiv: 1708.03528 [hep-ph] (cit. on pp. 17, 18, 20, 26, 107, 156).

[73] M. Diehl, P. Plößl, and A. Schäfer. "Proof of sum rules for double parton distributions in QCD". In: (2018). arXiv: 1811.00289 [hep-ph] (cit. on pp. 22, 32).

[74] Y. L. Dokshitzer. "Calculation of the Structure Functions for Deep Inelastic Scattering and e+ e- Annihilation by Perturbation Theory in Quantum Chromodynamics." In: *Sov. Phys. JETP* 46 (1977). [Zh. Eksp. Teor. Fiz.73,1216(1977)], pp. 641–653 (cit. on p. 25).

[75] V. N. Gribov and L. N. Lipatov. "Deep inelastic *ep* scattering in perturbation theory". In: *Sov. J. Nucl. Phys.* 15 (1972). [Yad. Fiz.15,781(1972)], pp. 438–450 (cit. on p. 25).

[76] G. Altarelli and G. Parisi. "Asymptotic Freedom in Parton Language". In: *Nucl. Phys.* B126 (1977), pp. 298–318. DOI: 10.1016/0550-3213(77)90384-4 (cit. on p. 25).

[77] J. R. Gaunt and W. J. Stirling. "Double Parton Scattering Singularity in One-Loop Integrals". In: *JHEP* 06 (2011), p. 048. DOI: 10.1007/JHEP06(2011)048. arXiv: 1103.1888 [hep-ph] (cit. on p. 26).

[78] R. Kirschner. "Generalized Lipatov-Altarelli-Parisi Equations and Jet Calculus Rules". In: *Phys. Lett.* B84 (1979), pp. 266–270. DOI: 10.1016/0370-2693(79)90300-9 (cit. on pp. 27, 57).

[79] V. P. Shelest, A. M. Snigirev, and G. M. Zinovev. "The Multiparton Distribution Equations in QCD". In: *Phys. Lett.* B113 (1982), p. 325. DOI: 10.1016/0370-2693(82)90049-1 (cit. on pp. 27, 57).

[80] G. S. Bali et al. "Two-current correlations in the pion on the lattice". In: *JHEP* 12 (2018), p. 061. DOI: 10.1007/JHEP12(2018)061. arXiv: 1807.03073 [hep-lat] (cit. on pp. 29, 31).

[81] H.-W. Lin et al. "Parton distributions and lattice QCD calculations: a community white paper". In: *Prog. Part. Nucl. Phys.* 100 (2018), pp. 107–160. DOI: 10.1016/j.ppnp.2018.01.007. arXiv: 1711.07916 [hep-ph] (cit. on p. 31).

[82] S.-J. Chang and S.-K. Ma. "Feynman rules and quantum electrodynamics at infinite momentum". In: *Phys. Rev.* 180 (1969), pp. 1506–1513. DOI: 10.1103/PhysRev.180.1506 (cit. on p. 34).

[83] J. B. Kogut and D. E. Soper. "Quantum Electrodynamics in the Infinite Momentum Frame". In: *Phys. Rev.* D1 (1970), pp. 2901–2913. DOI: 10.1103/PhysRevD.1.2901 (cit. on p. 34).

[84] T.-M. Yan. "Quantum field theories in the infinite momentum frame. 4. Scattering matrix of vector and Dirac fields and perturbation theory". In: *Phys. Rev.* D7 (1973), pp. 1780–1800. DOI: 10.1103/PhysRevD.7.1780 (cit. on p. 34).

[85] S. J. Brodsky and G. P. Lepage. "Exclusive Processes in Quantum Chromodynamics". In: *Adv. Ser. Direct. High Energy Phys.* 5 (1989), pp. 93–240. DOI: 10.1142/9789814503266_0002 (cit. on p. 34).

Bibliography

[86] W.-M. Zhang and A. Harindranath. "Light front QCD. 2: Two component theory". In: *Phys. Rev.* D48 (1993), pp. 4881–4902. DOI: 10.1103/PhysRevD.48.4881 (cit. on p. 34).

[87] N. E. Ligterink and B. L. G. Bakker. "Equivalence of light front and covariant field theory". In: *Phys. Rev.* D52 (1995), pp. 5954–5979. DOI: 10.1103/PhysRevD.52.5954. arXiv: hep-ph/9412315 [hep-ph] (cit. on p. 34).

[88] Y. V. Kovchegov and E. Levin. "Quantum chromodynamics at high energy". In: *Camb. Monogr. Part. Phys. Nucl. Phys. Cosmol.* 33 (2012), pp. 1–350. DOI: 10.1017/CBO9781139022187 (cit. on p. 34).

[89] J. Collins. "The non-triviality of the vacuum in light-front quantization: An elementary treatment". In: (2018). arXiv: 1801.03960 [hep-ph] (cit. on p. 34).

[90] J. C. Collins, D. E. Soper, and G. F. Sterman. "Soft Gluons and Factorization". In: *Nucl. Phys.* B308 (1988), pp. 833–856. DOI: 10.1016/0550-3213(88)90130-7 (cit. on pp. 36, 43, 44, 149).

[91] F. A. Ceccopieri. "An update on the evolution of double parton distributions". In: *Phys. Lett.* B697 (2011), pp. 482–487. DOI: 10.1016/j.physletb.2011.02.047. arXiv: 1011.6586 [hep-ph] (cit. on p. 58).

[92] J. Kalinowski, K. Konishi, and T. R. Taylor. "JET CALCULUS BEYOND LEADING LOGARITHMS". In: *Nucl. Phys.* B181 (1981), pp. 221–252. DOI: 10.1016/0550-3213(81)90351-5 (cit. on p. 59).

[93] J. Kalinowski et al. "Resolving QCD jets beyond leading order: quark decay probabilities". In: *Nucl. Phys.* B181 (1981), pp. 253–276. DOI: 10.1016/0550-3213(81)90352-7 (cit. on p. 59).

[94] F. A. Ceccopieri. "A second update on double parton distributions". In: *Phys. Lett.* B734 (2014), pp. 79–85. DOI: 10.1016/j.physletb.2014.05.015. arXiv: 1403.2167 [hep-ph] (cit. on pp. 61, 89).

[95] M. Diehl et al. "in preparation" (cit. on p. 64).

[96] R. K. Ellis, D. A. Ross, and A. E. Terrano. "The Perturbative Calculation of Jet Structure in e^+e^- Annihilation". In: *Nucl. Phys.* B178 (1981), pp. 421–456. DOI: 10.1016/0550-3213(81)90165-6 (cit. on pp. 65, 106).

[97] G. Calucci and D. Treleani. "Proton structure in transverse space and the effective cross-section". In: *Phys. Rev.* D60 (1999), p. 054023. DOI: 10.1103/PhysRevD.60.054023. arXiv: hep-ph/9902479 [hep-ph] (cit. on p. 66).

[98] D. Treleani. "Double parton scattering, diffraction and effective cross section". In: *Phys. Rev.* D76 (2007), p. 076006. DOI: 10.1103/PhysRevD.76.076006. arXiv: 0708.2603 [hep-ph] (cit. on p. 66).

[99] M. Diehl, T. Kasemets, and S. Keane. "Correlations in double parton distributions: effects of evolution". In: *JHEP* 05 (2014), p. 118. DOI: 10.1007/JHEP05(2014)118. arXiv: 1401.1233 [hep-ph] (cit. on p. 66).

[100]   J. Collins and T. Rogers. "Understanding the large-distance behavior of transverse-momentum-dependent parton densities and the Collins-Soper evolution kernel". In: *Phys. Rev.* D91.7 (2015), p. 074020. DOI: 10.1103/PhysRevD.91.074020. arXiv: 1412.3820 [hep-ph] (cit. on p. 67).

[101]   A. D. Martin et al. "Parton distributions for the LHC". In: *Eur. Phys. J.* C63 (2009), pp. 189–285. DOI: 10.1140/epjc/s10052-009-1072-5. arXiv: 0901.0002 [hep-ph] (cit. on p. 68).

[102]   R. K. Ellis, W. J. Stirling, and B. R. Webber. *QCD and Collider Physics*. Vol. 8. Cambridge Monographs on Particle Physics, Nuclear Physics and Cosmology. Cambridge University Press, 1996. DOI: 10.1017/CBO9780511628788 (cit. on pp. 70, 138).

[103]   C. Goebel, F. Halzen, and D. M. Scott. "Double Drell-Yan Annihilations in Hadron Collisions: Novel Tests of the Constituent Picture". In: *Phys. Rev.* D22 (1980), p. 2789. DOI: 10.1103/PhysRevD.22.2789 (cit. on p. 72).

[104]   B. Humpert. "ARE THERE MULTI - QUARK INTERACTIONS?" In: *Phys. Lett.* 131B (1983), pp. 461–467. DOI: 10.1016/0370-2693(83)90540-3 (cit. on p. 72).

[105]   B. Humpert and R. Odorico. "Multiparton Scattering and QCD Radiation as Sources of Four Jet Events". In: *Phys. Lett.* 154B (1985), p. 211. DOI: 10.1016/0370-2693(85)90587-8 (cit. on p. 72).

[106]   F. Halzen, P. Hoyer, and W. J. Stirling. "Evidence for Multiple Parton Interactions From the Observation of Multi - Muon Events in Drell-Yan Experiments". In: *Phys. Lett.* B188 (1987), pp. 375–378. DOI: 10.1016/0370-2693(87)91400-6 (cit. on p. 72).

[107]   J. Kuti and V. F. Weisskopf. "Inelastic lepton - nucleon scattering and lepton pair production in the relativistic quark parton model". In: *Phys. Rev.* D4 (1971), pp. 3418–3439. DOI: 10.1103/PhysRevD.4.3418 (cit. on p. 73).

[108]   K. P. Das and R. C. Hwa. "Quark-antiquark Recombination in the Fragmentation Region". In: *Phys. Lett.* 68B (1977). [Erratum: Phys. Lett.73B,504(1978)], p. 459. DOI: 10.1016/0370-2693(77)90469-5 (cit. on p. 73).

[109]   V. L. Korotkikh and A. M. Snigirev. "Double parton correlations versus factorized distributions". In: *Phys. Lett.* B594 (2004), pp. 171–176. DOI: 10.1016/j.physletb.2004.05.012. arXiv: hep-ph/0404155 [hep-ph] (cit. on p. 73).

[110]   S. J. Brodsky and G. R. Farrar. "Scaling Laws at Large Transverse Momentum". In: *Phys. Rev. Lett.* 31 (1973), pp. 1153–1156. DOI: 10.1103/PhysRevLett.31.1153 (cit. on p. 73).

[111]   S. J. Brodsky and G. R. Farrar. "Scaling Laws for Large Momentum Transfer Processes". In: *Phys. Rev.* D11 (1975), p. 1309. DOI: 10.1103/PhysRevD.11.1309 (cit. on p. 73).

[112]   T. Lalescu. *Introduction à la théorie des équations intégrales*. Librairie Scientifique A. Hermann, 1912 (cit. on p. 83).

[113] M. Diehl et al. "Two-loop splitting in double parton distributions". In: (2019). arXiv: 1902.08019 [hep-ph] (cit. on pp. 96, 136, 151).

[114] V. A. Smirnov. "Analytic tools for Feynman integrals". In: *Springer Tracts Mod. Phys.* 250 (2012), pp. 1–296. DOI: 10.1007/978-3-642-34886-0 (cit. on p. 96).

[115] K. G. Chetyrkin and F. V. Tkachov. "Integration by Parts: The Algorithm to Calculate beta Functions in 4 Loops". In: *Nucl. Phys.* B192 (1981), pp. 159–204. DOI: 10.1016/0550-3213(81)90199-1 (cit. on p. 97).

[116] F. V. Tkachov. "A Theorem on Analytical Calculability of Four Loop Renormalization Group Functions". In: *Phys. Lett.* 100B (1981), pp. 65–68. DOI: 10.1016/0370-2693(81)90288-4 (cit. on p. 97).

[117] S. G. Gorishnii et al. "Mincer: Program for Multiloop Calculations in Quantum Field Theory for the Schoonschip System". In: *Comput. Phys. Commun.* 55 (1989), pp. 381–408. DOI: 10.1016/0010-4655(89)90134-3 (cit. on p. 98).

[118] S. A. Larin, F. V. Tkachov, and J. A. M. Vermaseren. "The FORM version of MINCER". In: (1991) (cit. on p. 98).

[119] S. Laporta and E. Remiddi. "The Analytical value of the electron (g-2) at order alpha**3 in QED". In: *Phys. Lett.* B379 (1996), pp. 283–291. DOI: 10.1016/0370-2693(96)00439-X. arXiv: hep-ph/9602417 [hep-ph] (cit. on p. 98).

[120] S. Laporta. "High precision calculation of multiloop Feynman integrals by difference equations". In: *Int. J. Mod. Phys.* A15 (2000), pp. 5087–5159. DOI: 10.1016/S0217-751X(00)00215-7, 10.1142/S0217751X00002157. arXiv: hep-ph/0102033 [hep-ph] (cit. on p. 98).

[121] C. Anastasiou and A. Lazopoulos. "Automatic integral reduction for higher order perturbative calculations". In: *JHEP* 07 (2004), p. 046. DOI: 10.1088/1126-6708/2004/07/046. arXiv: hep-ph/0404258 [hep-ph] (cit. on p. 98).

[122] C. Studerus. "Reduze-Feynman Integral Reduction in C++". In: *Comput. Phys. Commun.* 181 (2010), pp. 1293–1300. DOI: 10.1016/j.cpc.2010.03.012. arXiv: 0912.2546 [physics.comp-ph] (cit. on p. 98).

[123] A. von Manteuffel and C. Studerus. "Reduze 2 - Distributed Feynman Integral Reduction". In: (2012). arXiv: 1201.4330 [hep-ph] (cit. on p. 98).

[124] A. V. Smirnov. "Algorithm FIRE – Feynman Integral REduction". In: *JHEP* 10 (2008), p. 107. DOI: 10.1088/1126-6708/2008/10/107. arXiv: 0807.3243 [hep-ph] (cit. on p. 98).

[125] A. V. Smirnov and V. A. Smirnov. "FIRE4, LiteRed and accompanying tools to solve integration by parts relations". In: *Comput. Phys. Commun.* 184 (2013), pp. 2820–2827. DOI: 10.1016/j.cpc.2013.06.016. arXiv: 1302.5885 [hep-ph] (cit. on p. 98).

[126] A. V. Smirnov. "FIRE5: a C++ implementation of Feynman Integral REduction". In: *Comput. Phys. Commun.* 189 (2015), pp. 182–191. DOI: 10.1016/j.cpc.2014.11.024. arXiv: 1408.2372 [hep-ph] (cit. on p. 98).

[127]   A. V. Smirnov and F. S. Chuharev. "FIRE6: Feynman Integral REduction with Modular Arithmetic". In: (2019). arXiv: 1901.07808 [hep-ph] (cit. on p. 98).

[128]   R. N. Lee. "LiteRed 1.4: a powerful tool for reduction of multiloop integrals". In: *J. Phys. Conf. Ser.* 523 (2014), p. 012059. DOI: 10.1088/1742-6596/523/1/012059. arXiv: 1310.1145 [hep-ph] (cit. on pp. 98, 124).

[129]   A. V. Kotikov. "Differential equations method: New technique for massive Feynman diagrams calculation". In: *Phys. Lett.* B254 (1991), pp. 158–164. DOI: 10.1016/0370-2693(91)90413-K (cit. on p. 99).

[130]   Z. Bern, L. J. Dixon, and D. A. Kosower. "Dimensionally regulated pentagon integrals". In: *Nucl. Phys.* B412 (1994), pp. 751–816. DOI: 10.1016/0550-3213(94)90398-0. arXiv: hep-ph/9306240 [hep-ph] (cit. on p. 99).

[131]   E. Remiddi. "Differential equations for Feynman graph amplitudes". In: *Nuovo Cim.* A110 (1997), pp. 1435–1452. arXiv: hep-th/9711188 [hep-th] (cit. on p. 99).

[132]   T. Gehrmann and E. Remiddi. "Differential equations for two loop four point functions". In: *Nucl. Phys.* B580 (2000), pp. 485–518. DOI: 10.1016/S0550-3213(00)00223-6. arXiv: hep-ph/9912329 [hep-ph] (cit. on p. 99).

[133]   J. M. Henn. "Multiloop integrals in dimensional regularization made simple". In: *Phys. Rev. Lett.* 110 (2013), p. 251601. DOI: 10.1103/PhysRevLett.110.251601. arXiv: 1304.1806 [hep-th] (cit. on pp. 99, 100).

[134]   R. N. Lee. "Reducing differential equations for multiloop master integrals". In: *JHEP* 04 (2015), p. 108. DOI: 10.1007/JHEP04(2015)108. arXiv: 1411.0911 [hep-ph] (cit. on p. 100).

[135]   O. Gituliar and V. Magerya. "Fuchsia: a tool for reducing differential equations for Feynman master integrals to epsilon form". In: *Comput. Phys. Commun.* 219 (2017), pp. 329–338. DOI: 10.1016/j.cpc.2017.05.004. arXiv: 1701.04269 [hep-ph] (cit. on p. 100).

[136]   J. Kuipers et al. "FORM version 4.0". In: *Comput. Phys. Commun.* 184 (2013), pp. 1453–1467. DOI: 10.1016/j.cpc.2012.12.028. arXiv: 1203.6543 [cs.SC] (cit. on p. 123).

[137]   V. Shtabovenko, R. Mertig, and F. Orellana. "New Developments in FeynCalc 9.0". In: *Comput. Phys. Commun.* 207 (2016), pp. 432–444. DOI: 10.1016/j.cpc.2016.06.008. arXiv: 1601.01167 [hep-ph] (cit. on p. 123).

[138]   M. Beneke and V. A. Smirnov. "Asymptotic expansion of Feynman integrals near threshold". In: *Nucl. Phys.* B522 (1998), pp. 321–344. DOI: 10.1016/S0550-3213(98)00138-2. arXiv: hep-ph/9711391 [hep-ph] (cit. on p. 125).

[139]   A. V. Smirnov, V. A. Smirnov, and M. Tentyukov. "FIESTA 2: Parallelizeable multiloop numerical calculations". In: *Comput. Phys. Commun.* 182 (2011), pp. 790–803. DOI: 10.1016/j.cpc.2010.11.025. arXiv: 0912.0158 [hep-ph] (cit. on p. 126).

[140] Z. Ligeti, I. W. Stewart, and F. J. Tackmann. "Treating the b quark distribution function with reliable uncertainties". In: *Phys. Rev.* D78 (2008), p. 114014. DOI: 10.1103/PhysRevD.78.114014. arXiv: 0807.1926 [hep-ph] (cit. on pp. 126, 136).

[141] J. C. Collins. "What exactly is a parton density?" In: *Acta Phys. Polon.* B34 (2003), p. 3103. arXiv: hep-ph/0304122 [hep-ph] (cit. on p. 127).

[142] A. V. Manohar and W. J. Waalewijn. "A QCD Analysis of Double Parton Scattering: Color Correlations, Interference Effects and Evolution". In: *Phys. Rev.* D85 (2012), p. 114009. DOI: 10.1103/PhysRevD.85.114009. arXiv: 1202.3794 [hep-ph] (cit. on p. 127).

[143] T. Becher and G. Bell. "Analytic Regularization in Soft-Collinear Effective Theory". In: *Phys. Lett.* B713 (2012), pp. 41–46. DOI: 10.1016/j.physletb.2012.05.016. arXiv: 1112.3907 [hep-ph] (cit. on p. 127).

[144] Y. Li, D. Neill, and H. X. Zhu. "An Exponential Regulator for Rapidity Divergences". In: (2016). arXiv: 1604.00392 [hep-ph] (cit. on p. 127).

[145] M. A. Ebert et al. "Subleading Power Rapidity Divergences and Power Corrections for q_T". In: (2018). arXiv: 1812.08189 [hep-ph] (cit. on p. 128).

[146] M. G. Echevarria, I. Scimemi, and A. Vladimirov. "Unpolarized Transverse Momentum Dependent Parton Distribution and Fragmentation Functions at next-to-next-to-leading order". In: *JHEP* 09 (2016), p. 004. DOI: 10.1007/JHEP09(2016)004. arXiv: 1604.07869 [hep-ph] (cit. on p. 128).

[147] J.-Y. Chiu et al. "The Rapidity Renormalization Group". In: *Phys. Rev. Lett.* 108 (2012), p. 151601. DOI: 10.1103/PhysRevLett.108.151601. arXiv: 1104.0881 [hep-ph] (cit. on p. 128).

[148] J.-Y. Chiu et al. "A Formalism for the Systematic Treatment of Rapidity Logarithms in Quantum Field Theory". In: *JHEP* 05 (2012), p. 084. DOI: 10.1007/JHEP05(2012)084. arXiv: 1202.0814 [hep-ph] (cit. on p. 128).

[149] A. Devoto and D. W. Duke. "Table of Integrals and Formulae for Feynman Diagram Calculations". In: *Riv. Nuovo Cim.* 7N6 (1984), pp. 1–39. DOI: 10.1007/BF02724330 (cit. on p. 137).

[150] E. G. Floratos, D. A. Ross, and C. T. Sachrajda. "Higher Order Effects in Asymptotically Free Gauge Theories: The Anomalous Dimensions of Wilson Operators". In: *Nucl. Phys.* B129 (1977). [Erratum: Nucl. Phys.B139,545(1978)], pp. 66–88. DOI: 10.1016/0550-3213(77)90020-7 (cit. on p. 138).

[151] E. G. Floratos, D. A. Ross, and C. T. Sachrajda. "Higher Order Effects in Asymptotically Free Gauge Theories. 2. Flavor Singlet Wilson Operators and Coefficient Functions". In: *Nucl. Phys.* B152 (1979), pp. 493–520. DOI: 10.1016/0550-3213(79)90094-4 (cit. on p. 138).

[152] A. Gonzalez-Arroyo, C. Lopez, and F. J. Yndurain. "Second Order Contributions to the Structure Functions in Deep Inelastic Scattering. 1. Theoretical Calculations". In: *Nucl. Phys.* B153 (1979), pp. 161–186. DOI: 10.1016/0550-3213(79)90466-8 (cit. on p. 138).

[153] A. Gonzalez-Arroyo and C. Lopez. "Second Order Contributions to the Structure Functions in Deep Inelastic Scattering. 3. The Singlet Case". In: *Nucl. Phys.* B166 (1980), pp. 429–459. DOI: 10.1016/0550-3213(80)90207-2 (cit. on p. 138).

[154] G. Curci, W. Furmanski, and R. Petronzio. "Evolution of Parton Densities Beyond Leading Order: The Nonsinglet Case". In: *Nucl. Phys.* B175 (1980), pp. 27–92. DOI: 10.1016/0550-3213(80)90003-6 (cit. on p. 138).

[155] W. Furmanski and R. Petronzio. "Singlet Parton Densities Beyond Leading Order". In: *Phys. Lett.* 97B (1980), pp. 437–442. DOI: 10.1016/0370-2693(80)90636-X (cit. on p. 138).

[156] E. G. Floratos, C. Kounnas, and R. Lacaze. "Higher Order QCD Effects in Inclusive Annihilation and Deep Inelastic Scattering". In: *Nucl. Phys.* B192 (1981), pp. 417–462. DOI: 10.1016/0550-3213(81)90434-X (cit. on p. 138).

[157] R. Hamberg and W. L. van Neerven. "The Correct renormalization of the gluon operator in a covariant gauge". In: *Nucl. Phys.* B379 (1992), pp. 143–171. DOI: 10.1016/0550-3213(92)90593-Z (cit. on p. 138).

[158] R. K. Ellis and W. Vogelsang. "The Evolution of parton distributions beyond leading order: The Singlet case". In: (1996). arXiv: hep-ph/9602356 [hep-ph] (cit. on p. 138).

[159] S. Moch, J. A. M. Vermaseren, and A. Vogt. "The Three loop splitting functions in QCD: The Nonsinglet case". In: *Nucl. Phys.* B688 (2004), pp. 101–134. DOI: 10.1016/j.nuclphysb.2004.03.030. arXiv: hep-ph/0403192 [hep-ph] (cit. on pp. 141, 149).

[160] A. Vogt, S. Moch, and J. A. M. Vermaseren. "The Three-loop splitting functions in QCD: The Singlet case". In: *Nucl. Phys.* B691 (2004), pp. 129–181. DOI: 10.1016/j.nuclphysb.2004.04.024. arXiv: hep-ph/0404111 [hep-ph] (cit. on pp. 141, 149).

[161] P. Breitenlohner and D. Maison. "Dimensional Renormalization and the Action Principle". In: *Commun. Math. Phys.* 52 (1977), pp. 11–38. DOI: 10.1007/BF01609069 (cit. on p. 151).